Gulf Stream Temperature, Salinity and Transport during the Last Millennium

by

David C. Lund

B.A., Geology, Carleton College 1993
M.S., Oceanography, Oregon State University 1997

Submitted in partial fulfillment of the requirements for the degree of

Doctor of Philosophy

at the
MASSACHUSETTS INSTITUTE OF TECHNOLOGY
and the
WOODS HOLE OCEANOGRAPHIC INSTITUTION

February, 2006

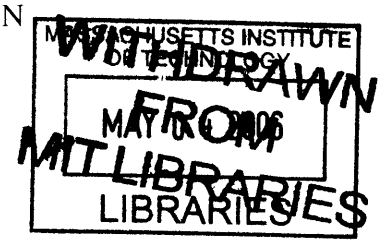

LINDGREN

Signature of Author: _____

Joint Program in Oceanography/Department of Geology and Geophysics
Massachusetts Institute of Technology and Woods Hole Oceanographic Institution
September 23, 2005

Certified by: _____

William B. Curry
Thesis Supervisor

Accepted by: _____

Gregory J. Hirth
Chair, Joint Committee for Geology and Geophysics
Woods Hole Oceanographic Institution

Gulf Stream Temperature, Salinity, and Transport during the Last Millennium

by

David C. Lund

Abstract

Benthic and planktonic foraminiferal $\delta^{18}O$ ($\delta^{18}O_c$) from a suite of well-dated, high-resolution cores spanning the depth and width of the Straits of Florida reveal significant changes in Gulf Stream cross-current density gradient during the last millennium. These data imply that Gulf Stream transport during the Little Ice Age (LIA: 1200-1850 A.D.) was 2-3 Sv lower than today. The timing of reduced flow is consistent with cold conditions in Northern Hemisphere paleoclimate archives, implicating Gulf Stream heat transport in centennial-scale climate variability of the last 1,000 years. The pattern of flow anomalies with depth suggests reduced LIA transport was due to weaker subtropical gyre wind stress curl.

The oxygen isotopic composition of Florida Current surface water ($\delta^{18}O_w$) near Dry Tortugas increased 0.4‰ during the course of the Little Ice Age (LIA: ~1200-1850 A.D.), equivalent to a salinity increase of 0.8-1.5 psu. On the Great Bahama Bank, where surface waters are influenced by the North Atlantic subtropical gyre, $\delta^{18}O_w$ increased by 0.3‰ during the last 200 years. Although a portion (~0.1‰) of this shift may be an artifact of anthropogenically-driven changes in surface water $\sum CO_2$, the remaining $\delta^{18}O_w$ signal implies a 0.4 to 1 psu increase in salinity after 200 yr BP. The simplest explanation of the $\delta^{18}O_w$ data is southward migration of the Atlantic Hadley circulation during the LIA. Scaling of the $\delta^{18}O_w$ records to salinity using the modern low-latitude $\delta^{18}O_w$-S slope produces an unrealistic reversal in the salinity gradient between the two sites. Only if $\delta^{18}O_w$ is scaled to salinity using a high-latitude $\delta^{18}O_w$-S slope can the records be reconciled. Changes in atmospheric ^{14}C paralleled shifts in Dry Tortugas $\delta^{18}O_w$, suggesting that variable solar irradiance paced centennial-scale Hadley cell migration and changes in Florida Current salinity during the last millennium.

Acknowledgements

I would like to thank my thesis advisor Bill Curry for the opportunity to work on a stimulating thesis project and his guidance over the past five years. I am also indebted to Jean Lynch-Stieglitz for her inspired idea to use foraminifera to estimate Gulf Stream density gradients. Each of my committee members, including Olivier Marchal, Terry Joyce, Delia Oppo, Jerry McManus, Lloyd Keigwin, and Mick Follows, have been generous with their time and provided insightful comments and suggestions throughout the course of my doctorate work. Dorinda Ostermann, Marti Jeglinski, Paige Cerulli, Simon Thorrold, and Scot Birdwhistle have been invaluable in the lab – without them this thesis wouldn't have been possible. Several fellow students have contributed to the stimulating environment in the MIT-WHOI Joint Program, including Peter Huybers, Mea Cook, Kristy Dahl, Rose Came and Matt Makou. I am grateful to the WHOI core lab for sample collection and archiving, the captain and crew of the R/V Knorr, and to the Sea Education Association for access to their vessels Westward and Cramer. I would also like to thank the National Science Foundation (NSF grant OCE-0096469) and WHOI Academic Programs for supporting this work.

On a personal level, many people have made Woods Hole a wonderful place to live. Oscar, Chris, Steph, Jason, Claudia, Henrik, Lara, Amy, Simon, and Andrea (and many others) – it has been a pleasure to get to know all of you and share the unique and rewarding experience of graduate school. And thank you for the dinner parties, triathlons, mountain bike rides at Otis, windsurfing days at Trunk River, and the occasional paddle across the Hole. I want to thank Max for spending time in the office with me and my daughter Etta for being the best possible distraction from thesis writing. And finally, I will be forever grateful to my wife Kate for her love, support, and patience – without her the last five years would have been a very different experience.

Table of Contents

Appendices

Chapter 1: Introduction

The salinity, temperature, and transport of the Gulf Stream are key variables that govern oceanic heat flux into the North Atlantic. If long-term variability in these parameters can be determined, then the Gulf Stream's role in climate change can be better understood. Since instrumental records are limited to the 20th century, centennial-scale shifts in Gulf Stream hydrographic properties must be inferred through clues left in ocean sediments. The Straits of Florida offer an ideal location for paleoceanographic reconstruction of the Gulf Stream. Sedimentation rates in this area are high due to input from continental and carbonate bank sources. Furthermore, the Florida Current (the name for the Gulf Stream within the Straits) is constrained by the surrounding topography. Variability in temperature, salinity and transport can therefore be ascribed to changes in the Gulf Stream itself, as opposed to changes in its position.

The primary goals of this thesis have been to: (1) verify that centennial-scale climate variability can be detected in planktonic foraminiferal $\delta^{18}O$ records from the Florida Straits; (2) determine whether the planktonic $\delta^{18}O$ signal was primarily a function of temperature or salinity; (3) reconstruct the density structure of the Florida Current using benthic $\delta^{18}O$ to estimate past changes in transport; and (4) compare the Florida Current data to other late Holocene paleoclimate archives to evaluate possible climate change mechanisms. The results of this research are detailed in Chapters 2, 3, and 4. Chapter 2 deals with long (>3000 year) planktonic $\delta^{18}O$ records and their relationship to

one another and to proxies of solar variability. Chapter 3 addresses the temperature and salinity components of the planktonic $\delta^{18}O$ records and the implied changes in the hydrologic cycle. Finally, Chapter 4 focuses on the benthic $\delta^{18}O$ records and the changes in Florida Current transport and water column stratification that their variability implies.

Recent paleoclimate research, particularly in the North Atlantic region, suggests that the ocean-atmosphere system is capable of significant variability on centennial time scales. The Little Ice Age, which occurred from ~1200 to 1850 A.D., was characterized by not only alpine glacier advances and unusually cool conditions in many parts of the Northern Hemisphere but also large-scale shifts in the mean position of the Atlantic Inter-Tropical Convergence Zone. Changes in solar irradiance may have triggered centennial- to millennial-scale climate variability during the Holocene, but solar forcing on its own appears to be too weak to explain climate anomalies such as the Little Ice Age. Either another driving mechanism was involved, or small changes in irradiance were amplified through a series of feedbacks internal to the climate system.

In Chapter 2, I show that sediment cores with high-sedimentation rates and well-resolved age models are capable of replicating planktonic $\delta^{18}O_c$ signals at frequencies as high as 1/250 years. This result gives us confidence that the $\delta^{18}O_c$ time series reflect real oceanographic variability as opposed to confounding factors associated with sediment accumulation, bioturbation, and winnowing. I also present evidence that Florida Current $\delta^{18}O_c$ varied coherently with proxies of atmospheric radiocarbon at low frequencies over

the last 5,000 years, suggesting a link between solar irradiance and either the surface temperature or salinity of the Gulf Stream during the mid- to late-Holocene.

In Chapter 3, I decompose the planktonic $\delta^{18}O_c$ signal of the last 1,200 years into its two primary parts, temperature and seawater $\delta^{18}O$ ($\delta^{18}O_w$), and find that the $\delta^{18}O_c$ variability was almost entirely a function of $\delta^{18}O_w$. On either side of the Florida Current the $\delta^{18}O_w$ results are very different – two cores from Dry Tortugas show the LIA was saltier than today, while two cores from the Great Bahama Bank show the LIA was fresher. These changes must be due to large-scale variability in the hydrologic cycle, most likely southward movement of the Hadley circulation. I also demonstrate that applying today's low-latitude seawater $\delta^{18}O_w$-S relationship to the observed LIA changes produces a reversal in the modern salinity gradient, an unrealistic scenario. Reasonable salinity changes can only be achieved if $\delta^{18}O_w$ is scaled to salinity using a thermocline or high-latitude $\delta^{18}O_w$-S relationship.

It is routinely suggested that variability in the meridional overturning circulation was either directly responsible for or intimately involved in amplifying centennial- to millennial-scale climate anomalies. In Chapter 4, I attempt to evaluate whether this occurred during the Little Ice Age using current shear and transport estimates based on benthic foraminiferal $\delta^{18}O_c$ data. The Florida Current acts as the northward surface compensation of the meridional overturning circulation as well as the western boundary of the North Atlantic subtropical gyre. Changes in either of these two components will

affect Gulf Stream flow and potentially the transport of heat into the North Atlantic. I show that transport during the LIA was ~10% lower than either today or 1100 yr BP. The primary implication is that lower oceanic heat flux may have contributed to the Little Ice Age cooling in the Northern Hemisphere. The data also suggest that the overturning circulation was relatively constant during the last millennium and any changes in oceanic heat transport were most likely wind-driven.

Chapter 2:

Late Holocene Variability in Florida Current Surface Density: Patterns and Possible Causes*

Abstract

Planktonic foraminiferal $\delta^{18}O$ time series from three well-dated, high sedimentation-rate cores near the Florida Keys (24.4°N, 83.3°W) exhibit repeated centennial to millennial-scale oscillations during the late Holocene. Isotopic shifts of 0.2-0.3‰ over the past 5,200 years represent changes in sea-surface temperature of 1.0-1.5°C or salinity variability of 1-2 psu. The largest significant isotopic events are centered at approximately 200, 2000, 3200, and prior to 4000 calendar years BP.

High Florida Current $\delta^{18}O$ during the Little Ice Age correlates with published records of high $\delta^{18}O$ in the Sargasso Sea and low SST off the coast of West Africa. An interval of generally low $\delta^{18}O$ in the Florida Straits from 1800 to 500 yr BP is synchronous with the Medieval Warm Period off West Africa but leads low $\delta^{18}O$ in the Sargasso Sea by several hundred years. Synchronous cooling across the subtropical gyre during the LIA is difficult to explain using interannual NAO patterns but may be consistent with the simulated effects of reduced solar irradiance.

At frequencies between 1/1000 and 1/300 years during the Late Holocene, Florida Current $\delta^{18}O$ is coherent with a published estimate of ^{14}C production rate. Radiocarbon production seems to lead $\delta^{18}O$ at these frequencies, but uncertainty in the phase calculation precludes a clear lead-lag relationship. At frequencies lower than 1/300 years, Florida Current $\delta^{18}O$ is coherent and in phase with atmospheric $\Delta^{14}C$. The coherence of $\Delta^{14}C$ and $\delta^{18}O$ at periods >1000 years implies oceanic circulation may play a role in modulating atmospheric radiocarbon on millennial time scales.

*Published as: Lund, D. C., and W. B. Curry (2004), Late Holocene variability in Florida Current surface density: Patterns and possible causes, *Paleoceanography, 19*, PA4001, doi:10.1029/2004PA001008. Reproduced with permission of the American Geophysical Union.

Late Holocene variability in Florida Current surface density: Patterns and possible causes

D. C. Lund

Massachusetts Institute of Technology/Woods Hole Oceanographic Institution Joint Program in Oceanography, Woods Hole Oceanographic Institution, Woods Hole, Massachusetts, USA

W. B. Curry

Department of Geology and Geophysics, Woods Hole Oceanographic Institution, Woods Hole, Massachusetts, USA

Received 14 January 2004; revised 28 May 2004; accepted 16 July 2004; published 5 October 2004.

[1] Planktonic foraminiferal $\delta^{18}O$ time series from three well-dated, high sedimentation rate cores near the Florida Keys (24.4°N, 83.3°W) exhibit repeated centennial to millennial-scale oscillations during the late Holocene. Isotopic shifts of 0.2–0.3‰ over the past 5200 years represent changes in sea-surface temperature (SST) of 1.0–1.5°C or salinity variability of 1–2 psu. The largest significant isotopic events are centered at approximately 200, 2000, 3200, and prior to 4000 calendar years BP. High Florida Current $\delta^{18}O$ during the Little Ice Age (LIA) correlates with published records of high $\delta^{18}O$ in the Sargasso Sea and low SST off the coast of west Africa. An interval of generally low $\delta^{18}O$ in the Florida Straits from 1800 to 500 years BP is synchronous with the Medieval Warm Period off west Africa but leads low $\delta^{18}O$ in the Sargasso Sea by several hundred years. Synchronous cooling across the subtropical gyre during the LIA is difficult to explain using interannual North Atlantic Oscillation patterns but may be consistent with the simulated effects of reduced solar irradiance. At frequencies between 1/1000 and 1/300 years during the Late Holocene, Florida Current $\delta^{18}O$ is coherent with a published estimate of ^{14}C production rate. Radiocarbon production seems to lead $\delta^{18}O$ at these frequencies, but uncertainty in the phase calculation precludes a clear lead-lag relationship. At frequencies lower than 1/300 years, Florida Current $\delta^{18}O$ is coherent and in phase with atmospheric $\Delta^{14}C$. The coherence of $\Delta^{14}C$ and $\delta^{18}O$ at periods >1000 years implies oceanic circulation may play a role in modulating atmospheric radiocarbon on millennial timescales. *INDEX TERMS:* 4215 Oceanography: General: Climate and interannual variability (3309); 4576 Oceanography: Physical: Western boundary currents; 4870 Oceanography: Biological and Chemical: Stable isotopes; *KEYWORDS* Holocene, Florida current, density

Citation: Lund, D. C., and W. B. Curry (2004), Late Holocene variability in Florida Current surface density: Patterns and possible causes, *Paleoceanography, 19*, PA4001, doi:10.1029/2004PA001008.

1. Introduction

[2] The Florida Current, the portion of the Gulf Stream confined to the Straits of Florida, is a key component of the North Atlantic circulation. The flow of the Florida Current (FC) reflects both wind-driven processes in the subtropical gyre and the surface compensating flow for North Atlantic Deep Water formation. The FC transports approximately 1.3 PW (1 PW = 10^{15} W) of heat across 24.5°N [*Larsen et al.*, 1992; *Ganachaud and Wunsch*, 2000] and therefore plays a key role in regulating the climate of the circum-North Atlantic region. While the Florida Current-Gulf Stream system is arguably one of the most studied features in modern oceanography, almost nothing is known about its behavior on centennial to millennial timescales. Observations are largely limited to sea surface temperature or snapshot flow estimates during the 20th century.

[3] Here we present evidence for long-term variability in the surface density of the Florida Current over the past 5200 years using the $\delta^{18}O$ of planktonic foraminifera. Stable isotopic data from three cores indicate the surface FC was denser (colder, saltier or both) during the Little Ice Age than either the Medieval Warm Period or today. The lowest $\delta^{18}O$ values in the Florida Current during the last 5200 years occurred from 2300 to 4000 years BP, significantly lower than either core top or $\delta^{18}O_{calcite}$ calculated using modern surface temperature and salinity observations. When considered with other published results [*Keigwin*, 1996; *deMenocal et al.*, 2000], it is possible that the entire subtropical gyre of the North Atlantic cooled during the Little Ice Age, a pattern unlike the interannual variations in the North Atlantic Oscillation [*deMenocal et al.*, 2000], but perhaps consistent with the simulated effects of reduced solar irradiance [*Rind and Overpeck*, 1993; *Shindell et al.*, 2001].

2. Background

2.1. Modern Oceanographic Setting

[4] The Florida Current, with an annual average flow of 31 Sv (1 Sv = 10^6 m^3 s^{-1}), is composed of two primary

0883-8305/04/2004PA001008$12.00

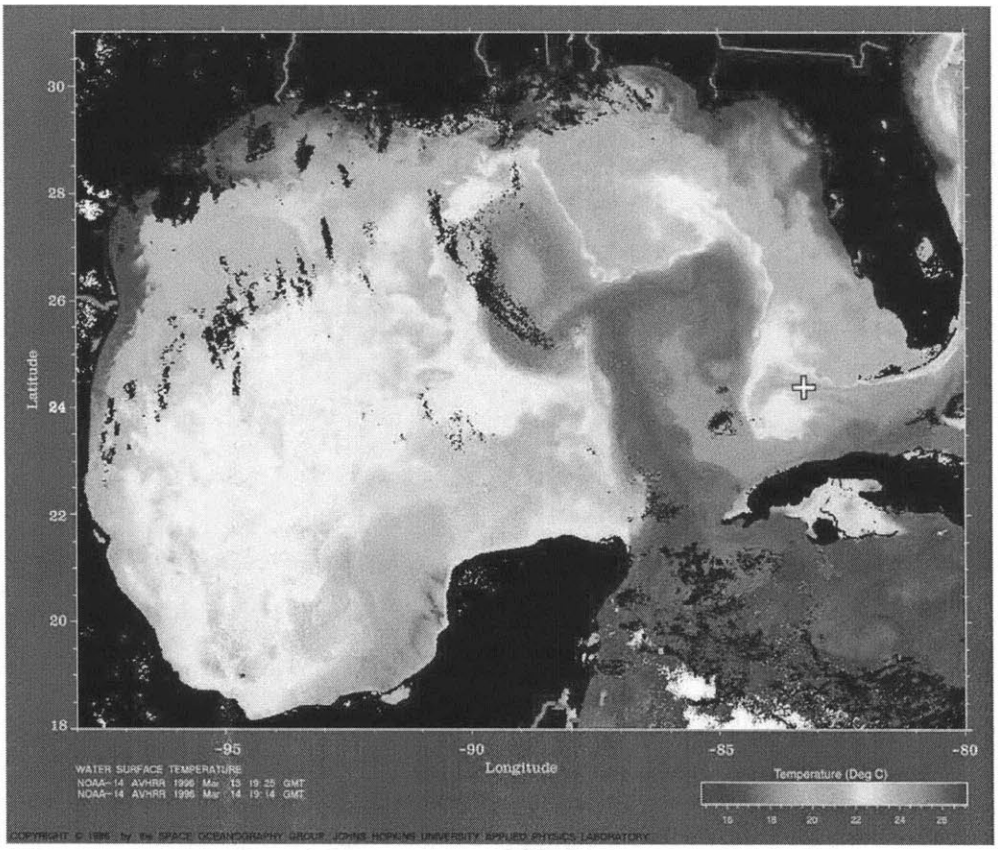

Figure 1. Advanced very high resolution radiometer (AVHRR)-based sea surface temperature estimates for the Gulf of Mexico and Florida Straits, 13–14 March 1996. SSTs in this figure vary from 15 to 27°C. The strong north-south temperature gradient near the core sites (plus symbol) is typical of winter conditions in this area (reprinted by permission from Ocean Remote Sensing Group, Johns Hopkins University Applied Physics Laboratory). See color version of this figure at back of this issue.

components; one from the wind-driven subtropical gyre (17 Sv) and the other from the tropical South Atlantic (14 Sv) [*Schmitz and Richardson*, 1991]. The fresh South Atlantic portion (<36 psu) accounts for the majority of the warmest water at the surface and coldest water near the bottom of the Florida Current (FC). In between these two components flows high salinity (>36 psu) water of the North Atlantic subtropical gyre [*Schmitz et al.*, 1993]. The estimate of the South Atlantic contribution is similar to the formation rate of North Atlantic Deep Water (13–14 Sv) implying that the South Atlantic portion of the FC compensates NADW formation [*Schmitz and McCartney*, 1993].

[5] The transport of the Florida Current varies on annual and interannual timescales. The best time series of FC variability are transport estimates based on the voltage difference in submarine telephone cables across the Straits of Florida. Using 16 years of data, *Baringer and Larsen* [2001] calculated an annual minimum of 30 Sv in January and maximum of 34 Sv in July. Decadal variations in FC transport of ±2 Sv seem to be negatively correlated with the NAO index, but the link between the two remains unclear due the limited length of the observations [*Baringer and Larsen*, 2001].

[6] Climatological sea surface temperatures at the coring sites discussed in this paper (near Dry Tortugas: ~24.5°N, 83.5°W) range from a summer maximum of approximately 30°C to a winter minimum of 24°C [*Levitus et al.*, 1994]. Satellite imagery indicates the presence of a strong meridional temperature gradient in this region from September through April, due to the juxtaposition of warm Florida Current water and colder water along the West Florida Shelf. An advanced very high resolution radiometer (AVHRR)-based SST map from mid-March 1996 shows the Loop Current penetrating into the Gulf of Mexico, then returning southward and eventually eastward into the Florida Straits (Figure 1). Northward incursions of the Loop Current and shedding of a large anticyclonic ring occurs on an aperiodic basis [*Vukovich*, 1988; *Sturges and Leben*, 2000].

[7] When the Loop Current is fully developed, frontal eddies propagated along its outer boundary generate cyclonic mesoscale features near Dry Tortugas [*Fratantoni et al.*, 1998]. The so-called Tortugas eddies persist on the order of 100 days and are eventually dislodged and taken downstream by meanders in the Florida Current [*Lee et al.*, 1995; *Fratantoni et al.*, 1998]. The presence of these eddies tends to cool SSTs near Dry Tortugas, except in the summer months when SSTs in the Gulf of Mexico and Florida Current are nearly homogeneous [*Levitus et al.*, 1994].

2.2. Little Ice Age Record

[8] The majority of our knowledge of the Little Ice Age comes from land-based historical and paleoclimate records. Historical accounts describe severe cold conditions in Europe and North America at intermittent periods during the LIA [*Grove*, 1988; *Jones and Bradley*, 1995]. Terrestrial paleoclimatic records, including Northern Hemisphere tree ring-based temperature reconstructions [*Bradley and Jones*, 1993; *Mann et al.*, 1999; *Esper et al.*, 2002], borehole temperature estimates [*Dahl-Jensen et al.*, 1998; *Huang et al.*, 2000], inferred temperatures from tropical and subtropical ice cores [*Thompson*, 1995], and glacial moraines in North America [*Denton and Karlén*, 1973] and New Zealand [*Chinn*, 1996] indicate the LIA was a hemispheric and perhaps global phenomenon.

[9] Several lines of evidence from marine sediments and coral records show that the surface North Atlantic was subject to centennial- and millennial-scale climate variability during the late Holocene culminating in the widespread effects of the Little Ice Age. Using planktonic foraminiferal $\delta^{18}O$, *Keigwin* [1996] estimated that SSTs in the Sargasso Sea during the Little Ice Age (LIA; ~50–450 years BP) were ~1°C cooler than today, while SSTs at 1000 years BP were ~1°C warmer. In the eastern part of the subtropical gyre, *deMenocal et al.* [2000] found a cooling of nearly 4°C during the LIA using foraminiferal-based faunal estimates of SST. In both locations, the LIA is preceded by relatively a warm interval, or so-called "medieval Warm Period" from roughly 700 to 1500 BP. The larger SST response in the eastern gyre is likely due to its proximity to the west African coast and greater sensitivity to wind-driven changes in upwelling. At the western edge of the gyre, corals from the Florida Keys and Puerto Rico experienced cooling of 1–3°C relative to today during the coldest intervals of the LIA [*Druffel*, 1982; *Winter et al.*, 2000].

[10] In the subpolar North Atlantic the pattern is more complicated. While *Keigwin and Pickart* [1999] have shown that LIA sediments south of Newfoundland contained lower concentrations of left coiling *N. pachyderma*, which would indicate local warming, *Bond et al.* [2001] observed increased flux of ice rafted debris (IRD) and the presence of colder-water fossils in the subpolar North Atlantic, consistent with generally colder conditions. *Keigwin and Pickart* [1999] likened the LIA to a prolonged negative phase of the NAO, but *deMenocal et al.* [2000] noted that cooling across the subtropical gyre during the LIA is unlike the NAO pattern. *Bond et al.* [2001] argued that episodic IRD events and cooling in the North Atlantic are tied to changes in the production rate of atmospheric ^{14}C and ^{10}Be, and proposed a link between solar irradiance, ocean circulation and climate on millennial timescales.

[11] Despite abundant historical and paleoclimatic evidence, there remain substantial gaps in our knowledge of the magnitude, timing, and spatial patterns of observed temperature anomalies during the late Holocene. As a result, there is no consensus on the mechanisms of climate change during this time. Fluctuations in solar output [*Eddy*, 1976; *Lean and Rind*, 1999; *Bond et al.*, 2001], volcanic activity [*Crowley*, 2000], North Atlantic Deep Water formation [*Bianchi and McCave*, 1999; *Keigwin and Boyle*, 2000; *Bond et al.*, 2001; *Oppo et al.*, 2003], the frequency of the El Niño Southern Oscillation [*Haug et al.*, 2001; *Cobb et al.*, 2003] and the North Atlantic Oscillation [*Keigwin*, 1996; *Keigwin and Pickart*, 1999], are all cited as possible causes of or contributors to Holocene climate variability. In this paper, our aim is to firmly establish the pattern and timing of surface density variations in the Florida Straits during the past 5000 years. With this information in hand, we hope to determine whether variations in NADW formation or shifts in NAO phase, two mechanisms that directly influence the Florida Current, may have contributed to events such as the Little Ice Age.

3. Methods and Materials

[12] The three sediment cores used for this study, W167-79GGC (530 m depth; 24°21.5′N, 83°20.9′W), KNR166-2-62MC-A (547 m depth; 24°19.6′N, 83°15.4′W), and C166A-8GGC (435 m depth; 24°23.1′N, 83°20.3′W) were raised from the Florida continental slope in an area of high sediment accumulation south of Dry Tortugas (Figure 1). Core samples were taken at intervals of 0.5 cm for 79GGC, 0.5 cm for 62MC, and 2 cm for 8GGC, equivalent to an average sample spacing of 21, 16, and 35 years, respectively (see next section). Planktonic foraminifera are abundant in each core, allowing for multiple replicate measurements at each stratigraphic level. For a typical sample, we used 10 *G. ruber* tests (white; 212–250 μm size fraction) per stable isotopic analysis, and measured four replicate analyses at each depth. Prior to analysis, we briefly sonicated each sample in methanol to remove detrital material from the foraminiferal shells.

[13] Isotopic samples from 79GGC and 8GGC were analyzed using a Finnigan MAT 252 coupled to a Kiel II automated carbonate device following the procedure outlined in the work of *Ostermann and Curry* [2000]. Calibration to VPDB scale was made using NBS-19 ($\delta^{18}O$ = −2.20‰ and $\delta^{13}C$ = 1.95‰). Long-term reproducibility (1σ) of NBS-19 (n > 2200) for this mass spectrometer system is ±0.07‰ for $\delta^{18}O$ and ±0.03‰ for $\delta^{13}C$ [*Ostermann and Curry*, 2000]. Samples from 62MC were run on a new Finnigan MAT 253 coupled to a Kiel III carbonate device. Replicate analyses of NBS-19 (n = 133) on this mass spectrometer yield a comparable analytical precision of ±0.08‰ for $\delta^{18}O$ and ±0.02‰ for $\delta^{13}C$.

4. Age Models

[14] The age model for W167-79GGC is based on 14 radiocarbon dates, the age model for C166A-8GGC has

Table 1. Radiocarbon Ages for W167-79GGC, C166A-8GGC, and KNR166-2-62MC-A[a]

Depth Range, cm	^{14}C Age, years	Error, years	Calendar Age, years BP	Model Age, years	Species
		W167-79GGC			
0–1	765	95	424	N/A	*G. sacculifer*
0–1	350	40	0	0	*G. ruber*
4–5	440	35	40	N/A	*G. sacculifer*
8–9	995	30	560	560	*G. sacculifer*
20–21	1270	25	796	796	*G. sacculifer*
31–31.5	1730	45	1278	1278	*G. sacculifer*
40.5–41	1870	30	1403	1403	*G. sacculifer*
54.5–55	2560	35	2272	2272	*G. sacculifer*
69–70	2800	35	2530	2530	*G. sacculifer*
84–84.5	3010	30	2759	2759	*G. sacculifer*
99–100	3470	30	3348	3348	*G. sacculifer*
114–115	4190	40	4266	4266	*G. sacculifer*
127–128	4810	45	5049	5210	*G. ruber*
127–128	5030	50	5371	5210	*G. sacculifer*
		C166A-8GGC			
0–1	155	30	0	0	*G. ruber*
1.5–2.5	465	40	60	60	*G. sacculifer*
26.5–27.5	795	35	447	504	*G. ruber*
26.5–27.5	995	35	560	504	*G. sacculifer*
38.5–39.5	1810	40	1338	N/A	*G. ruber*
38.5–39.5	1390	35	928	928	*G. sacculifer*
58.5–59.5	1690	120	1254	1254	*G. ruber*
58.5–59.5	1130	35	667	N/A	*G. sacculifer*
96.5–97.5	2370	40	1984	1913	*G. ruber*
96.5–97.5	2240	60	1842	1913	*G. sacculifer*
150.5–151.5	2920	35	2713	2849	*G. ruber*
150.5–151.5	3200	40	2985	2849	*G. sacculifer*
		KNR166-2-62MC-A			
0–1	>mod	N/A	post-1950 A.D.	0	*G. ruber*
29–29.5	1420	35	955	955	*G. ruber*

[a]We converted our raw ^{14}C values to calendar ages using CALIB 4.3 [*Stuiver et al.*, 1998] and a reservoir age of 400 years. See text for age model construction details.

12, and KNR166-2-62MC-A has two (see Table 1). The dates are based on either *Globigerinoides sacculifer* or *Globigerinoides ruber* from the >250 μm size fraction. In each case, the raw radiocarbon values were corrected for a 400-year reservoir effect and then converted to calendar ages using CALIB 4.3 [*Stuiver et al.*, 1998]. In some cases, analyses of *G. ruber* and *G. sacculifer* in the same core and at the same depth reveal age offsets of up to several hundred years, with no consistent pattern. For the gravity cores, we used the *G. ruber* values for the core top datum since the raw ^{14}C values of <400 years imply the presence of radiocarbon from nuclear testing, and hence a near-modern age. For the multicore 62MC the fraction of modern ^{14}C in the core top exceeds one, indicating an age younger than 1950 A.D. For each of the cores discussed here, the core top calendar age is assumed to be 0 cal (calendar) years BP, but this assumption is strongest for 62MC.

[15] Down core age control points in 79GGC are based on the *G. sacculifer* values, except the core bottom age, which is an average from both *G. sacculifer* and *G. ruber*. We omitted a ^{14}C measurement at 4.5 cm from the age model as it would require a sedimentation rate of >110 cm kyr^{-1} near the core top, an unrealistic value considering the average sedimentation rate of ~24 cm kyr^{-1} for 79GGC. Down core values for 8GGC at 27, 97, and 151 cm are two-species averages. The age control points for 8GGC are less certain at 39 and 59 cm, given the apparent age reversal in this range. Here we chose dates most consistent with the average sedimentation rate (53 cm kyr^{-1}); 928 years at 39 cm (*G. sacculifer*) and 1254 years at 59 cm (*G. ruber*).

5. The $\delta^{18}O$ Results

[16] Average values of *G. ruber* $\delta^{18}O$ at each stratigraphic depth reveal long-term trends in surface density in the three cores. In 79GGC, $\delta^{18}O$ values are highest (coldest temperatures and/or highest salinity) at approximately 200 years BP, 2000 years BP, and prior to 4000 years BP (Figure 2a). The lowest values of the entire record occur between approximately 2500 to 3500 years before present. In 8GGC, high $\delta^{18}O$ intervals are centered at 200 and 2000 years BP (Figure 2b), at about the same timing as events in 79GGC. In 8GGC, *G. ruber* $\delta^{18}O$ is lowest from ~1000 to 1700 years BP and prior to 2700 years BP. In 62MC, the shortest of the three records, there is an interval of high $\delta^{18}O$ centered at about 200 years BP (Figure 2c), similar to the nearby gravity cores

[17] At first glance, the scatter of *G. ruber* $\delta^{18}O$ values in each core appears to be unusually large, but much of the variance results from seasonal changes in the *G. ruber* population and our isotopic sampling and measurement strategy. Using time series of estimated monthly sea surface

temperature and climatological salinity at 24°N, 83°W [*Levitus et al.*, 1994], we calculated the seasonal $\delta^{18}O_{calcite}$ signal using a $\delta^{18}O$/SST relationship of 0.22‰/°C [*Epstein et al.*, 1953] and $\delta^{18}O$/salinity slope of 0.11‰/psu [*Fairbanks et al.*, 1992]. Since the annual changes in surface salinity are small compared to SST, the $\delta^{18}O$ variability is due primarily due to temperature. To simulate our sampling strategy, we sampled the calculated $\delta^{18}O_{calcite}$ time series randomly 10 times and took the average to simulate one $\delta^{18}O$ analysis of 10 *G. ruber* individuals. The calculated standard deviation of the resulting mean values is ±0.15‰ (σ_s, n = 10,000). Combining this with a mass spectrometer analytical error of ±0.08‰ (σ_m), we should expect a standard deviation for real measurements of ±0.17‰ ($\sigma^2 = \sigma_s^2 + \sigma_m^2$; *Killingley et al.* [1981]).

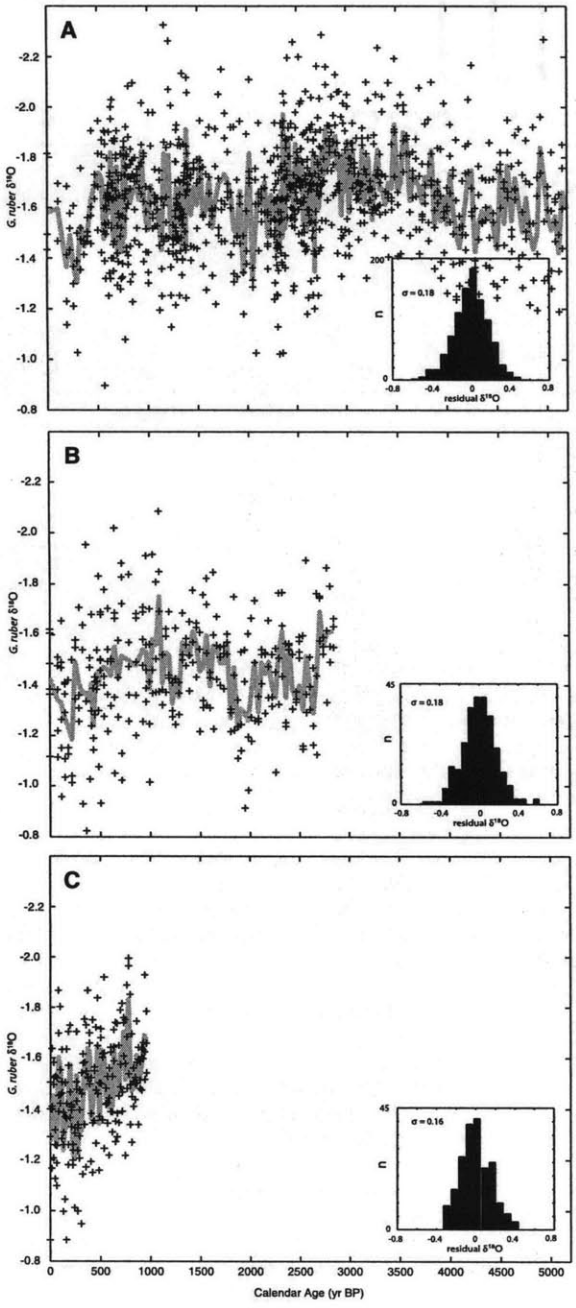

Figure 2. (a) Individual *G. ruber* $\delta^{18}O$ analyses for 79GGC (pluses) and average values at each depth (gray line). Intervals of heavy average $\delta^{18}O$ occur at approximately 200 years BP, 2000 years BP, and prior to 4000 years BP. Inset is the histogram for residual $\delta^{18}O$ values; residuals were calculated by subtracting the mean value at each depth from each $\delta^{18}O$ analysis. The distribution is approximately normal with a standard deviation of 0.18‰. (b) Same as previous, except for 8GGC. Intervals of heavy $\delta^{18}O$ occur at approximately 200 and 2000 years BP. Note the smaller number of samples relative to 79GGC and that mean $\delta^{18}O$ for 8GGC is ~0.2‰ heavier than for 79GGC. The standard deviation of $\delta^{18}O$ residuals is equal in the two cores. (c) Same as previous, except for 62MC. The highest average $\delta^{18}O$ occurred at approximately 200 years BP. The standard deviation of 0.16‰ for residual values is similar to that in 8GGC and 79GGC.

[18] The expected variance is almost identical to the values we observe: for 79GGC and 8GGC the 1σ standard deviation of residual $\delta^{18}O$ values is 0.18‰ (Figures 2a and 2b), while for 62MC the 1σ standard deviation of residuals is 0.16‰ (Figure 2c). We used residual values (individual $\delta^{18}O$ measurement minus the mean at each sampling depth) to ensure the calculated variance is independent of the mean climate state. In comparison to the predicted values, the variance in each core is not unusual, but what should be expected given the seasonal range in temperature and the likelihood that *G. ruber* is present at these sites year-round. Sediment trap studies [*Deuser*, 1987] and plankton tow data [*Williams et al.*, 1979] from the Sargasso Sea near Bermuda indicate year-round production of *G. ruber* (white) over an annual range of sea surface temperatures (20–28°C), comparable to that observed at our core sites in the Florida Straits (24–30°C).

[19] In each core, there are several one point excursions of depth-averaged $\delta^{18}O$ in excess of 0.3‰ (Figure 2). Many of the extreme $\delta^{18}O$ values probably can be explained by a disproportionate sampling of *G. ruber* individuals that calcified during the summer or winter months. To capture the mean $\delta^{18}O$ value in a sample with a precision approaching the limitations of the mass spectrometer requires approximately 200 individual *G. ruber* specimens, either with 200 individuals in one sample or with 20 samples of 10 individuals each. We accomplish the latter by smoothing with a 100 year moving average to group samples and calculate a stable mean $\delta^{18}O$ value (Figure 3). While making multiple measurements is more labor intensive than grouping samples together for a single analysis, the larger number of analyses reduces the standard error and the width of the confidence limits for each mean value.

[20] The confidence limits allow for quantitative evaluation of the difference between $\delta^{18}O$ values in various parts

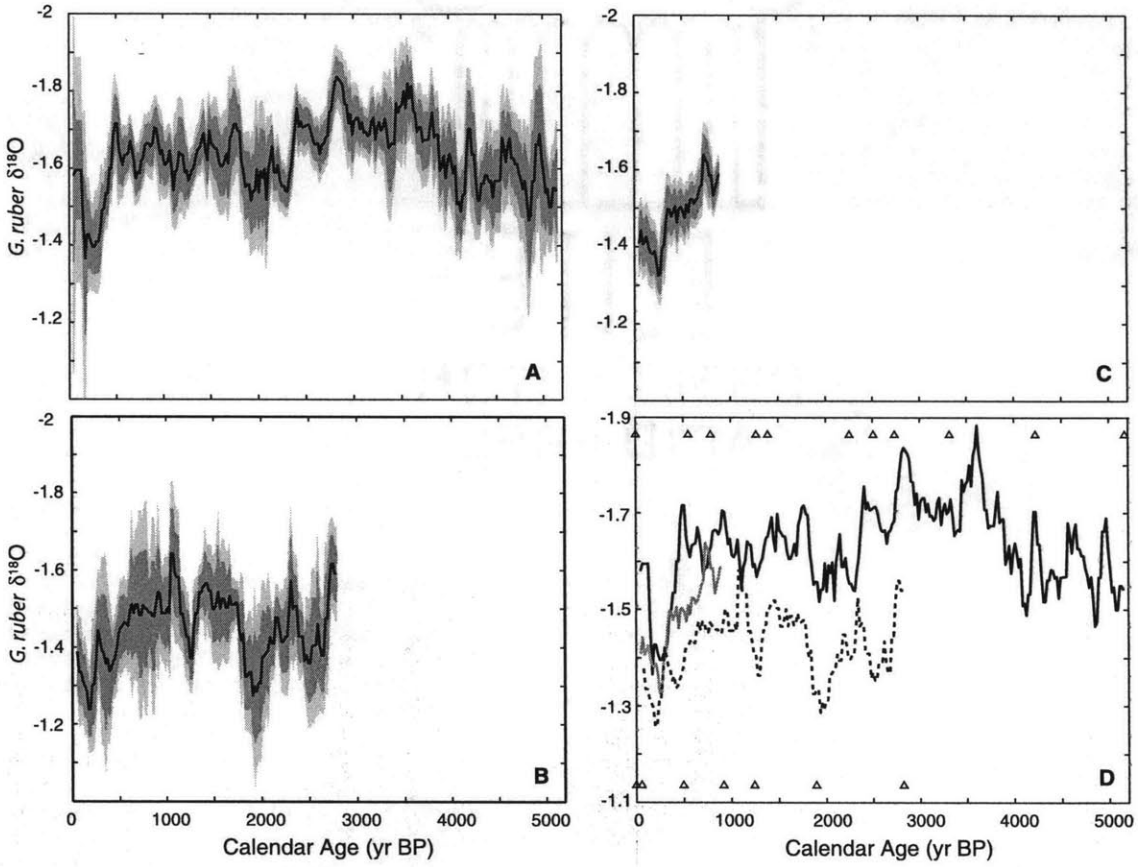

Figure 3. (a) One hundred year running mean *G. ruber* $\delta^{18}O$ for 79GGC, (b) 8GGC, and (c) 62MC. Mean values are represented by the black line. The 95% (light gray) and 80% (dark gray) confidence intervals were calculated using a t distribution. There are three periods of heavy $\delta^{18}O$ in 79GGC from ~100–400 years BP, ~1800–2300 years BP, and prior to 4000 years BP. (d) One hundred year running mean time series for all three cores (solid curve, 79 ggc; dashed curve, 8 ggc; gray curve, 62 mc). All three time series record low SST and/or high salinity conditions 200–300 years ago. Here 79GGC and 8GGC indicate an interval of high surface water density about 2000 years ago.

of the time series. For example, at 95% confidence, the mean $\delta^{18}O$ at 250 cal years BP in 79GGC is higher than the mean from ~500–1000 and 1300–1500 years BP; at 80% confidence, it is greater than any mean value between 500 and 1800 years BP (Figure 3a). Similar to the pattern indicated by the simpler depth averaging approach, there are three primary intervals of high $\delta^{18}O$ centered at 200 years BP, 2000 years BP, and prior to 4000 years BP. The 100-year moving average $\delta^{18}O$ for 8GGC is broadly similar to 79GGC, though it differs in detail. Using the 80% confidence interval as a guide, high $\delta^{18}O$ near 200 and 2000 years BP also occur in 8GGC (Figure 3b). At 95% confidence, however, the mean of the 200 years BP event is only greater than intervals from ~1000–1200, 1400–1500, and 1700–1800 years BP.

[21] The wider confidence limits in 8GGC relative 79GGC are due primarily to differences in sampling density: from 0–2850 years BP in 79GGC there are 613 $\delta^{18}O$ analyses, while in 8GGC there are 282. In contrast, the number of measurements in 62MC is comparable to the number in 79GGC from 0–1000 years BP (198 and 170, respectively). Similar to 79GGC, the $\delta^{18}O$ value at ~250 years BP in 62MC is significantly heavier than the mean $\delta^{18}O$ prior to 500 years BP, based on the 95% confidence interval (95% confidence interval (CI); Figure 3c). For both 79GGC and 62MC, the change in mean $\delta^{18}O$ from 1000 years BP to 250 years BP is 0.2–0.3‰ (95% CI). Since 250 years BP, $\delta^{18}O$ decreased 0.2‰ in 79GGC and 0.1‰ in 62MC (80% CI). In 8GGC, the $\delta^{18}O$ decrease in this time period of 0.1‰ is not significant at 80% confidence.

5.1. Surface Density Over Past 1000 Years

[22] Cores 79GGC and 62MC have high sampling density, exhibit similar changes in $\delta^{18}O$, and seem to provide a consistent picture of surface water $\delta^{18}O$ during the past 1000 years. Each core records a $\delta^{18}O$ increase of 0.2–0.3‰

from 1000 to 250 years BP, which if entirely due to temperature, is equivalent to a 1–1.5°C SST cooling. Similarly, a $\delta^{18}O$ decrease of 0.1–0.2‰ since 250 years BP may represent an SST warming of 0.5–1.0°C. If due to salinity, the $\delta^{18}O$ changes would require variability of 1–2 psu, assuming a $\delta^{18}O$/salinity relationship of 0.1–0.2‰/psu [*Fairbanks et al.*, 1992]. While on a seasonal basis salinity plays a minor role in controlling surface water $\delta^{18}O$, we cannot rule out longer term changes in salinity at these sites. Mg/Ca measurements in corals near Puerto Rico indicate that SSTs from 1987–1993 A.D. were 2 ± 1°C warmer than those from 1699–1703 A.D. [*Watanabe et al*, 2001], similar to the temperature change estimated from Sr/Ca in sclerosponges near Jamaica [*Haase-Schramm et al.*, 2003]. This shift is larger than implied by the $\delta^{18}O$ on the Florida Margin, but the discrepancy may be due to the lower resolution and bioturbation of the sediment records. Alternatively, lower salinity in the Florida Straits during the LIA may have masked changes in SST larger than those implied by planktonic $\delta^{18}O$.

[23] Changes in surface water pH may also influence the Florida Current $\delta^{18}O$. As pH increases, the primary form of dissolved inorganic carbon (DIC) in seawater shifts from bicarbonate to carbonate ion. Given that the carbonate ion is the isotopically lighter of the two species, the oxygen isotopic composition of DIC becomes lighter with increasing pH [*Zeebe*, 1999]. Theoretical considerations [*Zeebe*, 1999] and culturing experiments for *O. universa* [*Spero et al.*, 1997] yield a slope for $\delta^{18}O$ versus $[CO_3^{2-}]$ of ~0.002‰/(μmol kg^{-1}). Planktonic $\delta^{18}O$ during the Last Glacial Maximum may have decreased by up to 0.2‰ due lower atmospheric CO_2 and increased seawater $[CO_3^{2-}]$ [*Spero et al.*, 1997]. While we cannot rule out changes in $\delta^{18}O$ due to variable alkalinity, changes in atmospheric CO_2 during the Late Holocene have been small, on the order of 10 ppm [*Indermühle et al.*, 1999]. LGM-scale changes in CO_2 have occurred, but only in the past 200 years [*Etheridge et al.*, 1996], well after the observed increase in Florida Current planktonic $\delta^{18}O$ during the Little Ice Age.

[24] Prior to the LIA, *G. ruber* $\delta^{18}O$ indicates that Florida Current surface density was lower than core top values, which for 62MC are post-1950 AD, as well as lower than values calculated from modern hydrographic measurements. We calculated the $\delta^{18}O$ of calcite precipitated in equilibrium with modern surface waters ($\delta^{18}O_c$) by first determining $\delta^{18}O$ of water ($\delta^{18}O_w$) from annual average salinity and the regional relationship between $\delta^{18}O_w$ and salinity [*Lynch-Stieglitz et al.*, 1999]. We then determined $\delta^{18}O_c$ using annual average sea surface temperature and the empirical relationship between $\delta^{18}O_c$ and SST [e.g., *Kim and O'Neil*, 1997]. The predicted value for $\delta^{18}O_c$ is −1.5‰, indistinguishable from the core top values of −1.4 ± 0.1‰ (62MC), −1.6 ± 0.3‰ (79GGC) and −1 4 ± 0.2‰ (8GGC) (Figure 3). Of the three cores, the multicore provides the best estimate of modern $\delta^{18}O$, given its post-1950 A.D. core top age and relatively small uncertainty.

[25] *G. ruber* $\delta^{18}O$ is offset from equilibrium $\delta^{18}O_c$ by approximately −0.2‰ [*Fairbanks et al.*, 1982; *Curry et al.*, 1983; *Deuser*, 1987]. If we add 0.2‰ to the data to reflect this disequilibrium, then the core top value for 62MC would be 0.3‰ greater than $\delta^{18}O_c$ determined using modern hydrographic observations. Six years of sediment trap data from the Sargasso Sea indicate that seasonal changes in shell flux have little effect on annual average *G. ruber* $\delta^{18}O$ [*Deuser*, 1987], so the difference between the core top value and modern hydrography is unlikely to be caused by seasonal differences in productivity. If the seasonal pattern of *G. ruber* flux in the Florida Straits is similar to the Sargasso Sea, then the core top values may reflect real temperature and salinity differences from modern observations.

[26] Bioturbation makes the comparison of core top values to modern data difficult, but down core planktonic $\delta^{18}O$ can be evaluated relative to the 62MC core top. *G. ruber* $\delta^{18}O$ implies that hydrographic conditions at the location of 62MC prior to 500 years BP were warmer or less salty than post-1950 A. D. *G. ruber* ^{18}O in 79GGC from 500 to 2000 years BP (−1.65‰) and 2800 to 3500 years BP (−1.75‰) are also depleted relative to the 62MC core top value. This may reflect the SST gradients in this region as opposed to variations in $\delta^{18}O$ with time, however. Over the past 1000 years, the average 62MC $\delta^{18}O$ value is −1.45‰, compared to −1.55‰ for 79GGC.

5.2. Differences Between 8GGC and 79GGC

[27] Although down core variations in 79GGC and 8GGC mean $\delta^{18}O$ are similar, the absolute values in 8GGC are on average 0.15‰ greater than in 79GGC (Figure 3d). We believe the most likely explanation for this difference is the SST gradient between the coring sites. Maps of satellite-based SST estimates show a steep meridional SST gradient in this region during fall, winter, and spring, with temperature shifts of up to 5°C over only a few kilometers (Figure 1). Core 8GGC, located approximately 3 km north of 79GGC, likely has heavier $\delta^{18}O$ because it tends to experience cooler SSTs. The offset between 8GGC and 79GGC may have changed over the past 3000 years, but this difference is highly sensitive to uncertainty in the age model for each core.

5.3. Spectral Characteristics

[28] While the 79GGC and 8GGC $\delta^{18}O$ time series are similar to the eye, they are quite different in the frequency domain. We analyzed the depth-averaged (unsmoothed) $\delta^{18}O$ data (Figure 2) using multitaper spectral analysis [*Thomson*, 1982]. Each time series was linearly detrended and then interpolated using a constant sampling interval consistent with the mean time resolution of our $\delta^{18}O$ records (20 years for 79GGC and 35 years for 8GGC). The resulting spectral estimates were combined using the adaptive weighting scheme proposed by *Thomson* [1982]. A simple averaging of the spectra produces a similar result. The multitaper spectrum for 79GGC (Figure 4a) suggests periodic components in *G. ruber* $\delta^{18}O$ near 360, 190, 130, 100, and 80 years. In 8GGC, there appears to be a spectral peak at 130 years (Figure 4c). In both cores, similar features were observed using a hamming data taper and periodogram.

[29] The results of spectral analysis for any given core are highly sensitive to the age model employed. This is

particularly true for centennial-scale variability since age model errors are similar in magnitude to the derived periodic components. To test the robustness of the spectra, we created alternate age models for 8GGC and 79GGC using cubic spline rather than linear interpolation. In each case, the age model was forced to pass through the same radiocarbon control points, but abrupt changes in sedimentation rate were minimized by the spline model. While this option is not necessarily an improvement over the linear interpolation approach, it is equally plausible and demonstrates how age model uncertainty can affect the power spectrum.

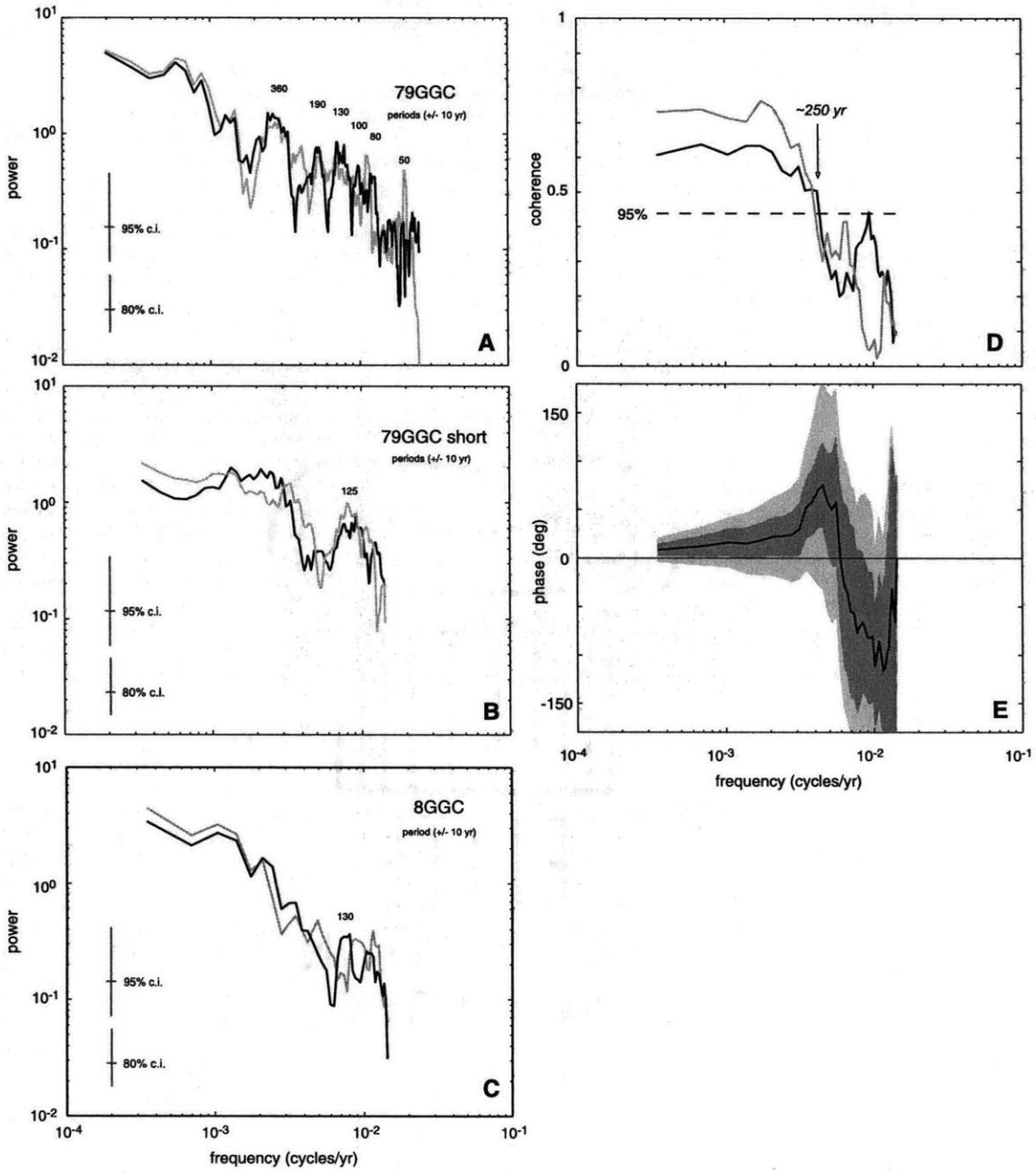

Figure 4

[30] On centennial timescales, the power spectra for the spline-based time series differ from those based on linear interpolation age models. The alternative 79GGC spectrum has peaks at periods of 360, 90, and 50 years (Figure 4a, gray curve). While there is power near 190 and 130 years, at neither period does it exceed the 95% confidence limit. The alternative spectrum for 8GGC appears to have one peak near 1/110 years, but it is not significant at the 80% level (Figure 4c). Only power at 1/360 years in 79GGC is a robust feature and it may represent a true periodic component in late Holocene planktonic $\delta^{18}O$ at this location. A complete analysis of the effects of dating uncertainty on spectral components would also take into account error in the ^{14}C control points. As such, the spline-based example given here provides a relatively optimistic view of spectral variability due to age model uncertainty.

[31] The interval from 0–2850 years in 79GGC has different spectral properties than the entire 5200-year record (Figure 4b). For both the linear and spline age models, there is a concentration of power at ~1/125 years and a broad peak between 1/1000 and 1/250 years. Cores 79GGC and 8GGC display coherent behavior at frequencies lower than ~1/250 years (Figure 4d). Nearly 35% of the coherence estimates exceed the 95% confidence level, all at low frequencies. Since neither core on its own exhibits obvious low-frequency periodic behavior, the coherence is a function of nonperiodic components in each time series. A similar result is found for the spline-based approach. Uncertainty in the radiocarbon-based chronologies and aliasing of the seasonal SST cycle make it difficult to estimate coherence at frequencies higher than 1/250 years.

[32] Low frequency changes in 79GGC $\delta^{18}O$ lead those in 8GGC by 30–50 years (Figure 5e). This could be a function of either age model error or different depth habitats for *G. ruber* and *G. sacculifer*. Each age model has ^{14}C tie point uncertainty due to analytical error (average ~50 years; Table 1), unknown changes in ^{14}C reservoir age, and bioturbation of foraminifera from adjacent depths. Ages between tie points have additional uncertainty due to variable sedimentation rate. While any one of these factors could account for a 50 year difference in the timing of similar $\delta^{18}O$ excursions in the two cores, it seems unlikely that age model uncertainty would produce a consistent offset across multiple frequencies. If *G. sacculifer* secretes more of its calcite in deeper, older water than *G. ruber* [*Duplessy et al.*, 1981], then the predominantly *G. sacculifer*-based age model for 79GGC would tend to be older than the 8GGC age model, similar to the phase relationship we observe (Figure 4e).

6. Discussion

6.1. Regional Ocean Dynamics

[33] A key question is whether the variability in the $\delta^{18}O$ records is representative of the Florida Current as a whole or due to the regional behavior of the Loop Current (LC) and Tortugas eddy system. Today, sea surface temperature at the core locations decreases due to the episodic formation of Tortugas eddies, which occur when the LC penetrates into the eastern Gulf of Mexico. When the LC retreats, water flows directly from the Yucatan Channel to the Straits of Florida, and Tortugas eddies fail to materialize (*Lee et al.* [1995]; see also http://e450.colorado.edu/realtime/gom_overlay/). As a result, the axis of the Florida Current shifts northward, and SST at the core sites increases (see http://fermi.jhuapl.edu/avhrr/gm/averages/index.html).

[34] While we cannot rule out that long-term shifts in the frequency of Tortugas eddy formation influenced our $\delta^{18}O$ records, instrumental data imply this process is an instability in the LC-Florida Current system unrelated to any obvious climate forcing. Northward penetration of the LC, a precursor to Tortugas eddy formation, lacks a clear seasonal signal and appears to be unrelated to Florida Current transport [*Maul and Vukovich*, 1993]. The shedding of anticyclonic rings from the LC, which occurs when the LC is well developed, also seems to be aperiodic [*Vukovich*, 1988; *Sturges and Leben*, 2000]. Potential vorticity flux through the Yucatan Channel may be an important control on LC development [*Candela et al.*, 2002], but it is unclear how climate variability would affect this flux. If Tortugas eddy formation is sensitive to changes in climate, our time series would indicate greater frequency of eddy formation, and

Figure 4. (a) Multitaper spectra for 79GGC. We calculated the spectrum for the 79GGC time series using two different age models, one using linear interpolation (dark line), and the other spline-based interpolation (gray line). In each case we used five discrete prolate spheroidal (Slepian) sequences with a time bandwidth product of 3 to window the data. For the linear age model, there are concentrations of power at periods 360, 190, 130, 100, and 80 years. The spline model yields different results, with the peaks near 360, 90, and 50 years. Confidence intervals are given by the vertical bars. (b) Multitaper spectra for 79GGC, 0–2850 years. The spectrum for each age model option indicates power near 1/125 years, significantly different than the spectra based on the longer time series. For the linear model, there is a broad spectral peak centered at 1/500 years. (c) Multitaper spectra for 8GGC. Only the linear age model yielded a significant peak, at 130 years. (d) Coherence for 79GGC and 8GGC (black curve, linear age model; gray curve, spline age model). Coherence was estimated using the multitaper window method with 15 windows and a time bandwidth product of 8. The MATLAB code used to estimate coherence and phase was provided by P. Huybers (http://web.mit.edu/~phuybers/www/Mfiles/index.html). The zero coherence level (horizontal dashed line; 95% confidence) indicates the two cores are coherent at frequencies lower than ~1/250 years. The lack of coherence at higher frequencies is likely a result of age model uncertainty. (e) Phase estimate for 79GGC and 8GGC. Across the low frequencies, 79GGC consistently leads 8GGC by 30–50 years. This offset is most likely related to the different foraminiferal species used for radiocarbon analyses to develop each age model (see text for details). Uncertainty in the phase estimate was determined using a Monte Carlo-based approach. The 95% and 80% confidence intervals are represented by the light gray and dark gray areas, respectively.

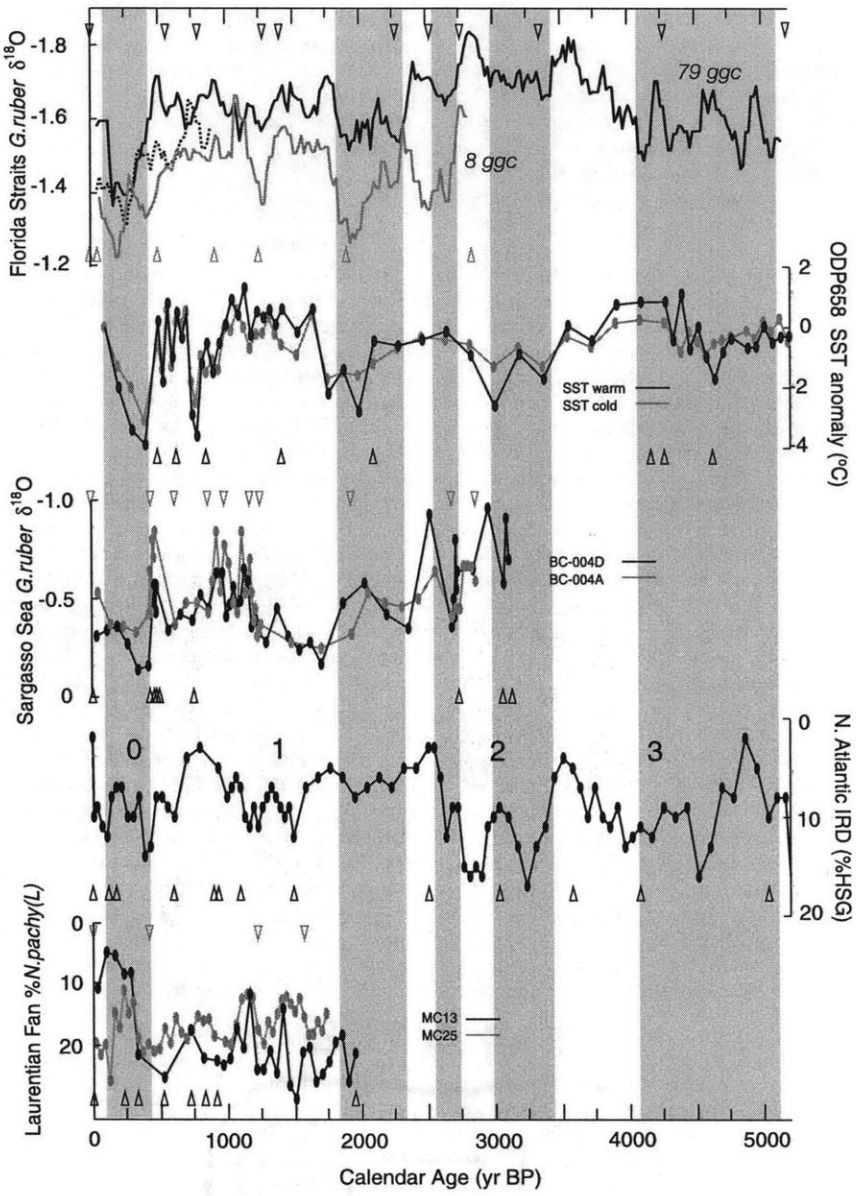

Figure 5. Comparison of the Florida Current $\delta^{18}O$ time series to paleoceanographic records from off the coast of west Africa (Site 658C; *deMenocal et al.* [2000]), the Sargasso Sea [*Keigwin*, 1996], the subpolar North Atlantic [*Bond et al.*, 2001], and south of Newfoundland [*Keigwin and Pickart*, 1999]. The vertical gray bars indicate intervals of generally heavy $\delta^{18}O$ in the Florida Current. Calendar ages for each time series are denoted with triangles. During the LIA, heavy $\delta^{18}O$ in 79GGC, 8GGC, and 62MC corresponds to enriched ^{18}O in the Sargasso Sea, SST cooling at Site 658C, increased ice-rafted debris (IRD) in the subpolar North Atlantic, and apparent warming (low % *N. pachyderma* (s.)) south of Newfoundland. The relative timing of earlier events is less clear, although high $\delta^{18}O$ in the Florida Straits generally corresponds to negative SST anomalies off the coast of west Africa.

presumably LC penetration, during intervals of high $\delta^{18}O$. Given the apparently stochastic nature of Tortugas eddy formation, however, we assume that their presence has little effect on mean Florida Current $\delta^{18}O$ on centennial and longer timescales.

6.2. North Atlantic Subtropical Gyre

[35] The $\delta^{18}O$ time series indicate the surface waters of the Florida Straits were cooler and/or more saline from approximately 50 to 400 cal years BP compared to today. This interval coincides very closely to the timing of the Little Ice Age observed in a variety of historical and paleoclimatic records. Similarly, a relatively warm and/or less saline interval from 450 to 1800 cal years BP encompasses the Medieval Warm Period. Several paleoceanographic records in the North Atlantic subtropical gyre are consistent with an SST cooling during the Little Ice Age (Figure 5). High $\delta^{18}O$ in the Florida Margin cores coincides with high $\delta^{18}O$ in the northwestern Sargasso Sea [*Keigwin*, 1996] and faunal-based estimates of SST cooling off the coast of west Africa (Site 658C; *deMenocal et al.* [2000]). At each of these three locations, there is a prominent event that began at approximately 400 years BP. The precise timing is difficult to constrain given age model uncertainty, but the apparent cooling is synchronous within chronological error at these three sites. Preceding this event at the coastal west Africa and Sargasso Sea sites is a similar but smaller amplitude cooling that began around 1000 A.D. This two-stage character of the LIA is not apparent in the Florida margin cores.

[36] At about 1000 years BP, surface water at the three subtropical gyre locations were apparently warmer or less saline than during the Little Ice Age. Prior to 1200 years BP, however, the records are quite different; in the Sargasso Sea, there is an interval of low $\delta^{18}O$ between 1200 and 800 years BP, while low $\delta^{18}O$ at the Florida Margin sites occurs from 1800 to 700 years BP, also an interval of warm SSTs off the coast of west Africa. To make the Sargasso Sea record consistent would require an age model adjustment of approximately 600 years in this interval; either the two Florida margin gravity cores and Site 658 are 600 years too old, the two Sargasso Sea box subcores are 600 years too young, or some combination of the two. This degree of age offset is unlikely to be caused by chronological errors, so it seems likely that the interval of low density in the Florida Current and high SST anomalies off the coast of west Africa began before the apparent warming in the Sargasso Sea.

[37] The timing of events in the subtropical gyre prior to the MWP is less clear, but overall it appears there were similar changes at each site. Intervals of high $\delta^{18}O$ centered at ~2000, 3200, and prior to 4000 cal years BP in the Florida Straits appear to be contemporary with cool SST events off the coast of west Africa (Figure 5). The two intervals of low $\delta^{18}O$ at 2400 and 2800 cal years BP in 79GGC are within dating error of similar excursions in the Sargasso Sea. Low $\delta^{18}O$ in 79GGC at ~2400 and 2800 cal years BP may coincide with the broad warming in site 658C from 2000 to 2800 cal years BP, but site 658C lacks two distinct events. Spectral analysis of site 658C and 79GGC show no significant coherent behavior if the full 5200-year 79GGC record is used, but the two sites are coherent at low frequencies (>1/300 years) if the analysis is limited to the 0–2000 years BP time span. The Sargasso Sea and 79GGC records are coherent between frequencies of ~1/1000 and 1/250 years for the common interval of 0 to 3000 years BP.

6.3. Subpolar North Atlantic

[38] The scope of the middle to late Holocene climate variability extends beyond the subtropical gyre into the subpolar North Atlantic. Marine sedimentary records of ice-rafted debris (IRD) imply that colder, ice-bearing waters episodically advected to the south and east of source regions in the Labrador and Nordic Seas [*Bond et al.*, 2001]. During the LIA, when the age control is robust, low apparent SSTs in the subtropical gyre correspond to IRD event 0, but there is no clear pattern for earlier events (Figure 5). IRD event 1 matches an interval of high $\delta^{18}O$ in the Sargasso Sea but it corresponds to warm SSTs at Site 658C and low $\delta^{18}O$ in the Florida Straits. IRD events 2 and 3 (at about 3000 years BP and 4500 years BP, respectively) overlap with intervals of both low and high $\delta^{18}O$ in the Florida Current. Asynchronous changes in the time domain are consistent with the lack of statistical coherence between Florida Straits $\delta^{18}O$ and subpolar North Atlantic IRD across all frequencies. At this stage it is difficult to determine whether the discrepancies between these records are real and reflect complex ocean-atmosphere dynamics, or an artifact of the age models and proxies used.

6.4. External Forcing

[39] Owing to the correlation of solar and climatic proxies at several sites, variability in late Holocene climate has been attributed in part to variations in solar forcing. Using a simple energy balance model, *Crowley* [2000] found that solar forcing accounts for a maximum of 31% of the temperature variance in the *Mann et al.* [1999] reconstruction from A.D. 1000–1850. Low solar activity inferred from low sunspot numbers during the Maunder Minimum (~1650–1710 A.D.) corresponds to high levels of atmospheric radiocarbon [*Eddy*, 1976], and cold Northern Hemisphere temperatures [*Bradley and Jones*, 1993]. It is estimated that solar irradiance was ~0.25% lower than today during the Maunder Minimum [*Lean et al.*, 1992].

[40] *Rind and Overpeck* [1993] simulated the climatic consequences of a 0.25% reduction in solar irradiance using an atmospheric general circulation model (AGCM). The model results produced a global annual average cooling of ~0.5°C, but the change in surface temperatures was spatially heterogeneous. The greatest cooling occurred over the continents (−1°C), while moderate warming occurred in and to the southeast of the Labrador Sea (+0.5°C). *Shindell et al.* [2001] found similar patterns using an updated AGCM that includes parameterizations of stratospheric ozone response to solar irradiance. Changes in oceanic circulation not included in these simulations may significantly alter the modeled SST patterns.

[41] The spatially variable temperature response of the models to decreased insolation is similar to that observed during the Little Ice Age. While temperatures in the Florida

Current, Sargasso Sea, and off the coast of west Africa all seemed to decrease, SSTs south of Newfoundland increased [*Keigwin and Pickart*, 1999]. The decrease in solar irradiance is also consistent with historical records of continental cooling during the LIA [*Grove*, 1988; *Jones and Bradley*, 1995] and borehole temperature evidence for a cold LIA in Greenland [*Dahl-Jensen et al.*, 1998]. *Shindell et al.* [2001] attributed the regional temperature pattern in their simulation to a shift in climatic conditions toward the low state of the Arctic Oscillation (or negative phase of the North Atlantic Oscillation (NAO)), where onshore flow of warm oceanic air is reduced during winter, generally resulting in cooler continents and warmer oceans in the circum-North Atlantic region. One exception to this pattern is the western subtropical North Atlantic, which cools during the NAO negative phase [*Walter and Graf*, 2002].

[42] If solar forcing played a dominant role in Holocene climate variability, we should find evidence of its influence in Florida Current $\delta^{18}O$. The spectrum for 79GGC has a concentration of power near 1/190 years (Figure 4a) and atmospheric $\Delta^{14}C$ has a well-known spectral peak at 1/200 years (Figure 6a; *Stuiver et al.* [1991]). In addition to 79GGC there are several late Holocene records from the Caribbean/Gulf of Mexico region that exhibit centennial-scale variability. A dominant period of ~200 years in Yucatan Peninsula drought records appears to be coherent with atmospheric $\Delta^{14}C$ [*Hodell et al.*, 2001]. Multiple centennial-scale features also appear in *G. sacculifer* abundance data from the Gulf of Mexico [*Poore et al.*, 2003] and *G. bulloides* abundance data from the Cariaco Basin [*Peterson et al.*, 1991].

[43] Although it is tempting to link Florida Current $\delta^{18}O$ and atmospheric $\Delta^{14}C$ because of their common spectral peak near 1/200 years, the two records are not coherent at this frequency (Figure 6b). Florida Current $\delta^{18}O$ and $\Delta^{14}C_{atm}$ are coherent near 1/100 and 1/50 years, but only if the linear interpolation age model for 79GGC is used. The two records may in fact be coherent in this part of the spectrum, but as is the case with 79GGC and 8GGC (Figure 4d), it appears that $\delta^{18}O$ signal noise and age model error preclude reliable coherence estimates at frequencies higher than 1/250 years. While Florida Current $\delta^{18}O$ and $\Delta^{14}C_{atm}$ lack coherence at timescales typically associated with solar variability, the two records are coherent at frequencies lower than ~1/300 years (Figure 6b). In general, $\delta^{18}O$ and $\Delta^{14}C_{atm}$ are in phase, although uncertainty in the estimate ranges from 10 to 50 degrees in the low frequencies (Figure 6c).

[44] The 79GGC $\delta^{18}O$ spectrum is also coherent at low frequencies with an estimate of Holocene ^{14}C production rate ($^{14}C_{pr}$). *Bond et al.* [2001] used a simple geochemical box model to simulate production rate changes necessary to yield the observed $\Delta^{14}C_{atm}$ signal. Although the $^{14}C_{pr}$ spectrum has a peak near 1/200 years (Figure 6d), it has less power at low frequencies than the linearly detrended $\Delta^{14}C_{atm}$ record (Figure 6a). Florida Current $\delta^{18}O$ and $^{14}C_{pr}$ are coherent at periods between ~300 and 1000 years (Figure 6e), but lack coherence at longer periods. While it appears that changes in $^{14}C_{pr}$ generally lead $\delta^{18}O$ (Figure 6f), the large error in the phase estimate makes it difficult to determine true leads or lags between the two time series.

[45] What climatic mechanism might cause surface density of the Florida Current and atmospheric $^{14}C_{pr}$ to vary together over centennial timescales? One possibility is that low solar irradiance caused ^{14}C production to increase and the surface ocean to cool. *Bond et al.* [2001] argued that centennial-scale increases in ice-rafted debris in the North Atlantic were coherent with high ^{14}C production rate and ice core ^{10}Be, or low apparent solar activity. On the basis of this correlation, the authors concluded that intervals of decreased solar irradiance during the past 12,000 years caused ice-bearing waters from the Labrador and Nordic Seas to more frequently advect to core sites in the northeast Atlantic.

[46] Atmospheric general circulation model results imply that parts of the North Atlantic subtropical gyre may have cooled by up to 1°C during the Maunder Minimum due to a solar irradiance-driven shift toward the NAO negative phase [*Shindell et al.*, 2001]. Although the simulated cooling in the Florida Straits is small (<0.2°C), changes in ocean circulation (which were not included in the AGCM) may have further amplified the cooling signal. Therefore in the frequency band of 1/1000 to 1/300 years, low solar activity (high $^{14}C_{pr}$) could lead to cooling in the Florida Straits and an increase in *G. ruber* $\delta^{18}O$.

6.5. Internal Forcing

[47] Internal climate system dynamics may act independently of solar activity to create Late Holocene climate variability. A prolonged negative phase of the North Atlantic Oscillation (NAO) has been invoked to explain cool SSTs in the Sargasso Sea and warm SSTs south of Newfoundland during the Little Ice Age (Figure 5) [*Keigwin and Pickart*, 1999]. On interannual timescales the negative phase of the NAO is characterized by warming in Greenland and off the coast of west Africa, however, patterns not observed during the LIA [*deMenocal et al.*, 2000]. Yet evaluating centennial-scale climate variability using the analogy of interannual NAO patterns may be misleading. If the climate system is forced toward one state of the NAO for decades or longer, the thermal inertia of the ocean and ocean-atmosphere feedbacks could create significantly different temperature anomalies. For instance, on multidecadal timescales the positive phase of the NAO is associated with warming in the subpolar gyre and cooling in the western subtropical Atlantic, opposite the interannual pattern [*Visbeck et al*, 2003]. This is apparently due to either increased oceanic meridional overturning or advection of warm SST anomalies from the western subtropical Atlantic [*Visbeck et al.*, 2003]. Therefore, if we were to use decadal-scale NAO patterns from observational data as an analogy for the Little Ice Age, the SST pattern during the LIA (warming south of Newfoundland and apparent cooling in the Florida Straits, Sargasso Sea, and off the coast of west Africa) would actually imply a shift toward the NAO positive phase.

[48] Changes in the frequency and magnitude of the El Niño Southern Oscillation may also contribute to Late Holocene climate variability. Coral $\delta^{18}O$ records show a

decreased zonal SST gradient in the equatorial Pacific during the Little Ice Age, possibly related to more frequent El Niño events during this time [*Hendy et al.*, 2002; *Cobb et al.*, 2003]. High-resolution terrestrial rainfall records from both the Yucatan Peninsula and the Cariaco Basin indicate the Little Ice Age represents unusually dry conditions in these two regions. Gastropod $\delta^{18}O$ in lake sediments from the Yucatan Peninsula reveal a greater prevalence of drought during the LIA [*Hodell et al.*, 2001, 2002], consistent with evidence for increased aridity inferred from trace

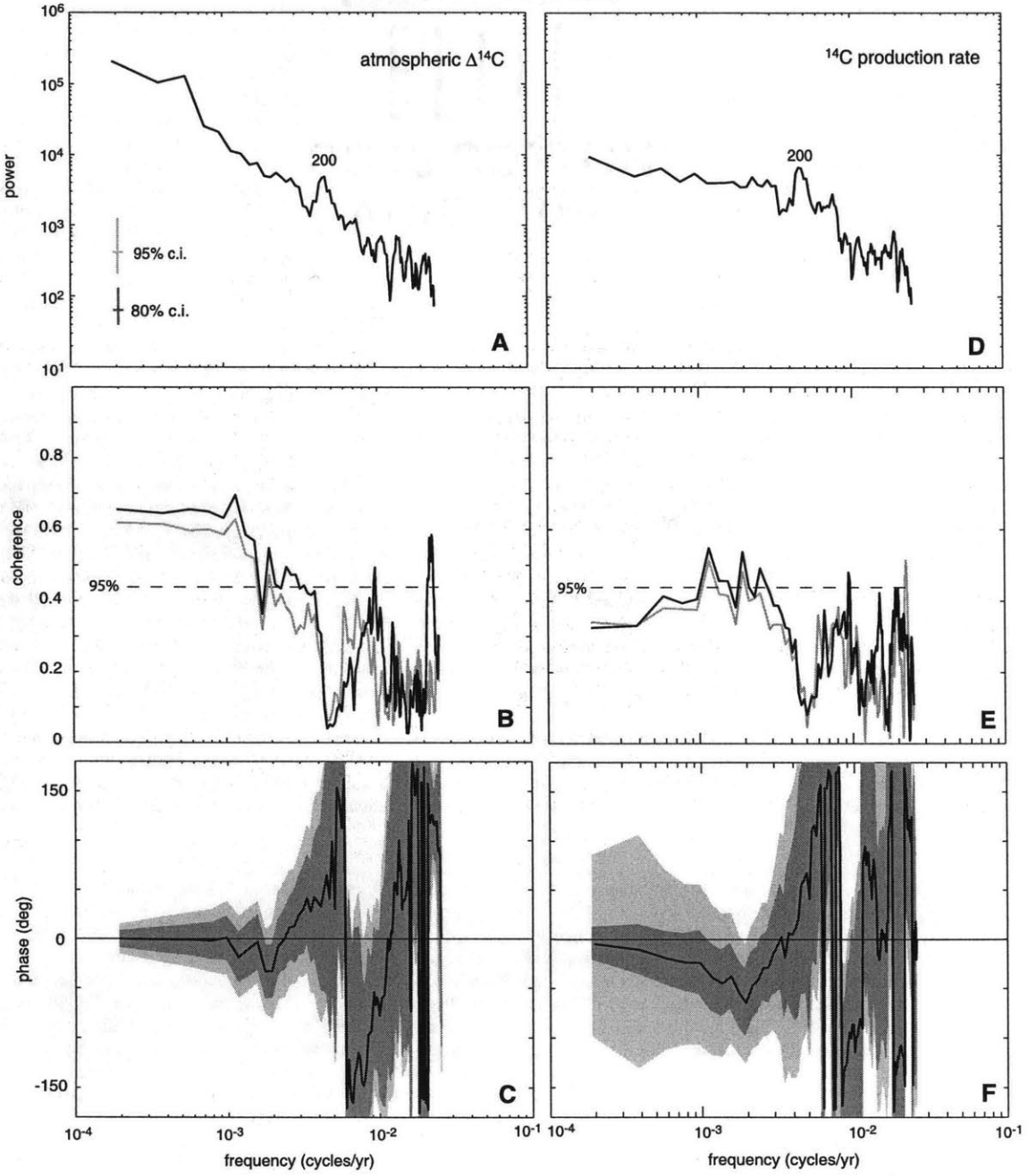

Figure 6

metals in the Cariaco Basin [*Haug et al.*, 2001]. In both cases, the rainfall records imply a southward shift of the intertropical convergence zone (ITCZ) during the LIA, perhaps as a result of a greater meridional temperature gradient in the North Atlantic or El Niño-like conditions in the equatorial Pacific [*Haug et al.*, 2001].

[49] If the Intertropical Convergence Zone shifted southward during the Little Ice Age, it could potentially increase the salinity of Florida Current (FC) surface waters. *Black et al.* [2004] invoke this mechanism as one possible explanation of the increase in Cariaco Basin planktonic $\delta^{18}O$ over the past 2000 years. Given that FC surface water is primarily south and equatorial Atlantic in origin [*Schmitz and Richardson*, 1991], it is not clear that a southward shift in ITCZ position would have a significant influence on FC surface salinity. If evaporation and precipitation patterns were similar to today during the LIA, then decreased Gulf Stream transport, and hence less export of salt from the subtropical gyre, could lead to more saline conditions in the Florida Current.

[50] A reduction in the cross-equatorial flow of warm surface waters which compensate North Atlantic Deep Water (NADW) would likely increase the North Atlantic SST gradient. Model simulations of strongly reduced NADW formation yield large meridional SST gradients in the North Atlantic and widespread cooling throughout the region [e.g., *Manabe and Stouffer*, 1988; *Schiller et al.*, 1997]. There is little direct evidence for a change in deep water production during the LIA, however. Benthic $\delta^{13}C$ data from the Bermuda Rise imply a decrease in the relative contribution of northern source deep waters during the Little Ice Age, but Cd/Ca analyses from the same cores show relatively little change [*Keigwin and Boyle*, 2000]. *Bianchi and McCave* [1999] suggest that sedimentary grain size evidence implies a reduction in Iceland-Scotland Overflow Water during the LIA. Benthic $\delta^{13}C$ data from the subpolar northeastern Atlantic are consistent with reduced NADW flow during some intervals of high ice rafting, implying meridional overturning may vary on millennial timescales during the Holocene [*Oppo et al.*, 2003], but this record ends prior to the LIA.

[51] The coherent and in-phase relationship between the detrended atmospheric $\Delta^{14}C$ and Florida Current $\delta^{18}O$ records at periods >1000 years (Figure 6b) raises the possibility that oceanic circulation influences the behavior of ^{14}C on millennial timescales. The relatively low coherence between ^{14}C production rate and $\delta^{18}O$ at these frequencies (Figure 6e) further implies that solar variability is not a likely driver of the $\delta^{18}O$ signal on longer timescales. Reduced meridional overturning circulation (MOC) may have caused both low SSTs in the subtropical gyre and less sequestration of radiocarbon in the deep ocean (higher $\Delta^{14}C_{atm}$). Model simulations of a shutdown of North Atlantic Deep Water yield SST cooling of ~1°C in the western subtropical gyre [*Manabe and Stouffer*, 1988; *Schiller et al.*, 1997]. While this could account for $\delta^{18}O$ changes in the Florida Current and Sargasso Sea during the LIA, there is no evidence in support of a NADW shutdown at this time. It is possible that the models lack adequate sensitivity to MOC variability or additional mechanisms such as the NAO play a role in amplifying the SST response.

[52] The idea that oceanic circulation had a significant influence on atmospheric $\Delta^{14}C$ during the Holocene is usually discredited due to the similarity of ^{14}C and ^{10}Be records at centennial timescales. *Beer et al.* [1988] simulated atmospheric $\Delta^{14}C$ using the concentration of ^{10}Be in the Camp Century ice core as a proxy for cosmogenic nuclide production. At frequencies higher than 1/1000 years, modeled and observed $\Delta^{14}C$ share approximately 36% of their variance during the late Holocene [*Beer et al*, 1988]. A similar degree of shared variance is found between bandpass filtered records of modeled ^{14}C production rate and ^{10}Be flux from the GRIP and GISPII ice cores [*Bond et al.*, 2001]. *Bard et al.* [2000] were able to closely model the detrended record of atmospheric $\Delta^{14}C$ for the past 1200 years using a ^{10}Be-based estimate of cosmogenic nuclide production from the South Pole. Since ^{14}C and ^{10}Be have different life histories, similar variability in each are most easily attributed to changes in production rate.

[53] On millennial timescales it is less clear that solar variability plays an important role in controlling atmospheric $\Delta^{14}C$. The long-term decrease in Holocene atmospheric $\Delta^{14}C$ is most likely due to increasing strength in the geomagnetic dipole, but offsets of ±20‰ between observed and geomagnetically driven changes in $\Delta^{14}C$ remain unex-

Figure 6. (a) Multitaper spectrum for atmospheric $\Delta^{14}C$, 0–5200 years BP, linearly detrended and sampled at 20-year intervals. The well-documented spectral peak near 1/200 years is apparent. Confidence intervals are given by the vertical bars (95%, gray; 80%, black). (b) Multitaper coherence for 79GGC and atmospheric $\Delta^{14}C$, 0–5200 years BP. Estimates for the 79GGC linear (black) and spline (gray) age model both indicate coherence at frequencies lower than 1/300 years. The linear model also has coherent features at higher frequencies, near 1/100 and 1/45 years, but these are lacking from the spline-based estimate. The 95% confidence limit is given by the horizontal dashed line. (c) Phase for 79GGC and atmospheric $\Delta^{14}C$. At low frequencies the records appear to be in phase. The 95% and 85% confidence limits, based on Monte Carlo simulations, are indicated by the light and dark gray areas, respectively. A similar phase relationship exists for the spline age model (not shown). Both coherence and phase were estimated using the MATLAB routine provided by P. Huybers. (d) Same as Figure 6a, except using the ^{14}C production rate time series from *Bond et al* [2001]. The spectrum also has significant power at 1/200 years but lacks the low-frequency power of $\Delta^{14}C$. (e) Multitaper coherence for 79GGC $\delta^{18}O$ and ^{14}C production rate 0–5200 years BP. Florida Current $\delta^{18}O$ and ^{14}C production rate are coherent at frequencies between ~1/1000 and 1/300 years but lack the lower frequency coherence apparent with $\Delta^{14}C$. (f) Phase for 79GGC $\delta^{18}O$ and radiocarbon production rate. At coherent frequencies, production rate leads $\delta^{18}O$, but only at the 80% confidence level.

plained [*Stuiver et al.*, 1991]. The $\Delta^{14}C$ offsets could be a function of undocumented millennial-scale solar variability, uncertainties in the geomagnetic reconstruction, or changes in the partitioning of carbon between the ocean, atmosphere, and terrestrial biosphere. While the data presented here are far too limited to choose between these possibilities, the coherence of Florida Current $\delta^{18}O$ and atmospheric $\Delta^{14}C$ at millennial timescales is consistent with an oceanic contribution.

7. Conclusion

[54] Planktonic foraminiferal oxygen isotopes indicate that the Florida Current was cooler or more saline during the Little Ice Age than today, and was relatively warm or fresh during the Medieval Warm Period. Much of the North Atlantic subtropical gyre responded in a similar manner. Given that the El Niño Southern Oscillation has little direct effect on SSTs in this region (see http://www.cdc.noaa.gov/ENSO/), it is unlikely that ENSO on its own was responsible for the gyre-wide hydrographic changes. A more feasible option is long-term changes in the behavior of the North Atlantic Oscillation. Results from an atmospheric general circulation model imply that low solar irradiance during the LIA may have triggered a shift toward the NAO negative phase, resulting in a cool subtropical gyre and warm subpolar gyre, similar to the observed pattern [*Shindell et al.*, 2001]. Alternatively, instrumental data indicate that on decadal and longer timescales, cool SST anomalies in the subtropical gyre and warm SST anomalies in the subpolar gyre are associated with the positive phase of the NAO [*Visbeck et al.*, 2003]. This pattern is apparently caused by oceanic advection of warm anomalies from the western subtropical Atlantic or enhanced meridional overturning circulation [*Visbeck et al*, 2003].

[55] The coherence and phasing of atmospheric ^{14}C production and Florida Current $\delta^{18}O$ during the Late Holocene implies that solar variability may influence FC surface density at frequencies between 1/300 and 1/1000 years. *Bond et al.* [2001] argue that a solar mechanism can account for the similarity between proxies of solar variability and ice-rafting in the subpolar North Atlantic. Solar irradiance-driven changes in surface temperature modeled by *Shindell et al.* [2001] underestimate the observed cooling in Greenland and the North Atlantic subtropical gyre by 1°C or more. Either model sensitivity to solar irradiance is too low, another mechanism is required to amplify the temperature response, or the subtropical gyre records reflect changes in salinity rather than temperature.

[56] One plausible option is that variability internal to the climate system influences Florida Current $\delta^{18}O$, ice-rafting in the North Atlantic and atmospheric $\Delta^{14}C$. Ocean general circulation models indicate the entire North Atlantic cools during severe reductions in NADW formation. Yet it seems unlikely that a change in NADW formation on its own caused the LIA cooling, given the warming south of Newfoundland at this time [*Keigwin and Pickart*, 1999]. If meridional overturning episodically slowed during the Late Holocene, it should lead to a cooling of the subtropical gyre, consistent with the pattern during the LIA. Reduced overturning would in turn limit sequestration of ^{14}C in the deep sea, and therefore cause an accumulation of ^{14}C in the atmosphere. The coherence between Florida Current $\delta^{18}O$ and atmospheric $\Delta^{14}C$ at periods greater than 1000 years implies that internal climate system variability may influence the low-frequency behavior of atmospheric radiocarbon during the Late Holocene.

[57] **Acknowledgments.** We would like to thank Olivier Marchal, Jean Lynch-Stieglitz, and two anonymous reviewers for their valuable comments and suggestions. We also thank Peter Huybers for use of his multitaper coherence routine and Dorinda Ostermann, Marti Jeglinski, Anne Edwards, and Shawn Johnson for technical support. We are grateful to the WHOI core lab for sample collection and archiving, the captain and crew of the R/V *Knorr*, and to the Sea Education Association for access to their vessels *Westward* and *Cramer*. This work was supported by NSF grants OCE-9905605 and OCE-0096469 This is WHOI contribution 11236.

References

Bard, E., G. Raisbeck, F. Yiou, and J. Jouzel (2000), Solar irradiance during the last 1200 years based on cosmogenic nuclides, *Tellus, Ser B, 52*, 985–992.

Baringer, M O., and J. C. Larsen (2001), Sixteen years of Florida Current transport at 27°N, *Geophys. Res. Lett., 28*, 3179–3182

Beer, J. U Siegenthaler, G. Bonami, R. C. Finkel, H Oeschger, M. Suter, and W. Wölfli (1988), Information on past solar activity and geomagnetism from 10Be in the Camp Century ice core, *Nature, 331*, 675–679.

Bianchi, G., and I N. McCave (1999), Holocene periodicity in North Atlantic climate and deep-ocean flow south of Iceland, *Nature, 397*, 515–517.

Black, D E., R. C. Thunell, A Kaplan, L C Peterson, and E J. Tappa (2004), A 2000-year record of Caribbean and tropical North Atlantic hydrographic variability, *Paleoceanography, 19*, PA2022, doi:10.1029/2003PA000982.

Bond, G , B. Kromer, J. Beer, R. Muscheler, M N. Evans, W. Showers, S. Hoffmann, R. Lotti-Bond, I. Hajdas, and G. Bonani (2001), Persistent solar influence on North Atlantic climate during the Holocene, *Science, 294, 2130–2136*

Bradley, R. S., and P. D. Jones (1993), Little Ice Age summer temperature variations. their nature and relevance to recent global warming trends, *Holocene, 3*, 367–376.

Candela, J., J Sheinbaum, J Ochoa, and A. Badan (2002), The potential vorticity flux through the Yucatan Channel and the Loop Current in the Gulf of Mexico, *Geophys Res Lett , 29*(22), 2059, doi:10.1029/2002GL015587

Chinn, T. J (1996), New Zealand glacier responses to climate change of the past century, *N Z J Geol. Geophys , 39*, 415–428.

Cobb, K. M , C D. Charles, H. Cheng, and R. L. Edwards (2003), El Niño/Southern Oscillation and tropical Pacific climate during the last millennium, *Nature, 424*, 271–276.

Crowley, T. J (2000), Causes of climate change over the past 1000 years, *Science, 289*, 270–277.

Curry, W. B., R C. Thunell, and S. Honjo (1983), Seasonal changes in the isotopic composition of planktonic foraminifera collected in Panama Basin sediment traps, *Earth Planet. Sci Lett., 64*, 33–43

Dahl-Jensen, D., K. Mosegaard, N. Gundestrup, G. D. Clow, S J. Johnsen, A. W Hansen, and N Balling (1998), Past temperatures directly from the Greenland ice sheet, *Science, 282*, 268–271

deMenocal, P , J Ortiz, T. Guilderson, and M. Sarnthein (2000), Coherent high- and low-latitude variability during the Holocene warm period, *Science, 288*, 2198–2202

Denton, G. H , and W. Karlén (1973), Holocene climatic variations-their pattern and possible cause, *Quat Res* , *3*, 155–205

Deuser, W. G. (1987), Seasonal variations in isotopic composition and deep-water fluxes of the tests of perennially abundant planktonic foraminifera of the Sargasso Sea: Results from sediment-trap collections and their paleoceanographic significance, *J Foraminiferal Res* , *17*, 14–27

Druffel, E M (1982), Banded corals: Changes in oceanic carbon-14 during the Little Ice Age, *Science*, *218*, 13–19.

Duplessy, J C , P. L Blanc, and A. W. H. Bé (1981), Oxygen-18 enrichment of planktonic foraminifera due to gametogenic calcification below the euphotic zone, *Science*, *213*, 1247–1250

Eddy, J M (1976), The Maunder Minimum, *Science*, *192*, 1189–1202.

Epstein, S., R Buchsbaum, H. A. Lowenstam, and H C. Urey (1953), Revised carbonate water isotopic temperature scale, *Geol Soc Am Bull* , *64*, 1315–1326

Esper, J , E R. Cook, and F H. Shweingruber (2002), Low-frequency signals in long tree-ring chronologies for reconstructing past temperature variability, *Science*, *295*, 2250–2253

Etheridge, D. M , L. P. Steele, R L Langenfelds, R. J. Francey, J. M. Barnola, and V. I Morgan (1996), Natural and anthropogenic changes in atmospheric CO2 over the last 1000 years from air in Antarctica ice and firn, *J Geophys Res* , *101*, 4115–4128

Fairbanks, R G., M Sverdlove, R Free, P H. Wiebe, and Allan W. H. Bé (1982), Vertical distribution and isotopic fractionation of living planktonic foraminifera from the Panama Basin, *Nature*, *298*, 841–844.

Fairbanks, R G , C. D Charles, and J. D Wright (1992), Origin of global meltwater pulses, in *Radiocarbon After Four Decades*, edited by R. E Taylor et al , pp. 473–500, Springer-Verlag, New York

Fratantoni, P. S , T. N Lee, G. P Podesta, and F Muller-Karger (1998), The influence of Loop Current perturbations on the formation and evolution of Tortugas eddies in the southern Straits of Florida, *J Geophys Res* , *103*, 24,759–24,779

Ganachaud, A , and C. Wunsch (2000), Improved estimates of global ocean circulation, heat transport and mixing from hydrographic data, *Nature*, *408*, 453–457.

Grove, J M. (1988), *The Little Ice Age*, 498 pp., Methuen, New York

Haase-Schramm, A., F. Bohm, A Eisenhauer, W Dullo, M M. Joachimski, B. Hansen, and J. Reitner (2003), Sr/Ca ratios and oxygen isotopes from sclerosponges· Temperature history of the Caribbean mixed layer and thermocline during the Little Ice Age, *Paleoceanography*, *18*(3), 1073, doi.10 1029/2002PA000830

Haug, G , K. A. Hughen, D M. Sigman, L C Peterson, and U. Rohl (2001), Southward migration of the ITCZ through the Holocene, *Science*, *293*, 1304–1308

Hendy, E J , M K Gagan, C. A Alibert, M T. McCulloch, J M. Lough, and P J. Isdale (2002), Abrupt decrease in tropical Pacific sea surface salinity at end of Little Ice Age, *Science*, *295*, 1511–1514

Hodell, D. A , M Brenner, J. H Curtis, and T. Guilderson (2001), Solar forcing of drought frequency in the Maya lowlands, *Science*, *292*, 1367–1370

Hodell, D A , et al (2002), The Little Ice Age in Mesoamerica, *Eos Trans AGU*, *83*(47), Fall Meet Suppl , Abstract PP61B-10

Huang, S , H N Pollack, and P. Shen (2000), Temperature trends over the past five centuries reconstructed from borehole temperatures, *Nature*, *403*, 756–758.

Indermuhle, A., et al. (1999), Holocene carbon-cycle dynamics based on CO_2 trapped in ice at Taylor Dome, *Antarctica, Nature*, *398*, 121–126

Jones, P. D., and R S Bradley (1995), Climate variations over the last 500 years, in *Climate Since A D 1500*, edited by R S Bradley and P D. Jones, pp 649–665, Routledge, New York

Keigwin, L (1996), The Little Ice Age and Medieval Warm Period in the Sargasso Sea, *Science*, *274*, 1504–1508.

Keigwin, L., and E. A Boyle (2000), Detecting Holocene changes in thermohaline circulation, *Proc Natl. Acad Sci U S.A.*, *97*, 1343–1346

Keigwin, L., and R S Pickart (1999), Slope Water Current over the Laurentian Fan on interannual to millennial time scales, *Science*, *286*, 520–523.

Killingley, J. S., R F. Johnson, and W. H Berger (1981), Oxygen and carbon isotopes of individual shells of planktonic foraminifera from Ontong-Java Plateau, equatorial Pacific, *Palaeogeogr Palaeoclimatol. Palaeoecol* , *33*, 193–204

Kim, S T., and J O'Neil (1997), Equilibrium and non-equilibrium oxygen isotope effects in synthetic carbonates, *Geochim Cosmochim Acta* , *61*, 3461–3475.

Larsen, J. C (1992), Transport and heat flux of the Florida Current at 27°N derived from cross-stream voltages and profiling data· Theory and observations, *Philos. Trans R Soc London A*, *338*, 169–236.

Lean, J., and D Rind (1999), Evaluating Sun-climate relationships since the Little Ice Age, *J Atmos. Terr Phys.*, *61*, 25–36.

Lean, J , A Skumanich, and O. White (1992), Estimating the Sun's radiative output during the Maunder Minimum, *Geophys Res Lett* , *19*, 1591–1594.

Lee, T. N , K Leaman, E. Williams, T. Berger, and L. Atkinson (1995), Florida Current meanders and gyre formation in the southern Straits of Florida, *J Geophys Res* , *100*, 8607–8620.

Levitus, S , R Burgett, and T. P Boyer (1994), *World Ocean Atlas*, U S Dept of Comm., Washington, D.C

Lynch-Stieglitz, J , W B Curry, and N Slowey (1999), A geostrophic estimate for the Florida Current from the oxygen isotope composition of benthic foraminifera, *Paleoceanography*, *14*, 360–373

Manabe, S , and R J Stouffer (1988), Two stable equilibria of a coupled ocean-atmosphere model, *J Clim* , *1*, 841–866.

Mann, M E., R S Bradley, and M K. Hughes (1999), Northern Hemisphere temperatures during the past millennium· Inferences, uncertainties, and limitations, *Geophys Res Lett* , *26*, 759–762

Maul, G , and F M Vukovich (1993), The relationship between variations in the Gulf of Mexico Loop Current and Straits of Florida volume transport, *J Phys Oceanogr* , *23*, 785–796

Oppo, D W , J F McManus, and J. L Cullen (2003), Deep water variability in the Holocene epoch, *Nature*, *422*, 277–278

Ostermann, D. R , and W B Curry (2000), Calibration of stable isotopic data: An enriched $\delta^{18}O$ standard used for source gas mixing detection and correction, *Paleoceanography*, *15*, 353–360

Peterson, L C , J. T Overpeck, N G. Kipp, and J Imbrie (1991), A high-resolution Late Quaternary upwelling record from the anoxic Cariaco Basin, Venezuela, *Paleoceanography*, *6*, 99–119

Poore, R Z , H J. Dowsett, S Verardo, and T. M. Quinn (2003), Millennial- to century-scale variability in Gulf of Mexico Holocene climate records, *Paleoceanography*, *18*(2), 1048, doi:10.1029/2002PA000868

Rind, D , and J Overpeck (1993), Hypothesized causes of decade- to century-scale climate variability. Climate model results, *Quat Sci Rev* , *12*, 357–374

Schiller, A , U Mikolajewicz, and R Voss (1997), The stability of the North Atlantic thermohaline circulation in a couple ocean-atmosphere general circulation model, *Clim Dyn.*, *13*, 325–347

Schmitz, W J , and M. S McCartney (1993), On the North Atlantic Circulation, *Rev Geophys* , *31*, 29–49.

Schmitz, W J., and P. Richardson (1991), On the sources of the Florida Current, *Deep Sea Res* , *38*, s379–s409.

Schmitz, W J , J. R Luyten, and R W Schmitt (1993), On the Florida Current T/S envelope, *Bull Mar Sci* , *53*, 1048–1065.

Shindell, D T., G A Schmidt, M. E Mann, D Rind, and A Waple (2001), Solar forcing of regional climate during the Maunder Minimum, *Science*, *294*, 2149–2152

Spero, H J., J. Bijma, D W. Lea, and B E Bemis (1997), Effect of seawater carbonate concentration on foraminiferal carbon and oxygen isotopes, *Nature*, *390*, 497–500.

Stuiver, M , T F Braziunas, B Becker, and B Kromer (1991), Climatic, solar, oceanic and geomagnetic influences on late-glacial and Holocene atmospheric $^{14}C/^{12}C$ change, *Quat Res* , *35*, 1–24.

Stuiver, M , P. J Reimer, E Bard, J W Beck, G. S. Burr, K. A. Hughen, B Kromer, F. G. McCormac, J. V. D Plicht, and M. Spurk (1998), INTCAL98 radiocarbon age calibration 24,000–0 cal BP, *Radiocarbon*, *40*, 1041–1083

Sturges, W , and R Leben (2000), Frequency of ring separations from the Loop Current in the Gulf of Mexico· A revised estimate, *J Phys Oceanogr* , *30*, 1814–1819

Thompson, L G (1995), Ice core evidence from Peru and China, in *Climate Since A D 1500*, edited by R. S Bradley and P D Jones, pp. 517–548, Routledge, New York

Thomson, D J. (1982), Spectrum estimation and harmonic analysis, *Proc IEEE*, *70*, 1055–1096.

Visbeck, M., E P Chassignet, R G Curry, T L Delworth, R. R Dickson, and G Krahmann (2003), The ocean's response to North Atlantic Oscillation variability, in *The North Atlantic Oscillation Climate Significance and Environmental Impact*, *Geophys Monogr Ser* , vol. 134, edited by J W Hurrell et al., pp 113–145, AGU, Washington, D. C.

Vukovich, F. M (1988), Loop Current boundary variations, *J Geophys Res* , *93*, 15,585–15,591

Walter, K , and H F Graf (2002), On the changing nature of the regional connection

between North Atlantic Oscillation and sea surface temperature, *J Geophys Res.*, *107*(D17), 4338, doi:10.1029/2001JD000850.

Watanabe, T., A. Winter, and T. Oba (2001), Seasonal changes in sea surface temperature and salinity during the Little Ice Age in the Caribbean Sea deduced from Mg/Ca and $^{18}O/^{16}O$ ratios in corals, *Mar Geol*, *173*, 21–35.

Williams, D. F., Allan W H. Bé, and R. G. Fairbanks (1979), Seasonal oxygen isotopic variations in living planktonic foraminifera off Bermuda, *Science*, *206*, 447–449.

Winter, A., H. Ishioroshi, T. Watanabe, T Oba, and J. Christy (2000), Caribbean sea surface temperatures: Two-to-three degrees cooler than present during the Little Ice Age, *Geophys Res Lett*, *27*, 3365–3368.

Zeebe, R E. (1999), An explanation of the effect of seawater carbonate concentration on foraminiferal oxygen isotopes, *Geochim Cosmochim Acta*, *63*, 2001–2007.

W. B Curry, Department of Geology and Geophysics, Woods Hole Oceanographic Institution, Woods Hole, MA 02543, USA.

D. C Lund, MIT/WHOI Joint Program in Oceanography, Woods Hole Oceanographic Institution, Wood Hole, MA 02543, USA (dlund@whoi edu)

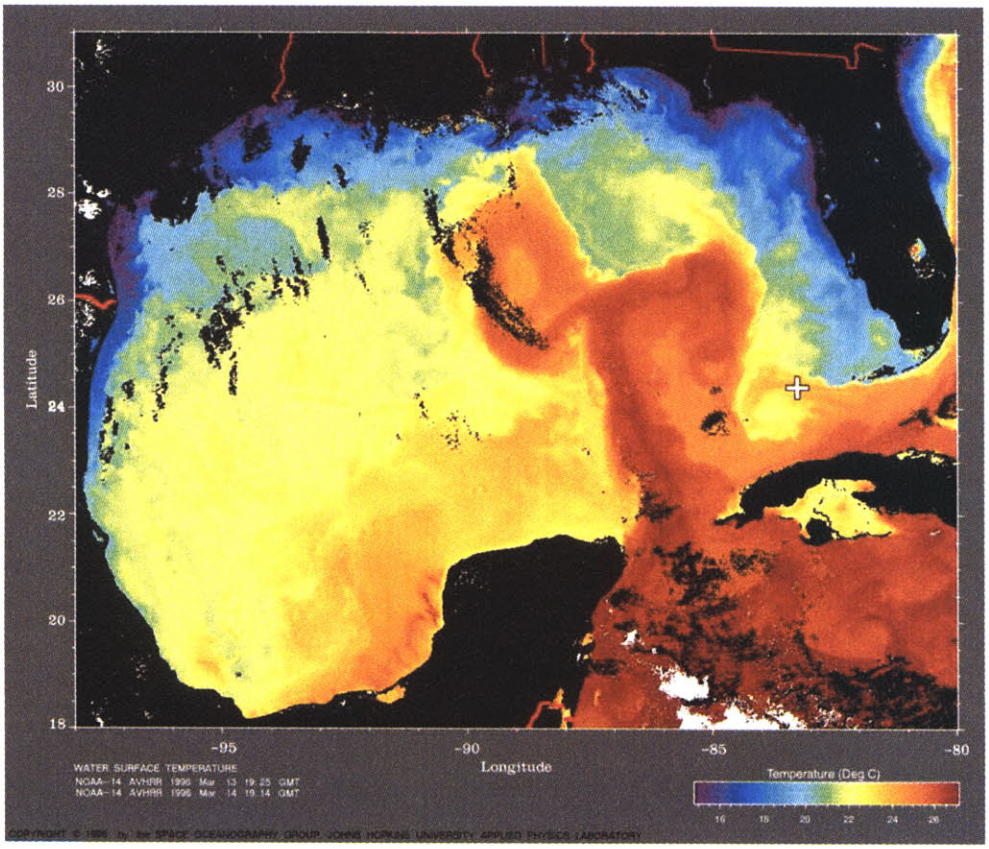

Figure 1. Advanced very high resolution radiometer (AVHRR)-based sea surface temperature estimates for the Gulf of Mexico and Florida Straits, 13–14 March 1996. SSTs in this figure vary from 15 to 27°C. The strong north-south temperature gradient near the core sites (plus symbol) is typical of winter conditions in this area (reprinted by permission from Ocean Remote Sensing Group, Johns Hopkins University Applied Physics Laboratory).

Chapter 3:

Florida Current Surface Temperature and Salinity Variability during the Last Millennium

Abstract

The salinity and temperature of the Florida Current are key parameters affecting the transport of heat into the North Atlantic, yet little is known about their variability on centennial time scales. Here we report replicated, high-resolution foraminiferal records of Florida Current surface hydrography for the last millennium from two coring sites, Dry Tortugas and the Great Bahama Bank. The oxygen isotopic composition of Florida Current surface water ($\delta^{18}O_w$) near Dry Tortugas increased by 0.4‰ during the course of the Little Ice Age (LIA: ~1200-1850 A.D.), which based on modern $\delta^{18}O_w$–salinity relationships is equivalent to a salinity increase of 0.8-1.5 psu.

On the Great Bahama Bank, where surface waters are influenced by the North Atlantic subtropical gyre, $\delta^{18}O_w$ increased by 0.3‰ during the last 200 years. Although a portion (~0.1‰) of this shift may be an artifact of anthropogenically-driven changes in surface water $\sum CO_2$, the remaining $\delta^{18}O_w$ signal implies a 0.4 to 1 psu increase in salinity after 200 yr BP. The simplest explanation of the $\delta^{18}O_w$ data is southward migration of the Atlantic Hadley circulation during the LIA. Scaling of the Dry Tortugas and Great Bahama Bank LIA $\delta^{18}O_w$ records to salinity using the modern low-latitude $\delta^{18}O_w$-S slope produces an unrealistic reversal in the salinity gradient between the two sites. Only if $\delta^{18}O_w$ is scaled to salinity using a high-latitude $\delta^{18}O_w$-S slope can the records be reconciled. Changes in atmospheric ^{14}C paralleled shifts in Dry Tortugas $\delta^{18}O_w$, suggesting that variable solar irradiance paced centennial-scale migration of the Atlantic Inter-Tropical Convergence Zone and changes in Florida Current salinity during the last millennium.

Sea-surface temperatures (SSTs) at Dry Tortugas were 0.5-1.0°C warmer during the LIA than the preceding and subsequent time intervals, possibly due to decreased frequency of Tortugas eddy formation. On the Great Bahama Bank, SSTs cooled by 0.5°C at the beginning of the Little Ice Age and gradually warmed towards modern values beginning at ~1450 A.D., well before the LIA termination. The SST data indicate surface temperature anomalies in the Northern Hemisphere were spatially heterogeneous during the latter portion of the Little Ice Age.

Introduction

The Little Ice Age was the most prominent climate event of the last millennium prior to the 20th century. Historical accounts describe severe cold conditions in Europe and North America at intermittent periods during the LIA (Grove, 1988; Bradley and Jones, 1995) and terrestrial paleoclimate data suggest the LIA was a global phenomenon (Bradley and Jones, 1993; Mann et al. 2000; Esper et al., 2002; Dahl-Jensen et al., 1998; Huang et al., 2000; Thompson, 1995; Chinn, 1996; Denton and Karlén, 1973). Reconstructions of North Atlantic sea-surface temperatures (SSTs) show that the eastern subtropical gyre cooled nearly 4°C during the LIA (deMenocal et al., 2000) while the Sargasso Sea cooled by ~1°C (Keigwin, 1996). The western edge of the gyre apparently cooled by 1-3°C relative to today during the coldest LIA intervals (Druffel, 1982; Winter et al., 2000). In both the eastern gyre and Sargasso Sea locations, the LIA was preceded by relatively a warm interval from ~500-1200 A.D., the so-called "Medieval Warm Period".

The Yucatan Peninsula (Hodell et al., 2005) and the Cariaco Basin (Haug et al., 2001) experienced unusually dry Little Ice Age conditions. The records can be interpreted as a southward shift of the Atlantic inter-tropical convergence zone (ITCZ), either as a result of a greater meridional temperature gradient in the North Atlantic or persistent El Niño-like conditions in the equatorial Pacific (Haug et al., 2001). Shifts in mean ITCZ position affect evaporation and precipitation in the tropical Atlantic and may

act to stabilize perturbations to the Atlantic overturning circulation by influencing Gulf Stream salinity (Vellinga et al., 2002).

Here we present evidence from multiple high-resolution sediment cores that Florida Current salinity increased during the Little Ice Age. The simplest explanation for this pattern is a southward shift of the Atlantic Inter-Tropical Convergence Zone (ITCZ) and increased evaporation minus precipitation (E-P) in the tropical Atlantic. These data support the suggestion that southward ITCZ migration caused dry LIA conditions in Central and South America (Haug et al., 2001; Hodell et al., 2005) and are consistent with simulations of increased aridity in the tropical North Atlantic in response to northern hemisphere cooling (Vellinga et al., 2002; Lohmann, 2003; Vellinga and Wu, 2004). On the eastern edge of the Florida Current, $\delta^{18}O_w$ was anomalously low during the Little Ice Age, due to southward movement of the Hadley circulation.

Oceanographic Setting

We used four sediment cores for this study, two from each side of the Florida Current, the portion of the Gulf Stream confined to the Straits of Florida. Cores KNR166-2-62MC-A and W167-79GGC were retrieved near Dry Tortugas, on the northwestern edge of the Florida Current (Figure 1). Cores KNR166-2-118MC-A and KNR166-2-125MC-D were retrieved from the Great Bahama Bank, on the eastern edge of Florida Current. Although separated in distance by only 400 km, the surface water at each location represents distinct oceanographic regimes. On the western side of the

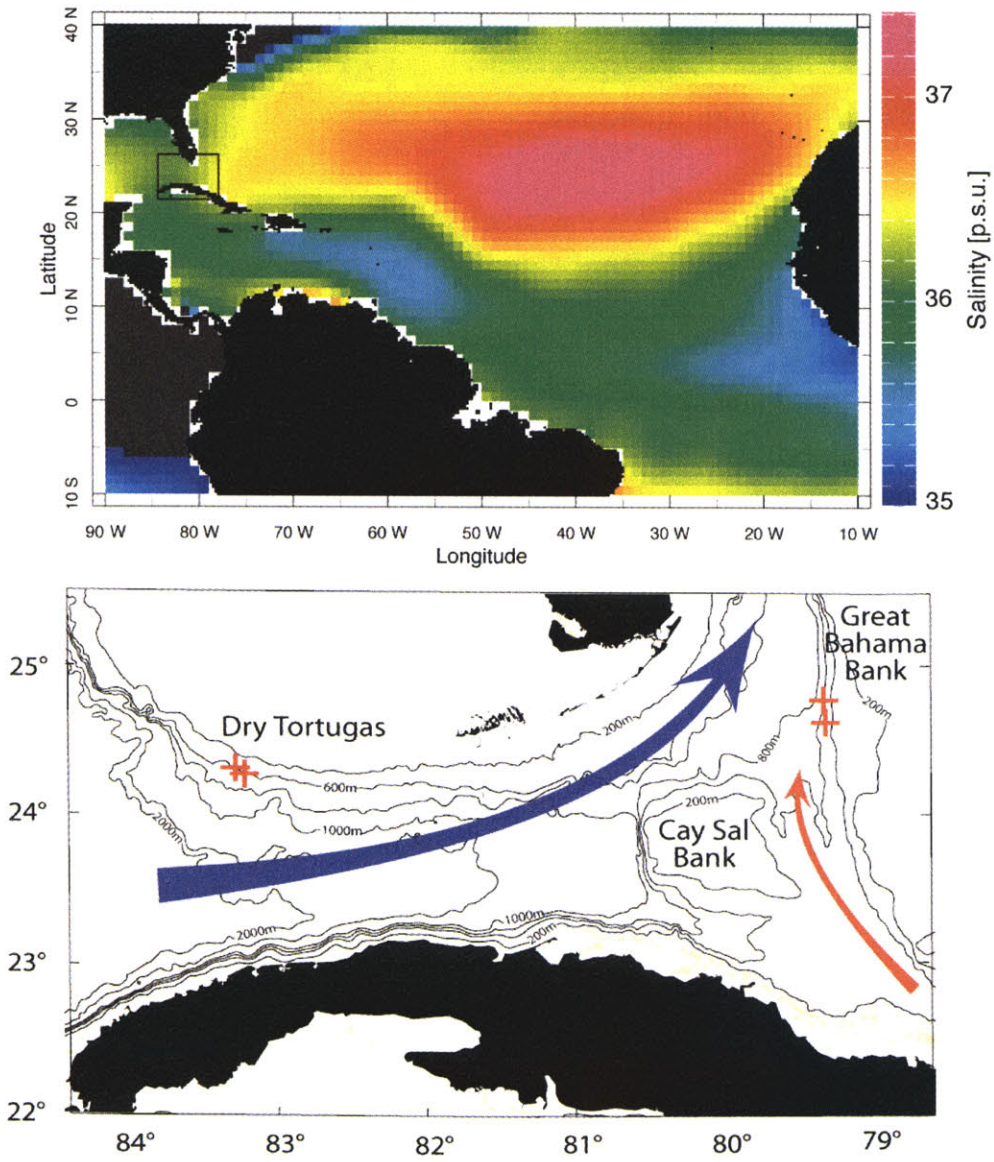

Figure 1

Top) Map of North Atlantic annual average salinity at 30 m depth (Levitus et al., 1994). High subtropical gyre salinities (> 36 psu) reflect positive E-P under the descending limb of the Hadley circulation, while low tropical North Atlantic salinities (< 36 psu) reflect negative E-P under the Inter-Tropical Convergence Zone. Inset rectangular box represents the region addressed in this study. Bottom) Bathymetric map of study region (200 m contour intervals). The Dry Tortugas sites, 62MC (547 m depth; 24°19.6' N, 83°15.4' W) and 79GGC (530 m depth; 24°21.5' N, 83°20.9' W), sit on the northwestern edge of the Florida Current (FC; blue arrow). The surface FC is dominated by low salinity water advected from the tropical North Atlantic via the Caribbean and into the Straits of Florida. The Great Bahama Bank sites, 118MC (531 m depth; 24°35.4' N, 79°16.1' W) and 125MC (694 m depth; 24°45.5' N, 79°17.5' W), reflect the influence of the FC as well as the relatively salty Santaren Current (red arrow) that originates in the North Atlantic subtropical gyre.

Florida Current, surface water is fresh due to the advection of low salinity waters from the tropical Atlantic (Schmitz and Richardson, 1991). Today, tropical Atlantic and Caribbean surface salinity is controlled largely by the excess rainfall relative to evaporation under the ascending branch of the Hadley circulation, the ITCZ. Rainfall associated with the annual migration of the ITCZ between 5°S and 15°N (Waliser and Gautier, 1993) is the primary reason surface water salinity is low in this region (Figure 1). This water is advected through the Caribbean and into the Straits of Florida via prevailing wind-driven and meridional overturning transports. Annual average salinity near Dry Tortugas is 36.1 with a seasonal and interannual range of approximately ±0.1 and ±0.2, respectively (Carton and Giese, 2005).

The Great Bahama Bank core sites reflect the influence of both the Florida Current and the Santaren Current, which is relatively salty due to the influence of the subtropical gyre. Higher salinities in the subtropical gyre reflect positive E-P conditions that occur under the dry, descending branch of the Hadley circulation and the convergence of surface water due to Ekman transport. Annual average salinity near the 118MC and 125MC cores sites is 36.2 (Carton and Giese, 2005). The seasonal and interannual range in salinity is approximately ±0.05 and ±0.15, respectively (Carton and Giese, 2005), somewhat smaller than the Dry Tortugas region.

Methods and Coretop Results

The hydrographic reconstructions presented here are based on paired measurements of oxygen isotopes and Mg/Ca in fossil shells of planktonic foraminifera. The $\delta^{18}O$ of calcite ($\delta^{18}O_c$) precipitated by foraminifera is a function of temperature (T) and $\delta^{18}O$ of the sea water ($\delta^{18}O_w$). By using paired measurements of oxygen isotopic composition [$\delta^{18}O_c \approx f(T, \delta^{18}O_w)$] and magnesium concentration [$Mg/Ca \approx f(T)$], it is possible to estimate $\delta^{18}O_w$, which is related to salinity through evaporation and precipitation at the ocean surface. We measured $\delta^{18}O_c$ and Mg/Ca in the surface dwelling foraminifer *G. ruber* in a suite of very high sedimentation rate cores from each side of the Florida Current to reconstruct salinity variability over the last millennium.

Age control

Down-core age control is based on multiple planktonic foraminiferal radiocarbon dates in each core (Table 1). Each date is based on an average of 8 mg *G. ruber* specimens from the > 250 μm size fraction. All three multi-core core tops in this study have >1 fraction modern radiocarbon, indicating that deposition occurred primarily after 1950 A. D. The one gravity core (79GGC) has a ^{14}C coretop age of 200 years, also indicating the presence of bomb radiocarbon, but to a lesser extent than the multi-cores. Raw radiocarbon ages were converted to calendar ages using CALIB 4.3 (Stuiver et al., 1998a), assuming a surface ocean reservoir age of 400 years. The average sampling interval for the four cores is as follows: 62MC, 16 years; 79GGC, 20 years; 118MC, 25 years; and 125MC, 50 years.

Sampling strategy

To address the potential bias of running $\delta^{18}O$ and Mg/Ca on separate groups of foraminifera, we decided to use one common population of approximately 100 individual *G. ruber* specimens (212-250 μm size fraction) for 62MC and 118MC, and 125MC. Each sample was sonicated in methanol, siphoned, dried at 70°C, crushed, weighed, and then split for isotopic and Mg/Ca analyses. The crushed sample was evenly distributed on a tray, and split using a fine brush to ensure the subsamples contained approximately equal portions of fine and coarse material. The weight equivalent of 40 *G. ruber* tests was removed and then split into four separate samples for stable isotopic determinations. We set the remainder aside for Mg/Ca analyses.

Depth range (cm)	^{14}C age (yr)	Error (yr)	Calage (yr BP)
KNR166-2-118MC-A			
0-1	>mod	N/A	0
12-14	635	25	282
36-37	1320	45	885
KNR166-2-125MC-D			
0-1	>mod	N/A	0
10-11	1250	30	780
27-28	1830	35	1360

Table 1
Radiocarbon ages for KNR166-2-118MC-A and KNR166-2-125MC-D. The columns are as follows: sample depth interval, raw radiocarbon age, analytical error, and calendar age. The core tops contain more radiocarbon than expected in modern samples, indicating contamination with bomb ^{14}C and post-1950 A.D. deposition ages. We calibrated the downcore raw ^{14}C values to calendar ages using CALIB 4.3 (Stuiver et al., 1998) and a reservoir age of 400 years. Each date is based on *G. ruber* from the >250 μm size fraction. See Lund and Curry (2004) for the W167-79GGC and KNR166-2-62MC-A age models.

Stable isotopes

Stable isotope analyses for 79GGC were run on a Finnigan MAT 252 coupled to a Kiel II carbonate device. Analyses for 62MC, 118MC, and 125MC were run on a Finnigan MAT 253 coupled to a Kiel III carbonate device. Calibration to VPDB scale was made using NBS-19 ($\delta^{18}O$ = -2.20‰ and $\delta^{13}C$ = 1.95‰). Reproducibility (1σ) of NBS-19 (n=461) for the MAT 253 system is ±0.08‰ for $\delta^{18}O$ and ±0.04‰ for $\delta^{13}C$. The 1σ values for NBS-19 on the MAT 252 were ±0.07‰ for $\delta^{18}O$ and ±0.03‰ for $\delta^{13}C$ (n>2200; Ostermann and Curry, 2000).

The isotope splits for 62MC, 118MC, and 125MC can be used to determine the degree of sample heterogeneity caused by the splitting procedure. If each isotope split represents the $\delta^{18}O$ of the sample population, then the variance of the residual $\delta^{18}O$ at each depth should be similar to the variance of the external standards. Residual values were determined by subtracting the mean $\delta^{18}O$ value at each depth from the individual measurements. The standard deviation of residual values for the cores is 0.09 per mil, close to the analytical error for NBS-19. The similarity of these statistics indicates that our splitting procedure created subsamples that are representative of the *G. ruber* population in each sample. A similar comparison is not possible for 79GGC since the variance of $\delta^{18}O$ analyses based on multiple measurements of 10 individuals is dominated by sampling rather than analytical uncertainty (Lund and Curry, 2004).

Mg/Ca analyses

The Mg/Ca analyses were based on either 50-60 individual foraminifera (79GGC) or their weight equivalent from a sample of 100 foraminifera (62MC, 118MC, and 125MC). To minimize bias due to matrix effects (Rosenthal et al., 1999), we weighed each Mg/Ca split individually to ensure it fell between 150 and 200 μg. Each sample was cleaned using a sequential three-step process, including clay removal, metal oxide reduction, and organic matter oxidation (Boyle and Keigwin, 1985; Rosenthal et al., 1997). All samples were run on a Finnigan Element 2 single collector ICP-MS.

Samples were corrected for drift using a 2% HNO_3 blank and a 50 ppm calcium standard. Analytical error was determined using three external standards with Mg/Ca ratios of 1.6, 3.2, and 4.8 mmol/mol. The analytical precision (1σ) for each standard was ±0.03 (n=12), ±0.04 (n=11), and ±0.05 mmol/mol (n=11), respectively. Mg/Ca ratios for the unknowns were typically in the 4.0 to 4.9 mmol/mol range. The average precision (1σ) for Mg/Ca splits, which reflects both analytical and sample processing uncertainty, is ±0.12 mmol/mol (n=82 pairs). Poorer precision for the unknowns primarily reflects sample heterogeneity due to the splitting and cleaning procedures.

We converted Mg/Ca values to sea-surface temperature using the calibration equation of Anand et al. (2003) for *G. ruber* (white), 250-350 μm [Mg/Ca(mmol/mol)= 0.34*exp(0.102*SST(°C))]. A Mg/Ca analytical precision of ±0.05 mmol/mol translates to an analytical temperature uncertainty of approximately ±0.1°C (1σ), whereas the

combined analytical and sample processing precision (±0.12 mmol/mol) corresponds to a SST uncertainty of ±0.25°C (1σ).

Calculated Dry Tortugas coretop SST values are 25.5°C (62MC) and 26.7°C (79GGC) (Figure 2). The annual average temperature at 30 m, the average depth for *G. ruber* calcification (Fairbanks, et al., 1982; Deuser, 1987), is 26.0°C (Levitus, 1994). On the Great Bahama Bank, coretop Mg/Ca-derived SSTs are 26.2°C (118MC) and 26.3°C (125MC) (Figure 3), compared to an annual average temperature of 26.3°C at 30 m depth (Levitus, 1994). The good agreement between Great Bahama Bank core tops and modern temperatures indicates that foraminiferal Mg/Ca in this location produces reasonable absolute temperature estimates. Although coretop and modern temperatures on near Dry Tortugas are well within the ±1°C calibration uncertainty (Anand et al., 2003), the match is not as precise as for the Great Bahama Bank sites. The 62MC and 79GGC cores are located near the strong temperature gradient along the northern edge of the Florida Current which exposes 79GGC to warmer waters and yields higher Mg/Ca-derived SSTs. Spatial SST variability at this scale (~10 km) is not captured by the coarse 1°x1° gridding of the Levitus SST database.

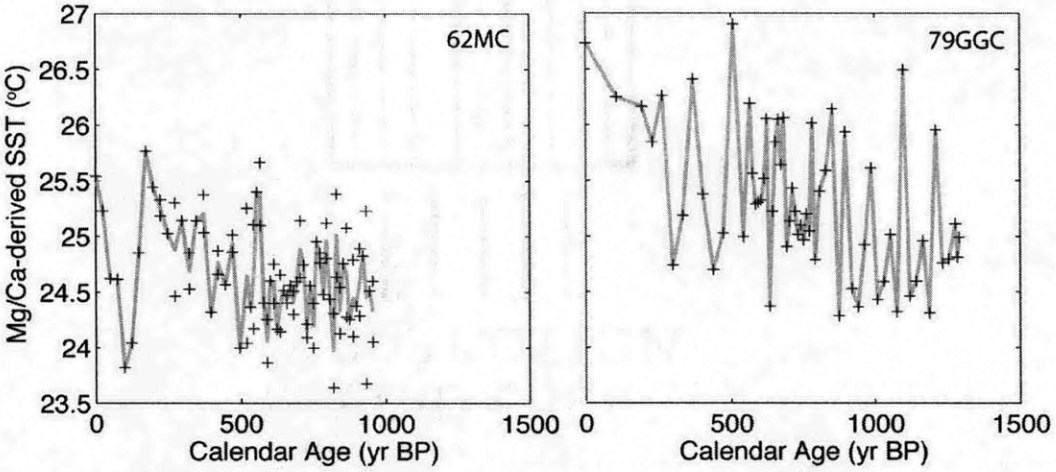

Figure 2
Left panel represents Mg/Ca-derived SSTs for 62MC based on *G. ruber* (white) 212-250 μm. Right panel represents the same for W167-79GGC. The plus symbols denote individual Mg/Ca analyses and the grey line is the average value at each stratigraphic level. SST estimates are based on the temperature calibration of Anand et al. (2003).

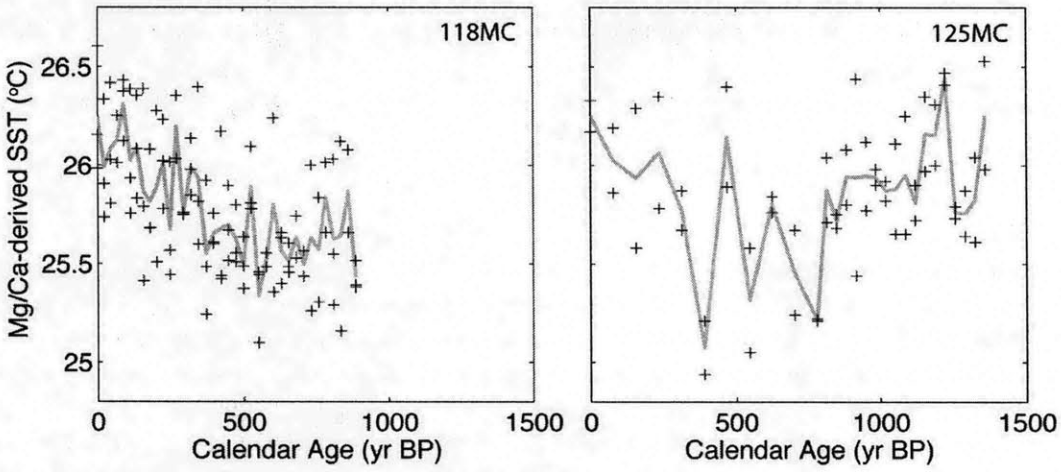

Figure 3
Same as Figure 2, but for the Great Bahama Bank multi-cores (118MC and 125MC).

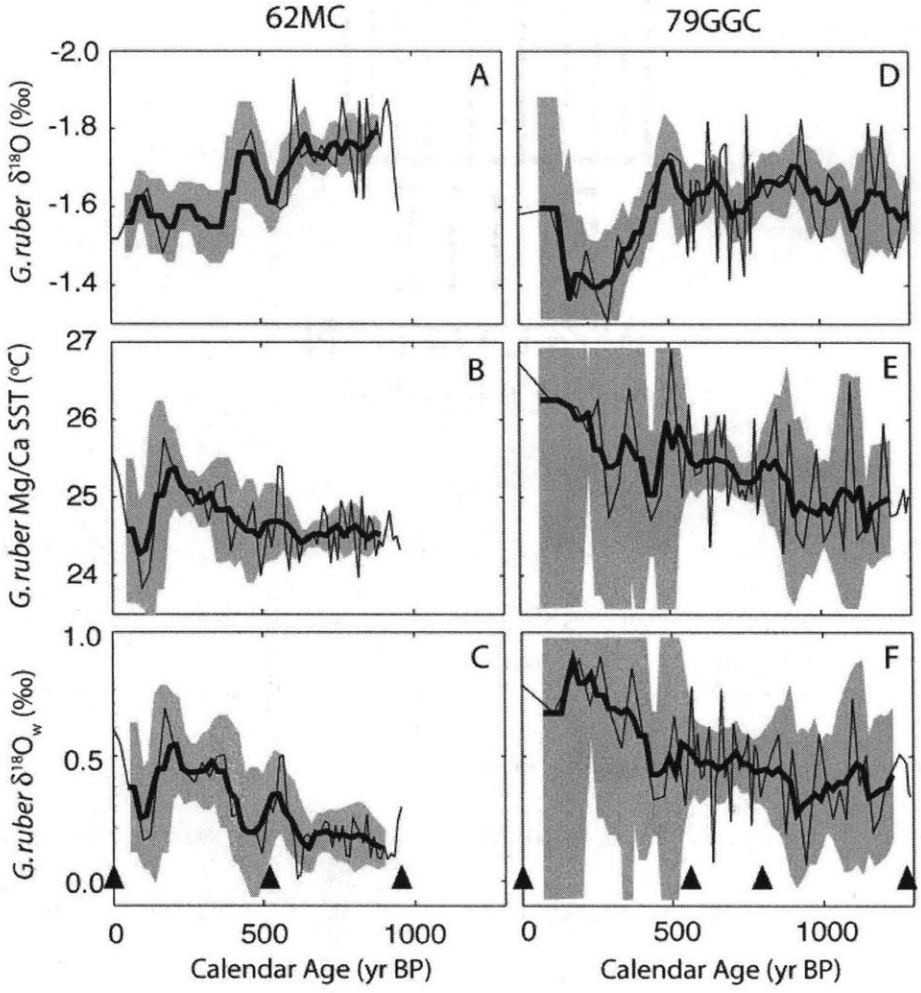

Figure 4

Left-hand column represents $\delta^{18}O_c$ (A), SST (B), and $\delta^{18}O_w$ (C) data from KNR166-2-62MC, based on *G. ruber* (white) 212-250 μm. Right-hand column represents $\delta^{18}O_c$ (D), SST (E), and $\delta^{18}O_w$ (F) data for W167-79GGC. The plotting convention is the same for each of the six subplots, which includes average value at each depth (thin black line), 100-year running mean (thick black line), and 95% confidence limits for the 100-year mean (shaded area). SST estimates are based on Mg/Ca analyses and the temperature calibration of Anand et al. (2003) and $\delta^{18}O_w$ was calculated using the equation of Kim and O'Neil (1997). $\delta^{18}O_w$ in each core was highest during the Little Ice Age. Calendar-calibrated radiocarbon dates (triangles) are given in the $\delta^{18}O_w$ plots. Despite being located only 10 km apart, 62MC $\delta^{18}O_w$ is approximately 0.2 per mil lower than 79GGC $\delta^{18}O_w$. This offset is most likely a function of using crushed foraminiferal tests for 62MC $\delta^{18}O$ analyses and whole tests for 79GGC (see Methods). The larger error envelope for 79GGC is due the smaller number of foraminifera used for the stable isotope and Mg/Ca analyses and fewer replicate Mg/Ca measurements.

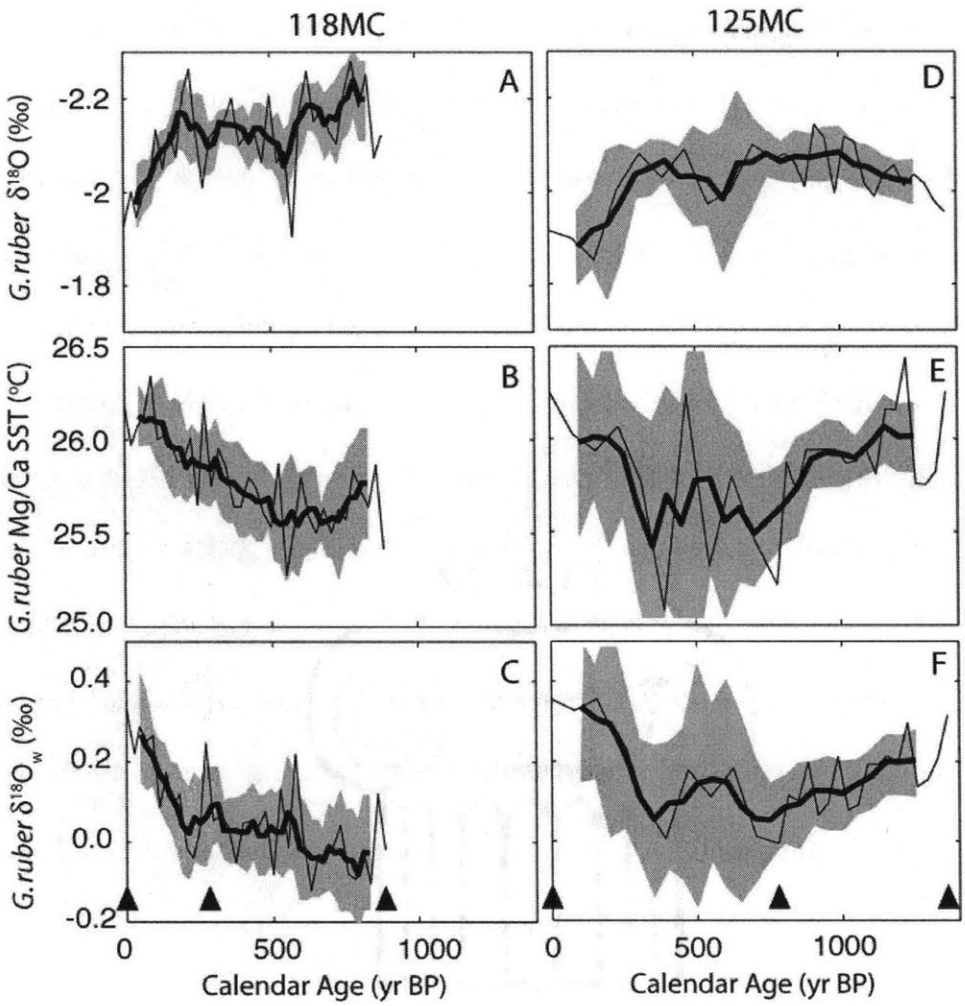

Figure 5

Left-hand column represents $\delta^{18}O_c$ (A), SST (B), and $\delta^{18}O_w$ (C) data from KNR166-2-118MC, based on *G. ruber* (white) 212-250 μm. Right-hand column represents $\delta^{18}O_c$ (D), SST (E), and $\delta^{18}O_w$ (F) data for KNR166-2-125MC. The plotting convention is the same as in Figure 4, except that the running average for 125MC was calculated using a 200-year running average to compensate for the lower sedimentation rate for this core. The wider error envelope for 125MC reflects the lower data density, even though the smoothing window used was twice as wide as for 118MC. $\delta^{18}O_c$ in both cores increased by 0.2 per mil over the last 300 years. Mg/Ca-derived SSTs were lower than today from 700 to 300 years BP, while those prior to 700 yr BP approached modern values. The $\delta^{18}O_w$ data imply that modern surface water at these sites is anomalously salty in the context of the last 1200 years.

$\delta^{18}O_w$ estimates

We calculated past changes in $\delta^{18}O_w$ using the isotopic fractionation vs. temperature relationship from Kim and O'Neil (1997) as presented by Lynch-Stieglitz et al. (1999). To evaluate whether the resulting values are reasonable, we compare the coretop $\delta^{18}O_w$ to estimates of surface water $\delta^{18}O_w$ based on modern $\delta^{18}O_w$-salinity observations. Since the Dry Tortugas sites are heavily influenced by tropical Atlantic surface waters, we used a $\delta^{18}O_w$/salinity regression based on data from the open ocean tropical Atlantic [$\delta^{18}O_w$(‰)= 0.26*S(psu)-8.44] (Schmidt et al., 1999). Assuming annual average salinity values of 36.1 near Dry Tortugas (Carton and Giese, 2005), the predicted coretop $\delta^{18}O_w$ is 0.95‰, somewhat larger than the 62MC and 79GGC coretop $\delta^{18}O_w$ values of 0.6‰ and 0.8‰, respectively (Figure 4c, f). For the Great Bahama Bank sites, the annual average salinity (36.2; Carton and Giese, 2005) and subtropical gyre $\delta^{18}O_w$/salinity regression [$\delta^{18}O_w$(‰)= 0.17*S(psu)-5.13] (Schmidt et al., 1999) yield a modern $\delta^{18}O_w$ of 1.02 per mil. This value is significantly higher than the 0.4‰ estimate for the 118MC and 125MC core tops (Figure 5c, f).

Although uncertainty in each coretop and surface water $\delta^{18}O_w$ estimate may account for some of the discrepancy, all four coretop values underestimate surface water $\delta^{18}O_w$. One possibility is that the measured *G. ruber* $\delta^{18}O$ does not represent the true equilibrium $\delta^{18}O$ value. Adding 0.2‰ to coretop $\delta^{18}O_w$ data to compensate for this disequilibrium (Deuser, 1987) would account for most of the surface water-coretop $\delta^{18}O_w$ discrepancy for 62MC and 79GGC but not for the Great Bahama Bank sites. The coretop

values for 118MC and 125MC would remain 0.4 per mil lower than modern even with this correction. This offset may reflect either a real difference in coretop and modern $\delta^{18}O_w$ values or spatial variability in the $\delta^{18}O_w$ / S relationship not captured by the Schmidt (1999) database.

Another potential source of error is whether whole or crushed foraminiferal tests were used for the stable isotope analyses. $\delta^{18}O$ values based on crushed foraminifera from 62MC are consistently 0.2 per mil lower than $\delta^{18}O$ values of whole foraminifera from the same samples (Figure 6). We observe no significant offset in $\delta^{13}C$ between the whole and crushed samples, so it is unlikely due to fractionation of CO_2 in the mass spectrometer. Keigwin and Jones (1990) found a similar pattern: the $\delta^{18}O$ of ground foraminifera was 0.2 per mil lower than the $\delta^{18}O$ of whole foraminifera, with no obvious difference in $\delta^{13}C$ values. This offset is likely due to either variable partitioning of oxygen isotopes amongst the products of the calcite-phosphoric acid reaction or diffusion of reaction products away from the particle surface associated with the production of CO_2 bubbles (Walters et al., 1972; Keigwin and Jones, 1990). Given that no fractionation occurs when crushed samples are acidified under elevated pressure to prevent foaming, it appears that the fractionation is most likely tied to the rate at which gas evolves during acidification (Walters et al., 1972). Swart et al. (1991) suggest that production of gas bubbles may encourage isotopic exchange between CO_2 and phosphoric acid, thus affecting the average isotopic value of the evolved carbon dioxide.

The apparent grain-size isotopic effect is analogous to temperature-driven changes in the fractionation factor. As the temperature and the reaction rate increase, the fractionation factor ($^{18}O/^{16}O_{calcite}/^{18}O/^{16}O_{CO2}$) decreases, leading to lower $\delta^{18}O$ values (e.g. Swart et al., 1991). For reasons that remain unclear, faster reaction rates associated with crushed samples apparently lead to a greater proportion of ^{16}O trapped as CO_2 and lower $\delta^{18}O$. Therefore, the low $\delta^{18}O_c$ and $\delta^{18}O_w$ in 62MC relative to 79GGC are most likely a function of crushing the 62MC samples prior to analysis. If the ~0.2 per mil offset between the cores were real, it would imply a salinity difference similar to the contrast observed between the subtropical gyre and tropical North Atlantic (~1 psu; Figure 1). Given that 62MC and 79GGC are located only 10 km apart, it is highly unlikely that their surface water $\delta^{18}O_w$ values are offset to this degree. Therefore, we conclude that the offset between coretop $\delta^{18}O_w$ for 62MC, 118MC, and 125MC and their respective modern $\delta^{18}O_w$ values can in part be attributed to the use of crushed samples for stable isotope analyses.

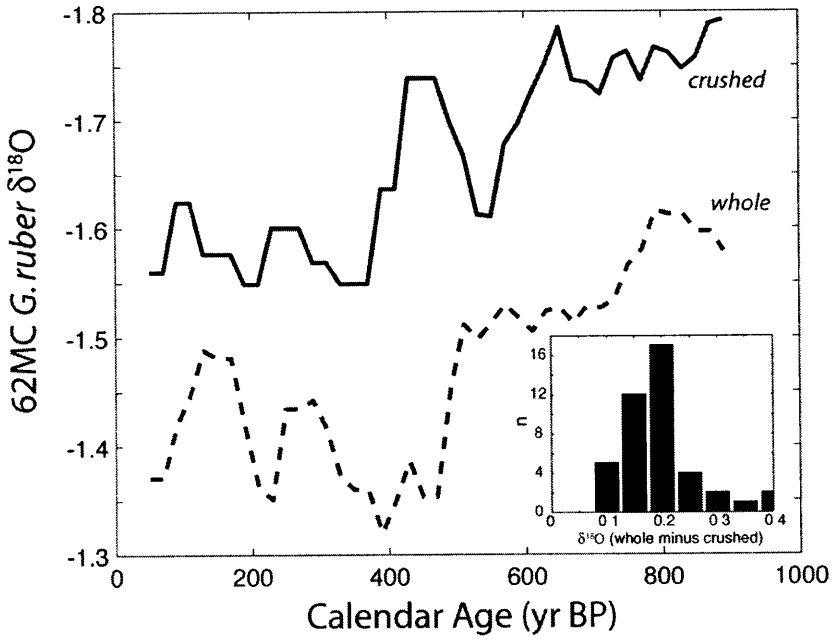

Figure 6

100-year running mean $\delta^{18}O_c$ for whole (dashed) and crushed (solid) foraminifera from 62MC. Inset) Histogram of whole $\delta^{18}O_c$ minus crushed $\delta^{18}O_c$ at each depth interval. The values based on whole foraminifera are consistently enriched in ^{18}O by 0.2 ‰. This offset may be due to variable isotopic exchange between phosphoric acid and evolved CO_2 associated with gas bubble production.

Downcore Results and Discussion

Surface water $\delta^{18}O_w$

Planktonic $\delta^{18}O_c$ and SST estimates from 62MC and 79GGC yield consistent changes in Florida Current $\delta^{18}O_w$ during the last 1,000 years. In 62MC, *G. ruber* $\delta^{18}O_c$ increased by approximately 0.2‰ over the past 900 years, with the largest change occurring from 400 yr BP to present (Figure 4a). The $\delta^{18}O_c$ increase is significant at the 95% confidence level and implies that Florida Current surface waters became progressively cooler, saltier, or both. Mg/Ca analyses of *G. ruber* indicate that SST was stable at 24.5°C from 900 to 500 yr BP, and then increased monotonically to ~25.5°C by 200 yr BP (Figure 4b). This SST maximum was followed by an abrupt 1°C decrease from 200 to 100 yr BP, and then a steady increase over the past 100 years. Reconciliation of the $\delta^{18}O_c$ and SST records requires $\delta^{18}O_w$ variability on the order of 0.4‰ (Figure 4c). Foraminiferal $\delta^{18}O_c$ in nearby core 79GGC was nearly constant from 1400 to 500 yr BP but then increased by 0.2-0.3 per mil at 500 yr BP (Figure 4d). Similar to 62MC, Mg/Ca-derived SSTs for 79GGC generally increase from 800 to 200 yr BP, although 79GGC is 0.9°C warmer on average over the past 800 years. This difference is similar to the coretop offset which reflects the strong SST gradient near Dry Tortugas (Methods).

The 79GGC time series extends the Dry Tortugas $\delta^{18}O_w$ record to 1400 yr BP and shows a distinct 0.1-0.2‰ increase at 900 yr BP, in addition to the larger 0.4‰ shift at

400 yr BP (Figure 4f). Although the absolute values for the Dry Tortugas $\delta^{18}O_w$ records are different, the magnitude and timing of their $\delta^{18}O_w$ variability is nearly identical. The parallel changes in the two records support their fidelity and indicate that each provides a robust signal of $\delta^{18}O_w$ variability at this location. The 0.2‰ offset between 62MC and 79GGC is caused by the difference in $\delta^{18}O_c$ from using whole versus crushed foraminifera for the stable isotopic analyses in these two cores (Methods).

On the Great Bahama Bank, significant changes in $\delta^{18}O_c$ and SST occurred during the past millennium, but with different timing than the Dry Tortugas sites. The largest change in 118MC $\delta^{18}O_c$ occurred from 200 yr BP to present (Figure 5a). A similar shift occurred about 100 years earlier in the 125MC record (Figure 5e). Since 118MC has better sampling resolution and chronological control than 125MC, the $\delta^{18}O_c$ increase most likely occurred after 200 yr BP. Mg/Ca-derived SSTs in 118MC increased gradually by 0.5°C from 500 yr BP to present (Figure 5b). Core 125MC extends the Great Bahama Bank SST record to 1400 yr BP and shows a ~0.5°C cooling at 800 yr BP, near the beginning of the LIA, and then a ~0.5°C warming at ~ 300 yr BP (Figure 5e). The combined $\delta^{18}O_c$ and SST records require that $\delta^{18}O_w$ along the Great Bahama Bank increased by ~0.3 per mil during the past 200 years (Figure 5c,f).

Sea-surface temperatures

The Great Bahama Bank results are inconsistent with foraminiferal SST estimates from the Sargasso Sea and the magnitude of LIA cooling inferred from Caribbean corals.

Rather than increasing after 400 yr BP, SSTs in the Sargasso Sea apparently decreased (Keigwin, 1996). This discrepancy may be due to the use of different SST proxies – $\delta^{18}O_c$ for the Sargasso Sea and Mg/Ca for the Great Bahama Bank. The data presented here suggest that high Sargasso Sea $\delta^{18}O_c$ after 200 yr BP may have be a result of high $\delta^{18}O_w$ rather than low SSTs. Estimates from Caribbean corals indicate SSTs were 1-3°C cooler than today during the coldest LIA intervals (Winter et al., 2000), significantly larger than the cooling along the Great Bahama Bank. The disagreement between the coral and Bahamas SST estimates may be due to the brief (~10 yr) time windows covered by the corals and signal smoothing in the foraminiferal records caused by bioturbation.

Interestingly, both Great Bahama Bank and Dry Tortugas SSTs warmed by ~0.5°C during the course of the LIA, from about 800 yr BP to 200 yr BP (Figure 7). As a result, the ~1.0°C cross-current SST gradient remained nearly constant during this time. Prior to 800 yr BP and after 200 yr BP, however, the cross-current gradient was 1.5-2.0°C, significantly larger than during the LIA interval. We believe this most likely reflects variable formation of Tortugas eddies, which today can shift SSTs at the 62MC and 79GGC core sites by >3°C for months at a time (SOG, Johns Hopkins; Fratantoni et al., 1998). Therefore, the LIA may have been characterized by reduced Tortugas eddy formation relative to the preceding and subsequent time intervals. This inference is opposite that based only on $\delta^{18}O_c$ from the Dry Tortugas sites (Lund and Curry, 2004). The apparent SST differences in 62MC and 79GGC over the past 600 years (Figure 7) are not significant at the 95% confidence level (Figure 4b, e).

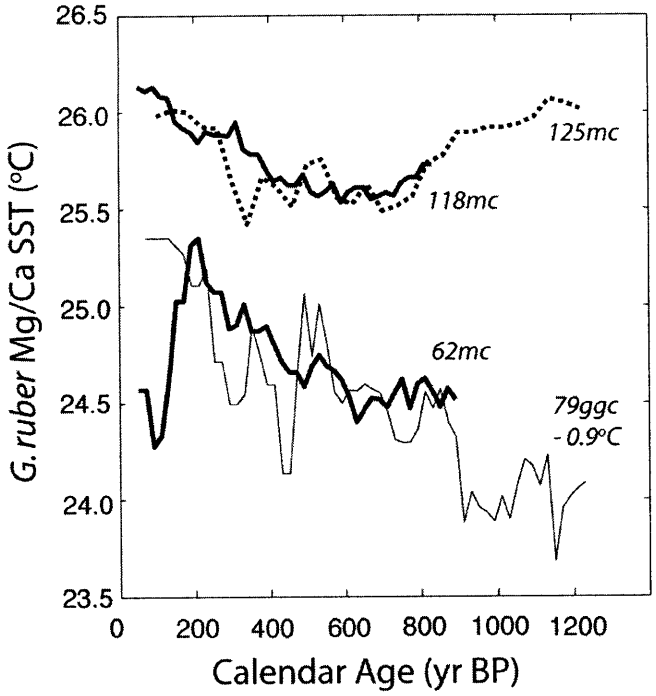

Figure 7
Compilation of smoothed SST records from the Great Bahama Bank (118MC-solid; 125MC-dashed) and Dry Tortugas (62MC-solid; 79GGC-thin solid). For clarity, the 79GGC time series was adjusted by –0.9°C (the average offset between 62MC and 79GGC from 0-800 yr BP). The largest cross-current SST gradient occurs prior to and after the Little Ice Age. All four time series indicate the Florida Current warmed by 0.5-1.0°C from 500 to 200 yr BP.

Carbonate Ion and ^{13}C Suess effects

Great Bahama Bank $\delta^{18}O_c$ (and hence calculated $\delta^{18}O_w$) may be influenced by decreasing surface water pH associated with the input of anthropogenic CO_2 over the past 200 years. As pH decreases, the greater proportion of bicarbonate to carbonate ion leads to isotopically heavier dissolved inorganic carbon, since bicarbonate is the more enriched of the two species (Zeebe, 1999). In laboratory culturing experiments, *G. ruber* $\delta^{18}O_c$ varies systematically with $[CO_3^{2-}]$ by a slope of -0.002±0.001‰/(μmol/kg) (Spero et al., 1999). During the last 200 years, surface North Atlantic subtropical gyre DIC has

increased ~60 μmol/kg due to anthropogenic CO_2 emissions (Sabine et al., 2004). Assuming constant near-surface alkalinity between the LIA and present (2400 μEq/kg; GEOSECS Stn. 31), we estimate that $[CO_3^{2-}]$ decreased by approximately 40 μmol/kg over this time interval (http://geosci.uchicago.edu/~archer/cgimodels/pco2.html), equivalent to a carbonate ion isotope effect on *G. ruber* $\delta^{18}O_c$ of +0.08±0.04‰. Therefore, approximately 0.1‰ of the $\delta^{18}O_w$ increase from the LIA to today may be attributed to decreasing surface water pH. If this is true, then the remainder (0.2‰) reflects increasing salinity of the surface North Atlantic subtropical gyre since the LIA.

Since carbonate ion concentration affects both the oxygen and carbon stable isotopes of foraminiferal calcite, it should be possible to verify the effect of pH on $\delta^{18}O_c$ using $\delta^{13}C_c$. Using a $[CO_3^{2-}]$ decrease of 40 μmol/kg and a *G. ruber* $\delta^{13}C_c/[CO_3^{2-}]$ relationship of -0.009±0.001‰/(μmol/kg) (Spero et al., 1999), the expected shift in $\delta^{13}C_c$ from LIA to present would be +0.35 per mil, similar to that observed in 118MC and 125MC (Figure 8a). However, if *G. ruber* $\delta^{13}C_c$ reliably records $\delta^{13}C$ of dissolved inorganic carbon ($\delta^{13}C_{DIC}$), it should reflect not only pH variability but also the influence of ^{13}C-depleted CO_2 from fossil fuel and biomass burning (the ^{13}C 'Suess effect'). Surface Atlantic $\delta^{13}C_{DIC}$ decreased by 0.8‰ over the past 200 years (Bohm et al., 1996), consistent with model estimates of mixed layer $\delta^{13}C_{DIC}$ driven by decreasing $\delta^{13}C$ of atmospheric CO_2 (Francey et al., 1999). Taking into account both the carbonate ion and Suess effects, the change in *G. ruber* $\delta^{13}C_c$ from 200 yr BP should be approximately –0.4 per mil, as opposed the observed signal of +0.3-0.4‰.

The 0.8‰ offset between predicted and observed $\delta^{13}C_c$ is either due to real changes in $\delta^{13}C_c$ or is an artifact of *G. ruber* vital effects. Increasing surface layer ΣCO_2 since the LIA would likely enhance biological carbon isotope fractionation and increase $\delta^{13}C_c$ (Jasper and Hayes, 1990; Hofmann et al., 1999). An increase in export production of ^{13}C-depleted organic matter could also enrich mixed layer ^{13}C of DIC. The situation is further complicated by the tendency of *G. ruber* $\delta^{18}C_c$ to be lower than ambient sea water $\delta^{13}C_{DIC}$. This offset is most likely a function of foraminiferal respiration, metabolic and growth rates, and symbiont photosynthesis, all of which are ecologically sensitive to oceanographic variability (Curry and Matthews, 1981; Spero and Lea, 1993; Russell and Spero, 2000). Regardless of the exact cause, it is clear *G. ruber* $\delta^{13}C_c$ on its own cannot be used to validate the effect of pH on $\delta^{18}O_c$.

The problematic nature of using *G. ruber* $\delta^{13}C_c$ as a proxy for $\delta^{13}C_{DIC}$ is further highlighted by the clear existence of the ^{13}C Suess effect in benthic foraminiferal $\delta^{13}C$ records from the Great Bahama Bank (Figure 8b). At water depths ranging from 250 to 700 m, four separate benthic time series show anomalous ^{13}C depletion during the past 200 years. The decrease in $\delta^{13}C_c$ near the core tops is unprecedented during the last millennium and the largest ^{13}C depletion occurs in the shallowest cores (<500 m), consistent with a surface ocean source of ^{13}C-depleted CO_2. This is the expected response to input of anthropogenic CO_2 into mid- to high-latitude North Atlantic surface waters and subsequent thermocline ventilation and transport along isopycnals into the subtropical gyre.

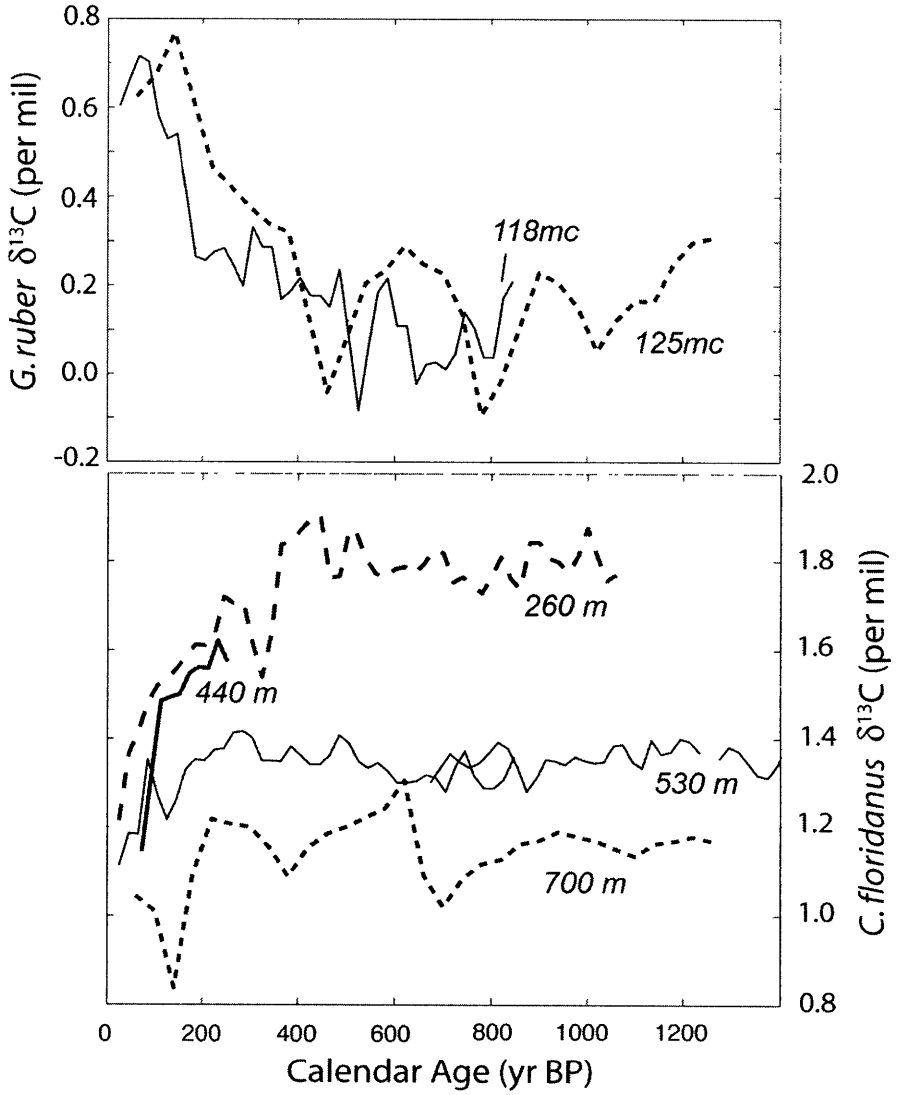

Figure 8

Great Bahama Bank *G. ruber* $\delta^{13}C$ (top) and *C. floridanus* $\delta^{13}C$ (bottom) over the past 1200 years. *C. floridanus* has been shown to reliably reflect the $\delta^{13}C_{DIC}$ gradient in the North Atlantic subtropical gyre thermocline (Slowey and Curry, 1995). Both the 118MC (solid) and 125MC (dashed) *G. ruber* $\delta^{13}C$ time series are 75-year running means. The benthic $\delta^{13}C$ time series are also 75-year running means, except for 125MC which was smoothed with a 150-year window. For raw data see Lund and Curry (in prep). *G. ruber* $\delta^{13}C$ increased during the past several hundred years, while the benthic $\delta^{13}C$ time series show the opposite trend. Although the planktonic $\delta^{13}C$ signal may reflect decreasing pH, it lacks the ^{13}C Suess effect apparent in the benthic $\delta^{13}C$ records (Lund and Curry, in prep) and other surface mixed layer $\delta^{13}C$ reconstructions (Bohm et al., 1996; Francey et al., 1999). We therefore conclude that additional metabolic or ecological factors account for the *G. ruber* $\delta^{13}C$ signal.

Sources of salinity variability

Florida Current $\delta^{18}O_w$ variability during the last millennium was most likely due large-scale changes in oceanic precipitation and evaporation. While variable flow of the Mississippi River and altered routing of oceanic currents may have played a minor role, the observed $\delta^{18}O_w$ signal is far too large to be explained by these mechanisms. Instead, southward migration of the Atlantic Hadley circulation during the Little Ice Age, in combination with a mean shift in thermocline $\delta^{18}O_w$, are the most likely mechanisms responsible for changes in $\delta^{18}O_w$ near Dry Tortugas and the Great Bahama Bank during the LIA.

Local/regional $\delta^{18}O_w$ effects

Input of isotopically light Mississippi River water may have influenced the Dry Tortugas $\delta^{18}O_w$ records, but only to a small extent. Today, the Mississippi River has an annual average flow rate of 0.015 Sv (Walker et al., 1994) and a $\delta^{18}O_w$ signature of –7‰ SMOW (Coplen and Kendall, 2000). Transport in the upper 100 m of the Florida Current is approximately 9 Sv (Schmitz and Richardson, 1991) with a $\delta^{18}O_w$ signature of ~0.9‰ (Methods).

If the isotopic signature of the oceanic and fluvial end members is held constant, the $\delta^{18}O_w$ increase in 62MC from 700 to 200 yr BP (0.4 per mil) would require Mississippi discharge to be ~33x higher at 700 yr BP (e.g. 0.015 Sv at 200 yr BP and 0.5 Sv at 700 yr BP). During the two-month peak of the 1993 flood event, one of the most

severe floods of the last century, the Mississippi discharge rate was 0.03 Sv (Walker et al., 1994), a doubling of the average rate, making even the 1993 flood too small to influence Florida Current $\delta^{18}O_w$ in a significant way. Given the unrealistic river flows required to create the observed changes in $\delta^{18}O_w$, and that these flow rates would have to persist for centuries, it is highly unlikely that variability in Mississippi River discharge significantly influenced Florida Current $\delta^{18}O_w$ during the last millennium.

On the Great Bahama Bank, variable current routing may have affected surface water $\delta^{18}O_w$ because the 118MC and 125MC core sites are located near the confluence of the Santaren and Florida Currents. Today, the Santaren Current supplies on average approximately 2 Sv of warm, salty water to the main flow of the Florida Current (Atkinson et al., 1995; Leaman et al., 1995). Lower Santaren Current flow during the LIA would likely result in lower salinity at the core sites. Despite the 0.2 psu difference in salinity on either side of the Florida Current, their $\delta^{18}O_w$ values are nearly equal (Methods). Therefore, reduced flow of the Santaren Current relative to the Florida Current during the LIA would not necessarily lead to lower surface water $\delta^{18}O_w$ along the Great Bahama Bank. If anything, increased Florida Current salinity during the LIA should lead to saltier conditions at the 118MC and 125MC core sites. What is remarkable is that LIA salinities on the GBB are anomalously low relative to coretop values, despite the proximity of the cores to the Florida Current (Figure 1).

Hadley Cell migration

The salinity changes on the Great Bahama Bank were very different than those at Dry Tortugas during the past 1,200 years. From 400 to 200 yr BP, when $\delta^{18}O_w$ was higher than today near Dry Tortugas, it was lower than today on the Great Bahama Bank (Figure 9). Beginning at 200 yr BP, $\delta^{18}O_w$ increased by ~0.2‰ on the Great Bahama Bank, while it decreased by 0.2-0.3‰ at Dry Tortugas. The largest cross-current difference in $\delta^{18}O_w$ occurred during the Little Ice Age, while the smallest offsets occurred from approximately 0 to 100 yr BP and 900 to 1200 yr BP. North-south movement of the Atlantic Hadley circulation is the most likely explanation of the observed $\delta^{18}O_w$ variability.

Given that Florida Current surface salinity is heavily influenced by E-P in the tropical Atlantic, reduced precipitation in this region during the Little Ice Age is the most logical cause of the observed changes. This interpretation is consistent with anomalously dry LIA conditions in the Yucatan Peninsula (Hodell et al., 2005) and northern South America near the Cariaco Basin (Haug et al., 2001). Comparison of Dry Tortugas $\delta^{18}O_w$ to the aridity record from the Cariaco Basin suggests a strong climatic link between the two (Figure 10). Cariaco Basin %Ti, which is assumed to be proportional to fluvial input, shows a long-term decrease beginning ~600 yr BP, with distinct minima clustered between 400 and 150 yr BP (Haug et al., 2001). The long-term drying of the Cariaco Basin region ended abruptly at 200 yr BP. Overall, the changes observed in 62MC and 79GGC $\delta^{18}O_w$ parallel those in Cariaco Basin %Ti. One mechanism that could cause this

common change is southward ITCZ migration, which would dry the watershed for the Cariaco Basin (Haug et al., 2001), and remotely force increased salinity in the Florida Current.

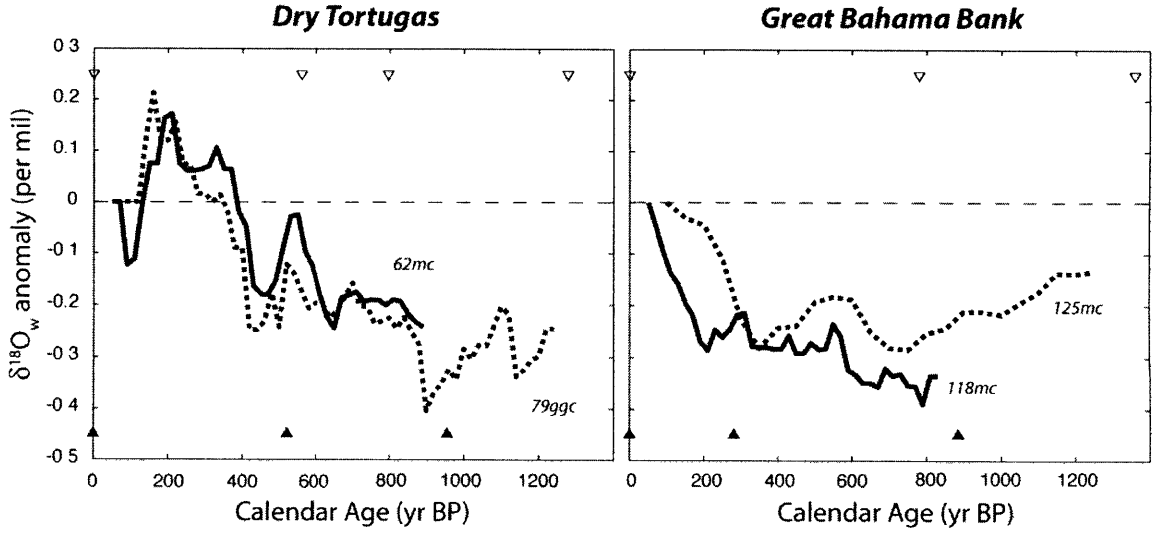

Figure 9

Left) Surface water $\delta^{18}O_w$ anomaly relative to coretop for the Dry Tortugas sites, 0-1400 yr BP (62MC, solid line; 79GGC, dashed line). Calendar age control points are given as triangles (62MC, solid; 79GGC, open). Right) Surface water $\delta^{18}O_w$ anomaly relative to coretop for the Great Bahama Bank sites 118MC (solid line) and 125MC (dashed line). If Great Bahama Bank surface layer [CO_3^{2-}] decreased by 60 μmol/kg over the past 200 years, then the $\delta^{18}O_w$ anomalies relative to coretop would be ~0.1 per mil less than plotted. The smallest offset between the Dry Tortugas and Great Bahama Bank $\delta^{18}O_w$ records occurred during two intervals: 0-100 yr BP and 900-1200 yr BP, coinciding with the modern and Medieval Warm Period, respectively. The largest offset occurred during the peak of the Little Ice Age (~100 to 400 yr BP).

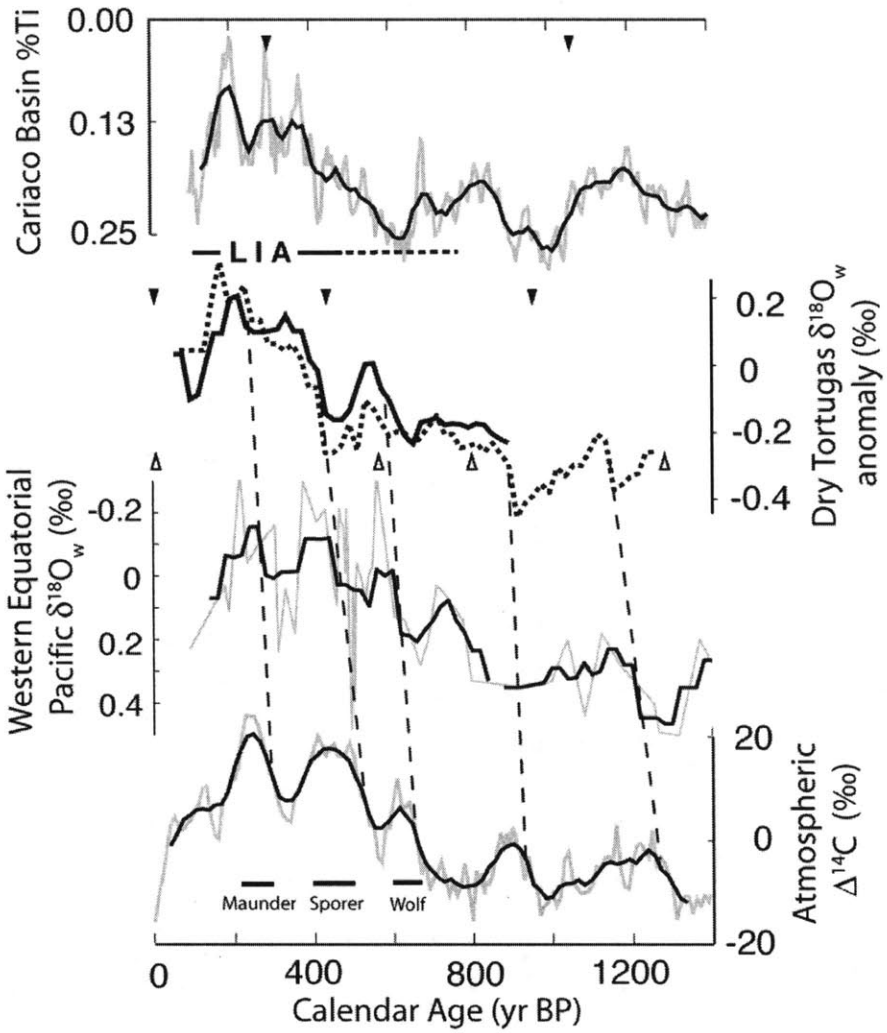

Figure 10

A) Cariaco Basin %Ti (grey, raw data; black, 80-year smooth) (Haug et al., 2001). Lower values imply greater aridity in northern Venezuela. B) Dry Tortugas $\delta^{18}O_w$ anomaly relative to core-top values (black, 62MC; dash, 79GGC; 100-year smooth). Increasing $\delta^{18}O_w$ indicates higher surface salinity. The saltiest Dry Tortugas and driest Cariaco Basin conditions occur during the LIA. Calendar age control points are noted with triangles. C) Western equatorial Pacific (WEP) $\delta^{18}O_w$ (grey, raw data; black, 100-year smooth) (Stott et al., 2004). Note y-axis is reversed. In general, the WEP and tropical Atlantic (Dry Tortugas) $\delta^{18}O_w$ records are anti-correlated. D) Tree-ring-based reconstruction of atmospheric radiocarbon (grey, 10-year bins; black, 80-year smooth) (Stuiver et al., 1998). Common $\Delta^{14}C_{atm}$ and tropical Atlantic $\delta^{18}O_w$ transitions also coincide with $\delta^{18}O_w$ transitions in the WEP (dashed black lines). Dry Tortugas and WEP $\delta^{18}O_w$ lags $\Delta^{14}C_{atm}$ by 50-100 years. A similar relationship exists with reconstructions of radiocarbon production rate (Bond et al., 2001; Marchal, 2005). The true phasing remains uncertain given the small lags involved (50-100 years) and the relatively large chronological uncertainties (>100 years).

On an interannual basis, southward migration of the Atlantic ITCZ can be caused by either an increased Atlantic cross-equatorial SST gradient or El Niño conditions in the equatorial Pacific (Chiang et al., 2002). Even slight (~0.2°C) cooling of the North Atlantic can force southward migration of the ITCZ, which in turn reduces precipitation in the tropical North Atlantic and creates a positive salinity anomaly in this region (Vellinga et al., 2002; Vellinga and Wu, 2004). The Florida Current $\delta^{18}O_w$ maxima and Cariaco Basin %Ti minima from 400 to 150 yr BP coincide with an interval of unusually cool conditions in several Northern Hemisphere records (Lamb, 1995; deMenocal et al., 2000; Dahl-Jensen et al., 1998; Huang et al., 2000). A southward shift in the ITCZ associated with Northern Hemisphere cooling can account for not only dry conditions near the Cariaco Basin (Haug et al., 2001), but also increased salinity of the Florida Current during the LIA.

Beginning at ~900 yr BP, $\delta^{18}O_w$ increased on the Florida Margin and decreased on the Great Bahama Bank, potentially reflecting southward migration of the Hadley cell and increased E-P in the tropical Atlantic and decreased E-P in the subtropical gyre. Several paleoclimate records indicate cooling in the North Atlantic region at about this time (Dahl-Jensen et al., 1998, Esper et al., 2002, deMenocal et al., 2000). The sharp decrease in $\delta^{18}O_w$ after 200 yr BP near Dry Tortugas and increase on Great Bahama Bank is consistent with warming since the LIA and an abrupt movement of the Hadley circulation to the north, causing relatively higher salinity in the subtropical gyre and lower salinity in the tropical Atlantic.

Surface ocean versus thermocline $\delta^{18}O_w$-S

The modern relationship between $\delta^{18}O_w$ and salinity in the tropical and subtropical Atlantic surface waters is described by a $\delta^{18}O_w$/S slope of approximately 0.2‰/psu (Figure 11a). In the subtropical gyre, $\delta^{18}O_w$ is high relative to the tropics since evaporation discriminates against ^{18}O. The resulting ^{16}O-enriched vapor rains out in the tropics and high-latitude Atlantic. At high latitudes, $\delta^{18}O$ decreases due to the preferential condensation of ^{18}O at cooler temperatures, making the $\delta^{18}O_w$/S slope steeper. Since these waters (up to ~45°N) ventilate the thermocline, the thermocline $\delta^{18}O_w$/S relationship (0.5‰/psu) is similar to that for the surface high-latitude North Atlantic.

Today, the Dry Tortugas and Bahamas sites differ by ~0.1‰ in $\delta^{18}O_w$ and ~0.2 psu in salinity (Figure 11a). During the LIA, $\delta^{18}O_w$ increased by 0.1‰ at Dry Tortugas and decreased by ~0.2‰ at the Great Bahama Bank. If this was a function of simply moving along the low latitude $\delta^{18}O_w$-S slope, this would imply LIA salinities of 36.5 at Dry Tortugas and 35.7 at the Bahamas (Figure 11b). This is unrealistic since it requires the surface North Atlantic subtropical gyre to be fresher than the tropical Atlantic (i.e. a reversal of the Hadley cell distribution of E-P). A more reasonable scenario involves southward migration of the Hadley circulation and its associated E-P patterns (Figure 11c). In this case, the tropical Atlantic becomes saltier along the 0.2‰ slope, but the subtropical gyre becomes fresher through greater influence of ^{18}O-depleted surface water from higher latitudes (equivalent to the thermocline $\delta^{18}O_w$-S line).

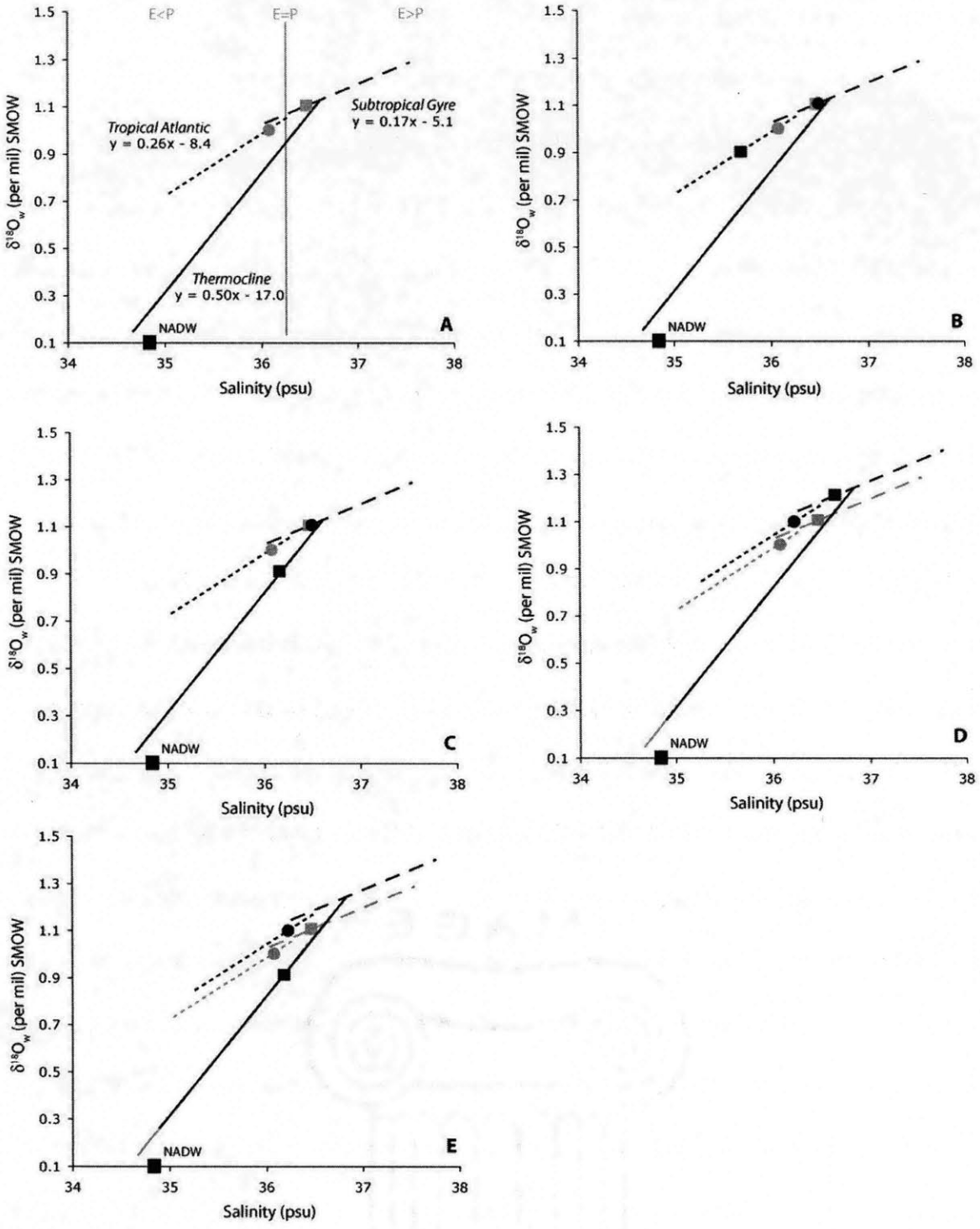
E<P
E=P
E>P
Tropical Atlantic
y = 0.26x - 8.4
Subtropical Gyre
y = 0.17x - 5.1
Thermocline
y = 0.50x - 17.0
NADW
A
B
C
D
E
δ18Ow (per mil) SMOW
Salinity (psu)

Figure 11

A) The modern $\delta^{18}O_w$-S regressions for the North Atlantic, including the tropics, subtropical gyre and thermocline (data from Schmidt et al., 1999). Since the thermocline is ventilated at mid- to high-latitudes, this line also represents the high-latitude surface North Atlantic. Based on modern annual average salinity of 36.1, the Dry Tortugas sites plot along the tropical relationship ($\delta^{18}O_w$ = 0.95; grey circle) where E-P (evaporation-precipitation) is negative. The Great Bahama Bank sites, with average salinity of 36.3, plot along the subtropical gyre line ($\delta^{18}O_w$ = 1.05; grey square), where E-P is positive. Today's average $\delta^{18}O_w$-S for North Atlantic Deep Water is noted with the solid square (Craig and Gordon, 1965). B) Little Ice Age $\delta^{18}O_w$ values at Dry Tortugas (black circle) were ~0.1‰ heavier than today while the Bahamas sites (black square) were ~0.2‰ lighter. Using the modern low-latitude slopes, this scenarios implies the Dry Tortugas sites were 1 psu saltier than the Bahamas, an unrealistic possibility. C) In the southward Hadley Cell migration case (see text), Dry Tortugas values increase along the low-latitude line as before, but now the Bahamas are influenced by a greater proportion of high-latitude ^{18}O-depleted water and therefore move along the 0.5‰ slope. The LIA salinity values remain reversed, but to a lesser extent than the previous scenario. D) An increase in the mean thermocline $\delta^{18}O_w$ of 0.1‰ moves all the lines upward along the 0.5‰ slope, easily accounting for the LIA Dry Tortugas $\delta^{18}O_w$ (black circle), but also causing the Bahamas to increase by 0.1‰ (black square), opposite the observed change. E) A combination of the models in C) and D), where the mean thermocline $\delta^{18}O_w$-S increases and the Hadley circulation migrates southward. This is the most realistic model for the data as it eliminates the pitfall of a reversed salinity gradient.

The situation depicted in Figure 11c allows $\delta^{18}O_w$ at Great Bahama Bank to be lower than Dry Tortugas and minimizes the LIA salinity difference between the two sites. Although less extreme than the first case, this scenario still requires a salinity gradient the reverse of today.

Surface water $\delta^{18}O_w$ is not only a function of evaporation and precipitation, but also the $\delta^{18}O_w$ of water with which it mixes. For the surface North Atlantic, this mixing component is the thermocline, characterized by a $\delta^{18}O_w$/S relationship of ~0.5‰/psu (Schmidt et al., 1999). If thermocline $\delta^{18}O_w$ and salinity varied during the LIA, it would likely be along the ~0.5‰/psu slope. Since the thermocline dominates the surface layer from a volumetric standpoint, the entire low latitude surface Atlantic $\delta^{18}O_w$/S relationship would also move along a thermocline slope to retain mass balance (Craig and Gordon, 1965). In this way, a 0.1‰ increase in mean thermocline $\delta^{18}O_w$ could account for the 0.1‰ increase at Dry Tortugas during the LIA (Figure 11d). The thermocline scenario would also require a positive shift in Great Bahama Bank $\delta^{18}O_w$, however, opposite that observed.

The scenario most consistent with the sign and magnitude of $\delta^{18}O_w$ variability in our records involves a combination of the thermocline and Hadley circulation models (Figure 11e). Higher mean thermocline $\delta^{18}O_w$ reduces the implied LIA salinity change at Dry Tortugas and southward migration of the Hadley cell and provides a mechanism for introducing ^{18}O-depleted surface waters into the subtropical gyre. This approach avoids

the pitfall of a reversed salinity gradient by moving each site in opposite directions along lines with 0.5‰/psu slopes. In fact, the only way to accommodate the opposing changes in $\delta^{18}O_w$ on either side of the Florida Current is to invoke the influence of high-latitude and thermocline waters. Using today's low-latitude 0.2‰/psu spatial $\delta^{18}O_w$-S relationship to estimate past changes in salinity yields unreasonable results (Figure 11b). If we use instead use the 0.5‰/psu slope, then LIA salinities at Dry Tortugas and Great Bahama Bank were nearly equal. This does not mean that salinities in the subtropical gyre and tropical Atlantic were also equal – today the salinity offset between these regions is on the order of ~1 psu, whereas the offset between the coring sites is only ~0.3 psu. During the LIA, therefore, the salinity gradient between the tropics and subtropical gyre was likely lower than today, but probably not zero.

El-Niño Southern Oscillation

Of course, the North Atlantic does not act independently of the remainder of the climate system. Anomalous atmospheric convection in the eastern equatorial Pacific during El Niño events forces subsidence and decreased precipitation over the tropical North Atlantic (Chiang et al., 2002). El Niño events also cause the main locus of rainfall to migrate into the central equatorial Pacific, away from its more typical location in the western equatorial Pacific (WEP) (http://www.cdc.noaa.gov/ENSO). Coral $\delta^{18}O$ records show a decreased equatorial Pacific zonal SST gradient during the LIA, possibly caused by more frequent El Niño events during this time (Hendy et al., 2002; Cobb et al., 2003). If the inter-annual model can be applied to longer time scales, El Niño-like conditions

would lead to decreased precipitation in the northern tropical Atlantic, as is observed, but also in the WEP. Available evidence shows that this did not occur. Low $\delta^{18}O_w$ in the WEP during the LIA (Stott et al., 2004) is inconsistent with the simple interannual model (Figure 10). Either ENSO played little role in Atlantic ITCZ movement or the MD81 $\delta^{18}O_w$ record reflects climatic processes other than ENSO.

Inter-basin vapor transport

Given that the Dry Tortugas and WEP $\delta^{18}O_w$ display similar but opposite variability during the last 1200 years (Figure 10), it is possible the records are linked via inter-basin vapor transport. From 900 to 200 yr BP, $\delta^{18}O_w$ increased by 0.6‰ near Dry Tortugas while it decreased by 0.5‰ in the WEP. Centennial-scale events in each record correspond remarkably well; positive $\delta^{18}O_w$ transitions in the Dry Tortugas records at approximately 200, 400, 600, and 1200 yr BP match negative $\delta^{18}O_w$ transitions in the WEP time series. Although the similarity of the two records is compelling, the inter-basin idea is problematic because the magnitude of the $\delta^{18}O_w$ changes in the two basins are comparable. If Atlantic to Pacific vapor transport is the sole mechanism involved, then the magnitude of the WEP $\delta^{18}O_w$ variability should be significantly smaller given the vastly greater size of the equatorial Pacific.

Since inter-basin changes in $\delta^{18}O_w$ of similar magnitude due to vapor transport seems unlikely, we believe it is more feasible that the Dry Tortugas and western equatorial Pacific $\delta^{18}O_w$ records responded independently to Northern Hemisphere

cooling during the Little Ice Age. Simulated WEP rainfall is anomalously high when North Atlantic SSTs are suppressed (Vellinga et al., 2002), apparently due to a weakened summer monsoon driven by cooling of Southeast Asia. We speculate that cold conditions in the Northern Hemisphere caused positive Florida Current $\delta^{18}O_w$ anomalies via southward migration of the Atlantic ITCZ and negative WEP $\delta^{18}O_w$ anomalies via a weaker Southeast Asian monsoon.

Role of solar variability

Reduced sunspot counts (Eddy, 1976), higher atmospheric $\Delta^{14}C$ ($\Delta^{14}C_{atm}$) (Stuiver et al. 1991) and greater ^{10}Be flux (Bard et al., 2000) all imply solar irradiance was lower than today during the LIA. High $\Delta^{14}C_{atm}$ during the Maunder, Spörer, and Wolf sunspot minima matches intervals of high Florida Current $\delta^{18}O_w$ and low western equatorial Pacific $\delta^{18}O_w$ (Figure 10). The $\delta^{18}O_w$ records appear to lag $\Delta^{14}C_{atm}$ by 50-100 years, assuming surface reservoir ages were similar to modern values over the past 1200 years. A similar lag is observed when comparing $\delta^{18}O_w$ with modeled estimates of radiocarbon production rate (Bond et al., 2001; Marchal, 2005). If this lag is correct, then it appears that solar variability paced not only migration of the North Atlantic subpolar front (Bond et al., 2001) but also centennial-scale hydrologic variability in both the tropical Atlantic and Pacific.

Numerical simulations of the evaporation-precipitation (E-P) response to reduced solar irradiance lack the positive E-P anomaly in the tropical North Atlantic and negative

E-P anomaly in the tropical South Atlantic characteristic of southward ITCZ migration (Rind and Overpeck, 1993). An imposed 1-2°C cooling across the entire North Atlantic is capable of creating the tropical Atlantic E-P dipole pattern, however (Rind and Overpeck, 1993). Dynamics of the ocean and atmosphere coupling not yet included in solar irradiance models may create very different temperature and E-P anomalies. Reduced northward surface heat transport associated with weaker meridional overturning or wind-driven subtropical gyre circulation may provide the cooling necessary to force ITCZ movement. Available paleoclimate evidence for reduced North Atlantic Deep Water production during the LIA is equivocal (Keigwin and Boyle, 2000).

Conclusions

The surface hydrography of the Florida Current was highly variable during the last millennium. Near Dry Tortugas, salinity increased by 0.8-1.5 psu during the course of the Little Ice Age. Similar although larger changes in tropical Atlantic salinity and northern hemisphere temperature are observed on glacial-interglacial and millennial timescales (Schmidt et al., 2004; Schmidt et al., 2004b). Thus this pattern of climate variability is not necessarily a manifestation of large continental ice sheets as it can occur under climatic boundary conditions very similar to today. Variable solar irradiance apparently paced shifts in Florida Current salinity during the last millennium, implying the transport of salt into the North Atlantic is sensitive to modest changes in solar forcing on centennial time scales. The lack of evidence for variable Atlantic overturning during the LIA (Keigwin and Boyle, 2000) suggests that southward ITCZ migration and increased Gulf Stream salinity may act to stabilize changes in North Atlantic Deep Water production, as is predicted by model studies (Vellinga et al., 2002).

On the Great Bahama Bank, where surface waters reflect the influence of the North Atlantic subtropical gyre, SST and $\delta^{18}O_w$ records display different variability than their Dry Tortugas counterparts. Sea-surface temperatures decreased by 0.5°C at the beginning of the LIA, consistent with the timing of cooling in several Northern Hemisphere temperature records. SSTs increased by 0.5°C about 200 yrs prior to the LIA termination, however, suggesting a more heterogeneous temperature anomaly pattern at the end of the LIA. If $\delta^{18}O_w$ on the Great Bahama Bank represents primarily

salinity rather than anthropogenically-driven pH effects, then surface salinity increased ~0.4 psu during the last 200 years, making the modern values the saltiest of the last millennium.

References

Atkinson, L. P., T. Berger, P. Hamilton, and E. Waddell, K. Leaman, and T. N. Lee (1995), Current meter observations in the Old Bahama Channel, *J. Geophys. Res., 100*, 8555-8560.

Anand, P., H. Elderfield, and M. H. Conte, Calibration of Mg/Ca thermometry in planktonic foraminifera from a sediment trap time series (2003), *Paleoceanography, 18(2)*, 1050, doi:10.1029/2002PA000846.

Bard, E., G. Raisbeck, F. Yiou, and J. Jouzel (2000), Solar irradiance during the last 1200 years based on cosmogenic nuclides, *Tellus, 52B*, 985-992.

Bohm, F., M. M. Joachimski, H. Lehnert, G. Morgenroth, W. Kretschmer, J. Vacelet, W. Chr. Dullo (1996), Carbon isotopic records from extant Caribbean and South Pacific sponges: Evolution of $\delta^{13}C$ in surface water DIC, *Earth and Planetary Science Letters, 139*, 291-303.

Bond, G., B. Kromer, J. Beer, R. Muscheler, M. N. Evans, W. Showers, S. Hoffmann, R. Lotti-Bond, I. Hajdas, and G. Bonami (2001), Persistent solar influence on North Atlantic climate during the Holocene, *Science, 294,* 2130-2136.

Boyle, E. A., and L. D. Keigwin (1985), Comparison of Atlantic and Pacific paleochemical records for the last 250,000 years: changes in deep ocean circulation and chemical inventories, *Earth Planet. Sci. Lett., 76*, 125-150.

Bradley, R. S., and P. D. Jones (1993), Little Ice Age summer temperature variations: their nature and relevance to recent global warming trends, *Holocene, 3*, 367-376.

Broecker, W. S., T. H. Peng, J. Jouzel, and G. Russell (1990), The magnitude of global fresh-water transports of importance to ocean circulation, *Clim. Dyn., 4*, 73-79.

Carton, J. A., and B. S. Giese (2005), SODA: A Reanalysis of Ocean Climate, submitted to *JGR-Oceans* (http://www.atmos.umd.edu/~carton/pdfs/carton&giese05.pdf)

Chiang. J. C. H., Y. Kushnir, and A. Giannini (2002), Deconstructing Atlantic ITCZ variability: Influence of the local cross-equatorial SST gradient and remote forcing from the eastern equatorial Pacific, *J. Geophys. Res., 107*, doi: 10.1029/2000JD000307.

Chinn, T. J. (1996), New Zealand glacier responses to climate change of the past century, *New Zealand Journal of Geology and Geophysics, 39*, 415-428.

Cobb, K. M., C. D. Charles, H. Cheng, and R. L. Edwards (2003), El Niño/Southern Oscillation and tropical Pacific climate during the last millennium, *Nature, 424*, 271-276.

Coplen, T. B., and C. Kendall (2000), Stable hydrogen and oxygen isotope ratios for selected sites of the U. S. Geological Survey's NASQAN and Benchmark Surface-water Networks, *U. S. Geological Survey Open-File Report 00-160.*

Craig H. and L. I. Gordon (1965), Isotopic Oceanography: Deuterium and oxygen 18 variations in the ocean and marine atmosphere, in *Symposium on Marine Geochemistry*, Graduate School of Oceanography, Univ. Rhode Island, Occ. Publ. No. 3, 277-374.

Curry, W. B. and R. K. Matthews (1981), Equilibrium ^{18}O fractionation in small size planktic foraminifera: Evidence from recent Indian Ocean sediments, *Marine Micropaleontology, 6*, 327-337.

Dahl-Jensen, D., K. Mosegaard, N. Gundestrup, G. D. Clow, S. J. Johnsen, A. W. Hansen, and N. Balling (1998), Past temperatures directly from the Greenland ice sheet, *Science, 282*, 268-271.

deMenocal, P., J. Ortiz, T. Guilderson, and M. Sarnthein (2000), Coherent high- and low-latitude variability during the Holocene warm period, *Science, 288*, 2198-2202,

Denton, G. H., and W. Karlén (1973), Holocene climatic variations – their pattern and possible cause, *Quat. Res., 3*, 155-205.

Deuser, W. G. (1987), Seasonal variations in isotopic composition and deep-water fluxes of the tests of perennially abundant planktonic foraminifera of the Sargasso Sea: results from sediment-trap collections and their paleoceanographic significance, *Journal of Foraminiferal Research, 17*, 14-27.

Druffel, E. M. (1982), Banded corals: Changes in oceanic carbon-14 during the Little Ice Age, *Science, 218*, 13-19.

Eddy, J. M. (1976), The Maunder Minimum, *Science, 192*, 1189-1202.

Esper, J., E. R. Cook, and F. H. Shweingruber (2002), Low-frequency signals in long tree-ring chronologies for reconstructing past temperature variability, *Science, 295*, 2250-2253.

Fairbanks, R. G., M Sverdlove, R. Free, P. H. Wiebe, and Allan W. H. Bé (1982), Vertical distribution and isotopic fractionation of living planktonic foraminifera from the Panama Basin, *Nature, 298*, 841-844.

Francey, R. J., C. E. Allison, D. M. Etheridge, C. M. Trudinger, I. G. Enting, M. Leuenberger, R. L. Langenfelds, E. Michel, and L. P. Steele (1999), A 1000-yr high precision record of $\delta^{13}C$ in atmospheric CO_2, *Tellus, 51B*, 170-193.

Fratantoni, P. S., T. N Lee, G. P. Podesta, and F. Muller-Karger (1998), The influence of Loop Current perturbations on the formation and evolution of Tortugas eddies in the southern Straits of Florida, *J. Geophys. Res., 103*, 24759-24779.

Grove, J. M. (1988), *The Little Ice Age*, Methuen, New York, 498 pp.

Haug, G., K. A. Hughen, D. M. Sigman, L. C. Peterson, and U. Rohl (2001), Southward migration of the ITCZ through the Holocene, *Science, 293*, 1304-1308.

Hendy, E. J., M. K. Gagan, C. A. Alibert, M. T. McCulloch, J. M. Lough, and P. J. Isdale (2002), Abrupt decrease in tropical Pacific sea surface salinity at end of Little Ice Age, *Science, 295*, 1511-1514.

Hodell, D. A., M. Brenner, J. H. Curtis, R. Medina-Gonzalez, E. Ildefonso-Chan Can, A. Albornaz-Pat, T. P. Guilderson (2005), Climate change on the Yucatan Peninsula during the Little Ice Age, *Quat. Res., 63*, 109-121.

Hofmann, M., W. S. Broecker, and J. Lynch-Stieglitz (1999), Influence of a $[CO_2(aq)]$ dependent biological C-isotope fractionation on glacial $^{13}C/^{12}C$ ratios in the ocean, *Global Biogeochemical Cycles, 13 (4)*, 873-883.

Huang, S., H. N. Pollack, and P. Shen (2000), Temperature trends over the past five centuries reconstructed from borehole temperatures, *Nature, 403*, 756-758.

Jasper, J. P., and J. M. Hayes, A carbon isotope record of CO_2 levels during the late Quaternary, *Nature, 347*, 462-464.

Keigwin, L. D., and G. A. Jones (1990), Deglacial climatic oscillations in the Gulf of California, *Paleoceanography, 5*, 1009-1023.

Keigwin, L. D., The Little Ice Age and Medieval Warm Period in the Sargasso Sea, *Science, 274*, 1504-1508 (1996).

Keigwin, L., and E. A. Boyle (2000), Detecting Holocene changes in thermohaline circulation, *Proceedings of the National Academy of Sciences 97*, 1343-1346.

Kim, S. T., and J. O'Neil (1997), Equilibrium and non-equilibrium oxygen isotope effects in synthetic carbonates, *Geochim. Cosmochim. Acta., 61*, 3461-3475.

Lamb, H., (1995) *Climate, History and the Modern World* (Routledge, London, New York, ed. 2).

Leaman, K. D., P. S. Vertes, L. P. Atkinson, T. N. Lee, P. Hamilton, and E. Waddell (1995), Transport, potential vorticity, and current/temperature structure across Northwest Providence and Santaren Channels and the Florida Current off Cay Sal Bank, *J. Geophys. Res., 100*, 8561-8569.

Levitus, S., R. Burgett, and T.P. Boyer, World Ocean Atlas (1994), Volume 3: Salinity & Volume 4: Temperature, NOAA Atlas NESDIS 3 & 4. U.S. Department of Commerce, Washington, D.C.

Lund, D. C., and W. B. Curry (2004), Late Holocene variability in Florida Current surface density: Patterns and possible causes, *Paleoceanography, 19*, PA4001, doi: 10.1029/2004PA001008.

Lynch-Stieglitz, J., W. B. Curry, and N. Slowey, A geostrophic estimate for the Florida Current from the oxygen isotope composition of benthic foraminifera, *Paleoceanography, 14*, 360-373, 1999.

Lohmann, G. (2003), Atmospheric and oceanic freshwater transport during weak Atlantic overturning circulation, *Tellus, 55A*, 438-449.

Mann, M. E., R. S. Bradley, M. K. Hughes (1999), Northern Hemisphere Temperatures during the past millennium: inferences, uncertainties, and limitations, *Geophys. Res. Lett., 26*, 759-762.

Marchal, O. (2005), Optimal estimation of atmospheric ^{14}C production over the Holocene: paleoclimate implications, *Climate Dynamics, 24*, 71-88.

Ostermann, D. R., and W. B. Curry (2000), Calibration of stable isotopic data: an enriched $\delta^{18}O$ standard used for source gas mixing detection and correction, *Paleoceanography, 15*, 353-360.

Rind, D., and J. Overpeck (1993), Hypothesized causes of decade- to century-scale climate variability: Climate model results, *Quaternary Science Reviews, 12*, 357-374.

Rosenthal, Y., E. A. Boyle, and L. Labeyrie (1997), Last glacial maximum paleochemistry and deepwater circulation in the Southern Ocean: Evidence from foraminiferal cadmium, *Paleoceanography, 12(6)*, 787-796.

Rosenthal, Y., M. P. Field, and R. M. Sherrell (1999), Precise determination of element/cadmium ratios in calcareous samples using sector field inductively coupled plasma mass spectrometry, *Anal. Chem., 71*, 3248-3253.

Russell, A. D., and H. J. Spero (2000), Field examination of the oceanic carbonate ion effect on stable isotopes in planktonic foraminifera, *Paleoceanography, 15(1)*, 43-52.

Sabine, C. L., R. A. Feely, N. Gruber, R. M. Key, K. Lee, J. L. Bullister,, R. Wannikof, C. S. Wong, D. W. R. Wallace, B. Tilbrook, F. J. Millero, T-H. Peng, A. Kozyr, T. Ono, and A. F. Rios (2004), The Oceanic Sink for Anthropogenic CO_2, *Science, 305*, 367-371.

Schmidt, G.A., G. R. Bigg and E. J. Rohling. 1999. "Global Seawater Oxygen-18 Database". http://www.giss.nasa.gov/data/o18data/

Schmidt, M. W., H. J. Spero, and D. W. Lea (2004), Links between salinity variation in the Caribbean and North Atlantic thermohaline circulation, *Nature, 428*, 160-163.

Schmidt, M. W., M. J. Vautravers, H. J. Spero (2004), *Eos Trans. AGU*, 85(47), Fall Meet. Suppl., Abstract PP44A-06.

Schmitz, W. J., and P. Richardson (1991), On the sources of the Florida Current, *Deep-Sea Research, 38*, s379-s409.

Slowey, N. C., and W. B. Curry (1995), Glacial-interglacial differences in circulation and carbon cycling within the upper western North Atlantic, Paleoceanography, 10(5), 715-732.

Spero, H. J., and D. W. Lea (1993), Intraspecific stable isotope variability in the planktic foraminifera Globigerinoides sacculifer: Results from laboratory experiments, *Marine Micropaleontology, 22*, 221-234.

Spero, H. J., J. Bijma, D. W. Lea, and A. D. Russell (1999), Deconvolving glacial ocean carbonate chemistry from the planktonic foraminifera carbon isotope record, in *Reconstructing Ocean History: A Window into the Future*, edited by F. Abrantes and A. Mix, pp. 329-342, Plenum, New York.

Stott, L., K. Cannariato, R. Thunnell, G. H. Haug, A. Koutavas, and S. Lund (2004), Decline of surface temperature and salinity in the western tropical Pacific Ocean in the Holocene epoch, *Nature, 431*, 56-59.

Stuiver, M., T. F. Braziunas, B. Becker, and B. Kromer (1991), Climatic, solar, oceanic and geomagnetic influences on late-glacial and Holocene atmospheric $^{14}C/^{12}C$ change, *Quat. Res., 35*, 1-24.

Stuiver, M., P. J. Reimer, E. Bard, J. W. Beck, G. S. Burr, K. A. Hughen, B. Kromer, F. G. McCormac (1998), J. v. d. Plicht, and M. Spurk, INTCAL98 radiocarbon age calibration 24,000 - 0 cal BP, Radiocarbon, 40, 1041-1083.

Swart, P. K., S. J. Burns, and J. J. Leder (1991), Fractionation of the stable isotopes of oxygen and carbon dioxide during the reaction of calcite with phosphoric acid as a function of temperature and technique, *Chemical Geology, 86*, 89-96.

Thompson, L. G. (1995), Ice core evidence from Peru and China, in *Climate Since A. D. 1500*, edited by R. S. Bradley and P. D. Jones, pp. 517-548, Routledge, New York.

Vellinga, M., R. A. Wood, and J. M. Gregory (2002), Processes governing the recovery of a perturbed thermohaline circulation in HadCM3, *J. Clim., 15*, 764-780.

Vellinga, M., and R. A. Wood (2002), Global climatic impacts of a collapse of the Atlantic thermohaline circulation, *Climatic Change, 54*, 251-257.

Vellinga, M., and P. Wu (2004), Low-latitude freshwater influence on centennial-scale variability of the Atlantic thermohaline circulation, *J. Clim., 17*, 4498-4511.

Waliser, D. E., and C. Gautier (1993), A satellite-derived climatology of the ITCZ, *J. Clim., 6*, 2162-2174.

Walker, N. D., L. J. Rouse, G. S. Fargion, and D. C. Biggs (1994), The Great Flood of summer 1993: Mississippi River discharge studied, *Earth in Space, 7(3)*, 11-14, American Geophysical Union.

Walters, L. J., G. E. Claypool, and P. W. Choquette (1972), Reaction rates and $\delta^{18}O$ variations for the carbonate –phosphoric acid preparation method, *Geochim. Cosmochim. Acta, 36*, 129-140.

Winter, A., H. Ishioroshi, T. Watanabe, T. Oba, and J. Christy (2000), Caribbean sea surface temperatures: two-to-three degrees cooler than present during the Little Ice Age, *Geophys. Res. Lett., 27,* 3365-3368.

Zeebe, R. E. (1999), An explanation of the effect of seawater carbonate concentration on foraminiferal oxygen isotopes, *Geochim. Cosmochim. Acta, 63*, 2001-2007.

Chapter 4:

Florida Current Density Structure and Transport during the Last Millennium

Abstract

The largest climate anomaly of the last millennium prior to the 20th century was the Little Ice (LIA; ~1200 to 1850 A. D.), an interval of generally cooler climatic conditions in the Northern Hemisphere. The primary goal of this work was to determine if the Gulf Stream was weaker during the LIA, and if so, whether it contributed to Northern Hemisphere cooling. Using a suite of well-dated, high-resolution cores spanning the depth and width of the Florida Current, we reconstructed the cross-current density gradient using benthic and planktonic foraminiferal $\delta^{18}O$. We found that the average density gradient and vertical current shear varied by ~10% during last millennium. Assuming a constant level of no motion at 850 m water depth, we estimate that LIA Florida Current transport was 2-3 Sv lower than today and ~1100 yr BP. The timing of reduced flow is consistent with anomalously cold conditions in several paleoclimate archives, implicating Gulf Stream heat transport as a contributor to centennial-scale climate variability during the last millennium.

Lower volume transport during the LIA occurred primarily in the 100-500 m depth range of the Florida Current, water which today originates in the wind-driven subtropical gyre. This suggests that low LIA flow was largely associated with weaker winds in the mid- to low-latitude North Atlantic. The water column at the Great Bahama Bank was more stratified during the LIA than today, as a result of denser water below the thermocline and less dense water above it. It is possible that the change in stratification was driven primarily by salinity. Saltier thermocline conditions may be linked to anomalously high salinity surface water in the Florida Current via thermocline ventilation at the northern edge of the gyre. Stratification was likely amplified by reduced wind-stress curl and Ekman pumping, limiting the exchange of water between the surface mixed layer and thermocline.

Introduction

The Florida Current, the portion of the Gulf Stream confined to the Straits of Florida, is a key component of the North Atlantic circulation. The flow of the Florida Current reflects both wind-driven processes in the subtropical gyre and the surface compensating flow for North Atlantic Deep Water formation. The Florida Current is a major component of the meridional overturning circulation which transports approximately 1.3 PW (1 PW = 10^{15} W) of heat across 24.5°N (Molinari et al., 1985; Larsen et al., 1992) and therefore plays a key role in regulating the climate of the North Atlantic region. While the Florida Current-Gulf Stream system is probably the most studied feature in modern oceanography, almost nothing is known about its behavior on centennial to millennial time scales. Observations are largely limited to sea-surface temperature or snapshot flow estimates during the 20th century.

Here we present evidence for centennial-scale variability in Florida Current subsurface density structure over the past 1,100 years based on the $\delta^{18}O$ of foraminifera. Overall, we find that the cross-current density gradient was remarkably constant during the last millennium, equivalent to transport variability on the order by 10%. Small but statistically significant changes transport did occur, however. Specifically, transport during the Medieval Warm Period (~1000 A. D.) was similar to today, while during the Little Ice Age (LIA; ~1200 to 1850 A. D.) it was 2-3 Sv lower. Therefore, the LIA, which is characterized by unusually cool Northern Hemisphere conditions, may have in part been caused by reduced northward oceanic heat transport. Reduced Gulf Stream flow may explain the apparent contradiction between modeled and proxy estimates of Northern Hemisphere temperature during the last millennium

Historical observations and modern flow estimates

Hydrographic surveys of the Gulf Stream began more than 150 years ago. Beginning in 1845, the U. S. Coast and Geodetic Survey, under the direction of A. D. Bache, constructed temperature sections at multiple locations along the flow axis of the Florida Current (Bache, 1860). Later in the 19th century, J. E. Pillsbury conducted a series of detailed Florida Current velocity measurements that would later be used to validate transport estimates based on the geostrophic method (Pillsbury, 1890; Wüst, 1924). Subsequent studies have utilized the geostrophic (e.g. Montgomery, 1941), dropsonde (Schmitz and Richardson, 1968; Niiler and Richardson, 1973), Pegasus acoustic profiler (Leaman et al., 1987; 1995), current meter (Schott et al., 1988) and voltage difference (Wertheim, 1954; Larsen, 1992; Baringer and Larsen, 2001) techniques to calculate Florida Current transport on daily to interannual time scales.

Depending on the time and place of measurement, transport of the Florida Current is estimated to be approximately 30 Sv (1 Sv=1x10^6 m^3 s^{-1}). Current meter data from Pillsbury suggest that annual average transport near Miami during the late 1880s was 25-29 Sv (Schmitz and Richardson, 1968), compared to 26 Sv estimated using hydrographic observations (Wust, 1924). From 1964-1970, average transport at Miami was 30 Sv (Niiler and Richardson, 1973). Further south, between Dry Tortugas and Havana, Pillsbury (1887), Montgomery (1941), and Wertheim (1954), estimated annual average transports of 27-28 Sv. These results are not directly comparable to those further north, however, given the input of flow from the Santaren Channel, located between Cay Sal and Great Bahama Bank (Figure 1). If we add 2 Sv to account for flow from the Santaren Channel (Leaman et al., 1995), the Dry Tortugas-Havana values range from 29 to 30 Sv, very similar to those at Miami.

The most complete record of Florida Current transport is that of Baringer and Larsen (2001). Based on current meter, Pegasus profilers, and cable voltage measurements from 1982-1998, they estimate an average transport of 32 Sv between West Palm Beach, FL, and Eight Mile Rock, Grand Bahamas Island. For comparison to flow estimates at Miami, it is necessary to adjust this value by 1 Sv to account for flow from the Northwest Providence Channel (Leaman et al., 1995). The resulting value of 31 Sv is similar to earlier estimates. Overall, the data suggest the annual average flow of the Florida Current varied by 5-15% during the last 110 years, with the lowest flows generally occurring in the late 19^{th} century and the highest in the late 20^{th} century.

The Florida Current consists of two primary components, one from the South Atlantic which is fresh (<36 psu) and the other from the North Atlantic subtropical gyre which is salty (>36 psu). The fresh component accounts for ~14 Sv of the total transport, is found at the surface (>24°C) and bottom (7-12°C) of the Florida Current, and acts as the northward flowing surface limb of the meridional overturning circulation (Schmitz and Richardson, 1991). The deepest portion of the Florida Current is most likely Antarctic Intermediate Water that has been modified through mixing with saltier water of the subtropical gyre. The wind-driven subtropical gyre component sits between the fresh South Atlantic water at the surface and deepest parts of the Florida Current, is characterized by intermediate temperatures (12-24°C), and accounts for ~17 Sv of the total flow (Schmitz et al., 1993). If the strength of either the wind-driven or meridional overturning circulation were weaker during the Little Ice Age, we should be able to detect it at our core sites in the Florida Straits.

Core location, age control, and core top results

The object of this study was to reconstruct Florida Current transport for the last 1,100 years using a suite of high-resolution sediment cores from the Straits of Florida. The cores were retrieved from two locations on either side of the Florida Current: Dry Tortugas and Great Bahama Bank (Figure 1). Near Dry Tortugas, we used 7 cores at 5 unique water depths, spanning 200 to 750 m. On the Great Bahama Bank, a total of 9 cores were used at 5 separate water depths ranging from 260 to 700 m. All the cores reported here, except W167-79GGC (Lund and Curry, 2004), were collected in January of 2002 aboard the R/V Knorr (cruise KNR166-2).

Age control

Down core age control is provided by multiple planktonic foraminiferal radiocarbon dates in each core (Tables 1 & 2). Each date is based on > 5 mg of *G. ruber* specimens from the > 250 μm size fraction. Several core tops have >1 fraction modern radiocarbon, indicating that deposition occurred primarily after 1950 A. D. (62MC, 118MC, 125MC, 133GGC, 134MC). Others have ^{14}C core top ages less than the 400-year surface water reservoir age for this area (3MC, 11MC, W167-79GGC, 94MC), indicating the presence of bomb radiocarbon, but to a lesser extent than those with >1 fraction modern ^{14}C. The only KNR166-2 sites without modern or near-modern core top material are those shallower than 400 m water depth near Dry Tortugas. We dated a total of 10 separate cores from 200 to 400 m in this region and none had core top ages < 900 ^{14}C years. Of these cores, three display a monotonic increase in age with depth (16MC,

49GGC, 50MC). Core 16MC has the most recent material, with a core top age of 960 ^{14}C years (Table 1). All raw radiocarbon ages were converted to calendar ages using CALIB 4.3 (Stuiver et al., 1998a) assuming a surface ocean reservoir age of 400 years.

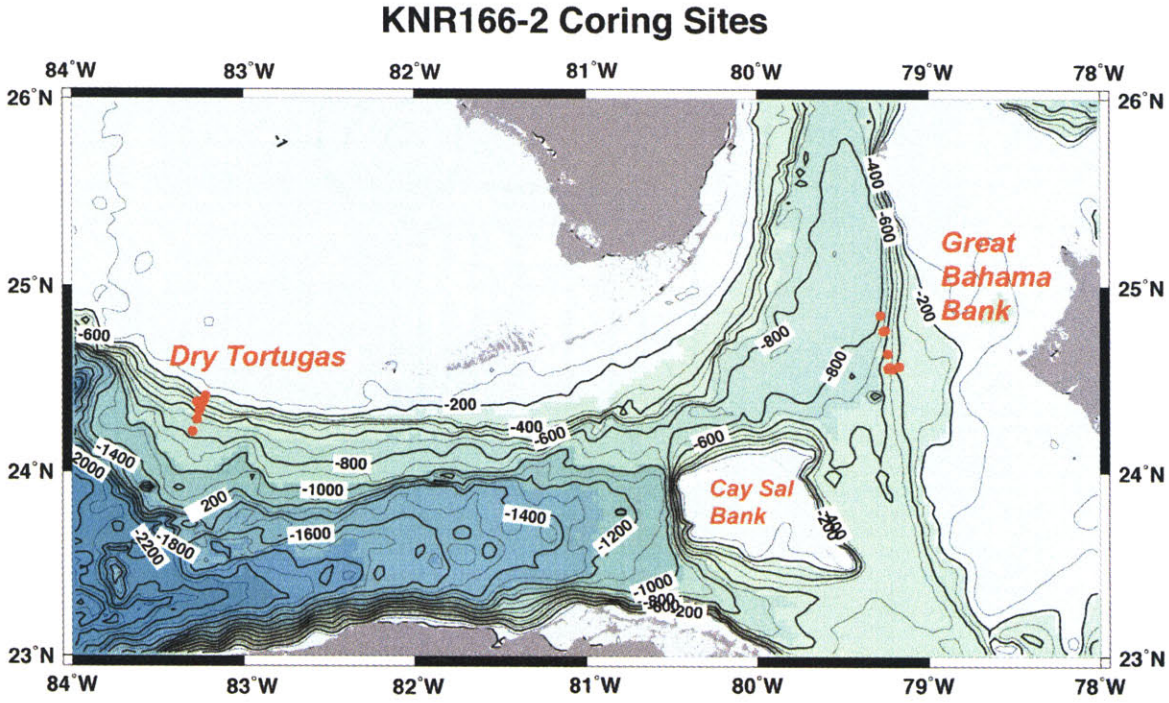

Figure 1
Bathymetric map of the locations of KNR166-2 cores used in this paper. Core depths spanned from 200 to 750 m near Dry Tortugas and 260 to 700 m along the Great Bahama Bank. Transport between the coring sites occurs in two channels: between Cay Sal Bank and Florida and Cay Sal Bank and the Great Bahama Bank (i.e. Santaren Channel). The total flow in the two channels is equivalent to that observed at Miami, approximately 31 Sv (Leaman et al., 1995; Baringer and Larsen, 2001).

Table 1. Dry Tortugas Radiocarbon Ages

Water Depth (m)	Core	Latitude (N)	Longitude (W)	Depth in core (cm)	^{14}C Age (yr)	Error (yr)	Calendar Age (yr BP)	Sedimentation Rate (mean) (cm/kyr)
198	50MC-E	*24 24.70*	*83 13.14*	0-1	1080	45	645	67
				24-25	1470	60	1010	
198	49GGC	*24 24.70*	*83 13.14*	0-1	1060	45	635	62
				50-51	1930	40	1490	
				111-112	2740	50	2430	
248	16MC-A	*24 23.72*	*83 13.53*	0-1	960	30	560	33
				37-38	2110	35	1710	
447	3MC-H	*24 23.04*	*83 20.33*	0-1	330	25	0	34
				18-19	930	30	536	
				37-38	1550	35	1104	
530	W167-79GGC	*24 21.50*	*83 20.90*	*see Lund & Curry (2004)*				
547	62MC-A	*24 19.60*	*83 15.40*	*see Lund & Curry (2004)*				
751	11MC-D	*24 13.18*	*83 17.75*	0-1	355	35	0	11
				8-9	1130	25	680	
				17-18	1810	25	1344	
				23-24	2500	35	2173	

*all cores are from cruise KNR166-2 (except W167-79GGC) and all dates based on >5 mg of *G. ruber* > 250 um (white and pink)

Table 2. Great Bahama Bank Radiocarbon Ages

Water Depth (m)	Core	Latitude (N)	Longitude (W)	Depth in core (cm)	^{14}C Age (yr)	Error (yr)	Calendar Age (yr BP)	Sedimentation Rate (mean) (cm/kyr)
259	94MC-C	*24 34.12*	*79 13.53*	0-2	215	35	0	65
				35-37	975	35	550	
259	93GGC	*24 34.12*	*79 13.53*	43-45	955	25	540	350
				90-93	1380	30	928	
				140-143	1480	30	1019	
				272-282	1630	60	1200	
304	105JPC	*24 33.83*	*79 13.77*	0-1	480	35	85	378
				1650-1651	4390	45	4450	
441	134MC-A	*24 50.16*	*79 13.11*	0-1	>Mod	n/a	0	59
				21-23	730	40	375	
445	133GGC	*24 50.16*	*79 13.11*	0-1	>Mod	n/a	0	121
				135-137	1570	35	1120	
531	118MC-A	*24 35.43*	*79 16.12*	0-1	>Mod	n/a	0	41
				12-14	635	25	282	
				36-37	1320	45	885	
528	117GGC	*24 35.44*	*79 16.12*	30-32	1090	30	649	110
				60-62	1430	30	962	
				88-90	1550	30	1101	
				147-150	2330	90	1954	
				200-210	2570	100	2224	
694	125MC-D	*24 45.45*	*79 17.45*	0-1	>Mod		0	20
				10-11	1250	30	780	
				27-28	1830	35	1360	
696	124GGC	*24 45.46*	*79 17.46*	7-8	865	35	490	26
				26-28	2020	25	1585.5	
				49-51	2460	30	2089.5	

*105JPC 0-1 cm based on mixed planktonics, 1650-1651 cm based on *G. ruber* and *G. sacculifer*

The sedimentation rates for the Dry Tortugas and Great Bahama Bank sites are uniformly high – all but one of the cores has a sedimentation rate in excess of 20 cm/kyr (The exception is 11MC, which has an accumulation rate of 11 cm/kyr.) On either side of the Florida Current, sedimentation rates increase with decreasing water depth. The highest accumulation rates are on the Great Bahama Bank, with several cores (e.g. 93GGC, 105JPC, 117GGC, and 133GGC) in excess of 100 cm/kyr.

Sampling strategy

Stable isotope analyses for the Florida Straits cores were based primarily on *Cibicidoides floridanus* from the >250 μm size fraction. At the deeper Dry Tortugas and Great Bahama Bank sites, we used *Planulina ariminensis* when necessary, also from the >250 μm size fraction. Both benthic foraminiferal species have been shown to precipitate calcite in equilibrium with ambient sea water, such that the $\delta^{18}O_{calcite}$-$\delta^{18}O_{seawater}$ difference follows a thermodynamic slope of ~0.2 per mil/°C (Slowey and Curry, 1995; Lynch-Stieglitz et al., 1999). We ran four $\delta^{18}O$ analyses at each stratigraphic level, each based on an individual benthic foraminifer test. Sonication of foraminifera to remove attached detrital material was performed as necessary and each foram was crushed prior to analysis to ensure thorough acidification. Stable isotope analyses were performed on a Finnigan MAT 253 coupled to a Kiel III carbonate device. Calibration to VPDB scale was made using NBS-19 ($\delta^{18}O$ = -2.20‰ and $\delta^{13}C$ = 1.95‰). Long-term reproducibility (1σ) of NBS-19 (n=461) for this mass spectrometer system is ±0.08‰ for $\delta^{18}O$ and ±0.04‰ for $\delta^{13}C$.

Density calibration

Foraminiferal $\delta^{18}O$, like seawater density, is a function of both temperature and salinity. As salinity increases and temperature decreases, both $\delta^{18}O$ and density increase. Therefore, if the relationship between salinity and $\delta^{18}O$ of seawater is known, and the difference between seawater and foraminiferal $\delta^{18}O$ is thermodynamically controlled, an empirical relationship between density and foraminiferal $\delta^{18}O$ can be created. We calculated σ_t values from CTD casts taken in the Florida Straits near our coring sites. We then estimated seawater $\delta^{18}O$ ($\delta^{18}O_w$) using the $\delta^{18}O_w$-S relationship from tropical and subtropical thermocline waters in the Atlantic ($\delta^{18}O_w = 0.50*S - 17.0$) (Schmidt et al., 1999), and the predicted $\delta^{18}O_c$ of *C. floridanus* and *P. ariminensis* precipitated in equilibrium with this water [$\delta^{18}O_c = (\delta^{18}O_w - 0.27) - 0.21*T + 3.38$] (Lynch-Stieglitz et al., 1999).

The resulting relationship between σ_t and $\delta^{18}O_c$ is shown in Figure 2. Using this regression, core top σ_t can be estimated and projected on onto two vertical profiles, one near Dry Tortugas and the other on Great Bahama Bank, creating what are essentially foram-based hydrographic stations. Comparison of core top foraminiferal and CTD density values from the KNR166-2 cruise in January 2002 (Figure 3) indicates the stable oxygen isotopic composition of *C. floridanus* and *P. ariminensis* reliably reflects the density structure of the Florida Current.

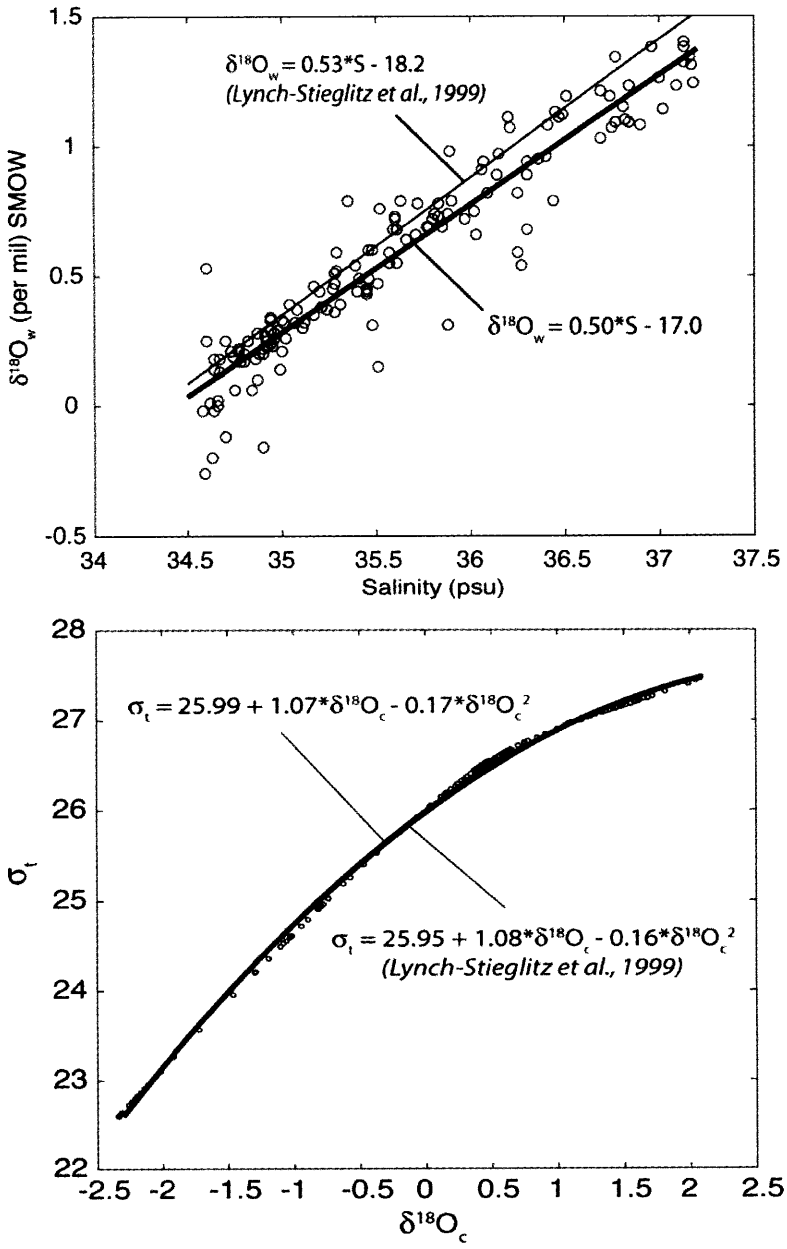

Figure 2.
Top) $\delta^{18}O$ of sea water ($\delta^{18}O_w$) versus salinity regressions. One is based on $\delta^{18}O_w$ -S pairs from GEOSECS stations 29 and 37 (dashed line; after Lynch-Stieglitz et al., 1999), and the other is based on a broader set of open-ocean thermocline data from the North Atlantic subtropical gyre and the tropical Atlantic (circles and solid line; Schmidt et al., 1999). Bottom) We used both $\delta^{18}O_w$ -S regressions in the paleotemperature equation for *Cibicidoides* species (see text) to obtain estimates of σ_t for given values of $\delta^{18}O_c$. Visually the two give very similar results, although in terms of absolute transport, the two differ by ~10%.

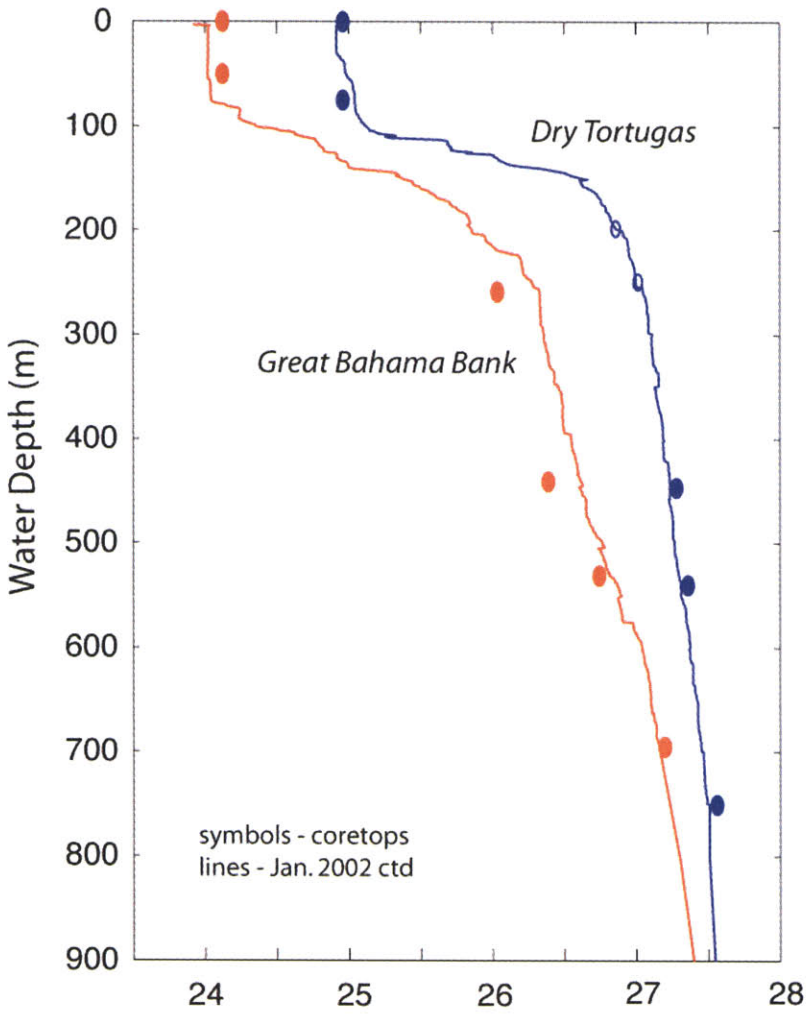

Figure 3
Comparison of sigma-t vs. depth based on core top foraminifera (solid symbols) with that calculated using T & S data from January 2002 CTD casts. Planktonic foraminifera are used to constrain mixed layer density. For comparison to the wintertime CTD data, Great Bahama Bank *G. ruber* $\delta^{18}O_c$, which reflects annual average mixed layer conditions (Deuser, 1987; Lund and Curry, 2004), was adjusted by +0.5 per mil to account for the difference between annual average and wintertime SSTs (2.5°C; Levitus, 1994). For the Dry Tortugas, *G. ruber* $\delta^{18}O_c$ was adjusted by +0.6 per mil to account for the 3°C offset between annual average and winter SSTs (Levitus, 1994). Overall, there is remarkably good agreement between the foram and CTD datasets. The primary discrepancy exists at mid-depths on the Great Bahama Bank. The offset is likely a function of the very different timescales for each proxy – individual CTD casts take a matter of hours whereas the core top sediments integrate over the last 50-100 years. The open blue symbols represent the assumed core top sigma-t values for 200 and 250 m depth near Dry Tortugas (see Figure 6).

The offsets between the January 2002 and foram σ_t data are most likely a function of short-term variability in Florida Current density not captured by the foraminiferal records. Flow of the Florida Current varies by up to ±8 Sv on weekly to monthly timescales and ±2-4 Sv on annual to interannual time scales (Niiler and Richardson, 1973; Baringer and Larsen, 2001). A portion of flow variability on annual time scales appears to be baroclinic (Niiler and Richardson, 1973) and should affect Florida Current density structure. It is therefore likely that the density values from January 2002 would be different than that inferred from coretop foraminifera, which represent approximately the last 50 years. Given the incompatible timescales of the CTD and foram-based density values, it is actually remarkable the two methods agree as well as they do.

Current shear and transport

Since benthic $\delta^{18}O_c$ reflects the cross-current density gradient in the Straits of Florida, it can be used to estimate vertical current shear. Based on the thermal wind equations, which combine the geostrophic and hydrostatic approximations, vertical current shear is proportional to the cross-current density gradient:

$$\frac{\partial v}{\partial z} = -\frac{g}{\rho_o f}\frac{\partial \rho}{\partial x}$$

$$\frac{\partial u}{\partial z} = \frac{g}{\rho_o f}\frac{\partial \rho}{\partial y}$$

where $\partial v/\partial z$ ($\partial u/\partial z$) is vertical shear of the meridional (zonal) velocity, g is the acceleration due to gravity, f is the coriolis parameter, ρ_o is a reference density, and $\partial \rho/\partial x$ ($\partial \rho/\partial y$) is the density gradient in the zonal (meridional) direction.

To estimate transport, a reference velocity must be either known or estimated to provide a constant of integration for the thermal wind equations. Typically, a level of no motion is assumed near the bottom of flow, but the exact depth at which this occurs is difficult to constrain without independent velocity measurements. Today, current meters show that near-zero velocities between Cay Sal Bank and Florida occur between 800 m and 1000 m (Leaman et al., 1995). Offshore of Key West, the level of no motion is deeper (~ 1000 m) but all velocities below 600 m are less than 5 cm/s (Hamilton et al., 2005). In the much shallower Santaren Channel, near-zero flow velocities occur near 600 m (Leaman et al., 1995). Given the wide range of possible choices, we used a level of no motion (850 m) that yields a core top transport of 31.5 Sv, consistent with modern instrumental estimates. If we assume a level of no motion at 900 m, the resulting transport is 33.3 Sv, higher than any published value of annual average flow for the Florida Current at this location.

Transport estimates were made using the geopotential method. This method utilizes the specific volume anomaly (δ), which requires independent knowledge of temperature and salinity. Since we lack this information, we instead use the thermosteric anomaly ($\Delta_{s,t}$), which is the primary component of δ in the upper 1000 m of the ocean and can be calculated directly from σ_t (Pond and Pickard, 1983). Using CTD data from January 2002, the estimated transport based on $\Delta_{s,t}$ and δ is 25.8 Sv and 28.0 Sv, respectively, a difference of ~10%. This error, while significant, is systematic and will affect absolute flow values, but not relative changes through time. We also approximate

pressure (p) at any given depth (z) using $p = z*10^4$ Pa (Pond and Pickard, 1983). The error compared to using the hydrostatic equation is minimal (<1% using January 2002 data) since the approximation is similar at each station and largely cancels when geopotential anomalies are differenced.

Downcore Results and Discussion

The density time series for the Florida Current are based on a total of over 3000 stable isotopic measurements, spanning from the surface to 750 m water depth and from today to 2000 years ago. Dry Tortugas and Great Bahama Bank planktonic foraminiferal $\delta^{18}O_c$ were used to constrain density variability in the surface mixed layer. The annual average mixed layer depth in this region is approximately 50 m (Levitus, 1994). Since this is similar to the depth habitat of *G. ruber* (Fairbanks et al., 1982), the planktonic $\delta^{18}O_c$ records should reliably record variations in surface water density. For the purposes of the geostrophic calculation, we assumed an annual average mixed layer thickness of 75 m for Dry Tortugas and 50 m for Great Bahama Bank to account for the greater wintertime mixed layer depth at Dry Tortugas (Figure 3).

Near Dry Tortugas, planktonic $\delta^{18}O_c$ was constant (within the 95% confidence limits) from 2000 to 900 yr BP, but then increased by 0.3‰ (σ_t = ~0.5) from 900 to 400 yr BP, with the largest shift after 600 yr BP (Figure 4). On the other side of the Florida Straits, surface density was stable from 2000 to 250 yr BP, and then increased by ~0.3 kg m^{-3} from 250 yr BP to present (Figure 5). The $\delta^{18}O_c$ signal at each site was primarily driven by changes in seawater $\delta^{18}O$ ($\delta^{18}O_w$) (Chapter 3). The net effect of the $\delta^{18}O_w$

variability was a positive shift in the cross-current density gradient from 900 to 250 yr BP, which was most pronounced after 600 yr BP.

The benthic foraminiferal $\delta^{18}O_c$ records also show clear shifts in water column density during the last millennium. At Dry Tortugas, benthic $\delta^{18}O_c$ decreased by ~0.1‰ from 900 to 200 yr BP at 450 and 540 m water depth, equivalent to a σ_t shift of 0.05-0.1 kg m^{-3} (Figure 6). At similar depths on the Great Bahama Bank, there was no comparable long-term decrease in $\delta^{18}O_c$ (Figure 7). As a result, the cross-current density gradient (and therefore vertical current shear) generally decreased from 900 to 200 yr BP. From 200 yr BP to present, $\delta^{18}O_c$ at all the Great Bahama Bank sites decreased by 0.1‰ ($\Delta\sigma_t = 0.1$), with no comparable change at Dry Tortugas. The converse occurred from 1100 yr BP, when density increased throughout the water column along Great Bahama Bank. Therefore, at mid-depths ($26.0 < \sigma_t < 27.2$), current shear decreased at ~1000 yr BP and then increased by a similar amount after 200 yr BP.

The shallow portion of the Florida Current was the most difficult to reconstruct given the lack of modern core top material near Dry Tortugas. To fill in this time gap, we assumed that the densities at zero age were equal to modern CTD values and then interpolated to the most recent $\delta^{18}O_c$ data. At both 200 and 250 m water depth, the resulting density trend is similar to that for the 450 and 540 m sites, giving us confidence that the interpolated points give a general sense of the centennial-scale density values from 500 yr BP to present.

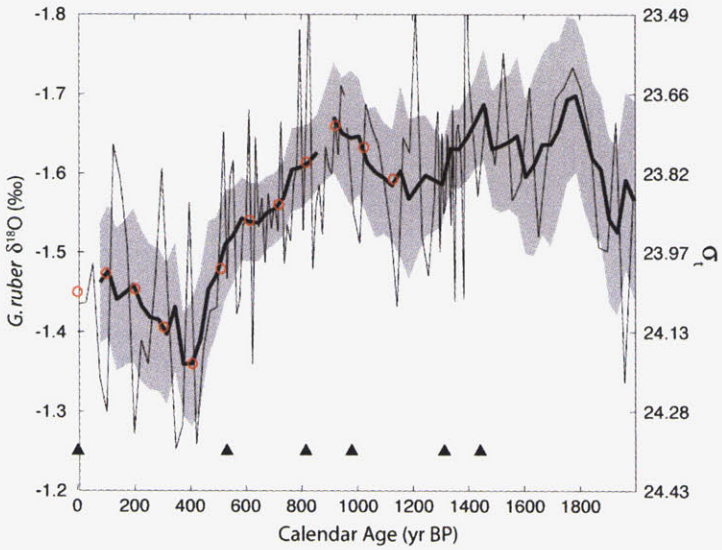

Figure 4

G. ruber $\delta^{18}O_c$ for the Dry Tortugas, based on two cores (62MC – 0-900 yr BP; 79GGC – 900-2000 yr BP). The right-hand axis is the equivalent change in sigma-t for the surface mixed layer. The data is presented as the average value at each depth (thin black line), the 100-year running mean (thick black line), and the 95% confidence limit on the 100-year mean (shaded area). Where overlap between cores occurred, the core with the narrower 95% confidence limit was used (in this case 62MC). The circles represent the interpolated values used in the transport calculation. Triangles represent calendar-corrected radiocarbon ages.

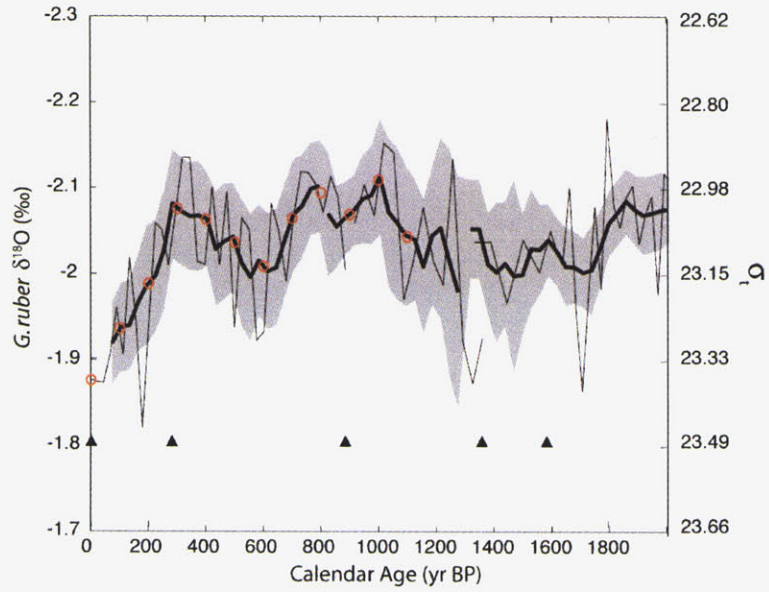

Figure 5

G. ruber $\delta^{18}O_c$ for the Great Bahama Bank, based on three cores (118MC – 0-900 yr BP; 125MC – 900-1300 yr BP; 124GGC – 1300-2000 yr BP). The plotting convention is the same as in Figure 4.

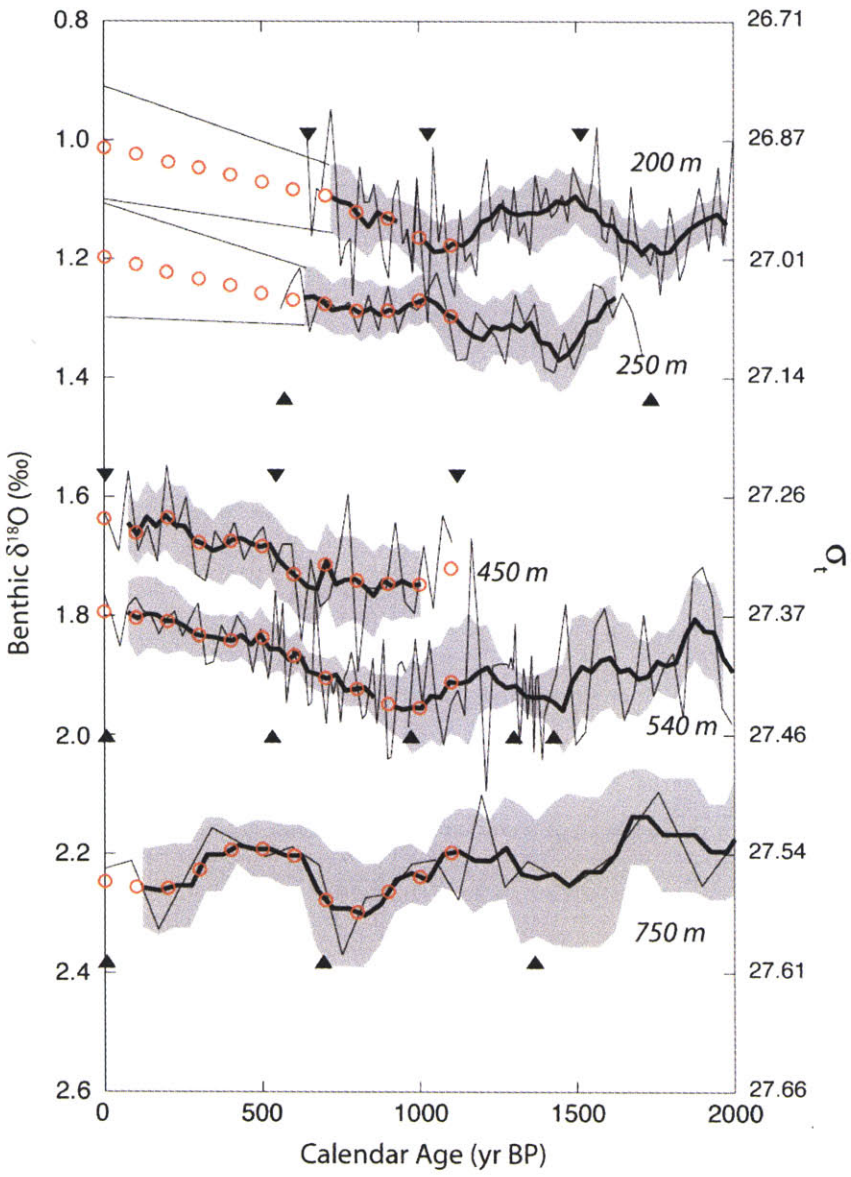

Figure 6

Benthic foraminiferal $\delta^{18}O_c$ time series for the Dry Tortugas. The plotting convention is the same as Figure 4. At 200 m, the record is based on two cores (50MC – 500-900 yr BP; 49GGC – 900-2000 yr BP). The record at 250 m is based entirely on 16MC. Given the lack of core material between 0 and 500 yr BP for these sites, we interpolated between modern sigma-t values based on CTDs (Figure 4) and the most recent core material. The resulting trend is similar to that in deeper cores. The maximum uncertainty in mean $\delta^{18}O_c$ at 200 and 250 m is ±0.1 per mil (since $\delta^{18}O_c$ at 250 m must always be larger than $\delta^{18}O_c$ at 200 m). We estimated uncertainty between 0 and 500 yr BP by interpolating between these values for each site to the uncertainty envelop for the core top material. The 450 m time series is based on 3MC, while at 540 m it is based on 62MC (0-900 yr BP) and 79GGC (900-2000 yr BP). At 700 m, the record is based entirely on 11MC. It is worth noting that the absence of radiocarbon dates below 1500 yr BP in some of the cores does not indicate we extrapolated their age models to 2000 yr BP. In each case there are radiocarbon dates older than 2000 yr BP that do not appear in the figure (see Table 1).

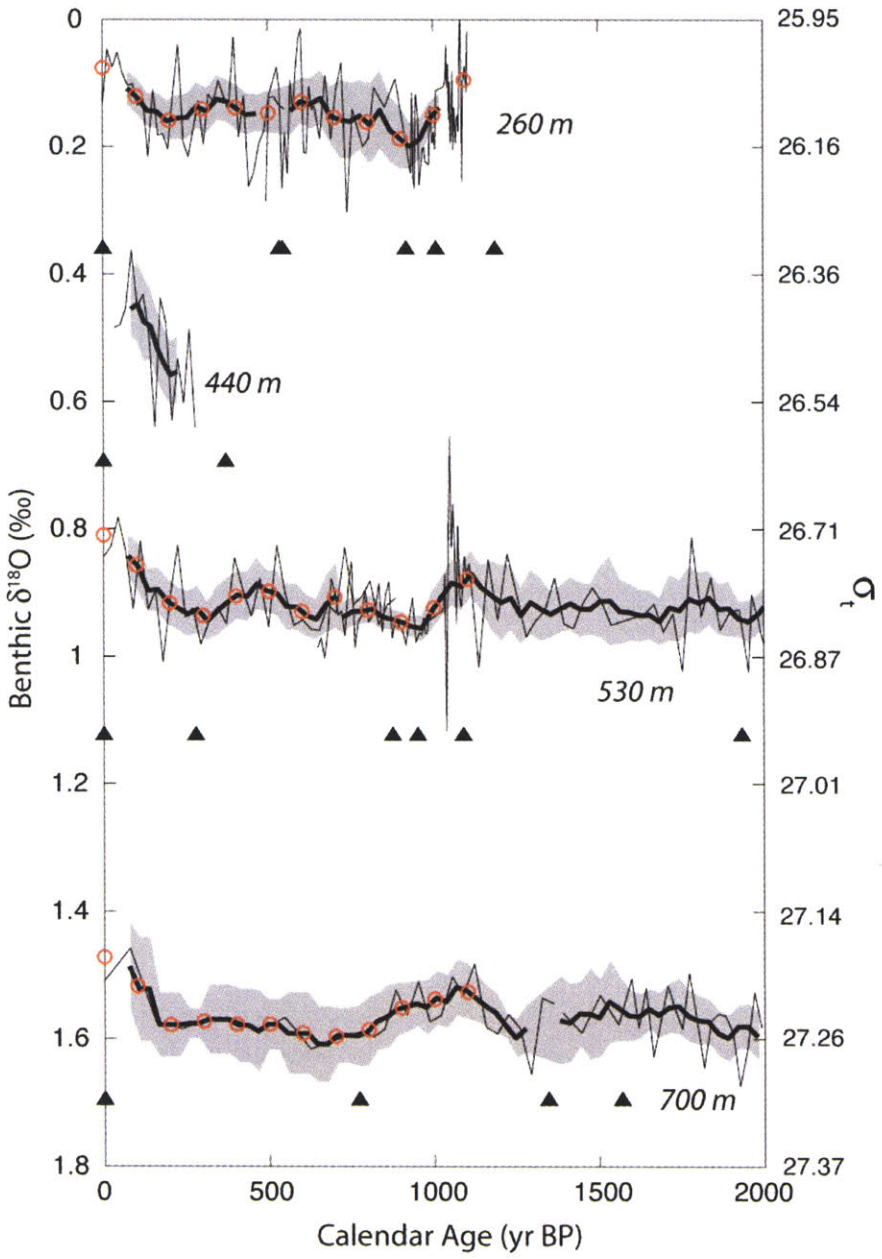

Figure 7

Benthic foraminiferal $\delta^{18}O_c$ time series for the Great Bahama Bank. The benthic record for this side of the Florida Current is more complete than for the Dry Tortugas, particularly in the time interval from 0-1100 yr BP. The record at 260 m is comprised of data from two cores (94MC – 0-500 yr BP; 93GGC – 500-1100 yr BP). The data at 440 m (134MC) was not used in the transport calculation as it is too short, but the trend of decreasing $\delta^{18}O_c$ over the past 200 years is consistent with that observed in all of the Bahamas benthic records. At 530 m, we used two cores (118MC – 0- 700 yr BP and 117GGC – 700-2000 yr BP) and at 700 m we also used two cores (125MC – 0-1300 yr BP and 124 GGC – 1300-2000 yr BP). In all cases where time overlap between two cores at a given water depth occurred, we used the mean value with the smaller uncertainty envelope.

We estimated the variance for the interpolated sections at 200 and 250 m depth at Dry Tortugas using a 95% confidence limit of ±0.1‰ for each site at 0 cal yr BP, which is equivalent the half the $\delta^{18}O_c$ difference between 200 and 250 m water depth. This is the largest possible variance given that the density at 250 m must always be greater than that at 200 m. We then scaled the error estimates back in time such that the error envelope converged with that based on core top material. Although this interpolation scheme ignores possible short-term shifts in mean density between 500 cal yr BP and today, it provides a conservative estimate of the overall density trend that is consistent with other Dry Tortugas cores and modern density observations.

Transport for the last millennium

Estimated Florida Current transport for the last millennium is shown in Figure 8. Over the past 1,100 years, transport varied by 2-3 Sv, or about 10% of the total flow. Compared to the 10-15 Sv flow reduction during the Last Glacial Maximum (Lynch-Stieglitz et al., 1999), the Late Holocene Florida Current is characterized by relatively small variations in volume transport. Despite the small signal, there is a clear interval of lower flow from 900 to 200 yr BP, coinciding with the Little Ice Age. Based on a Monte Carlo simulation, this shift in flow is statistically significant at the 95% confidence level and is 2-3 Sv lower than either the Medieval Warm Period (~1000 yr BP) or today. Flow is lowest from 600 to 200 yr BP, the approximate time of maximum cooling in several Northern Hemisphere temperature records (Dahl-Jensen et al., 1998; deMenocal et al., 2000; Keigwin, 1996). Nearly synchronous changes in Northern Hemisphere

temperature and reduced Florida Current baroclinic shear suggest that lower northward oceanic heat transport may have contributed to cooler Northern Hemisphere temperatures during the Little Ice Age.

If the level of no motion changed during the last millennium, it could substantially alter the flow time series in Figure 8. For example, a shift in the level of no motion from 850 to 950 m during the Little Ice Age, but with the same shear, would produce a total volume transport of ~31 Sv, equal to the modern value (Figure 9). Increasing the depth-averaged flow above 850 m by ~4 cm/s has a similar effect. On a seasonal basis, the mean flow of the Florida Current at Miami changes by 10-20 cm/s (Niiler and Richardson, 1973). In the context of the modern seasonal cycle, shifts in the mean flow of 4 cm/s seem entirely plausible. This may be a poor analog for the foram-based reconstruction, however, given the vastly different time scales involved and the higher bottom velocities observed near Miami (Niiler and Richardson, 1973) relative to Cay Sal Bank (Leaman et al., 1995). It is also possible that there was a decrease in mean flow or shoaling of the level of no motion during the LIA, which would amplify the signal in Figure 8. At this stage, these possibilities are unconstrained and therefore we have no choice but to interpret the record as it stands. For the remainder of the paper, I will assume that the level of no motion was constant during the last millennium.

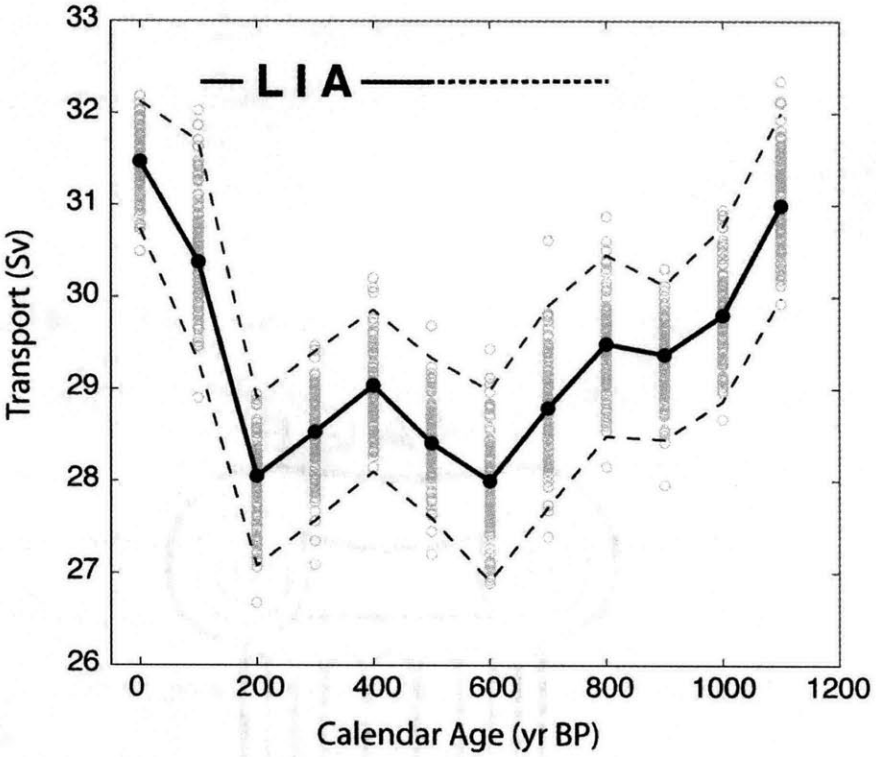

Figure 8
Estimated Florida Current transport for the last millennium. The most probable transport values (thick black line) are derived from the mean densities in Figures 4, 5, 6 and 7. The error envelope was estimated using a Monte Carlo approach. For a given time interval, transport was calculated using sigma-t values randomly sampled from the probability distribution in each core. We repeated this process 100 times at 0, 100, 200, …, and 1100 yr BP (grey circles). The 95% error envelope (dashed lines) averages ~ ±1 Sv and is defined as 2x the standard deviation of the transport estimates at each time interval. On average 95 out of 100 Monte Carlo-based values fall within this envelope. If the level of no motion remained constant, then Florida Current transport during the Little Ice Age was 2-3 Sv lower than either today or 1100 yr BP.

Flow variability versus depth

In addition to total transport, the foraminiferal density records yield information on the variability in transport with depth. Given that the wind-driven and meridional overturning components have characteristic density ranges in the Straits of Florida, we should be able to qualitatively assess if one of these two components was primarily responsible for past changes in flow. Low transport during the Little Ice Age is a

function of reduced flow throughout the water column, with the largest anomalies above 500 m (Figure 9). The transport profile for 1100 yr BP is very similar to today, with slightly lower values below 100 m and higher values above 100 m.

A richer picture of the flow variability appears when transport anomalies are contoured versus depth and time (Figure 10). We define anomalies as the difference in transport at each depth relative to the mean value for the past 1,100 years. The largest negative anomalies occur during the LIA and at depths from 100 to 500 m (or $24 < \sigma_t < 27$), the density range associated with waters from the North Atlantic subtropical gyre. Therefore, it appears that it was primarily the wind-driven rather than the meridional overturning component of the Florida Current that was responsible for low total transport during the LIA. Flow at the bottom of the Florida Current was also low during the LIA, indicating a weakening of the meridional overturning component. The intervals 0-100 yr BP and 1000-1100 yr BP are characterized by anomalously high transport, but they are unique in that the modern flow anomaly spans the entire water column, whereas at 1100 yr BP it is concentrated above $\sigma_t = 27.0$. This pattern suggests that the flow of upper Antarctic Intermediate Water was weaker at ~1100 yr BP than today.

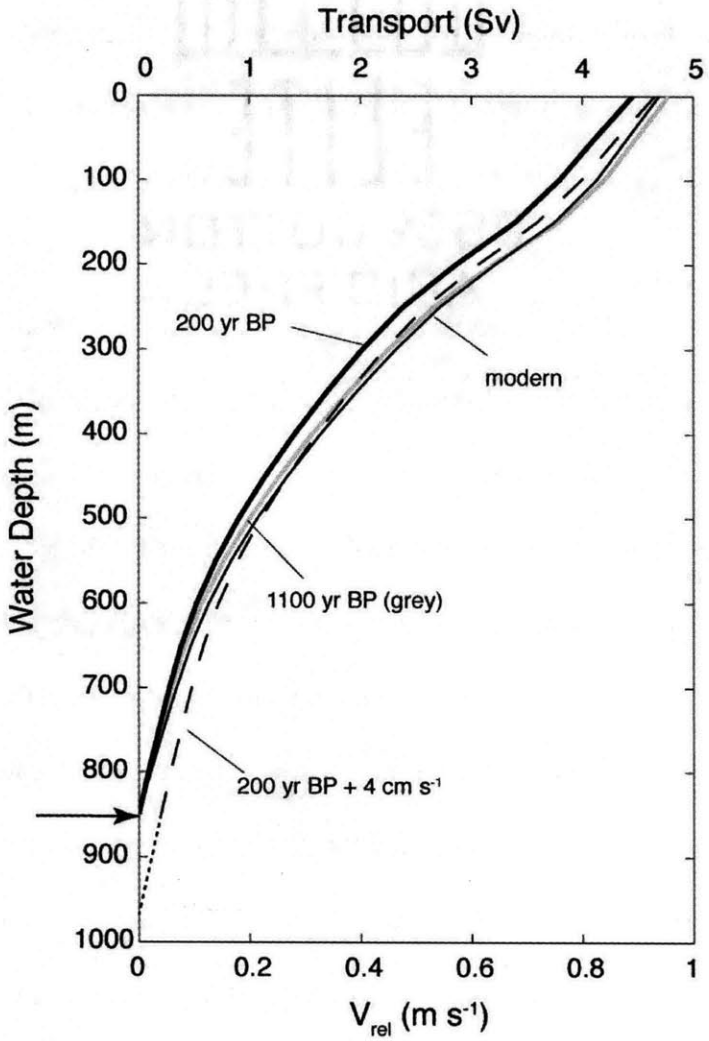

Figure 9

Velocity and transport profiles for today (thin black line), 200 yr BP (thick black line), and 1100 yr BP (grey line). Relative velocities (V_{rel}) were calculated assuming a scale-width of 100 km for the Florida Current. We define velocity to be 0 cm/s at 850 m, the level of no motion (arrow). A +0.4 cm/s increase in the mean or barotropic flow during the LIA (dashed line) compensates for the effect of reduced baroclinic shear, yielding a total transport of ~31 Sv, similar to the modern value. Moving the level of no motion to 950 m during the LIA has nearly the same effect (dotted line). (Transport is 0.2 Sv higher for a deeper level of no motion given the additional flow below 850 m.)

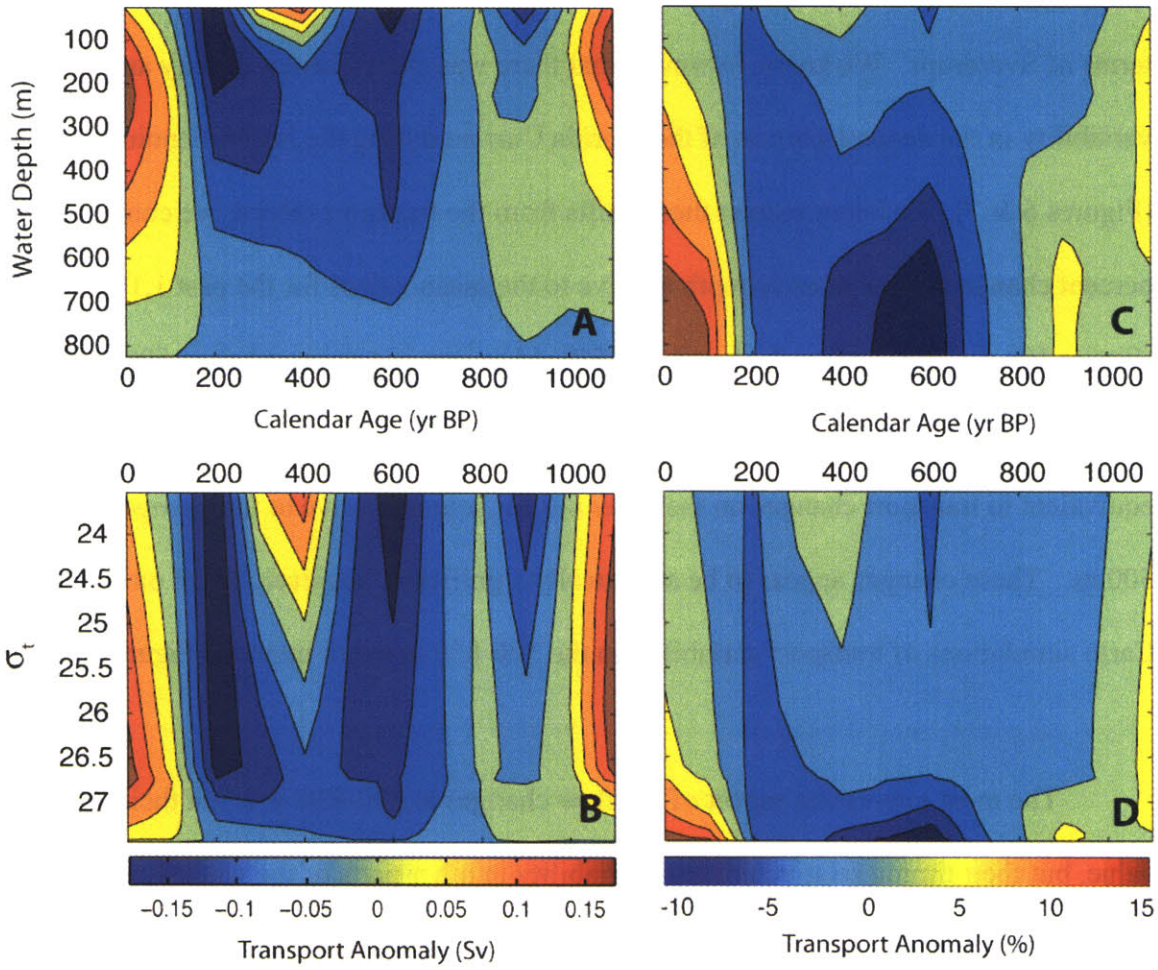

Figure 10

A) Flow anomaly vs. depth (Sv/50m), defined as transport at a given time minus average transport 0-1100 yr BP. Negative transport anomalies occur during the LIA and are largest in the depth range that is today dominated by flow from the North Atlantic subtropical gyre (100-500 m). B) Same as A), but using average cross-current sigma-t rather than depth. C) Percent flow anomaly vs. depth, defined at the percent change in transport at a given time relative to the 0-1100 yr BP average. Transport variability of ~25% occurred in the deepest portion of the Florida Current, with the lowest values early in the LIA and the highest values during the last 100 years. D) Same as C), except using sigma-t rather than depth.

Since transport below 500 m is generally low (~ 3 Sv), anomalies in this portion of the water column will be minimized relative to those above 500 m when expressed in terms of Sverdrups. We know, however, that there was cross-current density and shear variability in the deepest portion of the Florida Current during the last millennium (Figures 6 & 7). To better extract these shifts from the transport record, we contoured the percent change in flow at each depth relative to the mean values for the past 1,100 years (Figure 10c,d). This approach shows 15-25% reductions in transport below 500 m during the LIA relative to today. Given that flows for this depth range are ~ 3 Sv, this is equivalent to transport changes on the order 0.5 Sv, minor relative to the changes above 500 m. These changes appear to be statistically significant, however, based on Monte Carlo simulations of transport variability in the 500-850 m depth interval (Figure 11).

The most interesting aspect of the flow changes at 500-850 m is not their absolute value, but their timing relative to shear variability in other parts of the water column. Flow at the bottom of the Florida Current declined beginning at about ~ 900 yr BP (Figure 11, bottom), after the initial decrease in shear at mid-depth (Figure 11, middle). In terms of the two components of the Florida Current, the anomalies imply that decreased flow associated with the wind-driven subtropical gyre preceded the reduction in meridional overturning. At 200 yr BP, shear increased from 100-850 m, indicating flow of both the wind-driven and overturning components increased at the LIA termination.

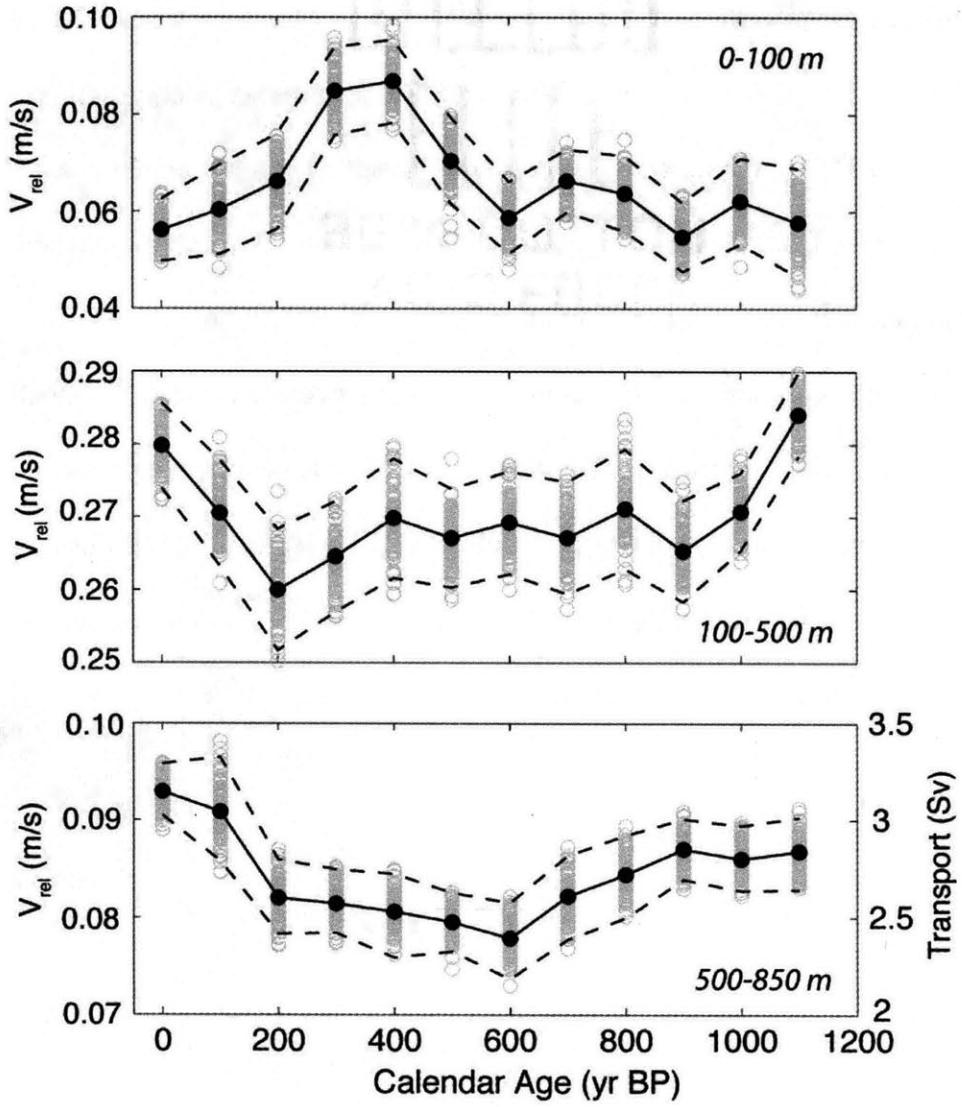

Figure 11

Top) Average velocity 0-100 m relative to velocity at 100 m (V_{rel}). Changing velocity shear in this layer contributes little to overall transport variability since the shear is small and does not translate upward in the water column. Middle) Average velocity 100-500 m relative to 500 m. Here the shear is five times larger than in the upper layer and 2-3 times larger than in the lower layer, meaning changes from 100-500 m will dominate the total transport signal. Bottom) Average velocity 500-850 m relative to 850 m. In the lowest layer, velocity scales directly to transport (right-axis) since there is no shear below 850 m. Although the changes in transport are small, they are statistically significant at the 95% confidence level, The shear anomalies suggest that decreased flow at mid-depths preceded decreased flow in the deepest portion of the Florida Current.

Error associated with salinity-$\delta^{18}O_w$ variability

To calculate past changes in density, we assumed the thermocline salinity and seawater $\delta^{18}O$ ($\delta^{18}O_w$) relationship was constant through time. Yet planktonic $\delta^{18}O_c$ and Mg/Ca time series from the Dry Tortugas and Great Bahama Bank show substantial changes in mixed layer $\delta^{18}O_w$ variability during the last millennium (Chapter 3). These changes are most reasonably explained by invoking an increase is mean thermocline $\delta^{18}O_w$ during the LIA (Figure 12). Although the planktonic data do not require a change in either the slope or intercept of the thermocline $\delta^{18}O_w$-S regression, it is possible that the $\delta^{18}O_w$-S slope changed during the LIA. In this section we examine the sensitivity of our transport estimates to reasonable changes in this slope.

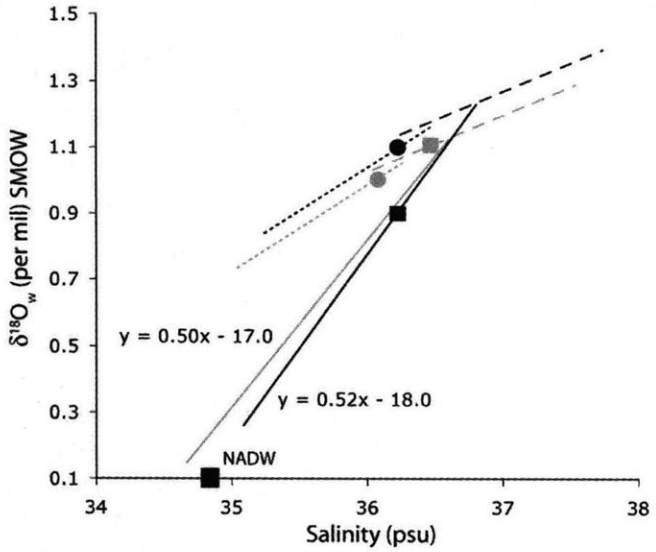

Figure 12
Schematic representation of the most likely change in North Atlantic $\delta^{18}O_w$-S relationships during the Little Ice Age (see Chapter 3). The grey lines represent today's $\delta^{18}O_w$-S relationships. Estimates of today's Great Bahama Bank (grey square) and Dry Tortugas (grey circle) surface water $\delta^{18}O_w$-S pairs are also given. LIA surface water $\delta^{18}O_w$ values (black symbols) suggest a greater proportion of ^{18}O-depleted water in the Sargasso Sea during the LIA and a higher mean thermocline $\delta^{18}O_w$ (see Chapter 3). The thermocline $\delta^{18}O_w$ –S slope may have also changed during the LIA – based on a 1‰ depletion in the freshwater end member, the thermocline slope would have been 0.52‰/psu (see text).

One way to alter the thermocline $\delta^{18}O_w$-S relationship would be to increase the meridional sea-surface temperature gradient, which would cause a depletion in ^{18}O of precipitation at high-latitudes. If temperatures in the region where subtropical gyre isopycnals outcrop cooled by ~1°C during the LIA (see next section), this would decrease rainfall $\delta^{18}O$ by 0.7‰ based on the relationship between $\delta^{18}O$ of precipitation and mean annual air temperature on land (Dansgaard, 1964). Since continental rainfall is generally more depleted in ^{18}O than oceanic rainfall, 0.7‰ is probably an overestimate of the LIA cooling effect on mean annual $^{18}O/^{16}O$ of oceanic precipitation. This effect may be offset by a greater temperature gradient in winter, however, when the thermocline is ventilated. As a rough estimate, we assume that LIA cooling lowered the $\delta^{18}O$ of the fresh-water end member by up to 1‰.

An isotopic depletion of the fresh-water end member results in a steeper $\delta^{18}O_w$-S slope (Figure 13, top) which in turn alters the polynomial fit to the $\delta^{18}O_c$ -σ_t data in the range occupied by the Dry Tortugas and Bahamas benthic $\delta^{18}O_c$ values (Figure 13, middle). The net effect is to increase density at Dry Tortugas more than the Bahamas, producing slightly higher transport values (~0.5 Sv) (Figure 13, bottom). Only if the fresh end member decreased by 4‰ would the resulting transport bias (~ 3 Sv) approach the observed signal for the last millennium (Lynch-Stieglitz et al., 1999). We therefore believe that the reconstructed transport is robust with respect to realistic long-term variability in the $\delta^{18}O$ of precipitation at high latitudes.

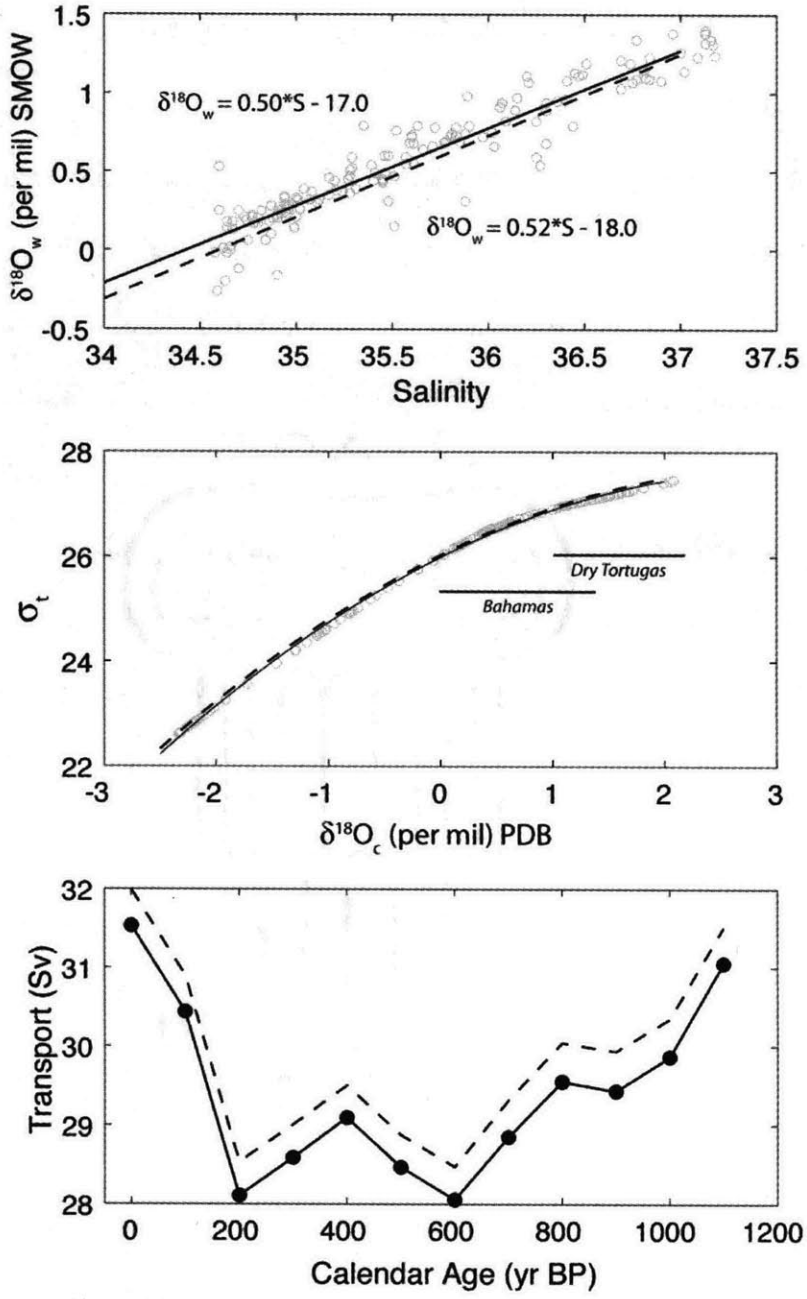

Figure 13

Top) The original (solid) and altered (dash) thermocline $\delta^{18}O_w$-S relationships, the latter having a 1 per mil more negative fresh end member. Middle) The effect of the alternative $\delta^{18}O_w$-S slope on the $\delta^{18}O_c$-σ_t regression. In the range of the benthic $\delta^{18}O_c$ data (horizontal bars), the altered $\delta^{18}O_c$-σ_t regression (dashed line) increases σ_t more for the Dry Tortugas than the Bahamas, and as a result amplifies the cross-current density gradient. Bottom) The resulting effect on transport is small, about +0.5 Sv.

Subtropical gyre thermocline properties and forcing

During the Little Ice Age, benthic $\delta^{18}O_c$ was 0.1‰ (σ_t ~0.1 kg m^{-3}) higher at all depths along the Great Bahama Bank relative to today (Figure 7). This change reflects a shoaling of isopycnals and thinning of the thermocline. In combination with the planktonic $\delta^{18}O_c$ results, which show the surface mixed layer has become anomalously dense during the last 200 years (Figure 5), it suggests there was significant variability in water column stratification during the last millennium. This is most easily observed in density profile anomalies, which we define as the density profile at a given time minus the core top profile (Figure 14). The least stratified interval of the last 1,100 years occurred from 200 yr BP to present. In absolute terms, today's surface to deep density gradient is 3.4 kg m^{-3}, whereas prior to 200 yr BP it was 3.8 kg m^{-3} (Figure 14, inset).

The North Atlantic subtropical gyre is the primary source of water on the salty eastern edge of the Florida Current (Schmitz et al., 1993). A comparison of hydrographic data from the Santaren Channel and the Sargasso Sea indicates the same is true for subsurface water at the Great Bahama Bank coring sites (Figure 15). Below σ_t ~ 27, Santaren Channel T-S pairs diverge from the Sargasso Sea values, presumably due to mixing with relatively fresh upper Antarctic Intermediate Water (AAIW). Although variable AAIW strength may have influenced Bahamas thermocline density in the past, its effect should be largest at the deepest sites. Instead, we observe a nearly constant shift in density at all depths, suggestive of forcing associated with the subtropical gyre.

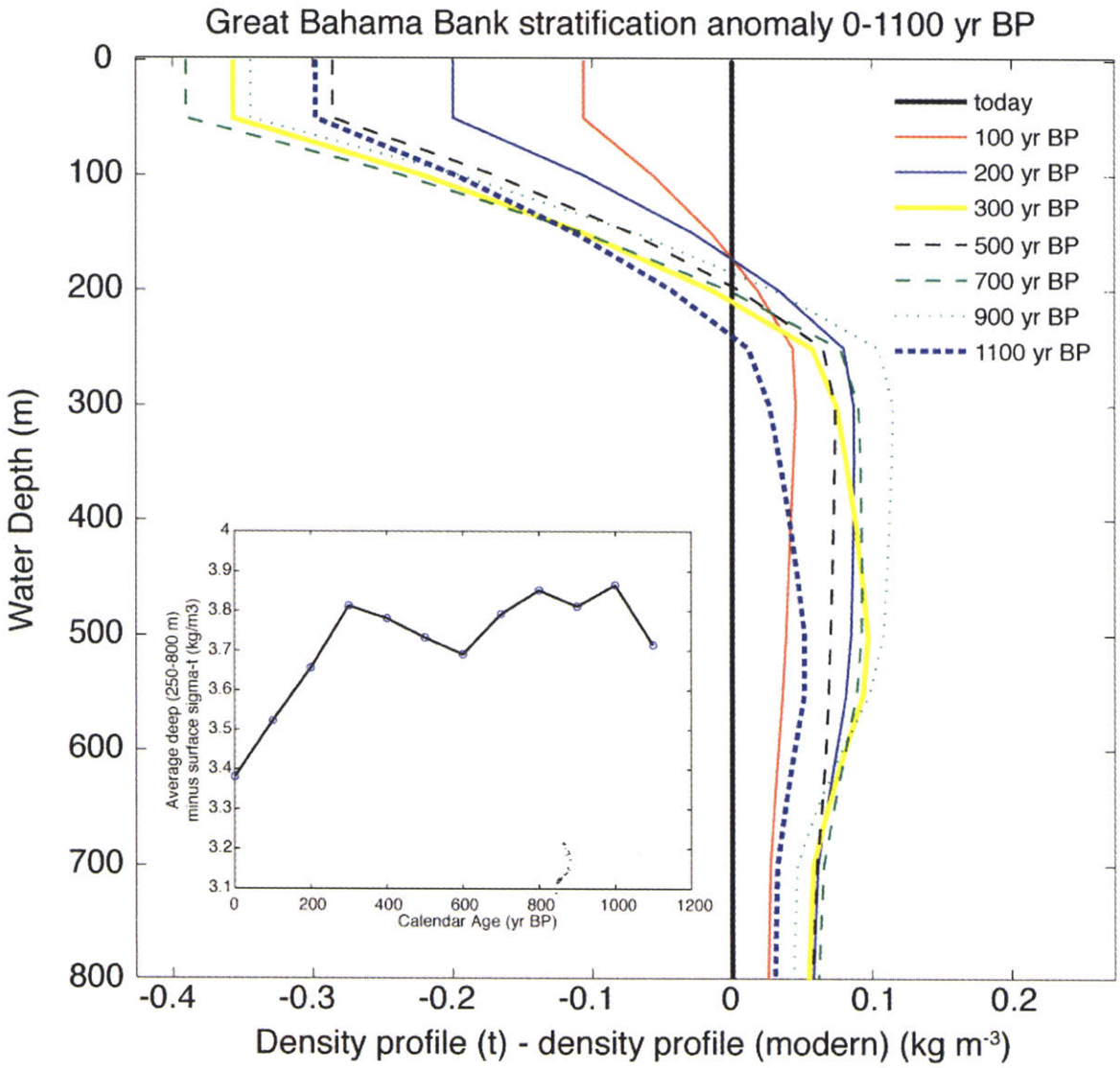

Figure 14

Density profile anomalies for the Great Bahama Bank, defined as the density profile at a given time minus the modern profile. The water column in the Santaren Channel has become progressively less stratified over the last 300 years. Inset) Alternate view of the same data – average deep (200-800 m) minus surface (0-100 m) sigma-t from 0-1100 yr BP. The surface to deep density gradient has decreased by ~0.4 sigma-t units from 300 yr BP to today. This is a function of both increasing salinity in the surface mixed layer (Chapter 3) and decreasing density in the thermocline. The profiles were constructed using the data in Figures 5 & 7, interpolated to 100 year time intervals and 50 m water depth intervals.

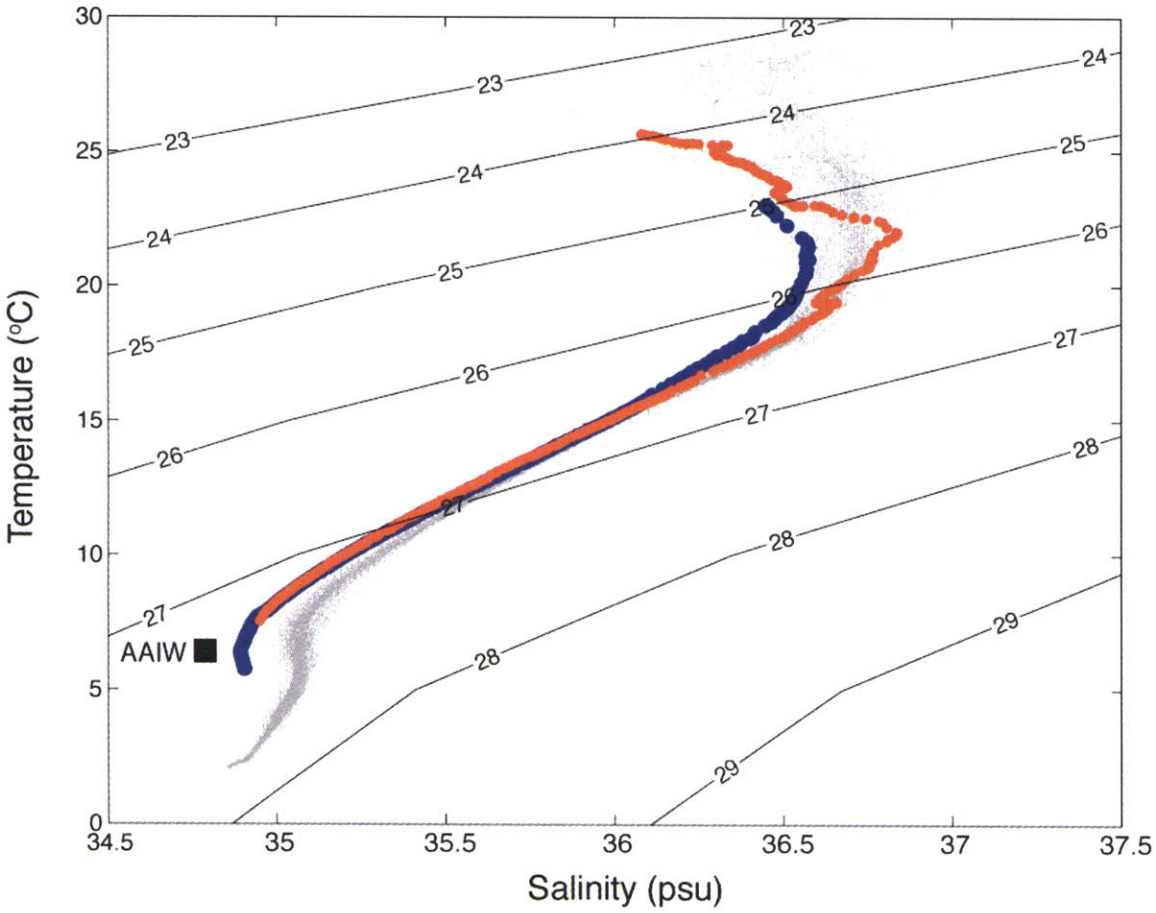

Figure 15
Salinity vs. in-situ temperature at Dry Tortugas (blue) and the Great Bahama Bank (red), January 2002. The grey dots are temperature and salinity pairs from the western Sargasso Sea for the last 60 years, spanning 22 to 27°N and 75 to 70°W (courtesy R. Curry). Contours represent lines of constant sigma-t. Thermocline waters in each Florida Straits location saltier than 36 psu are of subtropical gyre origin. Below 36 psu, both the Dry Tortugas and Santaren Channel data are fresher than the Sargasso Sea, reflecting the influence of mixing with upper Antarctic Intermediate Water (Schmitz et al., 1993). The approximate temperature and salinity of AAIW at 20°N is given by the solid black box (GEOSECS).

Stratification at Dry Tortugas shows a similar pattern to the Great Bahama Bank –during the last 200 years the water column was less stratified than earlier parts of the record (Figure 16). The exception is the interval from 400 to 200 yr BP when surface salinity at Dry Tortugas was unusually high (Chapter 3). In general, decreasing stratification over the last millennium was a function of variable density at both the surface and from 200-600 m (Figure 16). Today, the temperature and salinity properties of water in 200-600 m depth range on the western edge of the Florida Current can be traced to sections in the tropical North Atlantic (Schmitz et al., 1993). If this was also true in the past, then stratification in the tropical North Atlantic increased from 1100 yr BP to present, similar to the pattern for the subtropical gyre (Figure 16; inset). Overall, anomalies in thermocline density are larger at Great Bahama Bank than Dry Tortugas, suggesting a driving mechanism associated with the subtropical gyre as opposed to Antarctic Intermediate Water.

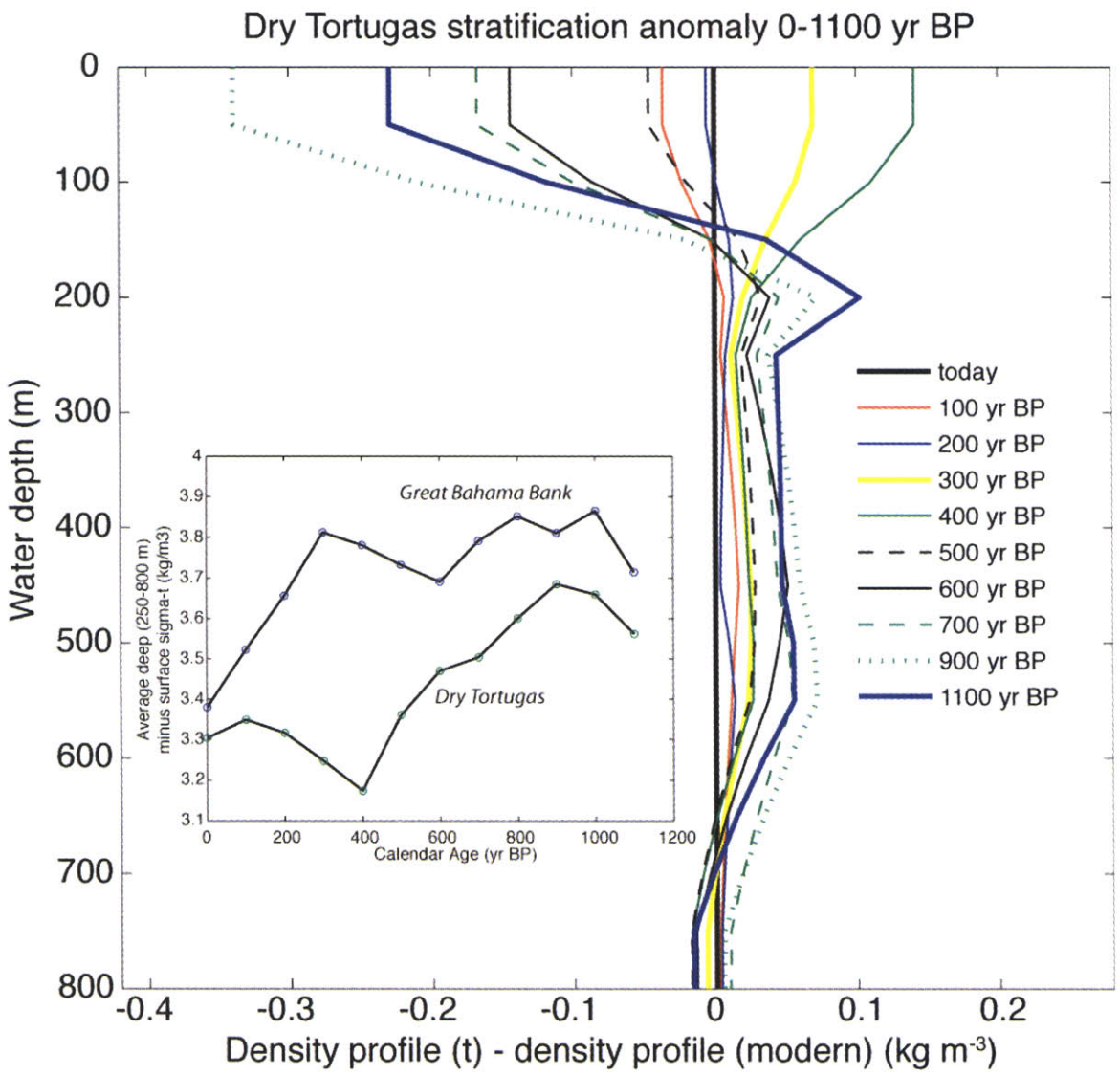

Figure 16

Same as Figure 14, except for Dry Tortugas. Like the Santaren Channel, the long-term decrease in stratification is a result of increasing salinity at the surface (Chapter 3) and decreasing thermocline density. A reversal in this trend occurred from 500-200 yr BP, driven by higher Dry Tortugas surface salinity during the LIA. Given that waters in this portion of the Florida Current T-S envelope can be traced to the tropical Atlantic (Schmitz et al., 1993), it suggests that stratification in both the tropical and subtropical Atlantic generally increased from 1100 yr BP to present (inset).

The hydrographic properties of the subtropical gyre are set in the mid- to high-latitude North Atlantic. During boreal winter, the 26.2 to 27.2 density surfaces outcrop at the base of the mixed layer between ~25°N and 45°N, where water is driven downward into the thermocline by Ekman pumping and then advected southward along isopycnal surfaces (Luyten et al., 1983). Given this trajectory, it is logical to trace changes in Great Bahama Bank density to surface mixed-layer conditions further north.

During the Little Ice Age, surface waters in the central and western subtropical gyre were 0.5°C to 1°C cooler than today (Chapter 3; Keigwin, 1996). South of Newfoundland (~43°N, 55°W), LIA sea-surface temperatures were up to 1°C warmer than modern (Keigwin and Pickart, 1999), while to the east (~44°N, 46°W), SSTs were perhaps 0.5°C cooler than today (Bond et al., 2001). Records of ice-rafted debris at this site and another east of Ireland (~55°N, 15°W), imply increased advection of cold, ice-bearing waters south and east from their source regions in the Nordic and Labrador Seas during the LIA (Bond et al., 2001). It is unknown whether these intervals of increased iceberg delivery were associated with significant salinity anomalies. Upper North Atlantic Deep Water along the Laurentian Slope was ~1°C colder during the LIA, suggesting that surface conditions in the source region of this water, the Labrador Sea, were also cooler (Marchitto and deMenocal, 2003). The terrestrial record supports general Northern Hemisphere cooling, with LIA negative anomalies of 0.5 to 1°C in the mid- to high-latitude North Atlantic (Dahl-Jensen et al., 1998; Esper et al., 2002; Lamb, 1995).

Overall, the available data indicate the surface North Atlantic during the LIA, including the subtropical gyre, was about 1°C cooler. If the entire isopycnal outcropping region cooled by 1°C, then it would increase the density of the thermocline σ_t by ~ 0.15-0.25, about twice the observed change. Therefore, a small (~0.5°C) homogeneous cooling of the mixed layer from ~25-45°N could possibly account for the systematic shift in density along the Great Bahama Bank. Alternatively, if temperature remained constant and the density change were entirely function of salinity, it would imply a salinity increase in the outcropping region of ~0.2 psu.

The shift in Great Bahama Bank water column stratification may be purely dynamical and independent of variable mixed layer temperature and salinity along the northern edge of the gyre. According to the theory of Luyten et al. (1983) the thickness of the subtropical gyre thermocline at a given latitude is proportional to the zonally integrated Ekman pumping at that latitude. In other words, thermocline depth at the Great Bahama Bank is primarily dependent on the wind stress curl at 24°N and is generally insensitive to wind-field variability at distant locations such as the isopycnal outcropping region. Therefore, a thinner LIA subtropical gyre thermocline may have been driven by reduced wind stress curl and Ekman pumping at 24°N. According to the Sverdrup relation, this would also reduce the meridional mass transport, consistent with our inference that lower Florida Current flow during the LIA was primarily wind-field related.

The ventilated thermocline model is based on the concept that once a density layer is insulated from direct wind forcing its potential vorticity will be conserved (Luyten et al., 1983). Such a layer will thin at lower latitudes to maintain a constant spin to thickness ratio. If the latitude at which a layer is ventilated were to shift southwards, for example, then the layer would become thinner to adjust for the reduction in its initial planetary vorticity. Increased mixed layer density in the mid- to high-latitude Atlantic during the Little Ice Age would cause isopycnals to outcrop further south, and should lead to thinner density layers at 24°N (Luyten et al., 1983b). The thickness of two density layers that comprise most of the subtropical gyre thermocline at Great Bahama Bank were essentially constant during the last millennium, however, suggesting the latitude at which they outcrop changed little over this time span (Figure 17).

The thickness ratio of density layers within the thermocline reflects the relative distance between their outcropping latitudes. A larger north-south mixed-layer density gradient would cause the deepest isopycnals to outcrop a lower latitudes, which in turn would affect the layer thickness ratio (Luyten et al., 1983b). Since layer thicknesses (and hence the layer ratio) at the Great Bahama Bank remained nearly constant during the last millennium, it implies there was little change in the meridional density gradient of the surface North Atlantic between ~25-45°N. The absolute and relative thickness of thermocline layers suggests that the mid-latitude surface density North Atlantic was remarkably stable during the last 1,100 years. This inference does not exclude the possibility of ~1°C cooler LIA sea-surface temperatures, but does imply that surface

salinity must have been lower (~0.2 psu) in order to compensate for the effect of cooling on seawater density. Alternatively, if salinity increased, then surface waters must have been warmer.

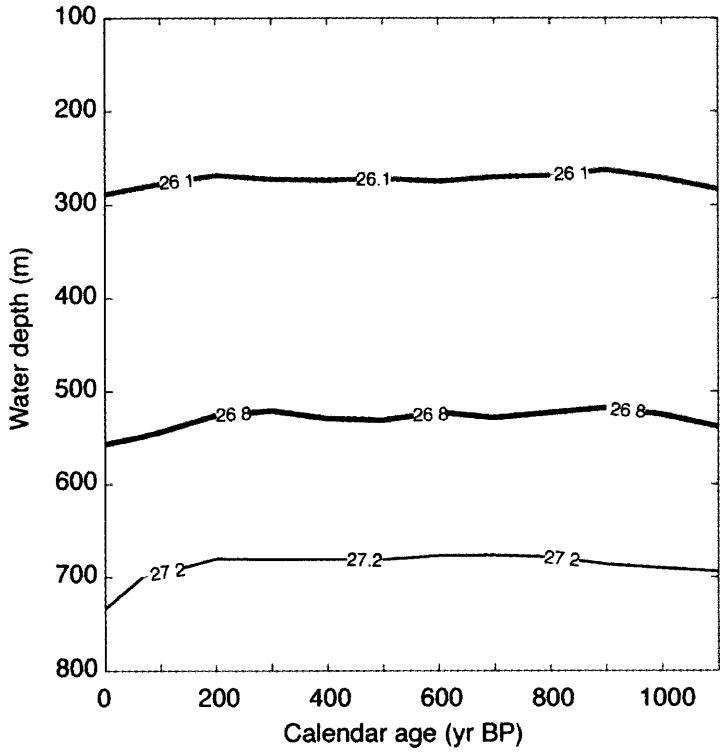

Figure 17
Thermocline isopycnal depth vs. time at Great Bahama Bank, 0-1100 yr BP. We chose to contour the three isopycnals that are best constrained by the available core material (26.1, 26.8, and 27.2; Figure 7). Over the last 1000 years, the thickness of the two layers defined by these isopycnals was essentially constant, implying little change in their outcropping latitude.

Heat transport

Heat flux into the North Atlantic can be estimated using the following equation:

$$Q = [\theta_{FC} - \theta_{NA}\ ]\ T_{FC}\ \rho C_p$$

where heat flux (Q) equals the difference in velocity-weighted mean temperature of the Florida Current (θ_{FC}) and deep water flowing southward out of the North Atlantic (θ_{NA}) multiplied by Florida Current transport (T_{FC}) and the constant ρC_p (0.0041 PW $°C^{-1}$ Sv^{-1}) (Larsen, 1992). Today, θ_{FC} and θ_{NA} are estimated to be 19.10 and 9.43°C, respectively (Larsen, 1992). Assuming a volume transport of 32 Sv, the northward heat flux is ~ 1.3 PW (1PW = 1 x 10^{15} W) (Molinari et al., 1990). On a monthly to annual basis, heat flux is driven primarily by T_{FC} since variability in θ_{FC} - θ_{NA} is small (Larsen, 1992). If θ_{FC} - θ_{NA} was similar to today during the LIA, then a 10% decrease in volume transport would reduce the northward oceanic heat flux by ~0.13 PW (or 1.3 x 10^{14} W). Alternatively, an increase in θ_{FC} of 1°C or decrease in θ_{NA} of 1°C could compensate for the effect of a 2-3 Sv transport reduction on heat flux.

Although we lack detailed information on the temperature structure of the Florida Current in the past, SSTs along Great Bahama Bank were ~ 0.5°C cooler during the Little Ice Age (Chapter 3). Since the upper 100 m of the Florida Current carries about 30% of the total transport (Schmitz and Richardson, 1991), this would have substantial leverage on θ_{FC} and would tend to magnify the LIA heat flux anomaly. Of course, this assumes either no change or an increase in θ_{NA}. Marchitto and deMenocal (2003) estimate that upper North Atlantic Deep Water was ~1°C cooler during the LIA. If we assume LIA

values of T_{FC} = 29 Sv, θ_{FC} = 18.5°C, and θ_{NA} = 8.4°C, northward oceanic heat transport would have been 1.2 PW, or 0.1 PW lower than today.

Given the number of variables involved, we can only speculate about how the oceanic heat flux varied in the past. We can however estimate the sensitivity of Northern Hemisphere temperature to a ~0.1 PW (1 x 10^{14} W) reduction in heat transport, and determine whether this change makes sense in light of available paleoclimate data. Averaged over the Northern Hemisphere (30°N to 90°N: 1.2 x 10^{14} m^2), 0.1 PW translates into a forcing on the order of -1 W m^{-2}. Climate system sensitivity estimates range from 0.3-1.0°C per W m^{-2}, with a best estimate of 0.5°C per W m^{-2} (IPCC, 1996). Combining the forcing and sensitivity values yields a temperature estimate of -0.3-1.0°C, with the best guess of -0.5°C. Although the majority of the temperature response would occur in the North Atlantic region, I chose to use a Northern Hemisphere average for comparison to available surface temperature reconstructions for the past millennium.

Effect of reduced heat transport on Northern Hemisphere climate

Variability in the Northern Hemisphere temperature reconstructions of Mann et al. (1999) and Crowley and Lowery (2000) is primarily attributed to solar, volcanic, and anthropogenic forcing (Crowley, 2000). Prior to the 20th century, solar and volcanic forcing alone can account for the estimated 0.1-0.2°C cooling that occurred during the LIA (Crowley, 2000). If this was the case, then it suggests the role of variable oceanic heat transport during the LIA was negligible and that our assumptions regarding level of

no motion or $\theta_{FC} - \theta_{NA}$ are in error. It is also possible that increased atmospheric heat transport could have compensated for the reduced Florida Current flow, resulting in little net change in surface temperature.

An alternative temperature reconstruction for the Northern Hemisphere shows centennial-scale temperature variability during the last millennium that is significantly larger than in the Mann et al. (1999) and Crowley and Lowery (2000) time series (Figure 18). Using a network of regionally-standardized tree ring records from temperature-sensitive locations, Esper et al. (2002) found that the Northern Hemisphere temperatures were on average ~ 0.5°C cooler than the Mann et al. (1999) time series during the Little Ice Age. The magnitude of this offset is consistent with our estimates of temperature change due to a weaker Gulf Stream, implying that oceanic heat transport may have played an important role in Little Ice Age cooling. If there was no change in oceanic heat flux during the last millennium, then either the Esper record is in error or another yet to be identified mechanism is required to explain the ~0.5°C cooling not accounted for by solar and volcanic forcing. Testing whether Gulf Stream heat flux played an important role in the LIA will require more detailed temperature estimates within the Florida Current and water flowing southward out of the North Atlantic. If oceanic heat transport played a significant role in the Little Ice Age, we should find the largest temperature anomalies in the North Atlantic region. Spatial analysis of the Esper et al. (2002) data should verify whether LIA temperature anomalies are consistent with an oceanic driver.

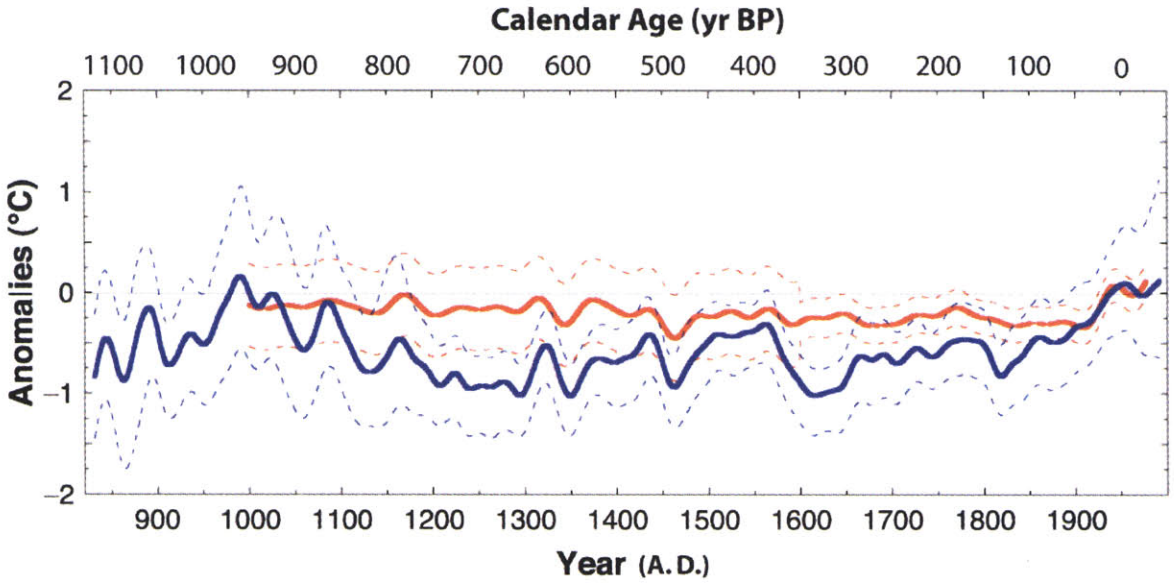

Figure 18

Northern Hemisphere temperature reconstructions for the last millennium (from Esper et al., 2002). The Esper record (blue) is on average 0.5°C cooler than the Mann et al. (1999) reconstruction (red) during the Little Ice Age. Both records were smoothed with a 40-year low pass filter. The offset between the reconstructions at centennial time scales is most likely a function of the differing techniques used to remove the biological growth trend from the tree-ring time series. Since the Esper et al. (2002) approach is designed specifically to preserve centennial-scale features typically lost to growth detrending, we believe it is a more reliable reconstruction of low-frequency Northern Hemisphere temperature variability during the last millennium.

Conclusions

The goal of this study was to reconstruct the density structure of the Florida Current over last millennium and infer from it whether the vertical current shear and transport varied on centennial time scales. If we assume that the level of no motion remained constant (within ±50 m), Florida Current transport was generally stable from 0-1000 yr BP, varying within 10% of the modern annual average of 31 Sv. The transport variability was not random, however. Flows were systematically 2-3 Sv lower from ~800 to 200 yr BP, the approximate time of the Little Ice Age. If we assume that the temperature difference between the Gulf Stream and water flowing southward out of the Atlantic was similar to today, then northward oceanic heat transport was ~1 x 10^{14} W lower during the LIA. The effect of such a reduction on Northern Hemisphere temperature is consistent with a least one independent surface temperature reconstruction for the last millennium. Although this result is suggestive, additional temperature data are required to conclusively link variable Florida Current transport to LIA cooling.

The changes in Florida Current density structure are driven primarily by variability at our Great Bahama Bank sites, those most influenced by the North Atlantic subtropical gyre. During the Little Ice Age, Bahamas thermocline density increased by ~0.1 kg/m^3, due to either changes in wind-stress curl at 24°N or a shift in temperature and salinity properties in the isopycnal outcropping region. In the first case, a reduction in wind-stress curl would limit Ekman pumping of mixed-layer water into the thermocline, leading to a more stratified water column and thinner thermocline. Consistent with this

idea, the water column at the Great Bahama Bank was more stratified prior to 200 yr BP. A LIA reduction in the wind-driven circulation would also explain why the largest transport anomalies occur from 100-500 m water depth in the Florida Current. Today water in this range can be traced primarily to the subtropical gyre. Future work will include calculating the change in Ekman pumping required to reduce Florida Current transport by 3 Sv, and then using this information in combination with the Luyten et al. (1983) ventilated thermocline theory to estimate the expected shift in thermocline depth. In doing so, it should be possible to determine whether the observed change in isopycnal depths can be attributed entirely to wind forcing or if variations in temperature and salinity are also necessary.

If variability in Great Bahama Bank thermocline density was a function of temperature or salinity, it would require either 0.5°C cooler or 0.2 psu saltier waters in the mid-latitude mixed layer where the thermocline is ventilated. Published records suggest that a 0.5°C LIA cooling for this region is reasonable. It is also possible that saltier conditions in the sub-surface subtropical gyre were linked to high salinity surface Gulf Stream waters (Chapter 3) via mid-latitude thermocline ventilation. Such a scenario is consistent with published models that show southward ITCZ migration increases the salt content of the surface tropical North Atlantic and this salt is then advected into the subtropical gyre via the Gulf Stream (Vellinga et al., 2002). In the models this process acts as a negative feedback on Northern Hemisphere cooling by stimulating North Atlantic Deep Water formation. Although we see little evidence for significant changes

in the meridional overturning circulation during the LIA, it is intriguing that the surface Florida Current achieved its highest salinity at 200 yr BP, just prior to the 3 Sv increase in transport from Little Ice Age to present.

References

Bache, A. D. (1860) Lecture on the Gulf Stream, prepared at the request of the American Association for the Advancement of Science, *American Journal of Science and Arts, 31 (90)*, 314-329.

Baringer, M. O., and J. C. Larsen (2001), Sixteen years of Florida Current transport at 27°N, *Geophys. Res. Lett., 28*, 3179-3182.

Bond, G., B. Kromer, J. Beer, R. Muscheler, M. N. Evans, W. Showers, S. Hoffmann, R. Lotti-Bond, I. Hajdas, and G. Bonami (2001), Persistent solar influence on North Atlantic climate during the Holocene, *Science, 294,* 2130-2136.

Crowley, T. J. and T. S. Lowery (2000), How warm was the Medieval Warm Period?, *Ambio, 29*, 51-54.

Crowley, T. J. (2000), Causes of climate change over the past 1000 years, *Science, 289*, 270-277.

Curry, R. (2005), http://www.whoi.edu/science/PO/hydrobase/HB2_home.htm

Dahl-Jensen, D., K. Mosegaard, N. Gundestrup, G. D. Clow, S. J. Johnsen, A. W. Hansen, and N. Balling (1998), Past temperatures directly from the Greenland ice sheet, *Science, 282*, 268-271.

deMenocal, P., J. Ortiz, T. Guilderson, and M. Sarnthein (2000), Coherent high- and low-latitude variability during the Holocene warm period, *Science, 288*, 2198-2202.

Dansgaard, W. (1964), Stable isotopes in precipitation, *Tellus XVI (4)*, 436-468.

Deuser, W. G. (1987), Seasonal variations in isotopic composition and deep-water fluxes of the tests of perennially abundant planktonic foraminifera of the Sargasso Sea: results from sediment-trap collections and their paleoceanographic significance, *Journal of Foraminiferal Research, 17*, 14-27.

Esper, J., E. R. Cook, and F. H. Shweingruber (2002), Low-frequency signals in long tree-ring chronologies for reconstructing past temperature variability, *Science, 295*, 2250-2253.

Fairbanks, R. G., M Sverdlove, R. Free, P. H. Wiebe, and Allan W. H. Bé (1982), Vertical distribution and isotopic fractionation of living planktonic foraminifera from the Panama Basin, *Nature, 298*, 841-844.

Hamilton, P., J. C. Larsen, K. D. Leaman, T. N. Lee, and E. Waddell (2005), Transports through the Straits of Florida, Journal of Physical Oceanography, 35, 308-322.

Inter-Governmental Panel on Climate Change (IPCC) (1996), *Climate Change 1995 – Contribution of Working Group I to the Second Assessment Report of the IPCC*, Cambridge University Press, UK.

Keigwin, L. D., The Little Ice Age and Medieval Warm Period in the Sargasso Sea, *Science, 274*, 1504-1508 (1996).

Keigwin, L., and R. S. Pickart, Slope Water Current over the Laurentian Fan on interannual to millennial time scales, *Science, 286*, 520-523, 1999.

Lamb, H., (1995) *Climate, History and the Modern World* (Routledge, London, New York, ed. 2).

Larsen, J.C., (1992) Transport and heat flux of the Florida Current at 27°N derived from cross-stream voltages and profiling data: theory and observations, *Philos. Trans. R. Soc. London A, 338*, 169-236.

Leaman, K. D., R. L. Molinari, and P. S. Vertes, Structure and variability of the Florida Current at 27°N: April 1982-July 1984, *Journal of Physical Oceanography, 17*, 565-583.

Leaman, K. D., P. S. Vertes, L. P. Atkinson, T. N. Lee, P. Hamilton, and E. Waddell (1995), Transport, potential vorticity, and current/temperature structure across Northwest Providence and Santaren Channels and the Florida Current off Cay Sal Bank, J. Geophys. Res., 100 (C5), 8561-8569.

Levitus, S., R. Burgett, and T.P. Boyer, World Ocean Atlas (1994), Volume 3: Salinity & Volume 4: Temperature, NOAA Atlas NESDIS 3 & 4. U.S. Department of Commerce, Washington, D.C.

Lund, D. C., and W. B. Curry (2004), Late Holocene variability in Florida Current surface density: Patterns and possible causes, *Paleoceanography, 19*, PA4001, doi: 10.1029/2004PA001008.

Luyten, J. R., J. Pedlosky, and H. Stommel (1983), The ventilated thermocline, *Journal of Physical Oceanography*, 13, 292-309.

Luyten, J., J. Pedlosky, and H. Stommel (1983b), Climatic inferences from the ventilated thermocline, *Climatic Change, 5,* 183-191.

Lynch-Stieglitz, J., W. B. Curry, and N. Slowey, A geostrophic estimate for the Florida Current from the oxygen isotope composition of benthic foraminifera, *Paleoceanography, 14*, 360-373, 1999.

Mann, M. E., R. S. Bradley, M. K. Hughes (1999), Northern Hemisphere Temperatures during the past millennium: inferences, uncertainties, and limitations, *Geophys. Res. Lett., 26*, 759-762.

Marchitto, T. M., and P. B. deMenocal (2003), Late Holocene variability of upper North Atlantic Deep Water temperature and salinity, *Geochem. Geophys. Geosyst., 4(12)*, 1100, doi:10.1029/2003GC000598.

Molinari, R. L., W. D. Wilson, and K. Leaman (1985), Volume and heat transports of the Florida Current: April 1982 through August 1983, *Science, 277*, 295-297.

Molinari, R. L., E. Johns, and J. F. Festa (1990), The annual cycle of meridional heat flux in the North Atlantic Ocean at 26.5N, *Journal of Physical Oceanography, 20*, 476-482.

Montgomery, R. B. (1941), Transport of the Florida Current off Habana, Journal of Marine Research, IV (3), 198-220.

Niiler, P. P. and W. S. Richardson (1973), Seasonal variability of the Florida Current, *Journal of Marine Research, 31 (3)*, 144-167.

Pillsbury, J. E. (1890) The Gulf Stream – A description of the methods employed in the investigation, and the results of the research, *Report of the Superintendent of the U. S. Coast and Geodetic Survey*, 173-184.

Pond, S., and G. L. Pickard (1983), *Introductory Dynamical Oceanography, 2nd edition*, Pergammon Press, Oxford, 329 pp.

Schmidt, G.A., G. R. Bigg and E. J. Rohling (1999) "Global Seawater Oxygen-18 Database". http://www.giss.nasa.gov/data/o18data/

Schmitz, W. J., and W. S. Richardson (1968), On the transport of the Florida Current, *Deep-Sea Research, 15*, 679-693.

Schmitz, W. J., and P. Richardson (1991), On the sources of the Florida Current, *Deep-Sea Research, 38*, s379-s409.

Schmitz, W. J., J. R. Luyten, and R. W. Schmitt (1993), On the Florida Current T/S envelope, *Bulletin of Marine Science, 53*, 1048-1065.

Schott, F. A., T. N. Lee, and R. Zantopp (1988), Variability and structure of the Florida Current in the period range of days to seasonal, Journal of Physical Oceanography, 18, 1209-1230.

Slowey, N. C., and W. B. Curry (1995), Glacial-interglacial differences in circulation and carbon cycling within the upper western North Atlantic, Paleoceanography, 10(5), 715-732.

Stuiver, M., P. J. Reimer, E. Bard, J. W. Beck, G. S. Burr, K. A. Hughen, B. Kromer, F. G. McCormac (1998), J. v. d. Plicht, and M. Spurk, INTCAL98 radiocarbon age calibration 24,000 - 0 cal BP, Radiocarbon, 40, 1041-1083.

Vellinga, M., R. A. Wood, and J. M. Gregory (2002), Processes governing the recovery of a perturbed thermohaline circulation in HadCM3, *J. Clim., 15*, 764-780.

Wertheim, G. K. (1954), Studies of the electric potential between Key West, Florida, and Havana, Cuba, *Transactions of the American Geophysical Union, 35 (6)*, 872-882.

Wüst, G., (1924) Florida- und Anillenstrom, eine Hydrodynamicsche Untersuchung. Veröffentlichungen del Insituts für Meereskunde an der Universität Berlin, Neue Folge, A12 (48pp).

Chapter 5: Summary and Conclusions

The four broad goals outlined at the beginning of this thesis were to: (1) use replicate planktonic foraminiferal $\delta^{18}O_c$ records to determine if centennial-scale oceanographic variability can be detected in the Florida Straits; (2) combine the planktonic $\delta^{18}O_c$ records with Mg/Ca data to evaluate Florida Current surface temperature and salinity during the last millennium; (3) estimate past changes in cross-current density gradient, vertical current shear, and transport using benthic foraminiferal $\delta^{18}O_c$ from cores spanning the depth and width of the Florida Current; and (4) evaluate the Florida Current data in the context of other records of Late Holocene climate variability and speculate on climate mechanisms most likely responsible for the observed changes.

Coherent variability in two long (>3000 year) planktonic $\delta^{18}O_c$ records retrieved near Dry Tortugas demonstrate the feasibility of using ocean sediments to address centennial-scale climate change in this location (Chapter 2). At frequencies higher than 1/250 years the records lack coherence, most likely due to age model error and aliasing of the seasonal sea-surface temperature cycle. The variance at a given stratigraphic level in each core can be described as a simple sum of variance due to mass spectrometer analytical error and variance associated with random sampling of the seasonal SST cycle. This suggests that on the decadal time-scale of individual samples (average sampling interval of 20-35 years) $\delta^{18}O_c$ variability was driven primarily by the seasonal SST cycle and that changes seawater $\delta^{18}O$ ($\delta^{18}O_w$) were minor.

In contrast, the planktonic $\delta^{18}O_c$ signal is driven almost entirely by $\delta^{18}O_w$ on centennial time scales (Chapter 3). The pattern of $\delta^{18}O_w$ variability at two Dry Tortugas sites indicates conditions were unusually salty during the LIA, consistent with published records that show anomalously dry conditions near the Cariaco Basin. Since the proxies used at Dry Tortugas and the Cariaco Basin are subject to very different sources of uncertainty, the parallel changes between them points to a common forcing mechanism. The most likely link is southward migration of the Inter-Tropical Convergence Zone (ITCZ), which would produce not only drier conditions near the Cariaco Basin, but also less precipitation in the tropical North Atlantic and therefore higher surface salinity. We assume that this anomaly would be advected to the Dry Tortugas sites by the prevailing surface ocean circulation.

On the Great Bahama Bank, replicate $\delta^{18}O_w$ records show that LIA surface salinity on the eastern edge of the Florida Current was lower than today, opposite the pattern observed at Dry Tortugas. This apparent contradiction is most likely a result of movement of not only the ascending limb of the Hadley circulation (the ITCZ) but also the descending limb. Southward movement of the Hadley cell during the LIA would likely reduce evaporation in the subtropical gyre and lead to lower surface salinity. Although the Dry Tortugas and Great Bahama Bank $\delta^{18}O_w$ signals move in the opposite directions during the Little Ice Age, they are not mirror images of one another, as would be expected if the $\delta^{18}O_w$ records were driven only by movement of freshwater between the subtropics and tropics. Rather, there appears to be at least one other end member

involved. Consistent with this idea, realistic salinity values can only be achieved if the LIA $\delta^{18}O_w$ data are scaled to salinity using a thermocline or high-latitude $\delta^{18}O_w$-S slope (~0.5‰/psu). The $\delta^{18}O_w$ are most easily explained through greater influence of high-latitude water at the Great Bahama Bank and a mean shift in thermocline $\delta^{18}O_w$.

Prior to 1,200 yr BP there is significant variability in the Dry Tortugas planktonic $\delta^{18}O_c$ records (Chapter 2). We currently lack Mg/Ca data from this time interval, so it unclear if the signal was primarily a function of temperature or $\delta^{18}O_w$. If the last 1,200 years can serve as a guide, the centennial-scale $\delta^{18}O_c$ variability from 1,200 to 5,200 yr BP was likely associated with salinity. The $\delta^{18}O_c$ signal is coherent with atmospheric radiocarbon ($\Delta^{14}C_{atm}$) and radiocarbon production rate ($^{14}C_{pr}$) at frequencies between 1/1000 and 1/300 years. Low coherence at high frequencies is likely due to age model uncertainty and aliasing of the seasonal cycle in the $\delta^{18}O_c$ time series as opposed to a true lack of common variance. At frequencies lower than 1/1000 years, $\delta^{18}O_c$ is coherent with $\Delta^{14}C_{atm}$ but not $^{14}C_{pr}$, suggesting that oceanic circulation may affect $\Delta^{14}C_{atm}$ on millennial time scales.

Although variable solar irradiance may have triggered centennial-scale climate variability during the late Holocene, solar forcing on its own appears to be too weak to explain climate anomalies such as the Little Ice Age. Either another driving mechanism was involved, or small changes in irradiance were amplified through a series of climate system feedbacks. To determine if the Gulf Stream played a role in the LIA, we

reconstructed the cross-current density gradient and vertical shear of the Florida Current for the last millennium. The results show that Florida Current vertical shear was lower during the Little Ice Age than both today and 1,100 yr BP. Assuming a constant level of no motion at 850 m, the changes in shear translate into LIA transports 2-3 Sv lower than the modern value of 31 Sv. Reduced flow occurred when the Northern Hemisphere was unusually cold, suggesting that Gulf Stream heat transport played an important role in the LIA. If we scale Florida Current volume flux to heat flux, then low flow would have cooled the Northern Hemisphere by up to 0.5°C, consistent with at least one temperature reconstruction for the Little Ice Age.

The Great Bahama Bank benthic foraminiferal $\delta^{18}O_c$ results can be interpreted in the context of ventilated thermocline theory, which states that (1) thermocline thickness at a particular location is a function of the zonally integrated Ekman pumping at the latitude, and (2) thickness of density layers within the thermocline is driven primarily by the latitude at which they outcrop. Based on density profiles from the Great Bahama Bank, it appears that the subtropical gyre thermocline thinned during the Little Ice Age. If this was a wind-driven phenomenon, it would suggest a reduction in subtropical gyre Ekman pumping and wind stress curl. The relatively constant thickness of density layers within the thermocline indicates little change in their outcropping latitude through time, which can be interpreted as a nearly constant mixed layer density at the northern edge of the subtropical gyre. An increase in mixed layer density would presumably cause isopycnals to outcrop at lower latitudes. It remains to be determined whether the

expected change in layer thickness due to a reasonable shift in LIA surface density is detectable using benthic foraminifera at the Great Bahama Bank.

Speculation

The variability in Great Bahama Bank thermocline density may be driven by salinity. Since we lack estimates of thermocline temperature, however, we cannot determine with certainty that salinity variations were involved. Nonetheless, it is instructive to estimate the change in salinity required to account for the Great Bahama Bank thermocline density anomaly during the LIA. The thermocline shift of +0.1‰ is equivalent to an increase in salinity of 0.2 psu (using a 0.5‰/psu slope). Given that the total mass of the gyre is approximately 1.35×10^{19} kg ($1025\ kg/m^3 * 800\ m * 5.9 \times 10^6\ m * 2.8 \times 10^{16}$ m), the mass of salt in the gyre today is roughly 4.877×10^{20} g (36 g/kg * 1.35×10^{19} kg). A salinity increase of 0.2 psu translates into about 3×10^{18} g more salt in the subtropical gyre during the LIA. The most likely salt source is the Gulf Stream – higher salt content in the surface Florida Current during the LIA may have altered subtropical gyre salinity via thermocline ventilation. Given a mass transport the upper 100 m of the Florida Current of approximately 2.9×10^{17} kg/yr ($1025\ kg/m^3 * 9$ Sv), a salinity increase of 0.2 psu would increase the salt flux by 6×10^{16} g/yr. To summarize:

	Total subtropical gyre salt (g)	Surface Florida Current Salt Flux (g/yr)
Today	4.877×10^{20}	1.050×10^{19}
Little Ice Age	4.904×10^{20}	1.056×10^{19}
Difference	$\sim 3 \times 10^{18}$	$\sim 6 \times 10^{16}$

From the Little Ice Age to present, the total reduction in salt input from the surface Florida Current was about 6 x 10^{18} g (6 x 10^{16} g/yr * 0.5 * 200 years), similar to the change in subtropical gyre salt inventory. This result suggests that higher Florida Current surface salinity could account for the density anomaly observed in the subtropical gyre during the Little Ice Age.

If we assume that salt preferentially accumulated in the subtropical as opposed to the tropical or subpolar thermocline, the Gulf Stream cross-current density gradient would be diminished. To maintain geostrophic balance, the vertical current shear would decrease. I speculate that during the LIA, southward ITCZ migration, perhaps triggered by decreased solar irradiance, led to higher Florida Current surface and subtropical gyre thermocline salinity, and this in turn reduced the flow of the Gulf Stream. Alternatively, southward ITCZ migration may reduce the strength of the trade winds over the subtropical gyre, which in turn would reduce the wind stress curl and transport of the Gulf Stream. In either scenario, a reduction in oceanic heat transport could amplify the climate system response to the small reductions in solar irradiance that occurred during the Little Ice Age.

Future Work

The results of this thesis raise several issues, including the relationship between Gulf Stream salinity and solar variability, the role of Gulf Stream heat transport in the Little Ice Age, and the cause of long-term trends in subtropical and tropical North

Atlantic stratification. As for the first issue, the existing Florida Current $\delta^{18}O_w$ time series are too short to establish the phase relationship with atmospheric $\Delta^{14}C$. A key future project will be to extend the $\delta^{18}O_w$ records to the mid-Holocene. Uncertainty in the ^{14}C reservoir age should be less problematic in a 5,000 year-long record, and so it may be possible to determine the relative phasing of $\delta^{18}O_w$ and cosmogenic nuclide production. Doing so will reveal whether centennial-scale changes in tropical Atlantic rainfall were due to internal climate system oscillations or external solar forcing. If $\delta^{18}O_w$ led ^{14}C production, then there must be ocean-atmosphere feedback mechanisms capable of independently generating centennial-scale climate variability. If the reverse was true, then small changes in solar irradiance may be capable of triggering widespread and abrupt shifts in the hydrologic cycle.

Further research is also necessary to better characterize the temperature structure of the Florida Current during the last millennium. Core top Mg/Ca ratios in the benthic foraminifer *C. floridanus* appear to reflect bottom water temperature and therefore may be useful in reconstructing thermocline variability in the past. This will greatly improve our ability to calculate heat transport and allow us to better estimate the effect of variable Gulf Stream strength on Northern Hemisphere temperature. In combination with $\delta^{18}O_c$, the benthic Mg/Ca data will allow for estimates of thermocline $\delta^{18}O_w$. Using this information it should be possible to verify whether the subtropical gyre was indeed saltier during the LIA and determine whether this change was consistent with reconstructions of Florida Current surface salinity.

Finally, we need to better understand the apparent long-term trend in water column stratification observed in both the subtropical and tropical North Atlantic from 1000 yr BP to today. This trend appears to be part of a longer millennial-scale pattern. Extension of the planktonic and benthic $\delta^{18}O_c$ records back in time will clarify the nature of this variability and allow for more informed speculation on its cause. For the time being, the trend toward less stratified conditions in the low-latitude Atlantic over the last millennium seems to signify either a long-term increase in wind stress curl or perhaps a warming and/or freshening of the thermocline.

APPENDIX A

Chapter 2 planktonic foraminiferal stable isotope data

COLUMN HEADERS:

CORE, DEPTH (cm), C13 (per mil), O18 (per mil), SPECIES

NOTE:

Each stable isotope analysis was based on an average of 10 *G. ruber-w* individuals.

CORE	DEPTH	C13	O18	SPECIES
W167-79GGC	0.5	0.627	-1.433	G. ruber-w
W167-79GGC	0.5	0.547	-1.493	G. ruber-w
W167-79GGC	0.5	0.425	-1.815	G. ruber-w
W167-79GGC	2	0.788	-1.467	G. ruber-w
W167-79GGC	2	0.322	-1.624	G. ruber-w
W167-79GGC	2	0.805	-1.696	G. ruber-w
W167-79GGC	3.25	0.831	-1.412	G. ruber-w
W167-79GGC	3.25	0.699	-1.23	G. ruber-w
W167-79GGC	3.25	0.847	-1.137	G. ruber-w
W167-79GGC	3.25	0.821	-1.685	G. ruber-w
W167-79GGC	3.75	0.573	-1.431	G. ruber-w
W167-79GGC	3.75	0.772	-1.577	G. ruber-w
W167-79GGC	3.75	0.48	-1.431	G. ruber-w
W167-79GGC	3.75	0.523	-1.517	G. ruber-w
W167-79GGC	4.25	0.69	-1.211	G. ruber-w
W167-79GGC	4.25	0.727	-1.299	G. ruber-w
W167-79GGC	4.25	0.633	-1.366	G. ruber-w
W167-79GGC	4.25	0.843	-1.607	G. ruber-w
W167-79GGC	4.75	0.615	-1.498	G. ruber-w
W167-79GGC	4.75	0.598	-1.388	G. ruber-w
W167-79GGC	4.75	0.805	-1.027	G. ruber-w
W167-79GGC	5.25	0.827	-1.474	G. ruber-w
W167-79GGC	5.25	0.336	-1.757	G. ruber-w
W167-79GGC	5.25	0.83	-1.354	G. ruber-w
W167-79GGC	5.25	0.483	-1.518	G. ruber-w
W167-79GGC	5.75	0.868	-1.455	G. ruber-w
W167-79GGC	5.75	0.762	-1.468	G. ruber-w
W167-79GGC	5.75	0.587	-1.413	G. ruber-w
W167-79GGC	6.25	-0.118	-1.465	G. ruber-w
W167-79GGC	6.25	0.77	-1.485	G. ruber-w
W167-79GGC	6.25	0.54	-1.503	G. ruber-w
W167-79GGC	6.25	0.536	-1.561	G. ruber-w
W167-79GGC	6.75	0.569	-1.457	G. ruber-w
W167-79GGC	6.75	0.728	-1.906	G. ruber-w
W167-79GGC	6.75	0.467	-1.603	G. ruber-w
W167-79GGC	6.75	0.639	-1.568	G. ruber-w
W167-79GGC	7.25	0.651	-1.635	G. ruber-w
W167-79GGC	7.25	0.449	-1.69	G. ruber-w
W167-79GGC	7.25	0.458	-1.732	G. ruber-w
W167-79GGC	7.75	0.46	-1.51	G. ruber-w
W167-79GGC	7.75	0.906	-1.684	G. ruber-w
W167-79GGC	7.75	0.387	-1.946	G. ruber-w
W167-79GGC	7.75	0.819	-1.815	G. ruber-w
W167-79GGC	8.25	0.568	-1.763	G. ruber-w
W167-79GGC	8.25	0.604	-1.421	G. ruber-w
W167-79GGC	8.25	0.295	-1.812	G. ruber-w
W167-79GGC	8.25	0.279	-1.87	G. ruber-w
W167-79GGC	8.75	0.399	-1.504	G. ruber-w
W167-79GGC	8.75	0.619	-1.597	G. ruber-w
W167-79GGC	8.75	0.774	-0.897	G. ruber-w
W167-79GGC	8.75	0.638	-1.906	G. ruber-w
W167-79GGC	9.25	0.413	-1.853	G. ruber-w
W167-79GGC	9.25	0.711	-1.9	G. ruber-w
W167-79GGC	9.25	0.577	-1.388	G. ruber-w

W167-79GGC	9.25	0.606	-1.538	G. ruber-w
W167-79GGC	9.75	0.409	-1.495	G. ruber-w
W167-79GGC	9.75	0.53	-1.608	G. ruber-w
W167-79GGC	9.75	0.503	-1.319	G. ruber-w
W167-79GGC	9.75	1.026	-1.531	G. ruber-w
W167-79GGC	10.25	0.626	-1.797	G. ruber-w
W167-79GGC	10.25	0.143	-1.638	G. ruber-w
W167-79GGC	10.25	0.662	-1.593	G. ruber-w
W167-79GGC	10.25	0.656	-1.648	G. ruber-w
W167-79GGC	10.75	0.394	-1.689	G. ruber-w
W167-79GGC	10.75	0.58	-1.659	G. ruber-w
W167-79GGC	10.75	0.634	-1.647	G. ruber-w
W167-79GGC	10.75	0.483	-1.657	G. ruber-w
W167-79GGC	11.25	0.211	-1.539	G. ruber-w
W167-79GGC	11.25	0.906	-1.252	G. ruber-w
W167-79GGC	11.25	0.762	-1.629	G. ruber-w
W167-79GGC	11.25	0.617	-1.902	G. ruber-w
W167-79GGC	11.75	0.688	-1.643	G. ruber-w
W167-79GGC	11.75	0.36	-1.724	G. ruber-w
W167-79GGC	11.75	0.447	-1.738	G. ruber-w
W167-79GGC	11.75	0.52	-1.34	G. ruber-w
W167-79GGC	12.25	0.796	-1.32	G. ruber-w
W167-79GGC	12.25	0.775	-1.954	G. ruber-w
W167-79GGC	12.25	0.375	-2.002	G. ruber-w
W167-79GGC	12.25	0.479	-2.001	G. ruber-w
W167-79GGC	12.75	0.471	-1.519	G. ruber-w
W167-79GGC	12.75	0.171	-1.698	G. ruber-w
W167-79GGC	12.75	0.618	-1.399	G. ruber-w
W167-79GGC	12.75	0.273	-2.029	G. ruber-w
W167-79GGC	13.25	0.676	-1.698	G. ruber-w
W167-79GGC	13.25	0.169	-1.678	G. ruber-w
W167-79GGC	13.25	0.286	-1.867	G. ruber-w
W167-79GGC	13.25	0.476	-1.63	G. ruber-w
W167-79GGC	13.75	0.658	-1.348	G. ruber-w
W167-79GGC	13.75	0.662	-1.638	G. ruber-w
W167-79GGC	13.75	0.548	-1.453	G. ruber-w
W167-79GGC	13.75	0.224	-1.399	G. ruber-w
W167-79GGC	14.25	0.337	-1.465	G. ruber-w
W167-79GGC	14.25	0.433	-1.876	G. ruber-w
W167-79GGC	14.25	0.534	-1.865	G. ruber-w
W167-79GGC	14.75	0.748	-1.81	G. ruber-w
W167-79GGC	14.75	0.804	-1.796	G. ruber-w
W167-79GGC	14.75	0.579	-1.668	G. ruber-w
W167-79GGC	15.25	0.355	-1.906	G. ruber-w
W167-79GGC	15.25	0.527	-1.74	G. ruber-w
W167-79GGC	15.25	0.749	-1.639	G. ruber-w
W167-79GGC	15.75	0.646	-1.528	G. ruber-w
W167-79GGC	15.75	0.581	-1.293	G. ruber-w
W167-79GGC	15.75	0.57	-1.419	G. ruber-w
W167-79GGC	16.25	0.518	-1.385	G. ruber-w
W167-79GGC	16.25	0.217	-1.71	G. ruber-w
W167-79GGC	16.25	-0.068	-1.576	G. ruber-w
W167-79GGC	16.75	0.549	-1.56	G. ruber-w
W167-79GGC	16.75	0.38	-1.649	G. ruber-w
W167-79GGC	16.75	0.461	-1.648	G. ruber-w

W167-79GGC	17.25	0.771	-1.486	G. ruber-w
W167-79GGC	17.25	0.29	-1.814	G. ruber-w
W167-79GGC	17.25	0.432	-1.278	G. ruber-w
W167-79GGC	17.75	0.216	-1.728	G. ruber-w
W167-79GGC	17.75	0.417	-1.319	G. ruber-w
W167-79GGC	17.75	0.58	-1.519	G. ruber-w
W167-79GGC	18.25	0.613	-1.378	G. ruber-w
W167-79GGC	18.25	0.663	-1.568	G. ruber-w
W167-79GGC	18.25	0.442	-1.326	G. ruber-w
W167-79GGC	18.75	0.307	-1.865	G. ruber-w
W167-79GGC	18.75	0.34	-1.841	G. ruber-w
W167-79GGC	18.75	0.07	-1.806	G. ruber-w
W167-79GGC	19.25	0.573	-1.731	G. ruber-w
W167-79GGC	19.25	0.143	-1.637	G. ruber-w
W167-79GGC	19.25	0.32	-1.079	G. ruber-w
W167-79GGC	19.75	0.677	-1.555	G. ruber-w
W167-79GGC	19.75	0.717	-1.656	G. ruber-w
W167-79GGC	19.75	0.129	-1.766	G. ruber-w
W167-79GGC	19.75	0.483	-1.922	G. ruber-w
W167-79GGC	19.75	0.041	-1.667	G. ruber-w
W167-79GGC	20.25	0.82	-1.804	G. ruber-w
W167-79GGC	20.25	0.531	-1.441	G. ruber-w
W167-79GGC	20.25	0.087	-1.597	G. ruber-w
W167-79GGC	20.25	0.15	-1.813	G. ruber-w
W167-79GGC	20.25	0.364	-1.423	G. ruber-w
W167-79GGC	20.25	0.496	-1.758	G. ruber-w
W167-79GGC	20.75	0.72	-1.882	G. ruber-w
W167-79GGC	20.75	0.088	-1.614	G. ruber-w
W167-79GGC	20.75	0.307	-1.723	G. ruber-w
W167-79GGC	20.75	0.514	-2.083	G. ruber-w
W167-79GGC	20.75	0.742	-1.409	G. ruber-w
W167-79GGC	20.75	0.681	-1.374	G. ruber-w
W167-79GGC	21.25	0.409	-1.675	G. ruber-w
W167-79GGC	21.25	0.436	-1.772	G. ruber-w
W167-79GGC	21.25	0.773	-1.833	G. ruber-w
W167-79GGC	21.25	0.467	-1.715	G. ruber-w
W167-79GGC	21.25	0.689	-1.307	G. ruber-w
W167-79GGC	21.25	0.636	-1.446	G. ruber-w
W167-79GGC	21.75	0.213	-1.733	G. ruber-w
W167-79GGC	21.75	0.155	-1.787	G. ruber-w
W167-79GGC	21.75	0.569	-1.228	G. ruber-w
W167-79GGC	21.75	0.376	-2.096	G. ruber-w
W167-79GGC	21.75	0.697	-1.336	G. ruber-w
W167-79GGC	21.75	0.733	-1.791	G. ruber-w
W167-79GGC	22.25	0.43	-1.799	G. ruber-w
W167-79GGC	22.25	0.262	-1.469	G. ruber-w
W167-79GGC	22.25	0.711	-1.592	G. ruber-w
W167-79GGC	22.25	0.799	-1.799	G. ruber-w
W167-79GGC	22.25	0.68	-1.725	G. ruber-w
W167-79GGC	22.25	0.549	-1.704	G. ruber-w
W167-79GGC	22.75	0.251	-1.705	G. ruber-w
W167-79GGC	22.75	0.393	-1.753	G. ruber-w
W167-79GGC	22.75	0.337	-1.729	G. ruber-w
W167-79GGC	22.75	0.538	-1.518	G. ruber-w
W167-79GGC	23.25	0.409	-1.452	G. ruber-w

W167-79GGC	23.25	0.446	-1.764	G. ruber-w
W167-79GGC	23.25	0.391	-1.679	G. ruber-w
W167-79GGC	23.75	0.17	-2.017	G. ruber-w
W167-79GGC	23.75	0.5	-1.851	G. ruber-w
W167-79GGC	23.75	0.052	-1.654	G. ruber-w
W167-79GGC	23.75	0.184	-1.78	G. ruber-w
W167-79GGC	24.25	0.593	-1.624	G. ruber-w
W167-79GGC	24.25	0.468	-1.386	G. ruber-w
W167-79GGC	24.25	0.402	-1.817	G. ruber-w
W167-79GGC	24.25	0.442	-1.804	G. ruber-w
W167-79GGC	24.75	0.48	-1.515	G. ruber-w
W167-79GGC	24.75	0.444	-1.584	G. ruber-w
W167-79GGC	24.75	0.512	-1.423	G. ruber-w
W167-79GGC	24.75	0.483	-1.684	G. ruber-w
W167-79GGC	25.25	0.737	-1.422	G. ruber-w
W167-79GGC	25.25	0.448	-1.302	G. ruber-w
W167-79GGC	25.25	-0.063	-1.979	G. ruber-w
W167-79GGC	25.25	0.578	-1.343	G. ruber-w
W167-79GGC	25.75	0.539	-1.846	G. ruber-w
W167-79GGC	25.75	0.178	-1.674	G. ruber-w
W167-79GGC	25.75	0.51	-1.616	G. ruber-w
W167-79GGC	25.75	0.846	-1.616	G. ruber-w
W167-79GGC	26.25	0.733	-1.574	G. ruber-w
W167-79GGC	26.25	0.41	-1.979	G. ruber-w
W167-79GGC	26.25	0.505	-1.558	G. ruber-w
W167-79GGC	26.25	0.027	-1.517	G. ruber-w
W167-79GGC	26.75	0.129	-1.526	G. ruber-w
W167-79GGC	26.75	0.113	-1.621	G. ruber-w
W167-79GGC	26.75	0.326	-1.752	G. ruber-w
W167-79GGC	26.75	0.505	-1.649	G. ruber-w
W167-79GGC	27.25	0.551	-1.527	G. ruber-w
W167-79GGC	27.25	0.208	-1.639	G. ruber-w
W167-79GGC	27.25	0.728	-1.592	G. ruber-w
W167-79GGC	27.75	0.694	-1.449	G. ruber-w
W167-79GGC	27.75	0.752	-1.195	G. ruber-w
W167-79GGC	27.75	-0.119	-1.748	G. ruber-w
W167-79GGC	27.75	0.374	-1.71	G. ruber-w
W167-79GGC	28.25	0.629	-1.486	G. ruber-w
W167-79GGC	28.25	0.901	-1.357	G. ruber-w
W167-79GGC	28.25	0.622	-1.634	G. ruber-w
W167-79GGC	28.25	0.345	-1.251	G. ruber-w
W167-79GGC	28.75	-0.041	-2.326	G. ruber-w
W167-79GGC	28.75	0.429	-1.861	G. ruber-w
W167-79GGC	28.75	1.006	-1.61	G. ruber-w
W167-79GGC	28.75	0.313	-1.465	G. ruber-w
W167-79GGC	29.25	0.331	-1.839	G. ruber-w
W167-79GGC	29.25	1.015	-1.485	G. ruber-w
W167-79GGC	29.25	0.336	-1.541	G. ruber-w
W167-79GGC	29.25	0.734	-1.641	G. ruber-w
W167-79GGC	29.75	0.667	-1.479	G. ruber-w
W167-79GGC	29.75	0.254	-2.07	G. ruber-w
W167-79GGC	29.75	0.7	-1.426	G. ruber-w
W167-79GGC	29.75	0.007	-2.263	G. ruber-w
W167-79GGC	30.25	0.146	-2.007	G. ruber-w
W167-79GGC	30.25	0.368	-1.128	G. ruber-w

W167-79GGC	30.25	0.769	-1.853	G. ruber-w
W167-79GGC	30.25	0.558	-1.254	G. ruber-w
W167-79GGC	30.25	0.425	-1.364	G. ruber-w
W167-79GGC	30.75	0.433	-1.53	G. ruber-w
W167-79GGC	30.75	0.783	-1.481	G. ruber-w
W167-79GGC	30.75	-0.056	-1.416	G. ruber-w
W167-79GGC	30.75	0.883	-1.476	G. ruber-w
W167-79GGC	30.75	0.585	-1.453	G. ruber-w
W167-79GGC	31.25	0.639	-1.589	G. ruber-w
W167-79GGC	31.25	0.485	-1.564	G. ruber-w
W167-79GGC	31.25	0.647	-1.215	G. ruber-w
W167-79GGC	31.25	0.556	-1.784	G. ruber-w
W167-79GGC	31.25	0.477	-1.7	G. ruber-w
W167-79GGC	31.75	0.233	-1.91	G. ruber-w
W167-79GGC	31.75	-0.34	-1.52	G. ruber-w
W167-79GGC	31.75	0.112	-1.419	G. ruber-w
W167-79GGC	31.75	0.439	-1.506	G. ruber-w
W167-79GGC	31.75	0.46	-1.782	G. ruber-w
W167-79GGC	32.25	0.631	-1.636	G. ruber-w
W167-79GGC	32.25	0.529	-1.93	G. ruber-w
W167-79GGC	32.25	0.269	-1.469	G. ruber-w
W167-79GGC	32.75	0.512	-1.608	G. ruber-w
W167-79GGC	32.75	0.203	-1.394	G. ruber-w
W167-79GGC	32.75	-0.413	-1.618	G. ruber-w
W167-79GGC	33.25	0.474	-1.616	G. ruber-w
W167-79GGC	33.25	0.705	-1.848	G. ruber-w
W167-79GGC	33.25	0.062	-1.487	G. ruber-w
W167-79GGC	33.75	-0.152	-1.469	G. ruber-w
W167-79GGC	33.75	0.687	-1.71	G. ruber-w
W167-79GGC	33.75	0.267	-1.469	G. ruber-w
W167-79GGC	34.25	0.333	-1.872	G. ruber-w
W167-79GGC	34.25	0.513	-1.253	G. ruber-w
W167-79GGC	34.25	0.528	-1.557	G. ruber-w
W167-79GGC	34.75	0.469	-1.592	G. ruber-w
W167-79GGC	34.75	0.069	-1.653	G. ruber-w
W167-79GGC	34.75	0.102	-1.703	G. ruber-w
W167-79GGC	35.25	0.254	-1.846	G. ruber-w
W167-79GGC	35.25	0.288	-1.59	G. ruber-w
W167-79GGC	35.25	0.212	-1.427	G. ruber-w
W167-79GGC	35.75	0.603	-1.564	G. ruber-w
W167-79GGC	35.75	0.666	-1.48	G. ruber-w
W167-79GGC	35.75	0.228	-1.56	G. ruber-w
W167-79GGC	36.25	0.642	-1.333	G. ruber-w
W167-79GGC	36.25	0.53	-2.134	G. ruber-w
W167-79GGC	36.25	0.049	-1.594	G. ruber-w
W167-79GGC	36.75	0.313	-1.392	G. ruber-w
W167-79GGC	36.75	0.688	-1.396	G. ruber-w
W167-79GGC	36.75	0.534	-1.53	G. ruber-w
W167-79GGC	37.25	0.443	-1.56	G. ruber-w
W167-79GGC	37.25	0.799	-1.853	G. ruber-w
W167-79GGC	37.25	0.905	-1.534	G. ruber-w
W167-79GGC	37.75	-0.011	-1.7	G. ruber-w
W167-79GGC	37.75	0.579	-1.575	G. ruber-w
W167-79GGC	37.75	0.287	-1.711	G. ruber-w
W167-79GGC	38.25	0.101	-1.739	G. ruber-w

W167-79GGC	38.25	0.156	-1.727	G. ruber-w
W167-79GGC	38.25	0.675	-1.451	G. ruber-w
W167-79GGC	38.75	-0.005	-1.503	G. ruber-w
W167-79GGC	38.75	0.533	-1.766	G. ruber-w
W167-79GGC	38.75	0.542	-1.505	G. ruber-w
W167-79GGC	39.25	-0.028	-1.649	G. ruber-w
W167-79GGC	39.25	-0.074	-1.244	G. ruber-w
W167-79GGC	39.25	0.346	-1.431	G. ruber-w
W167-79GGC	39.75	0.499	-1.775	G. ruber-w
W167-79GGC	39.75	0.161	-2.117	G. ruber-w
W167-79GGC	39.75	0.118	-1.845	G. ruber-w
W167-79GGC	40.25	-0.014	-2.058	G. ruber-w
W167-79GGC	40.25	0.28	-1.815	G. ruber-w
W167-79GGC	40.25	0.317	-1.727	G. ruber-w
W167-79GGC	40.25	0.012	-1.665	G. ruber-w
W167-79GGC	40.75	0.523	-1.692	G. ruber-w
W167-79GGC	40.75	0.315	-1.756	G. ruber-w
W167-79GGC	40.75	0.321	-1.751	G. ruber-w
W167-79GGC	40.75	-0.04	-1.672	G. ruber-w
W167-79GGC	41.25	0.476	-1.731	G. ruber-w
W167-79GGC	41.25	0.565	-1.717	G. ruber-w
W167-79GGC	41.25	0.545	-1.391	G. ruber-w
W167-79GGC	41.25	0.661	-1.447	G. ruber-w
W167-79GGC	41.75	0.496	-1.759	G. ruber-w
W167-79GGC	41.75	0.429	-1.442	G. ruber-w
W167-79GGC	41.75	0.077	-1.779	G. ruber-w
W167-79GGC	41.75	-0.058	-1.751	G. ruber-w
W167-79GGC	42.25	0.405	-1.437	G. ruber-w
W167-79GGC	42.25	0.109	-1.517	G. ruber-w
W167-79GGC	42.25	0.114	-1.792	G. ruber-w
W167-79GGC	42.25	0.186	-1.698	G. ruber-w
W167-79GGC	42.75	0.323	-1.754	G. ruber-w
W167-79GGC	42.75	-0.289	-1.947	G. ruber-w
W167-79GGC	42.75	0.323	-1.789	G. ruber-w
W167-79GGC	42.75	0.025	-1.714	G. ruber-w
W167-79GGC	43.25	0.252	-1.762	G. ruber-w
W167-79GGC	43.25	0.42	-1.368	G. ruber-w
W167-79GGC	43.25	0.555	-1.563	G. ruber-w
W167-79GGC	43.25	0.078	-1.571	G. ruber-w
W167-79GGC	43.75	0.653	-1.275	G. ruber-w
W167-79GGC	43.75	0.375	-1.734	G. ruber-w
W167-79GGC	43.75	0.457	-1.89	G. ruber-w
W167-79GGC	43.75	0.557	-1.461	G. ruber-w
W167-79GGC	44.25	0.383	-1.533	G. ruber-w
W167-79GGC	44.25	0.552	-1.721	G. ruber-w
W167-79GGC	44.25	0.307	-1.657	G. ruber-w
W167-79GGC	44.25	0.305	-1.921	G. ruber-w
W167-79GGC	44.75	0.615	-1.331	G. ruber-w
W167-79GGC	44.75	0.657	-1.587	G. ruber-w
W167-79GGC	44.75	0.148	-1.596	G. ruber-w
W167-79GGC	44.75	0.177	-1.567	G. ruber-w
W167-79GGC	45.25	0.146	-1.598	G. ruber-w
W167-79GGC	45.25	-0.053	-1.915	G. ruber-w
W167-79GGC	45.25	0.325	-1.764	G. ruber-w
W167-79GGC	45.25	0.832	-1.219	G. ruber-w

W167-79GGC	45.75	0.328	-2.051	G. ruber-w
W167-79GGC	45.75	0.123	-1.52	G. ruber-w
W167-79GGC	45.75	0.34	-1.49	G. ruber-w
W167-79GGC	45.75	0.454	-1.716	G. ruber-w
W167-79GGC	46.25	0.268	-2.15	G. ruber-w
W167-79GGC	46.25	0.628	-1.627	G. ruber-w
W167-79GGC	46.25	0.73	-1.592	G. ruber-w
W167-79GGC	46.25	0.618	-1.465	G. ruber-w
W167-79GGC	46.75	0.186	-1.977	G. ruber-w
W167-79GGC	46.75	0.432	-1.614	G. ruber-w
W167-79GGC	46.75	0.711	-1.466	G. ruber-w
W167-79GGC	46.75	-0.176	-1.878	G. ruber-w
W167-79GGC	47.25	0.516	-1.822	G. ruber-w
W167-79GGC	47.25	0.221	-1.695	G. ruber-w
W167-79GGC	47.25	0.024	-1.64	G. ruber-w
W167-79GGC	47.25	0.15	-1.663	G. ruber-w
W167-79GGC	47.75	0.516	-1.599	G. ruber-w
W167-79GGC	47.75	0.605	-1.414	G. ruber-w
W167-79GGC	47.75	0.217	-1.66	G. ruber-w
W167-79GGC	47.75	0.283	-1.921	G. ruber-w
W167-79GGC	48.25	0.41	-1.922	G. ruber-w
W167-79GGC	48.25	0.624	-1.458	G. ruber-w
W167-79GGC	48.25	0.835	-1.339	G. ruber-w
W167-79GGC	48.25	0.304	-1.307	G. ruber-w
W167-79GGC	48.75	0.529	-1.488	G. ruber-w
W167-79GGC	48.75	0.269	-1.327	G. ruber-w
W167-79GGC	48.75	0.689	-1.711	G. ruber-w
W167-79GGC	48.75	0.383	-1.481	G. ruber-w
W167-79GGC	49.25	0.652	-1.646	G. ruber-w
W167-79GGC	49.25	0.413	-1.615	G. ruber-w
W167-79GGC	49.25	0.492	-1.945	G. ruber-w
W167-79GGC	49.25	0.561	-1.456	G. ruber-w
W167-79GGC	49.75	0.761	-1.488	G. ruber-w
W167-79GGC	49.75	0.318	-1.344	G. ruber-w
W167-79GGC	49.75	0.497	-1.18	G. ruber-w
W167-79GGC	50.25	0.499	-1.587	G. ruber-w
W167-79GGC	50.25	0.466	-1.894	G. ruber-w
W167-79GGC	50.25	0.647	-1.377	G. ruber-w
W167-79GGC	50.25	0.198	-1.428	G. ruber-w
W167-79GGC	50.75	0.421	-1.744	G. ruber-w
W167-79GGC	50.75	0.414	-1.718	G. ruber-w
W167-79GGC	50.75	0.454	-1.699	G. ruber-w
W167-79GGC	50.75	0.164	-2.11	G. ruber-w
W167-79GGC	51.25	0.285	-1.286	G. ruber-w
W167-79GGC	51.25	0.894	-1.313	G. ruber-w
W167-79GGC	51.25	0.081	-1.361	G. ruber-w
W167-79GGC	51.75	0.419	-1.712	G. ruber-w
W167-79GGC	51.75	0.313	-1.756	G. ruber-w
W167-79GGC	51.75	0.246	-1.026	G. ruber-w
W167-79GGC	51.75	0.192	-1.615	G. ruber-w
W167-79GGC	52.25	0.693	-1.429	G. ruber-w
W167-79GGC	52.25	0.119	-1.938	G. ruber-w
W167-79GGC	52.25	0.238	-1.617	G. ruber-w
W167-79GGC	52.25	0.484	-1.656	G. ruber-w
W167-79GGC	52.75	0.792	-1.544	G. ruber-w

W167-79GGC	52.75	0.209	-1.639	G. ruber-w
W167-79GGC	52.75	0.349	-1.675	G. ruber-w
W167-79GGC	52.75	0.484	-1.585	G. ruber-w
W167-79GGC	53.25	0.07	-1.721	G. ruber-w
W167-79GGC	53.25	0.43	-1.824	G. ruber-w
W167-79GGC	53.25	0.409	-1.58	G. ruber-w
W167-79GGC	53.25	0.565	-1.678	G. ruber-w
W167-79GGC	53.75	0.082	-1.447	G. ruber-w
W167-79GGC	53.75	0.771	-1.358	G. ruber-w
W167-79GGC	53.75	0.387	-1.572	G. ruber-w
W167-79GGC	53.75	0.738	-1.456	G. ruber-w
W167-79GGC	53.75	0.506	-1.584	G. ruber-w
W167-79GGC	54.25	0.478	-1.782	G. ruber-w
W167-79GGC	54.25	0.845	-1.494	G. ruber-w
W167-79GGC	54.25	0.548	-1.781	G. ruber-w
W167-79GGC	54.25	0.689	-1.508	G. ruber-w
W167-79GGC	54.25	0.437	-1.787	G. ruber-w
W167-79GGC	54.25	0.803	-1.546	G. ruber-w
W167-79GGC	54.75	0.316	-1.671	G. ruber-w
W167-79GGC	54.75	0.406	-1.486	G. ruber-w
W167-79GGC	54.75	0.276	-1.623	G. ruber-w
W167-79GGC	54.75	1.029	-1.238	G. ruber-w
W167-79GGC	54.75	0.548	-1.555	G. ruber-w
W167-79GGC	54.75	0.451	-1.806	G. ruber-w
W167-79GGC	55.25	0.761	-1.509	G. ruber-w
W167-79GGC	55.25	0.527	-1.552	G. ruber-w
W167-79GGC	55.25	0.205	-1.938	G. ruber-w
W167-79GGC	55.25	0.472	-1.629	G. ruber-w
W167-79GGC	55.25	0.81	-1.303	G. ruber-w
W167-79GGC	55.75	0.273	-1.738	G. ruber-w
W167-79GGC	55.75	0.22	-1.695	G. ruber-w
W167-79GGC	55.75	0.512	-1.405	G. ruber-w
W167-79GGC	56.25	0.78	-1.438	G. ruber-w
W167-79GGC	56.25	0.863	-1.372	G. ruber-w
W167-79GGC	56.25	0.421	-1.462	G. ruber-w
W167-79GGC	56.25	0.673	-1.628	G. ruber-w
W167-79GGC	56.25	0.652	-1.257	G. ruber-w
W167-79GGC	56.75	0.653	-1.253	G. ruber-w
W167-79GGC	56.75	0.289	-1.129	G. ruber-w
W167-79GGC	56.75	0.511	-1.441	G. ruber-w
W167-79GGC	56.75	0.546	-1.641	G. ruber-w
W167-79GGC	56.75	0.558	-1.839	G. ruber-w
W167-79GGC	57.25	0.395	-1.584	G. ruber-w
W167-79GGC	57.25	0.587	-1.351	G. ruber-w
W167-79GGC	57.25	0.484	-1.45	G. ruber-w
W167-79GGC	57.25	0.543	-1.804	G. ruber-w
W167-79GGC	57.25	0.106	-1.709	G. ruber-w
W167-79GGC	57.75	0.606	-1.741	G. ruber-w
W167-79GGC	57.75	0.57	-1.021	G. ruber-w
W167-79GGC	57.75	0.757	-1.544	G. ruber-w
W167-79GGC	58.25	0.431	-1.548	G. ruber-w
W167-79GGC	58.25	0.608	-1.493	G. ruber-w
W167-79GGC	58.25	0.37	-1.444	G. ruber-w
W167-79GGC	58.75	0.401	-1.583	G. ruber-w
W167-79GGC	58.75	0.217	-1.765	G. ruber-w

W167-79GGC	58.75	0.442	-1.937	G. ruber-w
W167-79GGC	58.75	0.19	-1.631	G. ruber-w
W167-79GGC	58.75	0.503	-1.42	G. ruber-w
W167-79GGC	59.25	0.346	-1.383	G. ruber-w
W167-79GGC	59.25	0.528	-1.635	G. ruber-w
W167-79GGC	59.25	0.757	-1.751	G. ruber-w
W167-79GGC	59.25	0.509	-1.553	G. ruber-w
W167-79GGC	59.75	0.465	-1.373	G. ruber-w
W167-79GGC	59.75	0.799	-1.026	G. ruber-w
W167-79GGC	59.75	0.507	-1.637	G. ruber-w
W167-79GGC	59.75	0.182	-1.889	G. ruber-w
W167-79GGC	60.25	0.083	-1.919	G. ruber-w
W167-79GGC	60.25	0.659	-2.054	G. ruber-w
W167-79GGC	60.25	0.402	-1.946	G. ruber-w
W167-79GGC	60.75	0.743	-1.714	G. ruber-w
W167-79GGC	60.75	0.6	-2.018	G. ruber-w
W167-79GGC	60.75	0.396	-1.722	G. ruber-w
W167-79GGC	61.25	0.526	-1.776	G. ruber-w
W167-79GGC	61.25	0.735	-1.361	G. ruber-w
W167-79GGC	61.25	0.748	-1.409	G. ruber-w
W167-79GGC	61.75	0.71	-1.628	G. ruber-w
W167-79GGC	61.75	0.475	-1.868	G. ruber-w
W167-79GGC	61.75	0.858	-1.838	G. ruber-w
W167-79GGC	62.25	0.662	-1.873	G. ruber-w
W167-79GGC	62.25	0.845	-1.747	G. ruber-w
W167-79GGC	62.25	0.752	-1.73	G. ruber-w
W167-79GGC	62.75	0.701	-1.645	G. ruber-w
W167-79GGC	62.75	0.349	-1.561	G. ruber-w
W167-79GGC	62.75	0.167	-2.196	G. ruber-w
W167-79GGC	63.25	0.467	-1.918	G. ruber-w
W167-79GGC	63.25	0.509	-1.918	G. ruber-w
W167-79GGC	63.25	0.578	-1.805	G. ruber-w
W167-79GGC	63.75	0.352	-1.805	G. ruber-w
W167-79GGC	63.75	0.481	-1.682	G. ruber-w
W167-79GGC	63.75	0.351	-1.692	G. ruber-w
W167-79GGC	64.25	0.667	-1.672	G. ruber-w
W167-79GGC	64.25	0.467	-1.688	G. ruber-w
W167-79GGC	64.25	0.463	-1.558	G. ruber-w
W167-79GGC	64.75	0.531	-1.601	G. ruber-w
W167-79GGC	64.75	0.485	-1.936	G. ruber-w
W167-79GGC	64.75	0.887	-1.689	G. ruber-w
W167-79GGC	65.25	0.432	-1.882	G. ruber-w
W167-79GGC	65.25	0.6	-1.561	G. ruber-w
W167-79GGC	65.25	0.21	-1.527	G. ruber-w
W167-79GGC	65.75	0.707	-1.595	G. ruber-w
W167-79GGC	65.75	0.65	-1.273	G. ruber-w
W167-79GGC	65.75	0.297	-2.259	G. ruber-w
W167-79GGC	66.25	0.814	-1.683	G. ruber-w
W167-79GGC	66.25	0.735	-1.73	G. ruber-w
W167-79GGC	66.25	0.726	-1.291	G. ruber-w
W167-79GGC	66.75	0.712	-1.575	G. ruber-w
W167-79GGC	66.75	0.455	-1.521	G. ruber-w
W167-79GGC	66.75	0.589	-1.553	G. ruber-w
W167-79GGC	67.25	0.616	-1.661	G. ruber-w
W167-79GGC	67.25	0.379	-1.98	G. ruber-w

W167-79GGC	67.25	0.773	-1.919	G. ruber-w
W167-79GGC	67.75	0.829	-1.781	G. ruber-w
W167-79GGC	67.75	0.307	-1.7	G. ruber-w
W167-79GGC	67.75	0.693	-1.78	G. ruber-w
W167-79GGC	68.25	0.565	-1.634	G. ruber-w
W167-79GGC	68.25	0.926	-1.821	G. ruber-w
W167-79GGC	68.25	0.494	-1.626	G. ruber-w
W167-79GGC	68.75	0.879	-1.592	G. ruber-w
W167-79GGC	68.75	0.336	-1.796	G. ruber-w
W167-79GGC	68.75	1.067	-1.716	G. ruber-w
W167-79GGC	69.25	0.378	-2.2	G. ruber-w
W167-79GGC	69.25	0.727	-1.593	G. ruber-w
W167-79GGC	69.25	0.484	-1.496	G. ruber-w
W167-79GGC	69.75	0.385	-1.687	G. ruber-w
W167-79GGC	69.75	0.551	-2.014	G. ruber-w
W167-79GGC	69.75	0.233	-1.709	G. ruber-w
W167-79GGC	70.25	0.385	-1.835	G. ruber-w
W167-79GGC	70.25	0.739	-1.68	G. ruber-w
W167-79GGC	70.25	0.465	-1.617	G. ruber-w
W167-79GGC	70.75	0.398	-2.025	G. ruber-w
W167-79GGC	70.75	0.791	-1.46	G. ruber-w
W167-79GGC	70.75	0.901	-1.836	G. ruber-w
W167-79GGC	71.25	0.706	-1.702	G. ruber-w
W167-79GGC	71.25	0.639	-1.501	G. ruber-w
W167-79GGC	71.25	0.678	-1.784	G. ruber-w
W167-79GGC	71.75	0.167	-1.782	G. ruber-w
W167-79GGC	71.75	0.758	-1.891	G. ruber-w
W167-79GGC	71.75	0.419	-1.621	G. ruber-w
W167-79GGC	72.25	0.682	-1.623	G. ruber-w
W167-79GGC	72.25	0.557	-1.457	G. ruber-w
W167-79GGC	72.25	0.534	-1.528	G. ruber-w
W167-79GGC	72.75	0.578	-1.899	G. ruber-w
W167-79GGC	72.75	0.595	-1.501	G. ruber-w
W167-79GGC	72.75	0.681	-1.64	G. ruber-w
W167-79GGC	73.25	0.624	-1.714	G. ruber-w
W167-79GGC	73.25	0.816	-1.426	G. ruber-w
W167-79GGC	73.25	0.708	-1.728	G. ruber-w
W167-79GGC	73.75	0.309	-2.062	G. ruber-w
W167-79GGC	73.75	0.821	-1.693	G. ruber-w
W167-79GGC	73.75	0.61	-1.446	G. ruber-w
W167-79GGC	74.25	0.648	-1.434	G. ruber-w
W167-79GGC	74.25	0.604	-1.909	G. ruber-w
W167-79GGC	74.25	0.657	-1.18	G. ruber-w
W167-79GGC	74.75	0.53	-1.592	G. ruber-w
W167-79GGC	74.75	0.716	-1.793	G. ruber-w
W167-79GGC	74.75	0.428	-1.759	G. ruber-w
W167-79GGC	75.25	0.428	-1.872	G. ruber-w
W167-79GGC	75.25	0.506	-1.245	G. ruber-w
W167-79GGC	75.25	0.631	-1.664	G. ruber-w
W167-79GGC	75.75	0.521	-1.69	G. ruber-w
W167-79GGC	75.75	0.752	-1.571	G. ruber-w
W167-79GGC	75.75	0.686	-1.591	G. ruber-w
W167-79GGC	76.25	0.436	-1.54	G. ruber-w
W167-79GGC	76.25	0.865	-1.921	G. ruber-w
W167-79GGC	76.25	0.443	-1.737	G. ruber-w

W167-79GGC	76.75	0.862	-1.912	G. ruber-w
W167-79GGC	76.75	0.656	-1.699	G. ruber-w
W167-79GGC	76.75	0.747	-1.309	G. ruber-w
W167-79GGC	77.25	0.583	-1.673	G. ruber-w
W167-79GGC	77.25	0.335	-2.039	G. ruber-w
W167-79GGC	77.25	0.812	-1.546	G. ruber-w
W167-79GGC	77.75	0.557	-1.725	G. ruber-w
W167-79GGC	77.75	0.506	-1.932	G. ruber-w
W167-79GGC	77.75	0.368	-1.479	G. ruber-w
W167-79GGC	78.25	0.913	-1.509	G. ruber-w
W167-79GGC	78.25	0.568	-1.255	G. ruber-w
W167-79GGC	78.25	0.602	-1.822	G. ruber-w
W167-79GGC	78.75	0.547	-1.872	G. ruber-w
W167-79GGC	78.75	0.464	-1.867	G. ruber-w
W167-79GGC	78.75	0.463	-1.696	G. ruber-w
W167-79GGC	79.25	0.704	-1.427	G. ruber-w
W167-79GGC	79.25	0.589	-1.201	G. ruber-w
W167-79GGC	79.25	0.831	-1.416	G. ruber-w
W167-79GGC	79.75	0.64	-1.541	G. ruber-w
W167-79GGC	79.75	0.266	-1.807	G. ruber-w
W167-79GGC	79.75	0.718	-1.736	G. ruber-w
W167-79GGC	80.25	0.49	-1.585	G. ruber-w
W167-79GGC	80.25	0.728	-1.416	G. ruber-w
W167-79GGC	80.25	0.723	-1.902	G. ruber-w
W167-79GGC	80.75	0.857	-1.322	G. ruber-w
W167-79GGC	80.75	0.654	-2.163	G. ruber-w
W167-79GGC	80.75	0.78	-1.667	G. ruber-w
W167-79GGC	81.25	0.657	-1.781	G. ruber-w
W167-79GGC	81.25	-0.196	-1.689	G. ruber-w
W167-79GGC	81.25	0.873	-1.772	G. ruber-w
W167-79GGC	81.75	0.655	-1.959	G. ruber-w
W167-79GGC	81.75	0.6	-1.773	G. ruber-w
W167-79GGC	81.75	0.896	-1.253	G. ruber-w
W167-79GGC	82.25	0.707	-1.429	G. ruber-w
W167-79GGC	82.25	0.392	-1.722	G. ruber-w
W167-79GGC	82.25	0.757	-1.648	G. ruber-w
W167-79GGC	82.75	0.651	-1.844	G. ruber-w
W167-79GGC	82.75	0.282	-2.035	G. ruber-w
W167-79GGC	82.75	0.504	-1.514	G. ruber-w
W167-79GGC	83.25	0.564	-1.91	G. ruber-w
W167-79GGC	83.25	0.395	-1.441	G. ruber-w
W167-79GGC	83.25	0.749	-1.686	G. ruber-w
W167-79GGC	83.75	0.585	-1.656	G. ruber-w
W167-79GGC	83.75	0.544	-1.689	G. ruber-w
W167-79GGC	83.75	0.692	-1.694	G. ruber-w
W167-79GGC	83.75	0.323	-1.837	G. ruber-w
W167-79GGC	84.25	0.206	-2.287	G. ruber-w
W167-79GGC	84.25	0.512	-1.549	G. ruber-w
W167-79GGC	84.25	0.921	-1.692	G. ruber-w
W167-79GGC	84.25	0.658	-1.748	G. ruber-w
W167-79GGC	84.75	0.679	-1.708	G. ruber-w
W167-79GGC	84.75	0.513	-1.703	G. ruber-w
W167-79GGC	84.75	1.119	-1.794	G. ruber-w
W167-79GGC	85.25	0.875	-1.866	G. ruber-w
W167-79GGC	85.25	0.503	-1.547	G. ruber-w

W167-79GGC	85.25	0.736	-2.16	G. ruber-w
W167-79GGC	85.25	0.76	-2.089	G. ruber-w
W167-79GGC	85.75	0.609	-1.747	G. ruber-w
W167-79GGC	85.75	0.764	-1.63	G. ruber-w
W167-79GGC	85.75	0.542	-1.929	G. ruber-w
W167-79GGC	86.25	0.399	-1.875	G. ruber-w
W167-79GGC	86.25	0.133	-1.82	G. ruber-w
W167-79GGC	86.25	0.032	-1.846	G. ruber-w
W167-79GGC	86.25	0.705	-1.926	G. ruber-w
W167-79GGC	86.75	0.631	-2.042	G. ruber-w
W167-79GGC	86.75	1.023	-1.9	G. ruber-w
W167-79GGC	86.75	0.646	-1.747	G. ruber-w
W167-79GGC	86.75	0.336	-1.531	G. ruber-w
W167-79GGC	87.25	0.88	-1.864	G. ruber-w
W167-79GGC	87.25	0.638	-1.968	G. ruber-w
W167-79GGC	87.25	0.604	-1.649	G. ruber-w
W167-79GGC	87.25	0.345	-1.772	G. ruber-w
W167-79GGC	87.75	0.812	-1.93	G. ruber-w
W167-79GGC	87.75	0.612	-1.661	G. ruber-w
W167-79GGC	87.75	0.521	-2.129	G. ruber-w
W167-79GGC	87.75	0.036	-1.82	G. ruber-w
W167-79GGC	88.25	0.4	-1.419	G. ruber-w
W167-79GGC	88.25	0.206	-2.06	G. ruber-w
W167-79GGC	88.25	0.465	-1.686	G. ruber-w
W167-79GGC	88.25	0.234	-1.858	G. ruber-w
W167-79GGC	88.75	0.324	-1.808	G. ruber-w
W167-79GGC	88.75	0.232	-1.67	G. ruber-w
W167-79GGC	88.75	0.561	-1.696	G. ruber-w
W167-79GGC	88.75	0.057	-2.062	G. ruber-w
W167-79GGC	89.25	0.48	-1.478	G. ruber-w
W167-79GGC	89.25	0.651	-1.962	G. ruber-w
W167-79GGC	89.25	0.277	-1.514	G. ruber-w
W167-79GGC	89.25	0.616	-1.328	G. ruber-w
W167-79GGC	89.75	0.636	-2.016	G. ruber-w
W167-79GGC	89.75	0.53	-1.489	G. ruber-w
W167-79GGC	89.75	0.462	-1.937	G. ruber-w
W167-79GGC	90.25	0.341	-1.512	G. ruber-w
W167-79GGC	90.25	0.211	-1.83	G. ruber-w
W167-79GGC	90.25	0.153	-1.906	G. ruber-w
W167-79GGC	90.25	0.469	-1.411	G. ruber-w
W167-79GGC	90.75	0.758	-1.555	G. ruber-w
W167-79GGC	90.75	0.335	-2.05	G. ruber-w
W167-79GGC	90.75	0.417	-1.856	G. ruber-w
W167-79GGC	90.75	0.305	-2.004	G. ruber-w
W167-79GGC	91.25	0.657	-1.797	G. ruber-w
W167-79GGC	91.25	0.641	-1.448	G. ruber-w
W167-79GGC	91.25	0.646	-1.506	G. ruber-w
W167-79GGC	91.25	0.846	-1.409	G. ruber-w
W167-79GGC	91.25	0.443	-1.746	G. ruber-w
W167-79GGC	91.75	0.277	-1.774	G. ruber-w
W167-79GGC	91.75	0.607	-1.857	G. ruber-w
W167-79GGC	91.75	0.382	-1.795	G. ruber-w
W167-79GGC	91.75	0.686	-1.596	G. ruber-w
W167-79GGC	92.25	0.118	-1.858	G. ruber-w
W167-79GGC	92.25	0.293	-1.937	G. ruber-w

W167-79GGC	92.25	0.535	-1.679	G. ruber-w
W167-79GGC	92.25	0.586	-1.832	G. ruber-w
W167-79GGC	92.75	0.801	-1.76	G. ruber-w
W167-79GGC	92.75	0.281	-1.735	G. ruber-w
W167-79GGC	92.75	0.431	-1.778	G. ruber-w
W167-79GGC	92.75	0.634	-1.391	G. ruber-w
W167-79GGC	93.25	0.152	-1.632	G. ruber-w
W167-79GGC	93.25	0.526	-1.878	G. ruber-w
W167-79GGC	93.25	0.82	-1.699	G. ruber-w
W167-79GGC	93.25	0.011	-1.654	G. ruber-w
W167-79GGC	93.75	0.661	-1.636	G. ruber-w
W167-79GGC	93.75	0.419	-1.473	G. ruber-w
W167-79GGC	93.75	0.448	-1.735	G. ruber-w
W167-79GGC	93.75	0.746	-1.7	G. ruber-w
W167-79GGC	94.25	0.733	-1.592	G. ruber-w
W167-79GGC	94.25	0.635	-1.697	G. ruber-w
W167-79GGC	94.25	0.667	-1.538	G. ruber-w
W167-79GGC	94.25	0.875	-1.667	G. ruber-w
W167-79GGC	94.75	0.365	-1.85	G. ruber-w
W167-79GGC	94.75	0.941	-1.694	G. ruber-w
W167-79GGC	94.75	0.503	-1.918	G. ruber-w
W167-79GGC	94.75	0.315	-1.878	G. ruber-w
W167-79GGC	95.25	0.315	-1.54	G. ruber-w
W167-79GGC	95.25	0.325	-1.585	G. ruber-w
W167-79GGC	95.25	0.687	-1.579	G. ruber-w
W167-79GGC	95.25	0.424	-1.753	G. ruber-w
W167-79GGC	95.75	0.237	-1.733	G. ruber-w
W167-79GGC	95.75	0.567	-1.322	G. ruber-w
W167-79GGC	95.75	0.058	-2.099	G. ruber-w
W167-79GGC	95.75	0.95	-1.816	G. ruber-w
W167-79GGC	96.25	0.509	-1.673	G. ruber-w
W167-79GGC	96.25	0.404	-1.62	G. ruber-w
W167-79GGC	96.25	0.441	-2.027	G. ruber-w
W167-79GGC	96.25	0.465	-1.879	G. ruber-w
W167-79GGC	96.75	0.473	-1.63	G. ruber-w
W167-79GGC	96.75	0.478	-1.706	G. ruber-w
W167-79GGC	96.75	0.646	-1.674	G. ruber-w
W167-79GGC	96.75	0.436	-1.676	G. ruber-w
W167-79GGC	97.25	0.802	-1.675	G. ruber-w
W167-79GGC	97.25	0.82	-1.36	G. ruber-w
W167-79GGC	97.25	0.712	-1.593	G. ruber-w
W167-79GGC	97.25	0.77	-1.579	G. ruber-w
W167-79GGC	97.75	0.383	-1.855	G. ruber-w
W167-79GGC	97.75	0.447	-1.498	G. ruber-w
W167-79GGC	97.75	0.572	-1.604	G. ruber-w
W167-79GGC	97.75	0.301	-1.89	G. ruber-w
W167-79GGC	98.25	0.564	-1.648	G. ruber-w
W167-79GGC	98.25	0.59	-1.73	G. ruber-w
W167-79GGC	98.25	0.631	-1.59	G. ruber-w
W167-79GGC	98.25	0.172	-2.051	G. ruber-w
W167-79GGC	98.75	0.558	-2.236	G. ruber-w
W167-79GGC	98.75	0.804	-1.751	G. ruber-w
W167-79GGC	98.75	0.556	-1.728	G. ruber-w
W167-79GGC	98.75	0.82	-1.606	G. ruber-w
W167-79GGC	99.25	0.265	-1.7	G. ruber-w

W167-79GGC	99.25	0.154	-1.813	G. ruber-w
W167-79GGC	99.25	0.741	-1.611	G. ruber-w
W167-79GGC	99.25	0.645	-1.573	G. ruber-w
W167-79GGC	99.75	0.319	-0.94	G. ruber-w
W167-79GGC	99.75	0.438	-1.734	G. ruber-w
W167-79GGC	99.75	0.522	-1.983	G. ruber-w
W167-79GGC	99.75	0.461	-2.042	G. ruber-w
W167-79GGC	100.25	0.246	-1.48	G. ruber-w
W167-79GGC	100.25	0.467	-1.725	G. ruber-w
W167-79GGC	100.25	0.832	-1.582	G. ruber-w
W167-79GGC	100.25	0.459	-1.664	G. ruber-w
W167-79GGC	100.75	0.452	-1.404	G. ruber-w
W167-79GGC	100.75	0.175	-1.64	G. ruber-w
W167-79GGC	100.75	0.618	-2.097	G. ruber-w
W167-79GGC	100.75	0.185	-1.655	G. ruber-w
W167-79GGC	101.25	0.473	-1.64	G. ruber-w
W167-79GGC	101.25	0.147	-1.626	G. ruber-w
W167-79GGC	101.25	0.3	-1.592	G. ruber-w
W167-79GGC	101.25	0.2	-1.853	G. ruber-w
W167-79GGC	101.75	0.491	-1.913	G. ruber-w
W167-79GGC	101.75	0.36	-1.902	G. ruber-w
W167-79GGC	101.75	-0.182	-2.193	G. ruber-w
W167-79GGC	101.75	0.449	-1.724	G. ruber-w
W167-79GGC	102.25	0.71	-1.408	G. ruber-w
W167-79GGC	102.25	0.526	-2.007	G. ruber-w
W167-79GGC	102.25	0.458	-1.612	G. ruber-w
W167-79GGC	102.25	0.423	-1.662	G. ruber-w
W167-79GGC	102.75	0.645	-1.51	G. ruber-w
W167-79GGC	102.75	0.263	-2.05	G. ruber-w
W167-79GGC	102.75	0.39	-1.808	G. ruber-w
W167-79GGC	102.75	0.424	-1.417	G. ruber-w
W167-79GGC	103.25	-0.107	-1.867	G. ruber-w
W167-79GGC	103.25	0.276	-2.01	G. ruber-w
W167-79GGC	103.25	0.137	-1.743	G. ruber-w
W167-79GGC	103.25	0.413	-1.983	G. ruber-w
W167-79GGC	103.75	0.491	-1.888	G. ruber-w
W167-79GGC	103.75	0.559	-1.817	G. ruber-w
W167-79GGC	103.75	0.605	-1.886	G. ruber-w
W167-79GGC	103.75	0.34	-1.874	G. ruber-w
W167-79GGC	104.25	0.738	-1.583	G. ruber-w
W167-79GGC	104.25	0.458	-1.49	G. ruber-w
W167-79GGC	104.25	0.021	-1.813	G. ruber-w
W167-79GGC	104.75	-0.011	-1.717	G. ruber-w
W167-79GGC	104.75	0.477	-1.748	G. ruber-w
W167-79GGC	104.75	0.448	-1.64	G. ruber-w
W167-79GGC	104.75	0.51	-1.823	G. ruber-w
W167-79GGC	105.25	0.276	-1.514	G. ruber-w
W167-79GGC	105.25	0.602	-1.646	G. ruber-w
W167-79GGC	105.25	0.224	-1.874	G. ruber-w
W167-79GGC	105.25	0.263	-1.796	G. ruber-w
W167-79GGC	105.75	0.61	-1.513	G. ruber-w
W167-79GGC	105.75	0.251	-2.077	G. ruber-w
W167-79GGC	105.75	0.308	-1.727	G. ruber-w
W167-79GGC	105.75	0.566	-1.417	G. ruber-w
W167-79GGC	106.25	0.516	-1.574	G. ruber-w

W167-79GGC	106.25	0.375	-1.775	G. ruber-w
W167-79GGC	106.25	0.923	-1.566	G. ruber-w
W167-79GGC	106.25	0.417	-1.553	G. ruber-w
W167-79GGC	106.75	0.577	-1.691	G. ruber-w
W167-79GGC	106.75	0.971	-1.618	G. ruber-w
W167-79GGC	106.75	0.245	-1.65	G. ruber-w
W167-79GGC	106.75	0.447	-1.935	G. ruber-w
W167-79GGC	107.25	0.034	-1.774	G. ruber-w
W167-79GGC	107.25	0.387	-1.952	G. ruber-w
W167-79GGC	107.25	0.698	-1.541	G. ruber-w
W167-79GGC	107.25	0.503	-1.468	G. ruber-w
W167-79GGC	107.75	0.471	-1.816	G. ruber-w
W167-79GGC	107.75	0.482	-1.709	G. ruber-w
W167-79GGC	107.75	0.573	-2.099	G. ruber-w
W167-79GGC	107.75	0.475	-1.691	G. ruber-w
W167-79GGC	108.25	0.836	-1.359	G. ruber-w
W167-79GGC	108.25	0.295	-1.59	G. ruber-w
W167-79GGC	108.25	0.525	-1.649	G. ruber-w
W167-79GGC	108.25	0.502	-1.521	G. ruber-w
W167-79GGC	108.75	0.407	-1.667	G. ruber-w
W167-79GGC	108.75	0.647	-1.619	G. ruber-w
W167-79GGC	108.75	0.406	-1.704	G. ruber-w
W167-79GGC	108.75	0.911	-1.838	G. ruber-w
W167-79GGC	109.25	0.385	-1.835	G. ruber-w
W167-79GGC	109.25	0.686	-1.385	G. ruber-w
W167-79GGC	109.25	0.27	-1.322	G. ruber-w
W167-79GGC	109.25	0.398	-1.648	G. ruber-w
W167-79GGC	109.75	0.032	-2.016	G. ruber-w
W167-79GGC	109.75	0.035	-1.585	G. ruber-w
W167-79GGC	109.75	0.563	-1.422	G. ruber-w
W167-79GGC	109.75	0.521	-1.56	G. ruber-w
W167-79GGC	110.25	0.715	-1.605	G. ruber-w
W167-79GGC	110.25	0.722	-1.589	G. ruber-w
W167-79GGC	110.25	0.254	-1.68	G. ruber-w
W167-79GGC	110.25	0.307	-1.263	G. ruber-w
W167-79GGC	110.75	0.521	-1.807	G. ruber-w
W167-79GGC	110.75	0.387	-1.932	G. ruber-w
W167-79GGC	110.75	0.277	-1.543	G. ruber-w
W167-79GGC	110.75	0.468	-1.658	G. ruber-w
W167-79GGC	111.25	0.426	-1.751	G. ruber-w
W167-79GGC	111.25	0.685	-1.376	G. ruber-w
W167-79GGC	111.25	0.456	-1.496	G. ruber-w
W167-79GGC	111.25	0.533	-1.728	G. ruber-w
W167-79GGC	111.75	0.309	-1.25	G. ruber-w
W167-79GGC	111.75	0.494	-1.63	G. ruber-w
W167-79GGC	111.75	0.281	-1.237	G. ruber-w
W167-79GGC	111.75	0.418	-1.871	G. ruber-w
W167-79GGC	112.25	0.402	-1.567	G. ruber-w
W167-79GGC	112.25	0.036	-1.292	G. ruber-w
W167-79GGC	112.25	0.693	-1.382	G. ruber-w
W167-79GGC	112.25	0.432	-1.523	G. ruber-w
W167-79GGC	112.75	0.382	-1.387	G. ruber-w
W167-79GGC	112.75	0.424	-1.708	G. ruber-w
W167-79GGC	112.75	0.301	-1.493	G. ruber-w
W167-79GGC	112.75	0.625	-1.526	G. ruber-w

W167-79GGC	113.25	0.437	-1.738	G. ruber-w
W167-79GGC	113.25	0.383	-1.433	G. ruber-w
W167-79GGC	113.25	0.452	-1.846	G. ruber-w
W167-79GGC	113.25	0.25	-1.492	G. ruber-w
W167-79GGC	113.75	-0.489	-2.031	G. ruber-w
W167-79GGC	113.75	0.344	-1.742	G. ruber-w
W167-79GGC	113.75	0.381	-1.856	G. ruber-w
W167-79GGC	113.75	0.778	-1.306	G. ruber-w
W167-79GGC	114.25	0.085	-1.679	G. ruber-w
W167-79GGC	114.25	0.615	-1.585	G. ruber-w
W167-79GGC	114.25	-0.028	-2.167	G. ruber-w
W167-79GGC	114.25	0.36	-1.568	G. ruber-w
W167-79GGC	114.75	0.36	-1.391	G. ruber-w
W167-79GGC	114.75	0.458	-1.364	G. ruber-w
W167-79GGC	114.75	0.426	-1.599	G. ruber-w
W167-79GGC	114.75	0.871	-1.347	G. ruber-w
W167-79GGC	115.25	0.603	-1.26	G. ruber-w
W167-79GGC	115.25	0.269	-1.652	G. ruber-w
W167-79GGC	115.25	0.474	-1.474	G. ruber-w
W167-79GGC	115.25	0.154	-1.766	G. ruber-w
W167-79GGC	115.75	0.272	-1.539	G. ruber-w
W167-79GGC	115.75	0.57	-1.546	G. ruber-w
W167-79GGC	115.75	0.579	-1.546	G. ruber-w
W167-79GGC	115.75	0.497	-1.719	G. ruber-w
W167-79GGC	116.25	0.503	-1.602	G. ruber-w
W167-79GGC	116.25	0.674	-1.551	G. ruber-w
W167-79GGC	116.25	0.103	-1.372	G. ruber-w
W167-79GGC	116.25	0.321	-1.711	G. ruber-w
W167-79GGC	116.75	-0.002	-1.711	G. ruber-w
W167-79GGC	116.75	0.672	-1.482	G. ruber-w
W167-79GGC	116.75	0.154	-1.86	G. ruber-w
W167-79GGC	116.75	0.105	-1.363	G. ruber-w
W167-79GGC	117.25	0.493	-1.579	G. ruber-w
W167-79GGC	117.25	0.32	-1.301	G. ruber-w
W167-79GGC	117.25	0.397	-1.543	G. ruber-w
W167-79GGC	117.25	0.395	-1.715	G. ruber-w
W167-79GGC	117.75	0.392	-1.752	G. ruber-w
W167-79GGC	117.75	0.779	-1.449	G. ruber-w
W167-79GGC	117.75	0.446	-1.291	G. ruber-w
W167-79GGC	117.75	-0.009	-1.245	G. ruber-w
W167-79GGC	118.25	-0.025	-1.746	G. ruber-w
W167-79GGC	118.25	0.644	-1.6	G. ruber-w
W167-79GGC	118.25	0.724	-1.774	G. ruber-w
W167-79GGC	118.25	0.03	-1.82	G. ruber-w
W167-79GGC	118.75	0.35	-1.451	G. ruber-w
W167-79GGC	118.75	0.389	-1.704	G. ruber-w
W167-79GGC	118.75	0.513	-1.679	G. ruber-w
W167-79GGC	118.75	0.563	-1.316	G. ruber-w
W167-79GGC	119.25	0.098	-1.664	G. ruber-w
W167-79GGC	119.25	-0.142	-1.95	G. ruber-w
W167-79GGC	119.25	0.161	-1.64	G. ruber-w
W167-79GGC	119.25	0.655	-1.821	G. ruber-w
W167-79GGC	119.75	0.25	-1.485	G. ruber-w
W167-79GGC	119.75	0.53	-1.766	G. ruber-w
W167-79GGC	119.75	0.024	-1.428	G. ruber-w

W167-79GGC	119.75	0.581	-1.514	G. ruber-w
W167-79GGC	120.25	0.304	-1.671	G. ruber-w
W167-79GGC	120.25	0.371	-1.634	G. ruber-w
W167-79GGC	120.25	0.469	-1.89	G. ruber-w
W167-79GGC	120.25	0.575	-1.677	G. ruber-w
W167-79GGC	120.75	0.758	-1.366	G. ruber-w
W167-79GGC	120.75	0.589	-1.401	G. ruber-w
W167-79GGC	120.75	0.443	-1.78	G. ruber-w
W167-79GGC	120.75	0.382	-1.914	G. ruber-w
W167-79GGC	121.25	-0.28	-1.584	G. ruber-w
W167-79GGC	121.25	0.42	-1.732	G. ruber-w
W167-79GGC	121.25	0.438	-1.413	G. ruber-w
W167-79GGC	121.25	0.51	-1.285	G. ruber-w
W167-79GGC	121.75	0.048	-1.707	G. ruber-w
W167-79GGC	121.75	0.697	-1.477	G. ruber-w
W167-79GGC	121.75	-0.042	-1.869	G. ruber-w
W167-79GGC	121.75	0.626	-1.506	G. ruber-w
W167-79GGC	122.25	0.452	-1.537	G. ruber-w
W167-79GGC	122.25	0.203	-1.539	G. ruber-w
W167-79GGC	122.25	0.531	-1.695	G. ruber-w
W167-79GGC	122.25	0.554	-1.217	G. ruber-w
W167-79GGC	122.75	0.39	-1.922	G. ruber-w
W167-79GGC	122.75	0.399	-1.539	G. ruber-w
W167-79GGC	122.75	0.632	-1.314	G. ruber-w
W167-79GGC	122.75	0.479	-0.966	G. ruber-w
W167-79GGC	123.25	0.217	-1.417	G. ruber-w
W167-79GGC	123.25	0.599	-1.721	G. ruber-w
W167-79GGC	123.25	0.448	-1.196	G. ruber-w
W167-79GGC	123.25	0.719	-1.648	G. ruber-w
W167-79GGC	123.75	0.136	-1.739	G. ruber-w
W167-79GGC	123.75	0.613	-1.818	G. ruber-w
W167-79GGC	123.75	0.332	-1.963	G. ruber-w
W167-79GGC	124.25	0.333	-1.313	G. ruber-w
W167-79GGC	124.25	0.483	-1.546	G. ruber-w
W167-79GGC	124.25	0.057	-2.27	G. ruber-w
W167-79GGC	124.75	0.448	-1.592	G. ruber-w
W167-79GGC	124.75	0.574	-1.649	G. ruber-w
W167-79GGC	124.75	0.079	-1.685	G. ruber-w
W167-79GGC	124.75	0.737	-1.329	G. ruber-w
W167-79GGC	125.25	0.53	-1.589	G. ruber-w
W167-79GGC	125.25	0.357	-1.281	G. ruber-w
W167-79GGC	125.25	0.437	-1.351	G. ruber-w
W167-79GGC	125.25	0.366	-1.822	G. ruber-w
W167-79GGC	125.75	0.338	-1.467	G. ruber-w
W167-79GGC	125.75	0.09	-1.636	G. ruber-w
W167-79GGC	125.75	0.634	-1.543	G. ruber-w
W167-79GGC	125.75	0.413	-1.624	G. ruber-w
W167-79GGC	126.25	0.488	-1.654	G. ruber-w
W167-79GGC	126.25	0.314	-1.19	G. ruber-w
W167-79GGC	126.25	-0.124	-1.493	G. ruber-w
W167-79GGC	126.25	0.673	-1.349	G. ruber-w
W167-79GGC	126.75	0.492	-1.852	G. ruber-w
W167-79GGC	126.75	0.521	-1.438	G. ruber-w
W167-79GGC	126.75	0.464	-1.596	G. ruber-w
W167-79GGC	126.75	0.417	-1.759	G. ruber-w

W167-79GGC	127.5	0.366	-1.636	G. ruber-w
W167-79GGC	127.5	0.278	-1.481	G. ruber-w
W167-79GGC	127.5	0.443	-1.846	G. ruber-w
W167-79GGC	127.5	0.485	-1.384	G. ruber-w

CORE	DEPTH	C13	O18	SPECIES
C166A-8GGC	1	0.387	-1.621	G. ruber-w
C166A-8GGC	1	0.903	-1.384	G. ruber-w
C166A-8GGC	1	0.330	-1.116	G. ruber-w
C166A-8GGC	1	0.478	-1.363	G. ruber-w
C166A-8GGC	1	0.705	-1.606	G. ruber-w
C166A-8GGC	1	0.717	-1.487	G. ruber-w
C166A-8GGC	3	0.551	-1.382	G. ruber-w
C166A-8GGC	3	0.764	-1.114	G. ruber-w
C166A-8GGC	3	0.725	-1.478	G. ruber-w
C166A-8GGC	3	0.627	-1.512	G. ruber-w
C166A-8GGC	3	0.865	-1.219	G. ruber-w
C166A-8GGC	5	0.275	-1.492	G. ruber-w
C166A-8GGC	5	0.613	-1.263	G. ruber-w
C166A-8GGC	5	0.228	-1.151	G. ruber-w
C166A-8GGC	5	0.586	-0.957	G. ruber-w
C166A-8GGC	5	0.614	-1.655	G. ruber-w
C166A-8GGC	5	0.452	-1.470	G. ruber-w
C166A-8GGC	7	0.593	-1.364	G. ruber-w
C166A-8GGC	7	0.794	-1.108	G. ruber-w
C166A-8GGC	7	0.634	-1.412	G. ruber-w
C166A-8GGC	7	0.476	-1.291	G. ruber-w
C166A-8GGC	7	0.580	-1.034	G. ruber-w
C166A-8GGC	7	0.607	-1.405	G. ruber-w
C166A-8GGC	9	0.749	-1.421	G. ruber-w
C166A-8GGC	9	0.723	-1.152	G. ruber-w
C166A-8GGC	9	0.021	-1.127	G. ruber-w
C166A-8GGC	11	1.008	-1.039	G. ruber-w
C166A-8GGC	11	0.790	-1.013	G. ruber-w
C166A-8GGC	11	0.626	-1.502	G. ruber-w
C166A-8GGC	13	0.402	-1.550	G. ruber-w
C166A-8GGC	13	0.406	-1.345	G. ruber-w
C166A-8GGC	13	0.621	-1.579	G. ruber-w
C166A-8GGC	15	0.789	-1.707	G. ruber-w
C166A-8GGC	15	0.523	-1.360	G. ruber-w
C166A-8GGC	15	0.928	-1.309	G. ruber-w
C166A-8GGC	15	0.595	-1.255	G. ruber-w
C166A-8GGC	17	0.316	-1.541	G. ruber-w
C166A-8GGC	17	0.696	-0.928	G. ruber-w
C166A-8GGC	17	0.297	-1.638	G. ruber-w
C166A-8GGC	19	0.231	-1.954	G. ruber-w
C166A-8GGC	19	0.654	-1.335	G. ruber-w
C166A-8GGC	19	0.640	-0.823	G. ruber-w
C166A-8GGC	21	0.604	-1.509	G. ruber-w
C166A-8GGC	21	0.272	-1.471	G. ruber-w
C166A-8GGC	21	0.535	-1.026	G. ruber-w
C166A-8GGC	22	0.339	-1.680	G. ruber-w
C166A-8GGC	22	0.667	-1.298	G. ruber-w
C166A-8GGC	22	0.450	-1.238	G. ruber-w
C166A-8GGC	23	0.652	-1.388	G. ruber-w
C166A-8GGC	23	0.700	-1.190	G. ruber-w
C166A-8GGC	23	0.549	-1.143	G. ruber-w
C166A-8GGC	24	0.167	-1.434	G. ruber-w
C166A-8GGC	24	0.386	-1.282	G. ruber-w
C166A-8GGC	24	0.627	-1.414	G. ruber-w

C166A-8GGC	25	0.520	-1.540	G. ruber-w
C166A-8GGC	25	0.574	-1.416	G. ruber-w
C166A-8GGC	25	0.632	-1.384	G. ruber-w
C166A-8GGC	26	0.325	-1.831	G. ruber-w
C166A-8GGC	26	0.583	-1.076	G. ruber-w
C166A-8GGC	26	0.555	-1.299	G. ruber-w
C166A-8GGC	27	0.523	-1.504	G. ruber-w
C166A-8GGC	27	0.433	-1.499	G. ruber-w
C166A-8GGC	27	0.609	-0.931	G. ruber-w
C166A-8GGC	27	0.277	-1.689	G. ruber-w
C166A-8GGC	27	0.150	-1.679	G. ruber-w
C166A-8GGC	27	0.438	-1.460	G. ruber-w
C166A-8GGC	28	0.331	-1.778	G. ruber-w
C166A-8GGC	28	0.465	-1.436	G. ruber-w
C166A-8GGC	28	0.084	-1.401	G. ruber-w
C166A-8GGC	28	0.077	-1.276	G. ruber-w
C166A-8GGC	29	0.478	-1.363	G. ruber-w
C166A-8GGC	29	0.772	-1.217	G. ruber-w
C166A-8GGC	29	0.304	-1.543	G. ruber-w
C166A-8GGC	29	-0.097	-1.704	G. ruber-w
C166A-8GGC	29	0.754	-1.495	G. ruber-w
C166A-8GGC	30	0.445	-1.505	G. ruber-w
C166A-8GGC	30	1.018	-1.496	G. ruber-w
C166A-8GGC	30	0.311	-1.318	G. ruber-w
C166A-8GGC	31	0.443	-1.686	G. ruber-w
C166A-8GGC	31	1.053	-1.352	G. ruber-w
C166A-8GGC	31	0.790	-1.050	G. ruber-w
C166A-8GGC	31	0.923	-2.019	G. ruber-w
C166A-8GGC	31	0.594	-1.664	G. ruber-w
C166A-8GGC	32	0.580	-1.274	G. ruber-w
C166A-8GGC	32	0.516	-1.578	G. ruber-w
C166A-8GGC	32	0.661	-1.431	G. ruber-w
C166A-8GGC	33	0.791	-1.129	G. ruber-w
C166A-8GGC	33	0.382	-1.022	G. ruber-w
C166A-8GGC	33	0.478	-1.827	G. ruber-w
C166A-8GGC	33	0.434	-1.723	G. ruber-w
C166A-8GGC	33	0.168	-1.882	G. ruber-w
C166A-8GGC	35	0.316	-1.838	G. ruber-w
C166A-8GGC	35	0.851	-1.257	G. ruber-w
C166A-8GGC	35	0.652	-1.361	G. ruber-w
C166A-8GGC	35	0.559	-1.570	G. ruber-w
C166A-8GGC	35	0.380	-1.475	G. ruber-w
C166A-8GGC	37	0.320	-1.360	G. ruber-w
C166A-8GGC	37	0.656	-1.493	G. ruber-w
C166A-8GGC	37	0.797	-1.201	G. ruber-w
C166A-8GGC	37	0.279	-1.666	G. ruber-w
C166A-8GGC	37	0.521	-1.684	G. ruber-w
C166A-8GGC	39	0.648	-1.582	G. ruber-w
C166A-8GGC	39	0.731	-1.256	G. ruber-w
C166A-8GGC	39	-0.042	-1.709	G. ruber-w
C166A-8GGC	39	0.775	-1.690	G. ruber-w
C166A-8GGC	39	0.317	-1.480	G. ruber-w
C166A-8GGC	41	0.479	-1.561	G. ruber-w
C166A-8GGC	41	0.403	-1.334	G. ruber-w
C166A-8GGC	41	0.730	-1.461	G. ruber-w

C166A-8GGC	41	0.176	-1.911	G. ruber-w
C166A-8GGC	41	0.300	-1.389	G. ruber-w
C166A-8GGC	43	0.278	-1.247	G. ruber-w
C166A-8GGC	43	0.370	-1.015	G. ruber-w
C166A-8GGC	43	0.326	-1.563	G. ruber-w
C166A-8GGC	43	0.142	-1.414	G. ruber-w
C166A-8GGC	43	0.345	-1.702	G. ruber-w
C166A-8GGC	45	0.291	-1.916	G. ruber-w
C166A-8GGC	45	0.324	-1.461	G. ruber-w
C166A-8GGC	45	0.531	-1.368	G. ruber-w
C166A-8GGC	47	0.641	-1.506	G. ruber-w
C166A-8GGC	47	0.724	-1.372	G. ruber-w
C166A-8GGC	47	0.289	-1.808	G. ruber-w
C166A-8GGC	49	0.097	-1.849	G. ruber-w
C166A-8GGC	49	0.071	-1.692	G. ruber-w
C166A-8GGC	49	0.740	-1.375	G. ruber-w
C166A-8GGC	49	0.065	-2.085	G. ruber-w
C166A-8GGC	51	0.314	-1.383	G. ruber-w
C166A-8GGC	51	0.658	-1.322	G. ruber-w
C166A-8GGC	51	0.101	-1.522	G. ruber-w
C166A-8GGC	53	0.631	-1.623	G. ruber-w
C166A-8GGC	53	0.592	-1.594	G. ruber-w
C166A-8GGC	53	0.034	-1.373	G. ruber-w
C166A-8GGC	55	0.639	-1.690	G. ruber-w
C166A-8GGC	55	0.837	-1.430	G. ruber-w
C166A-8GGC	55	0.209	-1.441	G. ruber-w
C166A-8GGC	57	0.682	-1.410	G. ruber-w
C166A-8GGC	57	0.294	-1.275	G. ruber-w
C166A-8GGC	57	0.469	-1.299	G. ruber-w
C166A-8GGC	59	0.201	-1.626	G. ruber-w
C166A-8GGC	59	0.358	-1.426	G. ruber-w
C166A-8GGC	59	0.702	-1.245	G. ruber-w
C166A-8GGC	61	0.032	-1.368	G. ruber-w
C166A-8GGC	61	0.656	-1.412	G. ruber-w
C166A-8GGC	61	0.299	-1.283	G. ruber-w
C166A-8GGC	63	0.659	-1.522	G. ruber-w
C166A-8GGC	63	0.206	-1.502	G. ruber-w
C166A-8GGC	63	0.086	-1.686	G. ruber-w
C166A-8GGC	65	0.415	-1.561	G. ruber-w
C166A-8GGC	65	0.461	-1.586	G. ruber-w
C166A-8GGC	65	0.193	-1.479	G. ruber-w
C166A-8GGC	67	0.511	-1.652	G. ruber-w
C166A-8GGC	67	0.748	-1.519	G. ruber-w
C166A-8GGC	67	0.413	-1.377	G. ruber-w
C166A-8GGC	69	0.646	-1.776	G. ruber-w
C166A-8GGC	69	0.386	-1.571	G. ruber-w
C166A-8GGC	69	0.232	-1.491	G. ruber-w
C166A-8GGC	71	0.114	-1.646	G. ruber-w
C166A-8GGC	71	0.019	-1.433	G. ruber-w
C166A-8GGC	71	0.309	-1.629	G. ruber-w
C166A-8GGC	73	0.296	-1.544	G. ruber-w
C166A-8GGC	73	0.326	-1.609	G. ruber-w
C166A-8GGC	73	0.672	-1.217	G. ruber-w
C166A-8GGC	75	0.369	-1.758	G. ruber-w
C166A-8GGC	75	0.560	-1.340	G. ruber-w

C166A-8GGC	75	0.791	-1.312	G. ruber-w
C166A-8GGC	77	-0.211	-1.823	G. ruber-w
C166A-8GGC	77	0.698	-1.720	G. ruber-w
C166A-8GGC	77	0.198	-1.320	G. ruber-w
C166A-8GGC	77	0.166	-1.528	G. ruber-w
C166A-8GGC	79	0.565	-1.452	G. ruber-w
C166A-8GGC	79	0.256	-1.431	G. ruber-w
C166A-8GGC	79	0.303	-1.311	G. ruber-w
C166A-8GGC	81	0.211	-1.847	G. ruber-w
C166A-8GGC	81	0.330	-1.600	G. ruber-w
C166A-8GGC	81	0.595	-1.227	G. ruber-w
C166A-8GGC	83	0.072	-1.671	G. ruber-w
C166A-8GGC	83	0.565	-1.559	G. ruber-w
C166A-8GGC	83	0.703	-1.424	G. ruber-w
C166A-8GGC	85	0.283	-1.552	G. ruber-w
C166A-8GGC	85	0.286	-1.401	G. ruber-w
C166A-8GGC	85	0.252	-1.513	G. ruber-w
C166A-8GGC	87	0.454	-1.527	G. ruber-w
C166A-8GGC	87	0.941	-1.387	G. ruber-w
C166A-8GGC	87	0.916	-1.556	G. ruber-w
C166A-8GGC	89	0.488	-1.603	G. ruber-w
C166A-8GGC	89	0.807	-1.525	G. ruber-w
C166A-8GGC	89	0.276	-1.571	G. ruber-w
C166A-8GGC	91	0.497	-1.291	G. ruber-w
C166A-8GGC	91	0.631	-1.217	G. ruber-w
C166A-8GGC	91	0.503	-1.305	G. ruber-w
C166A-8GGC	93	0.188	-1.750	G. ruber-w
C166A-8GGC	93	0.852	-1.222	G. ruber-w
C166A-8GGC	93	0.527	-1.441	G. ruber-w
C166A-8GGC	95	0.460	-1.342	G. ruber-w
C166A-8GGC	95	0.470	-1.237	G. ruber-w
C166A-8GGC	95	0.641	-1.110	G. ruber-w
C166A-8GGC	97	0.138	-1.533	G. ruber-w
C166A-8GGC	97	0.659	-1.245	G. ruber-w
C166A-8GGC	97	0.463	-1.141	G. ruber-w
C166A-8GGC	99	0.235	-1.541	G. ruber-w
C166A-8GGC	99	0.626	-1.416	G. ruber-w
C166A-8GGC	99	0.611	-0.913	G. ruber-w
C166A-8GGC	101	0.465	-1.605	G. ruber-w
C166A-8GGC	101	0.414	-0.983	G. ruber-w
C166A-8GGC	101	0.752	-1.195	G. ruber-w
C166A-8GGC	103	0.454	-1.666	G. ruber-w
C166A-8GGC	103	0.320	-1.273	G. ruber-w
C166A-8GGC	103	0.610	-1.178	G. ruber-w
C166A-8GGC	105	0.513	-1.735	G. ruber-w
C166A-8GGC	105	0.369	-1.491	G. ruber-w
C166A-8GGC	105	0.666	-1.259	G. ruber-w
C166A-8GGC	107	0.297	-1.356	G. ruber-w
C166A-8GGC	107	0.647	-1.268	G. ruber-w
C166A-8GGC	107	0.713	-1.256	G. ruber-w
C166A-8GGC	109	0.511	-1.543	G. ruber-w
C166A-8GGC	109	0.464	-1.523	G. ruber-w
C166A-8GGC	109	0.015	-1.407	G. ruber-w
C166A-8GGC	111	0.419	-1.531	G. ruber-w
C166A-8GGC	111	0.762	-1.525	G. ruber-w

C166A-8GGC	111	0.737	-1.289	G. ruber-w
C166A-8GGC	113	-0.019	-1.656	G. ruber-w
C166A-8GGC	113	0.538	-1.351	G. ruber-w
C166A-8GGC	113	0.226	-1.475	G. ruber-w
C166A-8GGC	115	0.825	-1.524	G. ruber-w
C166A-8GGC	115	0.390	-1.317	G. ruber-w
C166A-8GGC	115	0.556	-1.354	G. ruber-w
C166A-8GGC	117	0.216	-1.547	G. ruber-w
C166A-8GGC	117	0.391	-1.054	G. ruber-w
C166A-8GGC	117	0.400	-1.454	G. ruber-w
C166A-8GGC	119	0.600	-1.325	G. ruber-w
C166A-8GGC	119	0.379	-1.765	G. ruber-w
C166A-8GGC	119	0.285	-1.510	G. ruber-w
C166A-8GGC	121	0.328	-1.636	G. ruber-w
C166A-8GGC	121	-0.068	-1.767	G. ruber-w
C166A-8GGC	121	0.620	-1.436	G. ruber-w
C166A-8GGC	123	0.386	-1.566	G. ruber-w
C166A-8GGC	123	0.184	-1.252	G. ruber-w
C166A-8GGC	123	0.368	-1.237	G. ruber-w
C166A-8GGC	125	0.184	-1.566	G. ruber-w
C166A-8GGC	125	0.868	-1.560	G. ruber-w
C166A-8GGC	125	0.275	-1.543	G. ruber-w
C166A-8GGC	127	0.331	-1.524	G. ruber-w
C166A-8GGC	127	0.673	-1.307	G. ruber-w
C166A-8GGC	127	0.646	-1.305	G. ruber-w
C166A-8GGC	129	0.598	-1.345	G. ruber-w
C166A-8GGC	129	0.564	-1.375	G. ruber-w
C166A-8GGC	129	0.434	-1.333	G. ruber-w
C166A-8GGC	131	0.329	-1.592	G. ruber-w
C166A-8GGC	131	0.594	-1.575	G. ruber-w
C166A-8GGC	131	0.747	-1.533	G. ruber-w
C166A-8GGC	131	0.628	-1.509	G. ruber-w
C166A-8GGC	131	0.516	-0.787	G. ruber-w
C166A-8GGC	133	0.236	-1.597	G. ruber-w
C166A-8GGC	133	0.338	-1.147	G. ruber-w
C166A-8GGC	133	0.967	-1.159	G. ruber-w
C166A-8GGC	135	0.671	-1.364	G. ruber-w
C166A-8GGC	135	-0.036	-1.894	G. ruber-w
C166A-8GGC	135	0.432	-1.292	G. ruber-w
C166A-8GGC	137	0.641	-1.304	G. ruber-w
C166A-8GGC	137	0.417	-1.513	G. ruber-w
C166A-8GGC	137	0.717	-1.395	G. ruber-w
C166A-8GGC	139	0.754	-1.239	G. ruber-w
C166A-8GGC	139	0.776	-1.163	G. ruber-w
C166A-8GGC	139	0.189	-1.470	G. ruber-w
C166A-8GGC	141	0.500	-1.763	G. ruber-w
C166A-8GGC	141	0.531	-1.125	G. ruber-w
C166A-8GGC	141	0.218	-1.438	G. ruber-w
C166A-8GGC	143	0.581	-1.752	G. ruber-w
C166A-8GGC	143	0.249	-1.745	G. ruber-w
C166A-8GGC	143	0.208	-1.577	G. ruber-w
C166A-8GGC	145	0.809	-1.590	G. ruber-w
C166A-8GGC	145	0.200	-1.554	G. ruber-w
C166A-8GGC	145	0.516	-1.525	G. ruber-w
C166A-8GGC	147	0.354	-1.617	G. ruber-w

C166A-8GGC	147	0.531	-1.332	G. ruber-w
C166A-8GGC	147	0.452	-1.865	G. ruber-w
C166A-8GGC	149	1.027	-1.792	G. ruber-w
C166A-8GGC	149	0.517	-1.493	G. ruber-w
C166A-8GGC	149	0.320	-1.555	G. ruber-w
C166A-8GGC	151	0.403	-1.664	G. ruber-w
C166A-8GGC	151	0.419	-1.633	G. ruber-w
C166A-8GGC	151	0.382	-1.551	G. ruber-w

CORE	DEPTH	C13	O18	SPECIES
KNR166-2-62MC-A	0.25	0.875	-0.883	G. ruber-w
KNR166-2-62MC-A	0.25	0.515	-1.505	G. ruber-w
KNR166-2-62MC-A	0.25	0.765	-1.291	G. ruber-w
KNR166-2-62MC-A	0.25	1.010	-1.401	G. ruber-w
KNR166-2-62MC-A	0.75	0.582	-1.399	G. ruber-w
KNR166-2-62MC-A	0.75	0.550	-1.167	G. ruber-w
KNR166-2-62MC-A	0.75	0.629	-1.637	G. ruber-w
KNR166-2-62MC-A	0.75	0.843	-1.410	G. ruber-w
KNR166-2-62MC-A	1.25	0.693	-1.522	G. ruber-w
KNR166-2-62MC-A	1.25	0.212	-1.208	G. ruber-w
KNR166-2-62MC-A	1.25	0.658	-1.582	G. ruber-w
KNR166-2-62MC-A	1.25	0.346	-1.496	G. ruber-w
KNR166-2-62MC-A	1.75	0.492	-1.260	G. ruber-w
KNR166-2-62MC-A	1.75	0.511	-1.126	G. ruber-w
KNR166-2-62MC-A	1.75	0.572	-1.527	G. ruber-w
KNR166-2-62MC-A	1.75	0.399	-1.318	G. ruber-w
KNR166-2-62MC-A	2.25	0.447	-1.187	G. ruber-w
KNR166-2-62MC-A	2.25	0.314	-1.099	G. ruber-w
KNR166-2-62MC-A	2.25	0.567	-1.256	G. ruber-w
KNR166-2-62MC-A	2.25	0.500	-1.521	G. ruber-w
KNR166-2-62MC-A	2.75	0.683	-1.698	G. ruber-w
KNR166-2-62MC-A	2.75	0.551	-1.453	G. ruber-w
KNR166-2-62MC-A	2.75	0.742	-1.868	G. ruber-w
KNR166-2-62MC-A	2.75	1.011	-1.391	G. ruber-w
KNR166-2-62MC-A	3.25	0.749	-1.422	G. ruber-w
KNR166-2-62MC-A	3.25	0.465	-1.552	G. ruber-w
KNR166-2-62MC-A	3.25	0.155	-1.803	G. ruber-w
KNR166-2-62MC-A	3.25	0.452	-1.456	G. ruber-w
KNR166-2-62MC-A	3.75	0.582	-1.506	G. ruber-w
KNR166-2-62MC-A	3.75	0.356	-1.632	G. ruber-w
KNR166-2-62MC-A	3.75	0.484	-1.284	G. ruber-w
KNR166-2-62MC-A	3.75	0.813	-1.463	G. ruber-w
KNR166-2-62MC-A	4.25	0.577	-1.387	G. ruber-w
KNR166-2-62MC-A	4.25	0.821	-1.260	G. ruber-w
KNR166-2-62MC-A	4.25	0.280	-1.309	G. ruber-w
KNR166-2-62MC-A	4.25	0.782	-0.997	G. ruber-w
KNR166-2-62MC-A	4.75	0.885	-1.505	G. ruber-w
KNR166-2-62MC-A	4.75	0.577	-1.502	G. ruber-w
KNR166-2-62MC-A	4.75	0.796	-1.046	G. ruber-w
KNR166-2-62MC-A	4.75	0.678	-1.370	G. ruber-w
KNR166-2-62MC-A	5.25	0.601	-1.364	G. ruber-w
KNR166-2-62MC-A	5.25	0.857	-1.634	G. ruber-w
KNR166-2-62MC-A	5.25	0.482	-1.422	G. ruber-w
KNR166-2-62MC-A	5.25	0.919	-0.884	G. ruber-w
KNR166-2-62MC-A	5.75	0.329	-1.260	G. ruber-w
KNR166-2-62MC-A	5.75	0.724	-1.704	G. ruber-w
KNR166-2-62MC-A	5.75	0.707	-1.181	G. ruber-w
KNR166-2-62MC-A	5.75	0.415	-1.570	G. ruber-w
KNR166-2-62MC-A	6.25	0.715	-1.366	G. ruber-w
KNR166-2-62MC-A	6.25	0.555	-1.729	G. ruber-w
KNR166-2-62MC-A	6.25	0.756	-1.729	G. ruber-w
KNR166-2-62MC-A	6.25	0.402	-1.466	G. ruber-w
KNR166-2-62MC-A	6.75	0.763	-1.417	G. ruber-w
KNR166-2-62MC-A	6.75	0.379	-1.395	G. ruber-w

KNR166-2-62MC-A	6.75	0.254	-1.331	G. ruber-w
KNR166-2-62MC-A	6.75	0.507	-1.408	G. ruber-w
KNR166-2-62MC-A	7.25	0.846	-1.199	G. ruber-w
KNR166-2-62MC-A	7.25	0.675	-1.261	G. ruber-w
KNR166-2-62MC-A	7.25	0.748	-1.180	G. ruber-w
KNR166-2-62MC-A	7.25	0.654	-1.238	G. ruber-w
KNR166-2-62MC-A	7.75	0.698	-1.327	G. ruber-w
KNR166-2-62MC-A	7.75	0.729	-1.012	G. ruber-w
KNR166-2-62MC-A	7.75	0.900	-1.305	G. ruber-w
KNR166-2-62MC-A	7.75	0.634	-1.370	G. ruber-w
KNR166-2-62MC-A	8.25	0.934	-1.506	G. ruber-w
KNR166-2-62MC-A	8.25	0.384	-1.431	G. ruber-w
KNR166-2-62MC-A	8.25	0.693	-1.477	G. ruber-w
KNR166-2-62MC-A	8.25	0.977	-1.703	G. ruber-w
KNR166-2-62MC-A	8.75	0.671	-0.999	G. ruber-w
KNR166-2-62MC-A	8.75	0.739	-1.237	G. ruber-w
KNR166-2-62MC-A	8.75	0.776	-1.339	G. ruber-w
KNR166-2-62MC-A	8.75	0.603	-1.326	G. ruber-w
KNR166-2-62MC-A	9.25	0.257	-1.294	G. ruber-w
KNR166-2-62MC-A	9.25	0.633	-1.207	G. ruber-w
KNR166-2-62MC-A	9.25	0.231	-1.396	G. ruber-w
KNR166-2-62MC-A	9.25	0.603	-1.475	G. ruber-w
KNR166-2-62MC-A	9.75	0.973	-1.460	G. ruber-w
KNR166-2-62MC-A	9.75	0.703	-0.948	G. ruber-w
KNR166-2-62MC-A	9.75	0.512	-1.542	G. ruber-w
KNR166-2-62MC-A	9.75	0.349	-1.637	G. ruber-w
KNR166-2-62MC-A	10.25	0.718	-1.144	G. ruber-w
KNR166-2-62MC-A	10.25	0.527	-1.579	G. ruber-w
KNR166-2-62MC-A	10.25	0.743	-1.615	G. ruber-w
KNR166-2-62MC-A	10.25	0.471	-1.252	G. ruber-w
KNR166-2-62MC-A	10.75	0.679	-1.340	G. ruber-w
KNR166-2-62MC-A	10.75	0.691	-1.753	G. ruber-w
KNR166-2-62MC-A	10.75	0.698	-1.583	G. ruber-w
KNR166-2-62MC-A	10.75	0.386	-1.797	G. ruber-w
KNR166-2-62MC-A	11.25	0.701	-1.172	G. ruber-w
KNR166-2-62MC-A	11.25	0.687	-1.548	G. ruber-w
KNR166-2-62MC-A	11.25	0.114	-1.730	G. ruber-w
KNR166-2-62MC-A	11.25	1.009	-1.286	G. ruber-w
KNR166-2-62MC-A	11.75	0.375	-1.868	G. ruber-w
KNR166-2-62MC-A	11.75	0.734	-1.525	G. ruber-w
KNR166-2-62MC-A	11.75	0.694	-1.521	G. ruber-w
KNR166-2-62MC-A	11.75	0.721	-1.328	G. ruber-w
KNR166-2-62MC-A	12.25	0.299	-1.699	G. ruber-w
KNR166-2-62MC-A	12.25	0.635	-1.658	G. ruber-w
KNR166-2-62MC-A	12.25	0.911	-1.498	G. ruber-w
KNR166-2-62MC-A	12.25	1.027	-1.475	G. ruber-w
KNR166-2-62MC-A	12.75	0.659	-1.383	G. ruber-w
KNR166-2-62MC-A	12.75	0.373	-1.522	G. ruber-w
KNR166-2-62MC-A	12.75	0.552	-1.193	G. ruber-w
KNR166-2-62MC-A	12.75	1.006	-1.458	G. ruber-w
KNR166-2-62MC-A	13.25	0.527	-1.151	G. ruber-w
KNR166-2-62MC-A	13.25	0.285	-1.751	G. ruber-w
KNR166-2-62MC-A	13.25	0.597	-1.346	G. ruber-w
KNR166-2-62MC-A	13.25	0.821	-1.382	G. ruber-w
KNR166-2-62MC-A	13.75	0.328	-1.355	G. ruber-w

KNR166-2-62MC-A	13.75	0.647	-1.549	G. ruber-w
KNR166-2-62MC-A	13.75	0.648	-1.564	G. ruber-w
KNR166-2-62MC-A	13.75	0.255	-1.533	G. ruber-w
KNR166-2-62MC-A	14.25	0.377	-1.474	G. ruber-w
KNR166-2-62MC-A	14.25	0.633	-1.266	G. ruber-w
KNR166-2-62MC-A	14.25	0.707	-1.721	G. ruber-w
KNR166-2-62MC-A	14.25	0.097	-1.567	G. ruber-w
KNR166-2-62MC-A	14.75	0.497	-1.460	G. ruber-w
KNR166-2-62MC-A	14.75	0.386	-1.648	G. ruber-w
KNR166-2-62MC-A	14.75	0.237	-1.838	G. ruber-w
KNR166-2-62MC-A	14.75	0.817	-1.641	G. ruber-w
KNR166-2-62MC-A	15.25	0.719	-1.503	G. ruber-w
KNR166-2-62MC-A	15.25	0.306	-1.159	G. ruber-w
KNR166-2-62MC-A	15.25	0.362	-1.371	G. ruber-w
KNR166-2-62MC-A	15.25	0.776	-1.272	G. ruber-w
KNR166-2-62MC-A	15.75	0.440	-1.680	G. ruber-w
KNR166-2-62MC-A	15.75	0.213	-1.715	G. ruber-w
KNR166-2-62MC-A	15.75	0.517	-1.500	G. ruber-w
KNR166-2-62MC-A	15.75	0.451	-1.556	G. ruber-w
KNR166-2-62MC-A	16.25	0.229	-1.616	G. ruber-w
KNR166-2-62MC-A	16.25	0.319	-1.357	G. ruber-w
KNR166-2-62MC-A	16.25	0.543	-1.602	G. ruber-w
KNR166-2-62MC-A	16.25	0.420	-1.420	G. ruber-w
KNR166-2-62MC-A	16.75	0.564	-1.246	G. ruber-w
KNR166-2-62MC-A	16.75	0.162	-1.920	G. ruber-w
KNR166-2-62MC-A	16.75	0.406	-1.619	G. ruber-w
KNR166-2-62MC-A	16.75	0.518	-1.351	G. ruber-w
KNR166-2-62MC-A	17.25	0.703	-1.419	G. ruber-w
KNR166-2-62MC-A	17.25	0.631	-1.482	G. ruber-w
KNR166-2-62MC-A	17.25	0.630	-1.421	G. ruber-w
KNR166-2-62MC-A	17.25	0.727	-1.492	G. ruber-w
KNR166-2-62MC-A	17.75	0.580	-1.345	G. ruber-w
KNR166-2-62MC-A	17.75	0.683	-1.528	G. ruber-w
KNR166-2-62MC-A	17.75	0.709	-1.425	G. ruber-w
KNR166-2-62MC-A	17.75	0.295	-1.863	G. ruber-w
KNR166-2-62MC-A	18.25	0.465	-1.443	G. ruber-w
KNR166-2-62MC-A	18.25	0.652	-1.561	G. ruber-w
KNR166-2-62MC-A	18.25	0.647	-1.219	G. ruber-w
KNR166-2-62MC-A	18.25	0.252	-1.764	G. ruber-w
KNR166-2-62MC-A	18.75	0.516	-1.623	G. ruber-w
KNR166-2-62MC-A	18.75	0.400	-1.391	G. ruber-w
KNR166-2-62MC-A	18.75	0.234	-1.642	G. ruber-w
KNR166-2-62MC-A	18.75	0.639	-1.471	G. ruber-w
KNR166-2-62MC-A	19.25	0.738	-1.389	G. ruber-w
KNR166-2-62MC-A	19.25	0.483	-1.310	G. ruber-w
KNR166-2-62MC-A	19.25	0.655	-1.528	G. ruber-w
KNR166-2-62MC-A	19.25	0.269	-1.744	G. ruber-w
KNR166-2-62MC-A	19.75	0.821	-1.643	G. ruber-w
KNR166-2-62MC-A	19.75	0.616	-1.589	G. ruber-w
KNR166-2-62MC-A	19.75	0.519	-1.711	G. ruber-w
KNR166-2-62MC-A	19.75	0.644	-1.582	G. ruber-w
KNR166-2-62MC-A	20.25	0.778	-1.273	G. ruber-w
KNR166-2-62MC-A	20.25	0.232	-1.741	G. ruber-w
KNR166-2-62MC-A	20.25	0.512	-1.352	G. ruber-w
KNR166-2-62MC-A	20.25	0.776	-1.442	G. ruber-w

KNR166-2-62MC-A	20.75	0.543	-1.736	G. ruber-w
KNR166-2-62MC-A	20.75	0.760	-1.292	G. ruber-w
KNR166-2-62MC-A	20.75	0.388	-1.384	G. ruber-w
KNR166-2-62MC-A	20.75	0.601	-1.595	G. ruber-w
KNR166-2-62MC-A	21.25	0.407	-1.649	G. ruber-w
KNR166-2-62MC-A	21.25	0.818	-1.451	G. ruber-w
KNR166-2-62MC-A	21.25	0.674	-1.347	G. ruber-w
KNR166-2-62MC-A	21.25	0.651	-1.477	G. ruber-w
KNR166-2-62MC-A	21.75	-0.011	-1.790	G. ruber-w
KNR166-2-62MC-A	21.75	0.508	-1.487	G. ruber-w
KNR166-2-62MC-A	21.75	0.496	-1.575	G. ruber-w
KNR166-2-62MC-A	21.75	0.687	-1.369	G. ruber-w
KNR166-2-62MC-A	22.25	0.627	-1.467	G. ruber-w
KNR166-2-62MC-A	22.25	0.811	-1.392	G. ruber-w
KNR166-2-62MC-A	22.25	0.758	-1.816	G. ruber-w
KNR166-2-62MC-A	22.25	0.293	-1.630	G. ruber-w
KNR166-2-62MC-A	22.75	0.453	-1.760	G. ruber-w
KNR166-2-62MC-A	22.75	0.200	-1.739	G. ruber-w
KNR166-2-62MC-A	22.75	0.645	-1.607	G. ruber-w
KNR166-2-62MC-A	22.75	0.326	-1.883	G. ruber-w
KNR166-2-62MC-A	23.25	0.409	-1.751	G. ruber-w
KNR166-2-62MC-A	23.25	0.748	-1.218	G. ruber-w
KNR166-2-62MC-A	23.25	0.324	-1.578	G. ruber-w
KNR166-2-62MC-A	23.25	0.599	-1.431	G. ruber-w
KNR166-2-62MC-A	23.75	0.500	-1.683	G. ruber-w
KNR166-2-62MC-A	23.75	0.132	-1.889	G. ruber-w
KNR166-2-62MC-A	23.75	0.398	-1.480	G. ruber-w
KNR166-2-62MC-A	23.75	0.439	-1.550	G. ruber-w
KNR166-2-62MC-A	24.25	0.412	-1.996	G. ruber-w
KNR166-2-62MC-A	24.25	0.650	-1.538	G. ruber-w
KNR166-2-62MC-A	24.25	0.561	-1.965	G. ruber-w
KNR166-2-62MC-A	24.25	0.620	-1.741	G. ruber-w
KNR166-2-62MC-A	24.75	0.654	-1.340	G. ruber-w
KNR166-2-62MC-A	24.75	0.583	-1.496	G. ruber-w
KNR166-2-62MC-A	24.75	1.354	-1.852	G. ruber-w
KNR166-2-62MC-A	24.75	0.643	-1.493	G. ruber-w
KNR166-2-62MC-A	25.25	0.499	-1.449	G. ruber-w
KNR166-2-62MC-A	25.25	0.280	-1.695	G. ruber-w
KNR166-2-62MC-A	25.25	0.385	-1.270	G. ruber-w
KNR166-2-62MC-A	25.25	0.741	-1.694	G. ruber-w
KNR166-2-62MC-A	25.75	0.548	-1.410	G. ruber-w
KNR166-2-62MC-A	25.75	0.591	-1.508	G. ruber-w
KNR166-2-62MC-A	25.75	0.830	-1.561	G. ruber-w
KNR166-2-62MC-A	25.75	0.387	-1.729	G. ruber-w
KNR166-2-62MC-A	26.25	0.271	-1.437	G. ruber-w
KNR166-2-62MC-A	26.25	0.533	-1.524	G. ruber-w
KNR166-2-62MC-A	26.25	0.151	-1.500	G. ruber-w
KNR166-2-62MC-A	26.25	0.635	-1.495	G. ruber-w
KNR166-2-62MC-A	26.75	0.551	-1.502	G. ruber-w
KNR166-2-62MC-A	26.75	0.691	-1.582	G. ruber-w
KNR166-2-62MC-A	26.75	0.225	-1.746	G. ruber-w
KNR166-2-62MC-A	26.75	0.512	-1.569	G. ruber-w
KNR166-2-62MC-A	27.25	0.404	-1.340	G. ruber-w
KNR166-2-62MC-A	27.25	0.550	-1.641	G. ruber-w
KNR166-2-62MC-A	27.25	0.555	-1.595	G. ruber-w

KNR166-2-62MC-A	27.25	0.806	-1.723	G. ruber-w
KNR166-2-62MC-A	27.75	0.390	-1.481	G. ruber-w
KNR166-2-62MC-A	27.75	0.295	-1.587	G. ruber-w
KNR166-2-62MC-A	27.75	0.644	-1.514	G. ruber-w
KNR166-2-62MC-A	27.75	0.348	-1.681	G. ruber-w
KNR166-2-62MC-A	28.25	0.368	-1.474	G. ruber-w
KNR166-2-62MC-A	28.25	0.644	-1.603	G. ruber-w
KNR166-2-62MC-A	28.25	0.383	-1.641	G. ruber-w
KNR166-2-62MC-A	28.25	0.288	-1.826	G. ruber-w
KNR166-2-62MC-A	28.75	0.319	-1.597	G. ruber-w
KNR166-2-62MC-A	28.75	0.414	-1.633	G. ruber-w
KNR166-2-62MC-A	28.75	0.615	-1.661	G. ruber-w
KNR166-2-62MC-A	28.75	0.576	-1.471	G. ruber-w
KNR166-2-62MC-A	29.25	0.610	-1.516	G. ruber-w
KNR166-2-62MC-A	29.25	0.236	-1.929	G. ruber-w
KNR166-2-62MC-A	29.25	0.516	-1.624	G. ruber-w
KNR166-2-62MC-A	29.25	0.315	-1.639	G. ruber-w
KNR166-2-62MC-A	29.75	0.360	-1.542	G. ruber-w
KNR166-2-62MC-A	29.75	0.383	-1.785	G. ruber-w
KNR166-2-62MC-A	29.75	0.326	-1.658	G. ruber-w
KNR166-2-62MC-A	29.75	-0.118	-1.913	G. ruber-w

APPENDIX B

Chapter 3 planktonic Mg/Ca and stable isotope data

NOTE:

Mg/Ca data is listed first, followed by stable istope data.

DRY TORTUGAS CORE SITES – Mg/Ca DATA

Note: Mg/Ca data for each stratigraphic level in 62MC-A is based on two splits (A&B) from the same group of ~100 crushed and homogenized *G. ruber* individuals. Mg/Ca ratios are given in mmol/mol. In certain cases, only one Mg/Ca analysis was run at a given core depth (where B_split is NaN).

CORE	DEPTH	A_split	B_split	SPECIES
KNR166-2-62MC-A	0.75	4.456	NaN	G. ruber-w
KNR166-2-62MC-A	1.75	4.187	NaN	G. ruber-w
KNR166-2-62MC-A	2.75	3.949	NaN	G. ruber-w
KNR166-2-62MC-A	3.75	4.708	NaN	G. ruber-w
KNR166-2-62MC-A	4.75	4.437	4.503	G. ruber-w
KNR166-2-62MC-A	5.75	4.122	4.491	G. ruber-w
KNR166-2-62MC-A	6.75	4.150	4.290	G. ruber-w
KNR166-2-62MC-A	7.75	4.524	4.369	G. ruber-w
KNR166-2-62MC-A	8.75	4.206	4.297	G. ruber-w
KNR166-2-62MC-A	9.75	4.293	4.361	G. ruber-w
KNR166-2-62MC-A	10.75	3.949	4.468	G. ruber-w
KNR166-2-62MC-A	11.75	4.401	4.001	G. ruber-w
KNR166-2-62MC-A	12.75	4.660	4.398	G. ruber-w
KNR166-2-62MC-A	13.75	3.879	4.035	G. ruber-w
KNR166-2-62MC-A	14.75	4.095	4.246	G. ruber-w
KNR166-2-62MC-A	15.75	3.990	4.205	G. ruber-w
KNR166-2-62MC-A	16.75	4.127	4.097	G. ruber-w
KNR166-2-62MC-A	17.75	4.054	4.141	G. ruber-w
KNR166-2-62MC-A	18.75	4.418	4.194	G. ruber-w
KNR166-2-62MC-A	19.75	4.018	3.969	G. ruber-w
KNR166-2-62MC-A	20.75	3.932	4.095	G. ruber-w
KNR166-2-62MC-A	21.75	4.251	4.290	G. ruber-w
KNR166-2-62MC-A	22.75	4.269	4.407	G. ruber-w
KNR166-2-62MC-A	23.75	3.791	4.058	G. ruber-w
KNR166-2-62MC-A	24.25	4.526	4.196	G. ruber-w
KNR166-2-62MC-A	24.75	3.983	4.156	G. ruber-w
KNR166-2-62MC-A	25.25	4.248	NaN	G. ruber-w
KNR166-2-62MC-A	25.75	4.387	4.045	G. ruber-w
KNR166-2-62MC-A	26.25	4.035	NaN	G. ruber-w
KNR166-2-62MC-A	26.75	3.973	4.262	G. ruber-w
KNR166-2-62MC-A	27.25	4.085	NaN	G. ruber-w
KNR166-2-62MC-A	27.75	4.049	NaN	G. ruber-w
KNR166-2-62MC-A	28.25	4.278	NaN	G. ruber-w
KNR166-2-62MC-A	28.75	3.806	4.457	G. ruber-w
KNR166-2-62MC-A	29.25	4.144	NaN	G. ruber-w
KNR166-2-62MC-A	29.75	4.183	3.954	G. ruber-w

Note: Mg/Ca data for each stratigraphic level in 79GGC is based on ~50 G. *ruber* individuals. Mg/Ca ratios are given in mmol/mol.

CORE	DEPTH	Mg/Ca	SPECIES
W167-79GGC	0.5	5.195	G. ruber-w
W167-79GGC	2	4.947	G. ruber-w
W167-79GGC	3.25	4.905	G. ruber-w
W167-79GGC	3.75	4.748	G. ruber-w
W167-79GGC	4.25	4.952	G. ruber-w
W167-79GGC	4.75	4.241	G. ruber-w
W167-79GGC	5.25	4.437	G. ruber-w
W167-79GGC	5.75	5.030	G. ruber-w
W167-79GGC	6.25	4.525	G. ruber-w
W167-79GGC	6.75	4.224	G. ruber-w
W167-79GGC	7.25	4.367	G. ruber-w
W167-79GGC	7.75	5.287	G. ruber-w
W167-79GGC	8.25	4.352	G. ruber-w
W167-79GGC	8.75	4.918	G. ruber-w
W167-79GGC	9.25	4.612	G. ruber-w
W167-79GGC	9.75	4.483	G. ruber-w
W167-79GGC	10.25	9.337	G. ruber-w
W167-79GGC	10.75	4.501	G. ruber-w
W167-79GGC	11.25	4.591	G. ruber-w
W167-79GGC	11.75	4.849	G. ruber-w
W167-79GGC	12.25	4.083	G. ruber-w
W167-79GGC	12.75	4.456	G. ruber-w
W167-79GGC	13.25	4.747	G. ruber-w
W167-79GGC	13.75	4.848	G. ruber-w
W167-79GGC	14.25	4.649	G. ruber-w
W167-79GGC	14.75	4.854	G. ruber-w
W167-79GGC	15.25	4.313	G. ruber-w
W167-79GGC	15.75	4.414	G. ruber-w
W167-79GGC	16.25	4.552	G. ruber-w
W167-79GGC	17.25	4.361	G. ruber-w
W167-79GGC	17.75	4.398	G. ruber-w
W167-79GGC	18.25	4.340	G. ruber-w
W167-79GGC	18.75	4.444	G. ruber-w
W167-79GGC	19.25	4.374	G. ruber-w
W167-79GGC	19.75	4.832	G. ruber-w
W167-79GGC	20.25	4.263	G. ruber-w
W167-79GGC	20.75	4.538	G. ruber-w
W167-79GGC	21.25	4.626	G. ruber-w
W167-79GGC	21.75	4.894	G. ruber-w
W167-79GGC	22.25	4.048	G. ruber-w
W167-79GGC	22.75	4.792	G. ruber-w
W167-79GGC	23.25	4.151	G. ruber-w
W167-79GGC	23.75	4.081	G. ruber-w
W167-79GGC	24.25	4.321	G. ruber-w
W167-79GGC	24.75	4.637	G. ruber-w
W167-79GGC	25.25	4.109	G. ruber-w
W167-79GGC	25.75	4.178	G. ruber-w
W167-79GGC	26.25	4.361	G. ruber-w
W167-79GGC	26.75	4.064	G. ruber-w
W167-79GGC	27.25	5.072	G. ruber-w

W167-79GGC	27.75	4.123	G. ruber-w
W167-79GGC	28.25	4.180	G. ruber-w
W167-79GGC	28.75	4.336	G. ruber-w
W167-79GGC	29.25	4.059	G. ruber-w
W167-79GGC	29.75	4.800	G. ruber-w
W167-79GGC	30.25	4.250	G. ruber-w
W167-79GGC	30.75	4.265	G. ruber-w
W167-79GGC	31.25	4.404	G. ruber-w
W167-79GGC	31.75	4.273	G. ruber-w
W167-79GGC	32.25	4.351	G. ruber-w

GREAT BAHAMA BANK CORE SITES – Mg/Ca DATA

Note: Mg/Ca data for each stratigraphic level in 118MC-A is based on two splits (A&B) from the same group of ~100 crushed and homogenized *G. ruber* individuals. Mg/Ca ratios are given in mmol/mol.

CORE	DEPTH	A_split	B_split	SPECIES
KNR166-2-118MC-A	0.5	4.898	5.128	G. ruber-w
KNR166-2-118MC-A	1.5	4.693	4.990	G. ruber-w
KNR166-2-118MC-A	2.5	4.727	5.033	G. ruber-w
KNR166-2-118MC-A	3.5	4.828	4.948	G. ruber-w
KNR166-2-118MC-A	4.5	5.010	4.882	G. ruber-w
KNR166-2-118MC-A	5.5	4.702	5.017	G. ruber-w
KNR166-2-118MC-A	6.5	4.863	5.000	G. ruber-w
KNR166-2-118MC-A	7.5	4.541	4.719	G. ruber-w
KNR166-2-118MC-A	8.5	4.666	4.667	G. ruber-w
KNR166-2-118MC-A	9.5	4.585	4.961	G. ruber-w
KNR166-2-118MC-A	10.5	4.714	4.938	G. ruber-w
KNR166-2-118MC-A	11.5	4.556	4.830	G. ruber-w
KNR166-2-118MC-A	12.5	4.838	5.000	G. ruber-w
KNR166-2-118MC-A	13.5	4.704	4.699	G. ruber-w
KNR166-2-118MC-A	14.5	4.812	4.890	G. ruber-w
KNR166-2-118MC-A	15.5	4.732	5.022	G. ruber-w
KNR166-2-118MC-A	16.5	4.575	4.463	G. ruber-w
KNR166-2-118MC-A	17.5	4.629	4.702	G. ruber-w
KNR166-2-118MC-A	18.5	4.553	4.546	G. ruber-w
KNR166-2-118MC-A	19.5	4.589	4.661	G. ruber-w
KNR166-2-118MC-A	20.5	4.586	4.723	G. ruber-w
KNR166-2-118MC-A	21.5	4.523	4.576	G. ruber-w
KNR166-2-118MC-A	22.5	4.713	4.869	G. ruber-w
KNR166-2-118MC-A	23.5	4.556	4.563	G. ruber-w
KNR166-2-118MC-A	26.5	4.644	4.535	G. ruber-w
KNR166-2-118MC-A	27.5	4.631	4.575	G. ruber-w
KNR166-2-118MC-A	33.5	4.485	4.605	G. ruber-w
KNR166-2-118MC-A	36.5	4.532	4.590	G. ruber-w

Note: Mg/Ca data for each stratigraphic level in 125MC-D is based on two splits (A&B) from the same group of ~100 crushed and homogenized *G. ruber* individuals. Mg/Ca ratios are given in mmol/mol.

CORE	DEPTH	A_split	B_split	SPECIES
KNR166-125MC-D	0.5	4.987	4.903	G. ruber-w
KNR166-125MC-D	1.5	4.917	4.750	G. ruber-w
KNR166-125MC-D	2.5	4.618	4.962	G. ruber-w
KNR166-125MC-D	3.5	4.998	4.710	G. ruber-w
KNR166-125MC-D	4.5	4.761	4.659	G. ruber-w
KNR166-125MC-D	5.5	4.329	4.448	G. ruber-w
KNR166-125MC-D	6.5	4.768	5.116	G. ruber-w
KNR166-125MC-D	7.5	4.618	4.372	G. ruber-w
KNR166-125MC-D	8.5	4.746	4.706	G. ruber-w
KNR166-125MC-D	9.5	4.663	4.461	G. ruber-w
KNR166-125MC-D	10.5	4.450	4.453	G. ruber-w
KNR166-125MC-D	11.5	4.844	4.682	G. ruber-w
KNR166-125MC-D	12.5	4.702	4.664	G. ruber-w
KNR166-125MC-D	13.5	4.723	4.861	G. ruber-w
KNR166-125MC-D	14.5	5.044	4.552	G. ruber-w
KNR166-125MC-D	15.5	4.883	4.707	G. ruber-w
KNR166-125MC-D	16.5	4.773	4.811	G. ruber-w
KNR166-125MC-D	17.5	4.784	4.735	G. ruber-w
KNR166-125MC-D	18.5	4.651	4.877	G. ruber-w
KNR166-125MC-D	19.5	4.947	4.653	G. ruber-w
KNR166-125MC-D	20.5	4.685	4.775	G. ruber-w
KNR166-125MC-D	21.5	4.805	5.000	G. ruber-w
KNR166-125MC-D	22.5	4.978	4.824	G. ruber-w
KNR166-125MC-D	23.5	5.028	5.059	G. ruber-w
KNR166-125MC-D	24.5	4.689	4.720	G. ruber-w
KNR166-125MC-D	25.5	4.647	4.758	G. ruber-w
KNR166-125MC-D	26.5	4.632	4.840	G. ruber-w
KNR166-125MC-D	27.5	4.814	5.089	G. ruber-w

DRY TORTUGAS CORE SITES – STABLE ISOTOPE DATA

COLUMN HEADERS:

CORE, DEPTH (cm), C13 (per mil), O18 (per mil), SPECIES

Note: The data for 62MC below is based on the same crushed and homogenized samples used for Mg/Ca analyses. These data are different than those generated for Chapter 2 (see Appendix A). Data for 79GGC is given in Appendix A.

CORE	DEPTH	C13	O18	SPECIES
KNR166-2-62MC-A	0.75	0.407	-1.554	G. ruber-w
KNR166-2-62MC-A	0.75	0.603	-1.483	G. ruber-w
KNR166-2-62MC-A	0.75	0.404	-1.445	G. ruber-w
KNR166-2-62MC-A	0.75	0.501	-1.441	G. ruber-w
KNR166-2-62MC-A	1.75	0.424	-1.697	G. ruber-w
KNR166-2-62MC-A	1.75	0.665	-1.556	G. ruber-w
KNR166-2-62MC-A	1.75	0.716	-1.495	G. ruber-w
KNR166-2-62MC-A	1.75	0.739	-1.460	G. ruber-w
KNR166-2-62MC-A	2.75	0.565	-1.643	G. ruber-w
KNR166-2-62MC-A	2.75	0.513	-1.627	G. ruber-w
KNR166-2-62MC-A	2.75	0.317	-1.624	G. ruber-w
KNR166-2-62MC-A	2.75	0.400	-1.543	G. ruber-w
KNR166-2-62MC-A	3.75	0.506	-1.504	G. ruber-w
KNR166-2-62MC-A	3.75	0.551	-1.427	G. ruber-w
KNR166-2-62MC-A	3.75	0.527	-1.367	G. ruber-w
KNR166-2-62MC-A	4.75	0.601	-1.690	G. ruber-w
KNR166-2-62MC-A	4.75	0.732	-1.547	G. ruber-w
KNR166-2-62MC-A	4.75	0.537	-1.512	G. ruber-w
KNR166-2-62MC-A	4.75	0.818	-1.495	G. ruber-w
KNR166-2-62MC-A	5.75	0.839	-1.598	G. ruber-w
KNR166-2-62MC-A	5.75	0.696	-1.539	G. ruber-w
KNR166-2-62MC-A	5.75	0.670	-1.522	G. ruber-w
KNR166-2-62MC-A	6.75	0.452	-1.602	G. ruber-w
KNR166-2-62MC-A	6.75	0.374	-1.582	G. ruber-w
KNR166-2-62MC-A	6.75	0.385	-1.508	G. ruber-w
KNR166-2-62MC-A	6.75	0.570	-1.331	G. ruber-w
KNR166-2-62MC-A	7.75	0.732	-1.582	G. ruber-w
KNR166-2-62MC-A	7.75	0.741	-1.514	G. ruber-w
KNR166-2-62MC-A	7.75	0.796	-1.425	G. ruber-w
KNR166-2-62MC-A	8.75	0.503	-1.790	G. ruber-w
KNR166-2-62MC-A	8.75	0.688	-1.777	G. ruber-w
KNR166-2-62MC-A	8.75	0.513	-1.623	G. ruber-w
KNR166-2-62MC-A	8.75	0.704	-1.400	G. ruber-w
KNR166-2-62MC-A	9.75	0.618	-1.777	G. ruber-w
KNR166-2-62MC-A	9.75	0.572	-1.755	G. ruber-w
KNR166-2-62MC-A	9.75	0.572	-1.740	G. ruber-w
KNR166-2-62MC-A	10.75	0.689	-1.712	G. ruber-w
KNR166-2-62MC-A	10.75	0.515	-1.647	G. ruber-w
KNR166-2-62MC-A	10.75	0.666	-1.501	G. ruber-w
KNR166-2-62MC-A	10.75	0.800	-1.453	G. ruber-w
KNR166-2-62MC-A	11.75	0.262	-1.775	G. ruber-w
KNR166-2-62MC-A	11.75	0.484	-1.625	G. ruber-w
KNR166-2-62MC-A	11.75	0.671	-1.438	G. ruber-w

KNR166-2-62MC-A	11.75	0.580	-1.417	G. ruber-w
KNR166-2-62MC-A	12.75	0.655	-1.606	G. ruber-w
KNR166-2-62MC-A	12.75	0.657	-1.549	G. ruber-w
KNR166-2-62MC-A	12.75	0.666	-1.508	G. ruber-w
KNR166-2-62MC-A	13.75	0.201	-1.697	G. ruber-w
KNR166-2-62MC-A	13.75	0.508	-1.601	G. ruber-w
KNR166-2-62MC-A	13.75	0.367	-1.508	G. ruber-w
KNR166-2-62MC-A	13.75	0.272	-1.466	G. ruber-w
KNR166-2-62MC-A	14.75	0.393	-2.023	G. ruber-w
KNR166-2-62MC-A	14.75	0.499	-1.853	G. ruber-w
KNR166-2-62MC-A	14.75	0.466	-1.837	G. ruber-w
KNR166-2-62MC-A	14.75	0.598	-1.800	G. ruber-w
KNR166-2-62MC-A	15.75	0.375	-1.778	G. ruber-w
KNR166-2-62MC-A	15.75	0.320	-1.674	G. ruber-w
KNR166-2-62MC-A	15.75	0.377	-1.609	G. ruber-w
KNR166-2-62MC-A	16.75	0.341	-1.783	G. ruber-w
KNR166-2-62MC-A	16.75	0.364	-1.772	G. ruber-w
KNR166-2-62MC-A	16.75	0.402	-1.670	G. ruber-w
KNR166-2-62MC-A	16.75	0.532	-1.593	G. ruber-w
KNR166-2-62MC-A	17.75	0.474	-1.749	G. ruber-w
KNR166-2-62MC-A	17.75	0.532	-1.671	G. ruber-w
KNR166-2-62MC-A	17.75	0.484	-1.572	G. ruber-w
KNR166-2-62MC-A	18.75	0.496	-1.812	G. ruber-w
KNR166-2-62MC-A	18.75	0.629	-1.787	G. ruber-w
KNR166-2-62MC-A	18.75	0.547	-1.639	G. ruber-w
KNR166-2-62MC-A	18.75	0.371	-1.597	G. ruber-w
KNR166-2-62MC-A	19.75	0.417	-1.726	G. ruber-w
KNR166-2-62MC-A	19.75	0.459	-1.712	G. ruber-w
KNR166-2-62MC-A	19.75	0.238	-1.667	G. ruber-w
KNR166-2-62MC-A	19.75	0.477	-1.619	G. ruber-w
KNR166-2-62MC-A	20.75	0.462	-1.731	G. ruber-w
KNR166-2-62MC-A	20.75	0.429	-1.709	G. ruber-w
KNR166-2-62MC-A	20.75	0.521	-1.646	G. ruber-w
KNR166-2-62MC-A	20.75	0.491	-1.536	G. ruber-w
KNR166-2-62MC-A	21.75	0.385	-2.051	G. ruber-w
KNR166-2-62MC-A	21.75	0.121	-1.853	G. ruber-w
KNR166-2-62MC-A	21.75	0.549	-1.740	G. ruber-w
KNR166-2-62MC-A	21.75	0.369	-1.728	G. ruber-w
KNR166-2-62MC-A	22.75	0.308	-1.896	G. ruber-w
KNR166-2-62MC-A	22.75	0.580	-1.699	G. ruber-w
KNR166-2-62MC-A	22.75	0.616	-1.620	G. ruber-w
KNR166-2-62MC-A	22.75	0.447	-1.615	G. ruber-w
KNR166-2-62MC-A	23.75	0.193	-1.674	G. ruber-w
KNR166-2-62MC-A	23.75	0.380	-1.618	G. ruber-w
KNR166-2-62MC-A	23.75	0.357	-1.604	G. ruber-w
KNR166-2-62MC-A	23.75	0.625	-1.449	G. ruber-w
KNR166-2-62MC-A	24.25	0.585	-2.075	G. ruber-w
KNR166-2-62MC-A	24.25	0.478	-1.809	G. ruber-w
KNR166-2-62MC-A	24.25	0.536	-1.741	G. ruber-w
KNR166-2-62MC-A	24.25	0.421	-1.660	G. ruber-w
KNR166-2-62MC-A	24.75	0.401	-1.712	G. ruber-w
KNR166-2-62MC-A	24.75	0.370	-1.695	G. ruber-w
KNR166-2-62MC-A	24.75	0.610	-1.559	G. ruber-w
KNR166-2-62MC-A	24.75	0.519	-1.362	G. ruber-w
KNR166-2-62MC-A	25.25	0.496	-1.940	G. ruber-w

KNR166-2-62MC-A	25.25	0.604	-1.719	G. ruber-w
KNR166-2-62MC-A	25.75	0.330	-1.832	G. ruber-w
KNR166-2-62MC-A	25.75	0.430	-1.771	G. ruber-w
KNR166-2-62MC-A	25.75	0.390	-1.680	G. ruber-w
KNR166-2-62MC-A	25.75	0.494	-1.673	G. ruber-w
KNR166-2-62MC-A	26.25	0.300	-1.772	G. ruber-w
KNR166-2-62MC-A	26.25	0.451	-1.724	G. ruber-w
KNR166-2-62MC-A	26.25	0.444	-1.686	G. ruber-w
KNR166-2-62MC-A	26.75	0.464	-1.940	G. ruber-w
KNR166-2-62MC-A	26.75	0.626	-1.744	G. ruber-w
KNR166-2-62MC-A	26.75	0.651	-1.708	G. ruber-w
KNR166-2-62MC-A	26.75	0.294	-1.692	G. ruber-w
KNR166-2-62MC-A	27.25	0.143	-1.836	G. ruber-w
KNR166-2-62MC-A	27.25	0.429	-1.751	G. ruber-w
KNR166-2-62MC-A	27.25	0.493	-1.706	G. ruber-w
KNR166-2-62MC-A	27.25	0.379	-1.580	G. ruber-w
KNR166-2-62MC-A	27.75	0.423	-1.851	G. ruber-w
KNR166-2-62MC-A	27.75	0.436	-1.799	G. ruber-w
KNR166-2-62MC-A	27.75	0.450	-1.782	G. ruber-w
KNR166-2-62MC-A	27.75	0.636	-1.778	G. ruber-w
KNR166-2-62MC-A	28.25	0.206	-1.904	G. ruber-w
KNR166-2-62MC-A	28.25	0.469	-1.848	G. ruber-w
KNR166-2-62MC-A	28.25	0.555	-1.815	G. ruber-w
KNR166-2-62MC-A	28.25	0.241	-1.791	G. ruber-w
KNR166-2-62MC-A	28.75	0.305	-1.837	G. ruber-w
KNR166-2-62MC-A	28.75	0.325	-1.769	G. ruber-w
KNR166-2-62MC-A	28.75	0.424	-1.729	G. ruber-w
KNR166-2-62MC-A	28.75	0.249	-1.728	G. ruber-w
KNR166-2-62MC-A	29.25	0.662	-1.705	G. ruber-w
KNR166-2-62MC-A	29.25	0.380	-1.630	G. ruber-w
KNR166-2-62MC-A	29.25	0.510	-1.593	G. ruber-w
KNR166-2-62MC-A	29.75	0.231	-1.637	G. ruber-w
KNR166-2-62MC-A	29.75	0.405	-1.540	G. ruber-w
KNR166-2-62MC-A	29.75	0.223	-1.464	G. ruber-w

GREAT BAHAMA BANK CORE SITES – STABLE ISOTOPE DATA

COLUMN HEADERS:

CORE, DEPTH (cm), C13 (per mil), O18 (per mil), SPECIES

Note: The data for 118MC and 125MC below is based on the same crushed and homogenized samples used for Mg/Ca analyses.

CORE	DEPTH	C13	O18	SPECIES
KNR166-2-118MC-A	0.5	0.631	-1.827	G. ruber-w
KNR166-2-118MC-A	0.5	0.614	-1.882	G. ruber-w
KNR166-2-118MC-A	0.5	0.504	-1.866	G. ruber-w
KNR166-2-118MC-A	0.5	0.701	-1.886	G. ruber-w
KNR166-2-118MC-A	1.5	0.328	-1.800	G. ruber-w
KNR166-2-118MC-A	1.5	0.625	-2.026	G. ruber-w
KNR166-2-118MC-A	1.5	0.553	-2.047	G. ruber-w
KNR166-2-118MC-A	1.5	1.633	-1.031	G. ruber-w
KNR166-2-118MC-A	2.5	0.716	-1.868	G. ruber-w
KNR166-2-118MC-A	2.5	0.578	-1.860	G. ruber-w
KNR166-2-118MC-A	2.5	0.718	-1.914	G. ruber-w
KNR166-2-118MC-A	2.5	0.566	-1.906	G. ruber-w
KNR166-2-118MC-A	3.5	0.672	-1.996	G. ruber-w
KNR166-2-118MC-A	3.5	0.759	-1.897	G. ruber-w
KNR166-2-118MC-A	3.5	0.807	-1.951	G. ruber-w
KNR166-2-118MC-A	3.5	0.754	-1.895	G. ruber-w
KNR166-2-118MC-A	4.5	0.639	-1.874	G. ruber-w
KNR166-2-118MC-A	4.5	0.689	-2.074	G. ruber-w
KNR166-2-118MC-A	4.5	0.394	-1.982	G. ruber-w
KNR166-2-118MC-A	4.5	0.748	-1.924	G. ruber-w
KNR166-2-118MC-A	5.5	0.432	-2.218	G. ruber-w
KNR166-2-118MC-A	5.5	0.569	-2.048	G. ruber-w
KNR166-2-118MC-A	5.5	0.589	-2.067	G. ruber-w
KNR166-2-118MC-A	5.5	0.473	-2.014	G. ruber-w
KNR166-2-118MC-A	6.5	0.531	-2.001	G. ruber-w
KNR166-2-118MC-A	6.5	0.423	-2.078	G. ruber-w
KNR166-2-118MC-A	6.5	0.611	-1.930	G. ruber-w
KNR166-2-118MC-A	7.5	0.368	-2.069	G. ruber-w
KNR166-2-118MC-A	7.5	0.511	-2.038	G. ruber-w
KNR166-2-118MC-A	7.5	0.687	-2.124	G. ruber-w
KNR166-2-118MC-A	7.5	0.583	-2.100	G. ruber-w
KNR166-2-118MC-A	8.5	0.254	-2.057	G. ruber-w
KNR166-2-118MC-A	8.5	0.117	-2.100	G. ruber-w
KNR166-2-118MC-A	8.5	0.336	-1.938	G. ruber-w
KNR166-2-118MC-A	8.5	0.340	-2.014	G. ruber-w
KNR166-2-118MC-A	9.5	0.249	-2.049	G. ruber-w
KNR166-2-118MC-A	9.5	0.039	-2.313	G. ruber-w
KNR166-2-118MC-A	9.5	0.433	-2.145	G. ruber-w
KNR166-2-118MC-A	9.5	0.270	-2.144	G. ruber-w
KNR166-2-118MC-A	10.5	0.182	-2.209	G. ruber-w
KNR166-2-118MC-A	10.5	-0.013	-2.488	G. ruber-w
KNR166-2-118MC-A	10.5	0.417	-2.020	G. ruber-w
KNR166-2-118MC-A	10.5	0.291	-2.103	G. ruber-w

KNR166-2-118MC-A	11.5	0.237	-1.907	G. ruber-w
KNR166-2-118MC-A	11.5	0.378	-2.010	G. ruber-w
KNR166-2-118MC-A	11.5	0.367	-2.169	G. ruber-w
KNR166-2-118MC-A	11.5	0.256	-2.165	G. ruber-w
KNR166-2-118MC-A	12.5	0.111	-1.886	G. ruber-w
KNR166-2-118MC-A	12.5	0.297	-1.981	G. ruber-w
KNR166-2-118MC-A	12.5	0.020	-2.138	G. ruber-w
KNR166-2-118MC-A	12.5	0.128	-1.800	G. ruber-w
KNR166-2-118MC-A	13.5	0.342	-2.024	G. ruber-w
KNR166-2-118MC-A	13.5	0.242	-2.122	G. ruber-w
KNR166-2-118MC-A	13.5	0.175	-2.023	G. ruber-w
KNR166-2-118MC-A	13.5	0.113	-2.063	G. ruber-w
KNR166-2-118MC-A	14.5	0.762	-2.042	G. ruber-w
KNR166-2-118MC-A	14.5	0.279	-2.133	G. ruber-w
KNR166-2-118MC-A	14.5	0.292	-2.090	G. ruber-w
KNR166-2-118MC-A	14.5	0.295	-2.060	G. ruber-w
KNR166-2-118MC-A	15.5	-0.028	-2.190	G. ruber-w
KNR166-2-118MC-A	15.5	0.124	-2.109	G. ruber-w
KNR166-2-118MC-A	15.5	0.131	-2.025	G. ruber-w
KNR166-2-118MC-A	15.5	0.322	-2.093	G. ruber-w
KNR166-2-118MC-A	16.5	0.045	-2.161	G. ruber-w
KNR166-2-118MC-A	16.5	0.031	-2.162	G. ruber-w
KNR166-2-118MC-A	16.5	0.486	-2.138	G. ruber-w
KNR166-2-118MC-A	17.5	-0.062	-2.079	G. ruber-w
KNR166-2-118MC-A	17.5	0.424	-1.937	G. ruber-w
KNR166-2-118MC-A	17.5	0.002	-2.155	G. ruber-w
KNR166-2-118MC-A	17.5	0.316	-2.037	G. ruber-w
KNR166-2-118MC-A	18.5	0.144	-2.155	G. ruber-w
KNR166-2-118MC-A	18.5	0.536	-2.054	G. ruber-w
KNR166-2-118MC-A	18.5	0.154	-2.044	G. ruber-w
KNR166-2-118MC-A	18.5	0.140	-2.065	G. ruber-w
KNR166-2-118MC-A	19.5	-0.033	-1.929	G. ruber-w
KNR166-2-118MC-A	19.5	0.032	-2.131	G. ruber-w
KNR166-2-118MC-A	19.5	0.423	-1.963	G. ruber-w
KNR166-2-118MC-A	19.5	-0.061	-2.304	G. ruber-w
KNR166-2-118MC-A	20.5	-0.081	-2.026	G. ruber-w
KNR166-2-118MC-A	20.5	0.381	-2.025	G. ruber-w
KNR166-2-118MC-A	20.5	0.302	-1.962	G. ruber-w
KNR166-2-118MC-A	21.5	0.279	-2.061	G. ruber-w
KNR166-2-118MC-A	21.5	0.239	-2.209	G. ruber-w
KNR166-2-118MC-A	21.5	0.248	-2.129	G. ruber-w
KNR166-2-118MC-A	21.5	0.143	-2.198	G. ruber-w
KNR166-2-118MC-A	22.5	-0.075	-1.916	G. ruber-w
KNR166-2-118MC-A	22.5	0.172	-1.919	G. ruber-w
KNR166-2-118MC-A	22.5	-0.247	-2.148	G. ruber-w
KNR166-2-118MC-A	22.5	-0.266	-2.034	G. ruber-w
KNR166-2-118MC-A	23.5	0.165	-1.989	G. ruber-w
KNR166-2-118MC-A	23.5	-0.025	-2.129	G. ruber-w
KNR166-2-118MC-A	23.5	0.330	-2.050	G. ruber-w
KNR166-2-118MC-A	23.5	0.248	-1.951	G. ruber-w
KNR166-2-118MC-A	24.5	0.113	-1.845	G. ruber-w
KNR166-2-118MC-A	25.5	0.109	-2.157	G. ruber-w
KNR166-2-118MC-A	25.5	0.302	-2.057	G. ruber-w
KNR166-2-118MC-A	25.5	0.168	-2.141	G. ruber-w
KNR166-2-118MC-A	25.5	0.289	-2.089	G. ruber-w

KNR166-2-118MC-A	26.5	-0.177	-2.256	G. ruber-w
KNR166-2-118MC-A	26.5	0.122	-2.144	G. ruber-w
KNR166-2-118MC-A	26.5	-0.157	-2.235	G. ruber-w
KNR166-2-118MC-A	27.5	-0.173	-2.245	G. ruber-w
KNR166-2-118MC-A	27.5	-0.034	-1.971	G. ruber-w
KNR166-2-118MC-A	27.5	0.064	-2.138	G. ruber-w
KNR166-2-118MC-A	27.5	0.121	-2.057	G. ruber-w
KNR166-2-118MC-A	28.5	0.228	-1.995	G. ruber-w
KNR166-2-118MC-A	28.5	-0.149	-2.209	G. ruber-w
KNR166-2-118MC-A	28.5	0.013	-2.092	G. ruber-w
KNR166-2-118MC-A	28.5	0.021	-2.236	G. ruber-w
KNR166-2-118MC-A	29.5	-0.260	-2.087	G. ruber-w
KNR166-2-118MC-A	29.5	0.220	-1.947	G. ruber-w
KNR166-2-118MC-A	29.5	0.042	-2.214	G. ruber-w
KNR166-2-118MC-A	30.5	0.085	-2.211	G. ruber-w
KNR166-2-118MC-A	30.5	0.124	-2.086	G. ruber-w
KNR166-2-118MC-A	30.5	-0.002	-1.870	G. ruber-w
KNR166-2-118MC-A	31.5	0.225	-2.152	G. ruber-w
KNR166-2-118MC-A	31.5	0.055	-2.275	G. ruber-w
KNR166-2-118MC-A	31.5	0.110	-2.117	G. ruber-w
KNR166-2-118MC-A	31.5	0.311	-2.119	G. ruber-w
KNR166-2-118MC-A	32.5	-0.122	-2.388	G. ruber-w
KNR166-2-118MC-A	32.5	0.206	-2.189	G. ruber-w
KNR166-2-118MC-A	32.5	-0.283	-2.219	G. ruber-w
KNR166-2-118MC-A	32.5	0.215	-2.091	G. ruber-w
KNR166-2-118MC-A	33.5	0.049	-2.057	G. ruber-w
KNR166-2-118MC-A	33.5	0.040	-2.191	G. ruber-w
KNR166-2-118MC-A	34.5	0.308	-2.063	G. ruber-w
KNR166-2-118MC-A	34.5	0.279	-2.140	G. ruber-w
KNR166-2-118MC-A	34.5	0.052	-2.477	G. ruber-w
KNR166-2-118MC-A	34.5	0.188	-2.093	G. ruber-w
KNR166-2-118MC-A	35.5	0.008	-2.083	G. ruber-w
KNR166-2-118MC-A	35.5	0.148	-1.960	G. ruber-w
KNR166-2-118MC-A	35.5	0.291	-2.017	G. ruber-w
KNR166-2-118MC-A	35.5	0.288	-2.043	G. ruber-w
KNR166-2-118MC-A	36.5	0.013	-2.070	G. ruber-w
KNR166-2-118MC-A	36.5	0.392	-2.182	G. ruber-w
KNR166-2-118MC-A	36.5	0.188	-1.970	G. ruber-w

CORE	DEPTH	C13	O18	SPECIES
KNR166-2-125MC-D	0.5	0.692	-2.200	G. ruber-w
KNR166-2-125MC-D	0.5	0.698	-1.827	G. ruber-w
KNR166-2-125MC-D	0.5	0.422	-1.921	G. ruber-w
KNR166-2-125MC-D	0.5	0.364	-2.190	G. ruber-w
KNR166-2-125MC-D	1.5	0.660	-1.717	G. ruber-w
KNR166-2-125MC-D	1.5	0.835	-1.889	G. ruber-w
KNR166-2-125MC-D	1.5	0.788	-1.880	G. ruber-w
KNR166-2-125MC-D	1.5	0.167	-1.980	G. ruber-w
KNR166-2-125MC-D	2.5	0.620	-1.922	G. ruber-w
KNR166-2-125MC-D	2.5	0.547	-1.874	G. ruber-w
KNR166-2-125MC-D	2.5	0.525	-1.778	G. ruber-w
KNR166-2-125MC-D	2.5	0.531	-2.106	G. ruber-w
KNR166-2-125MC-D	3.5	0.704	-2.021	G. ruber-w
KNR166-2-125MC-D	3.5	0.329	-2.045	G. ruber-w
KNR166-2-125MC-D	3.5	0.501	-1.898	G. ruber-w
KNR166-2-125MC-D	3.5	0.302	-2.215	G. ruber-w
KNR166-2-125MC-D	4.5	-0.331	-2.092	G. ruber-w
KNR166-2-125MC-D	4.5	0.185	-1.326	G. ruber-w
KNR166-2-125MC-D	4.5	0.561	-2.012	G. ruber-w
KNR166-2-125MC-D	4.5	0.252	-2.231	G. ruber-w
KNR166-2-125MC-D	4.5	0.068	-2.286	G. ruber-w
KNR166-2-125MC-D	4.5	-0.188	-2.078	G. ruber-w
KNR166-2-125MC-D	5.5	0.193	-2.000	G. ruber-w
KNR166-2-125MC-D	5.5	-0.110	-2.096	G. ruber-w
KNR166-2-125MC-D	5.5	-0.225	-1.954	G. ruber-w
KNR166-2-125MC-D	5.5	0.212	-2.205	G. ruber-w
KNR166-2-125MC-D	5.5	-0.363	-2.171	G. ruber-w
KNR166-2-125MC-D	6.5	0.257	-2.238	G. ruber-w
KNR166-2-125MC-D	6.5	0.321	-2.126	G. ruber-w
KNR166-2-125MC-D	6.5	0.200	-2.037	G. ruber-w
KNR166-2-125MC-D	6.5	0.504	-2.008	G. ruber-w
KNR166-2-125MC-D	6.5	0.135	-2.087	G. ruber-w
KNR166-2-125MC-D	7.5	0.041	-1.873	G. ruber-w
KNR166-2-125MC-D	7.5	0.109	-1.856	G. ruber-w
KNR166-2-125MC-D	7.5	0.479	-2.115	G. ruber-w
KNR166-2-125MC-D	7.5	0.428	-2.033	G. ruber-w
KNR166-2-125MC-D	7.5	0.339	-2.026	G. ruber-w
KNR166-2-125MC-D	8.5	0.633	-1.801	G. ruber-w
KNR166-2-125MC-D	8.5	0.394	-1.979	G. ruber-w
KNR166-2-125MC-D	8.5	0.316	-1.969	G. ruber-w
KNR166-2-125MC-D	8.5	0.368	-1.932	G. ruber-w
KNR166-2-125MC-D	8.5	0.312	-1.820	G. ruber-w
KNR166-2-125MC-D	9.5	0.194	-2.019	G. ruber-w
KNR166-2-125MC-D	9.5	0.404	-2.048	G. ruber-w
KNR166-2-125MC-D	9.5	0.216	-2.116	G. ruber-w
KNR166-2-125MC-D	9.5	0.502	-2.179	G. ruber-w
KNR166-2-125MC-D	9.5	0.023	-1.841	G. ruber-w
KNR166-2-125MC-D	10.5	0.509	-1.973	G. ruber-w
KNR166-2-125MC-D	10.5	-0.094	-2.199	G. ruber-w
KNR166-2-125MC-D	10.5	-0.297	-2.301	G. ruber-w
KNR166-2-125MC-D	10.5	0.373	-1.882	G. ruber-w
KNR166-2-125MC-D	10.5	-0.053	-2.091	G. ruber-w
KNR166-2-125MC-D	11.5	0.422	-1.785	G. ruber-w
KNR166-2-125MC-D	11.5	0.286	-1.960	G. ruber-w

KNR166-2-125MC-D	11.5	0.008	-2.027	G. ruber-w
KNR166-2-125MC-D	11.5	0.484	-2.043	G. ruber-w
KNR166-2-125MC-D	12.5	0.247	-2.034	G. ruber-w
KNR166-2-125MC-D	12.5	-0.198	-2.199	G. ruber-w
KNR166-2-125MC-D	12.5	0.051	-2.081	G. ruber-w
KNR166-2-125MC-D	12.5	-0.164	-1.968	G. ruber-w
KNR166-2-125MC-D	13.5	0.460	-1.886	G. ruber-w
KNR166-2-125MC-D	13.5	0.006	-2.064	G. ruber-w
KNR166-2-125MC-D	13.5	-0.106	-2.209	G. ruber-w
KNR166-2-125MC-D	13.5	0.192	-2.122	G. ruber-w
KNR166-2-125MC-D	14.5	0.177	-2.045	G. ruber-w
KNR166-2-125MC-D	14.5	0.675	-2.102	G. ruber-w
KNR166-2-125MC-D	14.5	0.474	-2.012	G. ruber-w
KNR166-2-125MC-D	14.5	0.329	-2.074	G. ruber-w
KNR166-2-125MC-D	15.5	0.038	-2.146	G. ruber-w
KNR166-2-125MC-D	15.5	0.863	-2.104	G. ruber-w
KNR166-2-125MC-D	15.5	0.472	-1.968	G. ruber-w
KNR166-2-125MC-D	15.5	-0.110	-2.195	G. ruber-w
KNR166-2-125MC-D	16.5	0.291	-2.093	G. ruber-w
KNR166-2-125MC-D	16.5	0.163	-2.070	G. ruber-w
KNR166-2-125MC-D	16.5	0.247	-2.166	G. ruber-w
KNR166-2-125MC-D	16.5	-0.181	-1.942	G. ruber-w
KNR166-2-125MC-D	17.5	0.234	-2.031	G. ruber-w
KNR166-2-125MC-D	17.5	0.137	-2.371	G. ruber-w
KNR166-2-125MC-D	17.5	0.251	-2.055	G. ruber-w
KNR166-2-125MC-D	17.5	-0.172	-2.310	G. ruber-w
KNR166-2-125MC-D	18.5	0.686	-2.215	G. ruber-w
KNR166-2-125MC-D	18.5	-0.215	-2.277	G. ruber-w
KNR166-2-125MC-D	18.5	0.098	-1.933	G. ruber-w
KNR166-2-125MC-D	18.5	-0.232	-2.142	G. ruber-w
KNR166-2-125MC-D	19.5	0.256	-2.157	G. ruber-w
KNR166-2-125MC-D	19.5	0.562	-2.068	G. ruber-w
KNR166-2-125MC-D	19.5	0.550	-1.655	G. ruber-w
KNR166-2-125MC-D	19.5	0.427	-1.988	G. ruber-w
KNR166-2-125MC-D	19.5	0.394	-1.984	G. ruber-w
KNR166-2-125MC-D	20.5	0.195	-1.911	G. ruber-w
KNR166-2-125MC-D	20.5	-0.387	-2.109	G. ruber-w
KNR166-2-125MC-D	20.5	0.563	-2.105	G. ruber-w
KNR166-2-125MC-D	20.5	0.630	-1.943	G. ruber-w
KNR166-2-125MC-D	21.5	-0.075	-2.200	G. ruber-w
KNR166-2-125MC-D	21.5	0.151	-2.103	G. ruber-w
KNR166-2-125MC-D	21.5	0.375	-1.928	G. ruber-w
KNR166-2-125MC-D	22.5	-0.577	-2.035	G. ruber-w
KNR166-2-125MC-D	22.5	0.261	-2.121	G. ruber-w
KNR166-2-125MC-D	22.5	-0.057	-1.891	G. ruber-w
KNR166-2-125MC-D	23.5	0.133	-2.046	G. ruber-w
KNR166-2-125MC-D	23.5	0.288	-2.233	G. ruber-w
KNR166-2-125MC-D	23.5	0.566	-1.684	G. ruber-w
KNR166-2-125MC-D	24.5	0.019	-2.287	G. ruber-w
KNR166-2-125MC-D	24.5	0.204	-2.002	G. ruber-w
KNR166-2-125MC-D	24.5	0.069	-2.115	G. ruber-w
KNR166-2-125MC-D	25.5	0.272	-2.246	G. ruber-w
KNR166-2-125MC-D	25.5	0.476	-1.652	G. ruber-w
KNR166-2-125MC-D	25.5	0.485	-1.869	G. ruber-w
KNR166-2-125MC-D	26.5	0.551	-1.888	G. ruber-w

KNR166-2-125MC-D	26.5	0.403	-1.888	G. ruber-w
KNR166-2-125MC-D	26.5	0.181	-1.842	G. ruber-w
KNR166-2-125MC-D	27.5	0.557	-1.926	G. ruber-w
KNR166-2-125MC-D	27.5	0.536	-2.096	G. ruber-w
KNR166-2-125MC-D	27.5	0.552	-1.755	G. ruber-w

APPENDIX C

Chapter 4 benthic and planktonic stable isotope data

COLUMN HEADERS:

CORE, DEPTH (cm), C13 (per mil), O18 (per mil), SPECIES

NOTE:
Each benthic stable isotope analysis is typically based on one individual foram from the > 250 µm size fraction. Planktonic data were based on an average of 10 *G. ruber* individuals from the 212-250 µm size fraction.

Data from the Dry Tortugas core sites is listed first, followed by data from the Great Bahama Bank core sites.

DRY TORTUGAS CORE SITES

CORE	DEPTH	C13	O18	SPECIES
KNR166-2-3MC-H	1	0.795	1.608	C. floridanus
KNR166-2-3MC-H	1	0.587	1.539	C. floridanus
KNR166-2-3MC-H	1	1.307	1.766	P. ariminensis
KNR166-2-3MC-H	1	0.976	1.589	C. floridanus
KNR166-2-3MC-H	2.5	0.766	1.793	C. floridanus
KNR166-2-3MC-H	2.5	0.740	1.668	C. floridanus
KNR166-2-3MC-H	2.5	1.208	1.617	P. ariminensis
KNR166-2-3MC-H	2.5	0.909	2.105	C. floridanus
KNR166-2-3MC-H	3.5	0.916	1.567	C. floridanus
KNR166-2-3MC-H	3.5	0.703	1.577	C. floridanus
KNR166-2-3MC-H	3.5	1.175	1.527	P. ariminensis
KNR166-2-3MC-H	3.5	1.264	1.640	P. ariminensis
KNR166-2-3MC-H	4.5	1.060	1.797	C. floridanus
KNR166-2-3MC-H	4.5	0.581	1.528	C. floridanus
KNR166-2-3MC-H	4.5	0.342	1.682	C. floridanus
KNR166-2-3MC-H	4.5	0.519	1.759	C. floridanus
KNR166-2-3MC-H	5.5	0.617	1.492	C. floridanus
KNR166-2-3MC-H	5.5	1.131	1.660	P. ariminensis
KNR166-2-3MC-H	5.5	1.170	1.729	P. ariminensis
KNR166-2-3MC-H	5.5	1.264	1.717	P. ariminensis
KNR166-2-3MC-H	6.5	0.725	1.890	C. floridanus
KNR166-2-3MC-H	6.5	0.648	1.620	C. floridanus
KNR166-2-3MC-H	6.5	1.147	1.659	P. ariminensis
KNR166-2-3MC-H	6.5	0.798	1.668	C. floridanus
KNR166-2-3MC-H	7.5	0.927	1.737	C. floridanus
KNR166-2-3MC-H	7.5	0.345	1.435	C. floridanus
KNR166-2-3MC-H	7.5	0.519	1.422	C. floridanus
KNR166-2-3MC-H	7.5	1.044	1.594	P. ariminensis
KNR166-2-3MC-H	8.5	0.693	1.675	C. floridanus
KNR166-2-3MC-H	8.5	0.755	1.682	C. floridanus
KNR166-2-3MC-H	8.5	1.229	1.585	P. ariminensis
KNR166-2-3MC-H	8.5	1.260	1.682	P. ariminensis
KNR166-2-3MC-H	9.5	0.735	1.639	C. floridanus
KNR166-2-3MC-H	9.5	0.401	1.359	C. floridanus
KNR166-2-3MC-H	9.5	1.230	1.727	P. ariminensis
KNR166-2-3MC-H	9.5	1.199	1.677	P. ariminensis
KNR166-2-3MC-H	10.5	0.945	1.946	C. floridanus
KNR166-2-3MC-H	10.5	0.879	1.654	P. ariminensis
KNR166-2-3MC-H	10.5	0.710	1.696	C. floridanus
KNR166-2-3MC-H	10.5	1.160	1.714	P. ariminensis
KNR166-2-3MC-H	10.5	1.096	1.564	P. ariminensis
KNR166-2-3MC-H	11.5	0.576	1.734	C. floridanus
KNR166-2-3MC-H	11.5	1.106	1.845	P. ariminensis
KNR166-2-3MC-H	11.5	1.254	1.755	P. ariminensis
KNR166-2-3MC-H	11.5	1.231	1.647	P. ariminensis
KNR166-2-3MC-H	12.5	1.010	1.740	C. floridanus
KNR166-2-3MC-H	12.5	0.986	1.836	C. floridanus
KNR166-2-3MC-H	12.5	0.951	1.701	C. floridanus
KNR166-2-3MC-H	12.5	1.225	1.598	P. ariminensis
KNR166-2-3MC-H	12.5	1.116	1.597	P. ariminensis

KNR166-2-3MC-H	13.5	0.725	1.703	C. floridanus
KNR166-2-3MC-H	13.5	1.206	1.753	P. ariminensis
KNR166-2-3MC-H	13.5	1.240	1.679	P. ariminensis
KNR166-2-3MC-H	13.5	1.134	1.604	P. ariminensis
KNR166-2-3MC-H	14.5	0.909	1.776	C. floridanus
KNR166-2-3MC-H	14.5	1.250	1.557	P. ariminensis
KNR166-2-3MC-H	14.5	1.126	1.601	P. ariminensis
KNR166-2-3MC-H	15.5	1.030	1.735	C. floridanus
KNR166-2-3MC-H	15.5	1.207	1.403	P. ariminensis
KNR166-2-3MC-H	15.5	0.941	1.981	C. floridanus
KNR166-2-3MC-H	16.5	1.154	1.659	C. floridanus
KNR166-2-3MC-H	16.5	0.865	1.746	C. floridanus
KNR166-2-3MC-H	16.5	1.234	1.665	P. ariminensis
KNR166-2-3MC-H	16.5	1.223	1.620	P. ariminensis
KNR166-2-3MC-H	17.5	0.875	1.687	C. floridanus
KNR166-2-3MC-H	17.5	1.213	1.478	P. ariminensis
KNR166-2-3MC-H	17.5	1.174	1.556	P. ariminensis
KNR166-2-3MC-H	17.5	0.865	1.864	C. floridanus
KNR166-2-3MC-H	17.5	1.077	1.669	P. ariminensis
KNR166-2-3MC-H	18.5	1.057	1.804	C. floridanus
KNR166-2-3MC-H	18.5	0.919	1.705	C. floridanus
KNR166-2-3MC-H	18.5	1.018	1.840	C. floridanus
KNR166-2-3MC-H	18.5	0.969	1.555	P. ariminensis
KNR166-2-3MC-H	19.5	1.028	1.899	C. floridanus
KNR166-2-3MC-H	19.5	0.532	1.660	C. floridanus
KNR166-2-3MC-H	19.5	1.065	1.482	P. ariminensis
KNR166-2-3MC-H	19.5	1.188	1.621	P. ariminensis
KNR166-2-3MC-H	20.5	1.023	1.701	C. floridanus
KNR166-2-3MC-H	20.5	1.159	1.552	P. ariminensis
KNR166-2-3MC-H	20.5	0.833	1.709	C. floridanus
KNR166-2-3MC-H	20.5	0.632	1.758	C. floridanus
KNR166-2-3MC-H	21.5	0.889	1.779	C. floridanus
KNR166-2-3MC-H	21.5	0.915	1.930	C. floridanus
KNR166-2-3MC-H	21.5	1.138	1.663	P. ariminensis
KNR166-2-3MC-H	21.5	1.190	1.816	C. floridanus
KNR166-2-3MC-H	22.5	0.800	1.653	C. floridanus
KNR166-2-3MC-H	22.5	0.913	1.683	C. floridanus
KNR166-2-3MC-H	22.5	0.791	1.766	C. floridanus
KNR166-2-3MC-H	22.5	0.885	1.723	C. floridanus
KNR166-2-3MC-H	23.5	0.818	1.537	C. floridanus
KNR166-2-3MC-H	23.5	1.090	1.944	C. floridanus
KNR166-2-3MC-H	23.5	0.691	1.708	C. floridanus
KNR166-2-3MC-H	23.5	0.875	1.949	C. floridanus
KNR166-2-3MC-H	24.5	1.045	1.794	C. floridanus
KNR166-2-3MC-H	24.5	0.928	1.904	C. floridanus
KNR166-2-3MC-H	24.5	1.275	1.591	P. ariminensis
KNR166-2-3MC-H	24.5	1.217	1.608	P. ariminensis
KNR166-2-3MC-H	25.5	0.928	1.595	C. floridanus
KNR166-2-3MC-H	25.5	0.883	1.653	C. floridanus
KNR166-2-3MC-H	25.5	1.121	1.692	P. ariminensis
KNR166-2-3MC-H	25.5	0.892	1.853	C. floridanus
KNR166-2-3MC-H	26.5	0.501	1.595	C. floridanus
KNR166-2-3MC-H	26.5	1.186	1.576	P. ariminensis
KNR166-2-3MC-H	26.5	1.111	1.512	P. ariminensis
KNR166-2-3MC-H	26.5	1.272	1.698	P. ariminensis

KNR166-2-3MC-H	27.5	0.575	1.817	C. floridanus
KNR166-2-3MC-H	27.5	1.166	1.765	P. ariminensis
KNR166-2-3MC-H	27.5	0.847	1.958	C. floridanus
KNR166-2-3MC-H	27.5	0.911	2.033	C. floridanus
KNR166-2-3MC-H	28.5	0.927	1.883	C. floridanus
KNR166-2-3MC-H	28.5	1.028	1.682	C. floridanus
KNR166-2-3MC-H	28.5	1.312	1.692	P. ariminensis
KNR166-2-3MC-H	28.5	0.629	1.775	C. floridanus
KNR166-2-3MC-H	29.5	0.731	1.957	C. floridanus
KNR166-2-3MC-H	29.5	1.019	1.768	C. floridanus
KNR166-2-3MC-H	29.5	0.576	1.588	C. floridanus
KNR166-2-3MC-H	29.5	1.208	1.702	P. ariminensis
KNR166-2-3MC-H	30.5	0.905	1.968	C. floridanus
KNR166-2-3MC-H	30.5	0.769	1.649	C. floridanus
KNR166-2-3MC-H	30.5	1.179	1.651	P. ariminensis
KNR166-2-3MC-H	30.5	1.243	1.748	P. ariminensis
KNR166-2-3MC-H	31.5	0.771	1.981	C. floridanus
KNR166-2-3MC-H	31.5	0.741	1.573	C. floridanus
KNR166-2-3MC-H	31.5	1.146	1.807	P. ariminensis
KNR166-2-3MC-H	31.5	1.217	1.550	P. ariminensis
KNR166-2-3MC-H	32.5	0.866	1.701	C. floridanus
KNR166-2-3MC-H	32.5	0.961	1.853	C. floridanus
KNR166-2-3MC-H	32.5	1.074	1.734	C. floridanus
KNR166-2-3MC-H	32.5	0.491	1.820	C. floridanus
KNR166-2-3MC-H	33.5	0.998	1.858	C. floridanus
KNR166-2-3MC-H	33.5	0.503	1.656	C. floridanus
KNR166-2-3MC-H	33.5	1.236	1.750	P. ariminensis
KNR166-2-3MC-H	33.5	0.686	1.918	C. floridanus
KNR166-2-3MC-H	34.5	0.842	1.779	C. floridanus
KNR166-2-3MC-H	34.5	1.013	1.585	C. floridanus
KNR166-2-3MC-H	34.5	1.207	1.730	P. ariminensis
KNR166-2-3MC-H	34.5	0.623	1.896	C. floridanus
KNR166-2-3MC-H	35.5	0.407	1.779	C. floridanus
KNR166-2-3MC-H	35.5	0.851	1.920	C. floridanus
KNR166-2-3MC-H	35.5	0.744	1.740	C. floridanus
KNR166-2-3MC-H	35.5	1.200	1.709	P. ariminensis
KNR166-2-3MC-H	36.5	0.480	1.713	C. floridanus
KNR166-2-3MC-H	36.5	1.250	1.636	P. ariminensis
KNR166-2-3MC-H	36.5	1.333	1.544	P. ariminensis
KNR166-2-3MC-H	36.5	1.236	1.717	P. ariminensis
KNR166-2-3MC-H	37.5	0.744	1.885	C. floridanus
KNR166-2-3MC-H	37.5	1.140	1.726	P. ariminensis
KNR166-2-3MC-H	37.5	1.155	1.647	P. ariminensis
KNR166-2-3MC-H	37.5	0.954	1.659	C. floridanus

CORE	DEPTH	C13	O18	SPECIES
KNR166-2-11MC-D	0.5	0.915	2.173	C. floridanus
KNR166-2-11MC-D	0.5	1.009	2.358	C. floridanus
KNR166-2-11MC-D	0.5	0.981	2.202	C. floridanus
KNR166-2-11MC-D	0.5	0.903	2.128	C. sp.
KNR166-2-11MC-D	0.5	1.135	2.267	C. sp.
KNR166-2-11MC-D	1.5	1.005	2.020	C. floridanus
KNR166-2-11MC-D	1.5	0.985	2.402	C. floridanus
KNR166-2-11MC-D	1.5	1.010	2.289	C. floridanus
KNR166-2-11MC-D	1.5	0.934	2.285	C. sp.
KNR166-2-11MC-D	1.5	1.035	2.141	C. sp.
KNR166-2-11MC-D	2.5	0.984	2.254	C. floridanus
KNR166-2-11MC-D	2.5	0.948	2.332	C. floridanus
KNR166-2-11MC-D	2.5	0.979	2.418	C. floridanus
KNR166-2-11MC-D	2.5	0.886	2.342	C. floridanus
KNR166-2-11MC-D	2.5	0.768	2.290	C. sp.
KNR166-2-11MC-D	3.5	0.871	2.159	C. floridanus
KNR166-2-11MC-D	3.5	0.884	2.467	C. floridanus
KNR166-2-11MC-D	3.5	0.940	2.216	C. floridanus
KNR166-2-11MC-D	3.5	0.749	2.370	C. floridanus
KNR166-2-11MC-D	3.5	1.158	2.210	C. sp.
KNR166-2-11MC-D	3.5	0.838	2.030	C. sp.
KNR166-2-11MC-D	4.5	0.909	2.206	C. floridanus
KNR166-2-11MC-D	4.5	0.946	2.434	C. floridanus
KNR166-2-11MC-D	4.5	0.782	2.404	C. floridanus
KNR166-2-11MC-D	4.5	0.982	2.282	C. floridanus
KNR166-2-11MC-D	4.5	0.895	2.121	C. sp.
KNR166-2-11MC-D	4.5	0.858	2.144	C. sp.
KNR166-2-11MC-D	5.5	0.781	2.140	C. floridanus
KNR166-2-11MC-D	5.5	0.900	2.174	C. floridanus
KNR166-2-11MC-D	5.5	0.756	2.227	C. floridanus
KNR166-2-11MC-D	5.5	0.847	2.132	C. floridanus
KNR166-2-11MC-D	5.5	1.098	2.232	C. sp.
KNR166-2-11MC-D	6.5	0.882	2.227	C. floridanus
KNR166-2-11MC-D	6.5	0.953	2.226	C. floridanus
KNR166-2-11MC-D	6.5	0.857	2.212	C. floridanus
KNR166-2-11MC-D	6.5	0.972	2.085	C. floridanus
KNR166-2-11MC-D	6.5	0.887	2.212	C. sp.
KNR166-2-11MC-D	6.5	0.962	2.268	C. floridanus
KNR166-2-11MC-D	7.5	1.046	2.269	C. floridanus
KNR166-2-11MC-D	7.5	1.165	2.402	C. sp-puffy
KNR166-2-11MC-D	7.5	0.888	2.249	C. sp-puffy
KNR166-2-11MC-D	7.5	0.936	2.048	C. sp.
KNR166-2-11MC-D	7.5	0.980	2.200	C. sp.
KNR166-2-11MC-D	7.5	0.929	2.045	C. sp.
KNR166-2-11MC-D	8.5	0.955	2.217	C. floridanus
KNR166-2-11MC-D	8.5	0.862	2.291	C. floridanus
KNR166-2-11MC-D	8.5	1.033	2.917	C. floridanus
KNR166-2-11MC-D	8.5	0.936	2.144	C. sp.
KNR166-2-11MC-D	8.5	0.982	2.223	C. sp.
KNR166-2-11MC-D	9.5	1.073	2.622	C. floridanus
KNR166-2-11MC-D	9.5	1.028	2.390	C. floridanus
KNR166-2-11MC-D	9.5	1.019	2.488	C. floridanus
KNR166-2-11MC-D	9.5	0.918	2.082	C. floridanus
KNR166-2-11MC-D	9.5	0.848	2.265	C. floridanus

KNR166-2-11MC-D	10.5	0.907	2.186	C. floridanus
KNR166-2-11MC-D	10.5	0.971	2.454	C. floridanus
KNR166-2-11MC-D	10.5	1.022	2.479	C. floridanus
KNR166-2-11MC-D	10.5	0.959	2.150	C. floridanus
KNR166-2-11MC-D	10.5	1.047	2.101	C. sp.
KNR166-2-11MC-D	11.5	0.903	2.322	C. floridanus
KNR166-2-11MC-D	11.5	1.010	2.270	C. floridanus
KNR166-2-11MC-D	11.5	0.993	2.310	C. floridanus
KNR166-2-11MC-D	11.5	0.855	2.216	C. sp
KNR166-2-11MC-D	11.5	0.864	2.219	C. sp.
KNR166-2-11MC-D	12.5	1.034	2.302	C. floridanus
KNR166-2-11MC-D	12.5	0.920	2.193	C. floridanus
KNR166-2-11MC-D	12.5	0.866	2.165	C. floridanus
KNR166-2-11MC-D	12.5	0.957	2.131	C. sp
KNR166-2-11MC-D	12.5	0.959	2.207	C. floridanus
KNR166-2-11MC-D	13.5	0.888	2.345	C. floridanus
KNR166-2-11MC-D	13.5	0.924	2.354	C. floridanus
KNR166-2-11MC-D	13.5	0.968	2.100	C. floridanus
KNR166-2-11MC-D	13.5	0.837	2.164	C. floridanus
KNR166-2-11MC-D	13.5	0.860	2.086	C. sp.
KNR166-2-11MC-D	14.5	0.818	2.333	C. floridanus
KNR166-2-11MC-D	14.5	1.024	2.433	C. floridanus
KNR166-2-11MC-D	14.5	1.009	2.231	C. floridanus
KNR166-2-11MC-D	14.5	0.941	2.148	C. floridanus
KNR166-2-11MC-D	14.5	1.093	2.240	C. sp.
KNR166-2-11MC-D	15.5	1.208	2.218	P. ariminensis
KNR166-2-11MC-D	15.5	0.335	2.811	C. floridanus
KNR166-2-11MC-D	15.5	0.950	2.175	C. sp.
KNR166-2-11MC-D	15.5	0.966	2.145	C. sp
KNR166-2-11MC-D	15.5	1.026	2.054	C. sp.
KNR166-2-11MC-D	15.5	0.722	1.993	C. sp.
KNR166-2-11MC-D	15.5	0.819	2.063	C. sp.
KNR166-2-11MC-D	16.5	0.968	2.154	C. floridanus
KNR166-2-11MC-D	16.5	0.936	2.330	C. floridanus
KNR166-2-11MC-D	16.5	1.097	2.580	C. floridanus
KNR166-2-11MC-D	16.5	0.902	2.011	C. floridanus
KNR166-2-11MC-D	16.5	0.475	1.952	C. sp.
KNR166-2-11MC-D	16.5	0.979	2.204	C. sp.
KNR166-2-11MC-D	17.5	0.898	2.363	C. floridanus
KNR166-2-11MC-D	17.5	0.963	2.219	C. floridanus
KNR166-2-11MC-D	17.5	0.917	2.236	C. floridanus
KNR166-2-11MC-D	17.5	0.962	2.041	C. floridanus
KNR166-2-11MC-D	17.5	1.095	2.202	C. sp.
KNR166-2-11MC-D	18.5	0.972	2.565	C. floridanus
KNR166-2-11MC-D	18.5	1.061	2.288	C. floridanus
KNR166-2-11MC-D	18.5	1.205	2.320	C. sp.
KNR166-2-11MC-D	18.5	0.933	2.034	C. floridanus
KNR166-2-11MC-D	18.5	0.999	2.059	C. sp.
KNR166-2-11MC-D	19.5	1.022	2.410	C. floridanus
KNR166-2-11MC-D	19.5	1.079	2.316	C. floridanus
KNR166-2-11MC-D	19.5	0.888	2.196	C. sp.
KNR166-2-11MC-D	19.5	1.121	2.151	C. floridanus
KNR166-2-11MC-D	19.5	0.920	2.134	C. sp.
KNR166-2-11MC-D	20.5	0.494	2.464	C. floridanus
KNR166-2-11MC-D	20.5	1.261	2.127	P. ariminensis

KNR166-2-11MC-D	20.5	1.016	2.268	C. floridanus
KNR166-2-11MC-D	20.5	0.875	2.073	C. floridanus
KNR166-2-11MC-D	20.5	1.117	2.117	C. sp.
KNR166-2-11MC-D	20.5	1.096	1.899	C. sp.
KNR166-2-11MC-D	20.5	1.036	2.089	C. sp.
KNR166-2-11MC-D	21.5	0.917	2.392	C. floridanus
KNR166-2-11MC-D	21.5	1.067	2.390	C. floridanus
KNR166-2-11MC-D	21.5	0.977	2.132	C. floridanus
KNR166-2-11MC-D	21.5	0.856	2.156	C. floridanus
KNR166-2-11MC-D	21.5	1.131	2.193	C. sp.
KNR166-2-11MC-D	22.5	1.276	2.306	P. ariminensis
KNR166-2-11MC-D	22.5	1.228	2.248	P. ariminensis
KNR166-2-11MC-D	22.5	1.035	2.052	C. sp.
KNR166-2-11MC-D	22.5	0.873	1.968	C. sp
KNR166-2-11MC-D	22.5	1.032	2.118	C. sp.
KNR166-2-11MC-D	22.5	1.043	2.178	C. sp.
KNR166-2-11MC-D	22.5	1.061	2.214	C. sp.
KNR166-2-11MC-D	23.5	1.076	2.340	C. floridanus
KNR166-2-11MC-D	23.5	1.032	2.457	C. floridanus
KNR166-2-11MC-D	23.5	1.002	2.141	C. sp.
KNR166-2-11MC-D	23.5	0.971	1.908	C. sp
KNR166-2-11MC-D	23.5	1.087	2.150	C. sp.

CORE	DEPTH	C13	O18	SPECIES
KNR166-2-16MC-A	0.5	1.024	1.167	C. floridanus
KNR166-2-16MC-A	0.5	0.571	1.175	C. floridanus
KNR166-2-16MC-A	0.5	0.403	1.371	C. floridanus
KNR166-2-16MC-A	0.5	0.449	1.425	C. floridanus
KNR166-2-16MC-A	0.5	0.170	1.400	C. floridanus
KNR166-2-16MC-A	1.5	0.487	1.129	C. floridanus
KNR166-2-16MC-A	1.5	0.719	1.395	C. floridanus
KNR166-2-16MC-A	1.5	0.318	1.055	C. floridanus
KNR166-2-16MC-A	1.5	0.522	1.440	C. floridanus
KNR166-2-16MC-A	1.5	0.610	1.197	C. floridanus
KNR166-2-16MC-A	2.5	0.672	1.263	C. floridanus
KNR166-2-16MC-A	2.5	0.399	1.238	C. floridanus
KNR166-2-16MC-A	2.5	0.704	1.203	C. floridanus
KNR166-2-16MC-A	2.5	0.434	1.332	C. floridanus
KNR166-2-16MC-A	2.5	0.360	1.041	C. floridanus
KNR166-2-16MC-A	3.5	0.763	1.289	C. floridanus
KNR166-2-16MC-A	3.5	0.537	1.376	C. floridanus
KNR166-2-16MC-A	3.5	0.737	1.391	C. floridanus
KNR166-2-16MC-A	3.5	0.783	1.319	C. floridanus
KNR166-2-16MC-A	3.5	0.401	1.241	C. floridanus
KNR166-2-16MC-A	4.5	0.568	1.163	C. floridanus
KNR166-2-16MC-A	4.5	0.647	1.395	C. floridanus
KNR166-2-16MC-A	4.5	0.773	1.320	C. floridanus
KNR166-2-16MC-A	4.5	0.793	1.179	C. floridanus
KNR166-2-16MC-A	5.5	0.557	1.269	C. floridanus
KNR166-2-16MC-A	5.5	0.553	1.312	C. floridanus
KNR166-2-16MC-A	5.5	0.775	1.330	C. floridanus
KNR166-2-16MC-A	5.5	0.707	1.182	C. floridanus
KNR166-2-16MC-A	6.5	0.748	1.422	C. floridanus
KNR166-2-16MC-A	6.5	0.569	1.102	C. floridanus
KNR166-2-16MC-A	6.5	0.893	1.365	C. floridanus
KNR166-2-16MC-A	6.5	0.570	1.260	C. floridanus
KNR166-2-16MC-A	7.5	0.698	1.303	C. floridanus
KNR166-2-16MC-A	7.5	0.904	1.217	C. floridanus
KNR166-2-16MC-A	7.5	0.712	1.411	C. floridanus
KNR166-2-16MC-A	7.5	0.650	1.162	C. floridanus
KNR166-2-16MC-A	8.5	0.749	1.186	C. floridanus
KNR166-2-16MC-A	8.5	0.480	1.443	C. floridanus
KNR166-2-16MC-A	8.5	0.555	1.509	C. floridanus
KNR166-2-16MC-A	8.5	0.323	1.338	C. floridanus
KNR166-2-16MC-A	9.5	0.797	1.184	C. floridanus
KNR166-2-16MC-A	9.5	0.934	1.390	C. floridanus
KNR166-2-16MC-A	9.5	0.579	1.256	C. floridanus
KNR166-2-16MC-A	9.5	0.705	1.215	C. floridanus
KNR166-2-16MC-A	10.5	0.572	1.260	C. floridanus
KNR166-2-16MC-A	10.5	0.977	1.224	C. floridanus
KNR166-2-16MC-A	10.5	0.864	1.453	C. floridanus
KNR166-2-16MC-A	10.5	0.487	1.343	C. floridanus
KNR166-2-16MC-A	11.5	0.933	1.317	C. floridanus
KNR166-2-16MC-A	11.5	0.720	1.194	C. floridanus
KNR166-2-16MC-A	11.5	0.724	1.142	C. floridanus
KNR166-2-16MC-A	11.5	0.910	1.330	C. floridanus
KNR166-2-16MC-A	12.5	0.934	1.329	C. floridanus
KNR166-2-16MC-A	12.5	0.979	1.365	C. floridanus

KNR166-2-16MC-A	12.5	0.334	1.212	C. floridanus
KNR166-2-16MC-A	12.5	0.724	1.391	C. floridanus
KNR166-2-16MC-A	13.5	0.615	1.224	C. floridanus
KNR166-2-16MC-A	13.5	0.897	1.234	C. floridanus
KNR166-2-16MC-A	13.5	0.767	1.280	C. floridanus
KNR166-2-16MC-A	13.5	0.622	1.365	C. floridanus
KNR166-2-16MC-A	14.5	0.665	1.331	C. floridanus
KNR166-2-16MC-A	14.5	0.425	1.212	C. floridanus
KNR166-2-16MC-A	14.5	0.623	1.366	C. floridanus
KNR166-2-16MC-A	14.5	0.913	1.234	C. floridanus
KNR166-2-16MC-A	15.5	0.855	1.321	C. floridanus
KNR166-2-16MC-A	15.5	0.612	1.239	C. floridanus
KNR166-2-16MC-A	15.5	0.864	1.278	C. floridanus
KNR166-2-16MC-A	15.5	0.621	1.179	C. floridanus
KNR166-2-16MC-A	16.5	0.817	1.383	C. floridanus
KNR166-2-16MC-A	16.5	0.833	1.001	C. floridanus
KNR166-2-16MC-A	16.5	0.651	1.261	C. floridanus
KNR166-2-16MC-A	16.5	0.669	1.248	C. floridanus
KNR166-2-16MC-A	17.5	0.889	1.256	C. floridanus
KNR166-2-16MC-A	17.5	0.889	1.256	C. floridanus
KNR166-2-16MC-A	17.5	0.988	1.411	C. floridanus
KNR166-2-16MC-A	17.5	0.620	1.292	C. floridanus
KNR166-2-16MC-A	17.5	0.869	1.210	C. floridanus
KNR166-2-16MC-A	18.5	0.618	1.502	C. floridanus
KNR166-2-16MC-A	18.5	0.757	1.590	C. floridanus
KNR166-2-16MC-A	18.5	0.541	1.239	C. floridanus
KNR166-2-16MC-A	19.5	0.672	1.220	C. floridanus
KNR166-2-16MC-A	19.5	0.730	1.532	C. floridanus
KNR166-2-16MC-A	19.5	0.782	1.202	C. floridanus
KNR166-2-16MC-A	19.5	0.673	1.519	C. floridanus
KNR166-2-16MC-A	20.5	0.683	1.269	C. floridanus
KNR166-2-16MC-A	20.5	1.057	1.310	C. floridanus
KNR166-2-16MC-A	20.5	0.777	1.124	C. floridanus
KNR166-2-16MC-A	20.5	0.562	1.453	C. floridanus
KNR166-2-16MC-A	21.5	0.734	1.399	C. floridanus
KNR166-2-16MC-A	21.5	0.843	1.210	C. floridanus
KNR166-2-16MC-A	21.5	0.691	1.314	C. floridanus
KNR166-2-16MC-A	21.5	0.489	1.323	C. floridanus
KNR166-2-16MC-A	22.5	0.435	1.226	C. floridanus
KNR166-2-16MC-A	22.5	0.884	1.343	C. floridanus
KNR166-2-16MC-A	22.5	0.738	1.348	C. floridanus
KNR166-2-16MC-A	22.5	0.659	1.407	C. floridanus
KNR166-2-16MC-A	23.5	0.577	1.399	C. floridanus
KNR166-2-16MC-A	23.5	0.778	1.212	C. floridanus
KNR166-2-16MC-A	23.5	0.675	1.319	C. floridanus
KNR166-2-16MC-A	23.5	0.724	1.573	C. floridanus
KNR166-2-16MC-A	24.5	0.670	1.357	C. floridanus
KNR166-2-16MC-A	24.5	0.859	1.308	C. floridanus
KNR166-2-16MC-A	24.5	0.864	1.203	C. floridanus
KNR166-2-16MC-A	24.5	0.621	1.173	C. floridanus
KNR166-2-16MC-A	25.5	0.683	1.255	C. floridanus
KNR166-2-16MC-A	25.5	0.726	1.269	C. floridanus
KNR166-2-16MC-A	25.5	0.791	1.487	C. floridanus
KNR166-2-16MC-A	25.5	0.449	1.226	C. floridanus
KNR166-2-16MC-A	26.5	0.667	1.245	C. floridanus

KNR166-2-16MC-A	26.5	0.748	1.527	C. floridanus
KNR166-2-16MC-A	26.5	0.618	1.067	C. floridanus
KNR166-2-16MC-A	26.5	0.652	1.261	C. floridanus
KNR166-2-16MC-A	27.5	0.716	1.280	C. floridanus
KNR166-2-16MC-A	27.5	0.694	1.407	C. floridanus
KNR166-2-16MC-A	27.5	0.626	1.382	C. floridanus
KNR166-2-16MC-A	27.5	0.391	1.459	C. floridanus
KNR166-2-16MC-A	28.5	0.628	1.312	C. floridanus
KNR166-2-16MC-A	28.5	0.823	1.570	C. floridanus
KNR166-2-16MC-A	28.5	0.964	1.323	C. floridanus
KNR166-2-16MC-A	28.5	0.860	1.357	C. floridanus
KNR166-2-16MC-A	29.5	0.608	1.230	C. floridanus
KNR166-2-16MC-A	29.5	0.644	1.454	C. floridanus
KNR166-2-16MC-A	29.5	0.966	1.339	C. floridanus
KNR166-2-16MC-A	29.5	0.670	1.272	C. floridanus
KNR166-2-16MC-A	30.5	0.662	1.544	C. floridanus
KNR166-2-16MC-A	30.5	0.465	1.357	C. floridanus
KNR166-2-16MC-A	30.5	0.700	1.444	C. floridanus
KNR166-2-16MC-A	30.5	0.648	1.192	C. floridanus
KNR166-2-16MC-A	31.5	0.755	1.376	C. floridanus
KNR166-2-16MC-A	31.5	0.618	1.221	C. floridanus
KNR166-2-16MC-A	31.5	0.918	1.410	C. floridanus
KNR166-2-16MC-A	31.5	0.664	1.339	C. floridanus
KNR166-2-16MC-A	32.5	0.634	1.157	C. floridanus
KNR166-2-16MC-A	32.5	0.937	1.280	C. floridanus
KNR166-2-16MC-A	32.5	0.567	1.374	C. floridanus
KNR166-2-16MC-A	32.5	0.640	1.153	C. floridanus
KNR166-2-16MC-A	33.5	0.729	1.281	C. floridanus
KNR166-2-16MC-A	33.5	0.850	1.173	C. floridanus
KNR166-2-16MC-A	33.5	0.765	1.223	C. floridanus
KNR166-2-16MC-A	33.5	0.584	1.317	C. floridanus
KNR166-2-16MC-A	34.5	0.721	1.368	C. floridanus
KNR166-2-16MC-A	34.5	0.815	1.272	C. floridanus
KNR166-2-16MC-A	34.5	1.053	1.443	C. floridanus
KNR166-2-16MC-A	34.5	0.823	1.250	C. floridanus
KNR166-2-16MC-A	35.5	0.784	1.157	C. floridanus
KNR166-2-16MC-A	35.5	0.634	1.235	C. floridanus
KNR166-2-16MC-A	35.5	0.567	1.373	C. floridanus
KNR166-2-16MC-A	35.5	0.689	1.262	C. floridanus
KNR166-2-16MC-A	36.5	0.704	1.390	C. floridanus
KNR166-2-16MC-A	36.5	0.818	1.240	C. floridanus
KNR166-2-16MC-A	36.5	0.522	1.265	C. floridanus
KNR166-2-16MC-A	36.5	0.884	1.258	C. floridanus
KNR166-2-16MC-A	37.5	0.696	1.386	C. floridanus
KNR166-2-16MC-A	37.5	0.696	1.386	C. floridanus
KNR166-2-16MC-A	37.5	0.697	1.259	C. floridanus
KNR166-2-16MC-A	37.5	0.866	1.498	C. floridanus
KNR166-2-16MC-A	37.5	0.752	1.411	C. floridanus

CORE	DEPTH	C13	O18	SPECIES
KNR166-2-49GGC	4.5	0.736	1.190	C. floridanus
KNR166-2-49GGC	4.5	0.898	1.300	C. floridanus
KNR166-2-49GGC	5.5	0.871	1.131	C. floridanus
KNR166-2-49GGC	6.5	0.691	1.133	C. floridanus
KNR166-2-49GGC	6.5	0.491	1.311	C. floridanus
KNR166-2-49GGC	7.5	0.674	1.154	C. floridanus
KNR166-2-49GGC	8.5	0.838	1.039	C. floridanus
KNR166-2-49GGC	8.5	0.701	1.290	C. floridanus
KNR166-2-49GGC	9.5	0.652	1.228	C. floridanus
KNR166-2-49GGC	10.5	0.878	1.224	C. floridanus
KNR166-2-49GGC	10.5	0.900	1.251	C. floridanus
KNR166-2-49GGC	11.5	0.844	1.086	C. floridanus
KNR166-2-49GGC	12.5	0.905	1.146	C. floridanus
KNR166-2-49GGC	12.5	0.847	1.277	C. floridanus
KNR166-2-49GGC	13.5	0.830	1.126	C. floridanus
KNR166-2-49GGC	14.5	0.620	1.239	C. floridanus
KNR166-2-49GGC	14.5	0.802	1.183	C. floridanus
KNR166-2-49GGC	15.5	0.757	1.342	C. floridanus
KNR166-2-49GGC	16.5	0.845	1.188	C. floridanus
KNR166-2-49GGC	16.5	0.594	1.319	C. floridanus
KNR166-2-49GGC	17.5	0.702	1.194	C. floridanus
KNR166-2-49GGC	18.5	0.755	1.407	C. floridanus
KNR166-2-49GGC	18.5	0.784	1.307	C. floridanus
KNR166-2-49GGC	19.5	0.744	1.149	C. floridanus
KNR166-2-49GGC	20.5	0.889	1.026	C. floridanus
KNR166-2-49GGC	20.5	0.991	1.254	C. floridanus
KNR166-2-49GGC	20.5	0.388	1.329	C. floridanus
KNR166-2-49GGC	20.5	0.565	1.216	C. floridanus
KNR166-2-49GGC	21.5	0.739	1.251	C. floridanus
KNR166-2-49GGC	21.5	0.936	1.196	C. floridanus
KNR166-2-49GGC	21.5	0.677	1.157	C. floridanus
KNR166-2-49GGC	21.5	0.863	0.874	C. floridanus
KNR166-2-49GGC	22.5	0.892	1.345	C. floridanus
KNR166-2-49GGC	22.5	0.725	1.061	C. floridanus
KNR166-2-49GGC	22.5	0.656	1.116	C. floridanus
KNR166-2-49GGC	22.5	0.889	1.166	C. floridanus
KNR166-2-49GGC	23.5	0.937	1.256	C. floridanus
KNR166-2-49GGC	23.5	0.786	1.252	C. floridanus
KNR166-2-49GGC	23.5	0.740	1.360	C. floridanus
KNR166-2-49GGC	23.5	0.689	1.361	C. floridanus
KNR166-2-49GGC	24.5	0.688	0.971	C. floridanus
KNR166-2-49GGC	24.5	0.855	1.487	C. floridanus
KNR166-2-49GGC	24.5	0.887	1.361	C. floridanus
KNR166-2-49GGC	24.5	0.451	1.052	C. floridanus
KNR166-2-49GGC	25.5	0.769	1.285	C. floridanus
KNR166-2-49GGC	25.5	0.862	1.135	C. floridanus
KNR166-2-49GGC	25.5	0.596	1.162	C. floridanus
KNR166-2-49GGC	25.5	0.852	1.099	C. floridanus
KNR166-2-49GGC	26.5	0.630	1.141	C. floridanus
KNR166-2-49GGC	26.5	0.744	1.067	C. floridanus
KNR166-2-49GGC	26.5	0.738	1.135	C. floridanus
KNR166-2-49GGC	26.5	0.548	1.088	C. floridanus
KNR166-2-49GGC	27.5	0.761	1.247	C. floridanus
KNR166-2-49GGC	27.5	0.580	1.139	C. floridanus

KNR166-2-49GGC	27.5	0.503	1.315	C. floridanus
KNR166-2-49GGC	27.5	0.671	1.148	C. floridanus
KNR166-2-49GGC	28.5	0.769	1.529	C. floridanus
KNR166-2-49GGC	28.5	0.633	1.054	C. floridanus
KNR166-2-49GGC	28.5	0.715	1.379	C. floridanus
KNR166-2-49GGC	28.5	0.747	1.086	C. floridanus
KNR166-2-49GGC	29.5	0.527	1.172	C. floridanus
KNR166-2-49GGC	29.5	0.805	1.081	C. floridanus
KNR166-2-49GGC	29.5	0.501	1.182	C. floridanus
KNR166-2-49GGC	29.5	0.769	1.032	C. floridanus
KNR166-2-49GGC	30.5	0.740	1.175	C. floridanus
KNR166-2-49GGC	30.5	0.506	1.206	C. floridanus
KNR166-2-49GGC	30.5	0.580	1.192	C. floridanus
KNR166-2-49GGC	30.5	0.721	1.213	C. floridanus
KNR166-2-49GGC	31.5	1.008	1.156	C. floridanus
KNR166-2-49GGC	31.5	0.726	1.223	C. floridanus
KNR166-2-49GGC	31.5	0.731	1.252	C. floridanus
KNR166-2-49GGC	31.5	0.817	1.129	C. floridanus
KNR166-2-49GGC	32.5	0.855	1.106	C. floridanus
KNR166-2-49GGC	32.5	0.485	1.311	C. floridanus
KNR166-2-49GGC	32.5	0.584	1.392	C. floridanus
KNR166-2-49GGC	32.5	0.613	1.108	C. floridanus
KNR166-2-49GGC	33.5	1.020	1.097	C. floridanus
KNR166-2-49GGC	33.5	0.730	1.100	C. floridanus
KNR166-2-49GGC	33.5	0.388	1.136	C. floridanus
KNR166-2-49GGC	33.5	0.781	1.038	C. floridanus
KNR166-2-49GGC	34.5	0.706	0.978	C. floridanus
KNR166-2-49GGC	34.5	0.781	0.946	C. floridanus
KNR166-2-49GGC	34.5	0.652	1.098	C. floridanus
KNR166-2-49GGC	34.5	0.565	1.106	C. floridanus
KNR166-2-49GGC	35.5	0.733	1.111	C. floridanus
KNR166-2-49GGC	35.5	0.840	1.104	C. floridanus
KNR166-2-49GGC	35.5	0.515	1.293	C. floridanus
KNR166-2-49GGC	35.5	0.674	1.101	C. floridanus
KNR166-2-49GGC	36.5	1.050	1.710	C. floridanus
KNR166-2-49GGC	36.5	0.722	1.137	C. floridanus
KNR166-2-49GGC	36.5	0.511	1.190	C. floridanus
KNR166-2-49GGC	36.5	0.802	1.057	C. floridanus
KNR166-2-49GGC	37.5	0.647	1.267	C. floridanus
KNR166-2-49GGC	37.5	0.543	1.012	C. floridanus
KNR166-2-49GGC	37.5	0.789	1.109	C. floridanus
KNR166-2-49GGC	37.5	0.694	1.015	C. floridanus
KNR166-2-49GGC	38.5	1.160	1.086	C. floridanus
KNR166-2-49GGC	38.5	0.550	1.228	C. floridanus
KNR166-2-49GGC	38.5	0.686	1.118	C. floridanus
KNR166-2-49GGC	39.5	0.594	1.328	C. floridanus
KNR166-2-49GGC	39.5	0.884	1.011	C. floridanus
KNR166-2-49GGC	39.5	0.686	1.123	C. floridanus
KNR166-2-49GGC	39.5	0.741	1.100	C. floridanus
KNR166-2-49GGC	40.5	0.952	0.984	C. floridanus
KNR166-2-49GGC	40.5	0.887	1.273	C. floridanus
KNR166-2-49GGC	40.5	0.937	1.267	C. floridanus
KNR166-2-49GGC	40.5	0.710	1.230	C. floridanus
KNR166-2-49GGC	41.5	0.487	1.316	C. floridanus
KNR166-2-49GGC	41.5	0.681	1.241	C. floridanus

KNR166-2-49GGC	41.5	0.586	1.206	C. floridanus
KNR166-2-49GGC	41.5	0.677	0.967	C. floridanus
KNR166-2-49GGC	42.5	0.596	1.289	C. floridanus
KNR166-2-49GGC	42.5	0.864	1.149	C. floridanus
KNR166-2-49GGC	42.5	0.636	1.168	C. floridanus
KNR166-2-49GGC	42.5	0.977	1.096	C. floridanus
KNR166-2-49GGC	43.5	0.704	1.091	C. floridanus
KNR166-2-49GGC	43.5	0.628	1.508	C. floridanus
KNR166-2-49GGC	43.5	0.949	1.182	C. floridanus
KNR166-2-49GGC	43.5	0.781	1.025	C. floridanus
KNR166-2-49GGC	44.5	0.669	1.465	C. floridanus
KNR166-2-49GGC	44.5	0.958	1.212	C. floridanus
KNR166-2-49GGC	44.5	0.911	1.392	C. floridanus
KNR166-2-49GGC	44.5	0.590	1.116	C. floridanus
KNR166-2-49GGC	45.5	0.746	1.314	C. floridanus
KNR166-2-49GGC	45.5	0.792	0.748	C. floridanus
KNR166-2-49GGC	45.5	0.862	1.050	C. floridanus
KNR166-2-49GGC	45.5	0.764	1.209	C. floridanus
KNR166-2-49GGC	46.5	0.607	1.132	C. floridanus
KNR166-2-49GGC	46.5	0.585	1.315	C. floridanus
KNR166-2-49GGC	46.5	0.339	1.300	C. floridanus
KNR166-2-49GGC	46.5	0.896	0.956	C. floridanus
KNR166-2-49GGC	47.5	0.728	1.495	C. floridanus
KNR166-2-49GGC	47.5	0.808	1.085	C. floridanus
KNR166-2-49GGC	47.5	0.770	1.263	C. floridanus
KNR166-2-49GGC	47.5	0.931	1.150	C. floridanus
KNR166-2-49GGC	48.5	0.762	1.071	C. floridanus
KNR166-2-49GGC	48.5	0.874	1.092	C. floridanus
KNR166-2-49GGC	48.5	0.810	1.062	C. floridanus
KNR166-2-49GGC	48.5	0.886	1.145	C. floridanus
KNR166-2-49GGC	49.5	0.594	1.277	C. floridanus
KNR166-2-49GGC	49.5	0.695	1.054	C. floridanus
KNR166-2-49GGC	49.5	0.773	1.123	C. floridanus
KNR166-2-49GGC	49.5	0.564	1.092	C. floridanus
KNR166-2-49GGC	50.5	0.824	1.045	C. floridanus
KNR166-2-49GGC	52.5	0.775	1.265	C. floridanus
KNR166-2-49GGC	52.5	0.550	1.018	C. floridanus
KNR166-2-49GGC	52.5	0.896	1.168	C. floridanus
KNR166-2-49GGC	52.5	0.490	1.100	C. floridanus
KNR166-2-49GGC	53.5	0.737	1.198	C. floridanus
KNR166-2-49GGC	53.5	0.777	1.048	C. floridanus
KNR166-2-49GGC	53.5	0.746	1.096	C. floridanus
KNR166-2-49GGC	54.5	0.903	0.998	C. floridanus
KNR166-2-49GGC	54.5	0.671	1.161	C. floridanus
KNR166-2-49GGC	54.5	0.763	1.244	C. floridanus
KNR166-2-49GGC	54.5	0.828	0.857	C. floridanus
KNR166-2-49GGC	55.5	0.491	1.067	C. floridanus
KNR166-2-49GGC	55.5	0.768	1.210	C. floridanus
KNR166-2-49GGC	55.5	0.762	1.136	C. floridanus
KNR166-2-49GGC	55.5	0.677	0.978	C. floridanus
KNR166-2-49GGC	56.5	0.577	1.039	C. floridanus
KNR166-2-49GGC	56.5	0.774	1.077	C. floridanus
KNR166-2-49GGC	56.5	0.679	1.430	C. floridanus
KNR166-2-49GGC	56.5	0.805	1.107	C. floridanus
KNR166-2-49GGC	57.5	0.622	1.245	C. floridanus

KNR166-2-49GGC	57.5	0.647	1.144	C. floridanus
KNR166-2-49GGC	57.5	0.697	1.159	C. floridanus
KNR166-2-49GGC	57.5	0.828	1.137	C. floridanus
KNR166-2-49GGC	58.5	0.414	0.924	C. floridanus
KNR166-2-49GGC	58.5	0.635	1.452	C. floridanus
KNR166-2-49GGC	58.5	0.578	1.199	C. floridanus
KNR166-2-49GGC	58.5	0.759	1.209	C. floridanus
KNR166-2-49GGC	59.5	0.608	1.051	C. floridanus
KNR166-2-49GGC	59.5	0.761	1.234	C. floridanus
KNR166-2-49GGC	59.5	0.524	1.195	C. floridanus
KNR166-2-49GGC	59.5	0.858	1.136	C. floridanus
KNR166-2-49GGC	60.5	0.698	1.124	C. floridanus
KNR166-2-49GGC	60.5	0.806	1.332	C. floridanus
KNR166-2-49GGC	60.5	0.780	1.190	C. floridanus
KNR166-2-49GGC	60.5	0.697	1.300	C. floridanus
KNR166-2-49GGC	61.5	0.794	1.144	C. floridanus
KNR166-2-49GGC	61.5	0.593	1.273	C. floridanus
KNR166-2-49GGC	61.5	0.821	1.137	C. floridanus
KNR166-2-49GGC	61.5	0.511	1.724	C. floridanus
KNR166-2-49GGC	62.5	0.609	1.059	C. floridanus
KNR166-2-49GGC	62.5	0.622	1.274	C. floridanus
KNR166-2-49GGC	62.5	0.742	0.900	C. floridanus
KNR166-2-49GGC	63.5	0.665	1.323	C. floridanus
KNR166-2-49GGC	63.5	0.764	1.161	C. floridanus
KNR166-2-49GGC	63.5	0.833	0.969	C. floridanus
KNR166-2-49GGC	63.5	0.858	1.170	C. floridanus
KNR166-2-49GGC	64.5	0.882	1.298	C. floridanus
KNR166-2-49GGC	64.5	0.818	1.061	C. floridanus
KNR166-2-49GGC	64.5	0.972	1.170	C. floridanus
KNR166-2-49GGC	64.5	0.905	1.253	C. floridanus
KNR166-2-49GGC	65.5	0.462	1.312	C. floridanus
KNR166-2-49GGC	65.5	0.633	1.120	C. floridanus
KNR166-2-49GGC	65.5	0.924	1.162	C. floridanus
KNR166-2-49GGC	65.5	0.753	1.169	C. floridanus
KNR166-2-49GGC	66.5	2.513	5.966	C. floridanus
KNR166-2-49GGC	66.5	0.758	1.373	C. floridanus
KNR166-2-49GGC	66.5	0.686	0.702	C. floridanus
KNR166-2-49GGC	66.5	0.436	1.045	C. floridanus
KNR166-2-49GGC	67.5	0.437	0.894	C. floridanus
KNR166-2-49GGC	67.5	0.742	1.323	C. floridanus
KNR166-2-49GGC	67.5	0.810	1.224	C. floridanus
KNR166-2-49GGC	67.5	0.884	1.258	C. floridanus
KNR166-2-49GGC	68.5	0.980	1.306	C. floridanus
KNR166-2-49GGC	68.5	0.615	1.340	C. floridanus
KNR166-2-49GGC	68.5	0.871	1.250	C. floridanus
KNR166-2-49GGC	68.5	0.708	1.140	C. floridanus
KNR166-2-49GGC	69.5	0.784	1.070	C. floridanus
KNR166-2-49GGC	69.5	0.810	1.271	C. floridanus
KNR166-2-49GGC	69.5	0.719	1.175	C. floridanus
KNR166-2-49GGC	69.5	0.921	1.192	C. floridanus
KNR166-2-49GGC	70.5	0.460	0.997	C. floridanus
KNR166-2-49GGC	70.5	0.630	1.156	C. floridanus
KNR166-2-49GGC	70.5	0.646	1.198	C. floridanus
KNR166-2-49GGC	70.5	0.871	1.180	C. floridanus
KNR166-2-49GGC	71.5	0.882	1.056	C. floridanus

KNR166-2-49GGC	71.5	0.680	1.208	C. floridanus
KNR166-2-49GGC	71.5	0.669	1.202	C. floridanus
KNR166-2-49GGC	71.5	0.771	1.188	C. floridanus
KNR166-2-49GGC	72.5	0.836	1.085	C. floridanus
KNR166-2-49GGC	72.5	0.878	1.307	C. floridanus
KNR166-2-49GGC	72.5	0.822	1.386	C. floridanus
KNR166-2-49GGC	73.5	0.307	1.210	C. floridanus
KNR166-2-49GGC	73.5	0.774	1.235	C. floridanus
KNR166-2-49GGC	73.5	0.783	1.185	C. floridanus
KNR166-2-49GGC	73.5	0.847	1.948	C. floridanus
KNR166-2-49GGC	74.5	0.868	1.333	C. floridanus
KNR166-2-49GGC	74.5	0.658	1.141	C. floridanus
KNR166-2-49GGC	74.5	0.779	1.202	C. floridanus
KNR166-2-49GGC	74.5	0.702	1.144	C. floridanus
KNR166-2-49GGC	75.5	0.834	1.123	C. floridanus
KNR166-2-49GGC	75.5	0.963	1.215	C. floridanus
KNR166-2-49GGC	75.5	0.728	1.046	C. floridanus
KNR166-2-49GGC	75.5	0.723	1.106	C. floridanus
KNR166-2-49GGC	76.5	0.814	1.135	C. floridanus
KNR166-2-49GGC	76.5	0.902	1.088	C. floridanus
KNR166-2-49GGC	76.5	0.919	1.014	C. floridanus
KNR166-2-49GGC	76.5	0.393	1.780	C. floridanus
KNR166-2-49GGC	77.5	0.787	1.134	C. floridanus
KNR166-2-49GGC	77.5	0.746	1.087	C. floridanus
KNR166-2-49GGC	77.5	0.934	1.157	C. floridanus
KNR166-2-49GGC	77.5	0.619	1.123	C. floridanus
KNR166-2-49GGC	78.5	0.560	1.254	C. floridanus
KNR166-2-49GGC	78.5	0.630	1.206	C. floridanus
KNR166-2-49GGC	78.5	0.751	1.140	C. floridanus
KNR166-2-49GGC	78.5	0.777	1.144	C. floridanus
KNR166-2-49GGC	79.5	0.763	1.028	C. floridanus
KNR166-2-49GGC	79.5	0.611	1.226	C. floridanus
KNR166-2-49GGC	79.5	0.627	1.148	C. floridanus
KNR166-2-49GGC	79.5	0.655	1.029	C. floridanus
KNR166-2-49GGC	80.5	0.571	1.077	C. floridanus
KNR166-2-49GGC	80.5	0.363	1.375	C. floridanus
KNR166-2-49GGC	80.5	0.840	1.197	C. floridanus
KNR166-2-49GGC	80.5	0.466	0.860	C. floridanus
KNR166-2-49GGC	81.5	0.749	1.167	C. floridanus
KNR166-2-49GGC	81.5	0.678	1.109	C. floridanus
KNR166-2-49GGC	81.5	0.958	1.093	C. floridanus
KNR166-2-49GGC	81.5	0.640	1.334	C. floridanus
KNR166-2-49GGC	82.5	0.625	1.048	C. floridanus
KNR166-2-49GGC	82.5	0.677	1.150	C. floridanus
KNR166-2-49GGC	82.5	0.692	1.112	C. floridanus
KNR166-2-49GGC	82.5	0.625	1.115	C. floridanus
KNR166-2-49GGC	83.5	0.869	1.012	C. floridanus
KNR166-2-49GGC	83.5	0.708	1.275	C. floridanus
KNR166-2-49GGC	83.5	0.879	1.066	C. floridanus
KNR166-2-49GGC	83.5	0.979	0.929	C. floridanus
KNR166-2-49GGC	84.5	0.874	1.207	C. floridanus
KNR166-2-49GGC	84.5	0.866	1.369	C. floridanus
KNR166-2-49GGC	84.5	0.642	1.305	C. floridanus
KNR166-2-49GGC	84.5	0.680	1.283	C. floridanus
KNR166-2-49GGC	85.5	0.675	1.272	C. floridanus

KNR166-2-49GGC	85.5	0.733	1.238	C. floridanus
KNR166-2-49GGC	85.5	0.613	1.022	C. floridanus
KNR166-2-49GGC	85.5	0.576	1.298	C. floridanus
KNR166-2-49GGC	86.5	0.778	1.061	C. floridanus
KNR166-2-49GGC	86.5	0.777	1.321	C. floridanus
KNR166-2-49GGC	86.5	0.940	1.099	C. floridanus
KNR166-2-49GGC	87.5	0.849	1.169	C. floridanus
KNR166-2-49GGC	87.5	0.605	1.147	C. floridanus
KNR166-2-49GGC	87.5	0.876	0.995	C. floridanus
KNR166-2-49GGC	87.5	0.797	1.060	C. floridanus
KNR166-2-49GGC	88.5	0.776	1.090	C. floridanus
KNR166-2-49GGC	88.5	0.733	1.172	C. floridanus
KNR166-2-49GGC	88.5	0.758	1.179	C. floridanus
KNR166-2-49GGC	88.5	0.808	1.041	C. floridanus
KNR166-2-49GGC	89.5	0.768	1.156	C. floridanus
KNR166-2-49GGC	89.5	0.601	1.242	C. floridanus
KNR166-2-49GGC	89.5	0.447	1.078	C. floridanus
KNR166-2-49GGC	89.5	0.452	1.353	C. floridanus

CORE	DEPTH	C13	O18	SPECIES
KNR166-2-50MC-E	0.5	0.735	1.252	C. floridanus
KNR166-2-50MC-E	0.5	0.790	1.191	C. floridanus
KNR166-2-50MC-E	0.5	0.737	1.022	C. floridanus
KNR166-2-50MC-E	0.5	0.519	0.951	C. floridanus
KNR166-2-50MC-E	1.5	0.641	0.970	C. floridanus
KNR166-2-50MC-E	1.5	0.740	0.819	C. floridanus
KNR166-2-50MC-E	1.5	0.589	1.298	C. floridanus
KNR166-2-50MC-E	1.5	0.757	1.026	C. floridanus
KNR166-2-50MC-E	2.5	0.789	1.056	C. floridanus
KNR166-2-50MC-E	2.5	0.746	1.310	C. floridanus
KNR166-2-50MC-E	2.5	0.575	0.963	C. floridanus
KNR166-2-50MC-E	2.5	0.696	1.108	C. floridanus
KNR166-2-50MC-E	3.5	0.928	1.340	C. floridanus
KNR166-2-50MC-E	3.5	0.706	1.087	C. floridanus
KNR166-2-50MC-E	3.5	0.316	1.109	C. floridanus
KNR166-2-50MC-E	3.5	0.814	1.066	C. floridanus
KNR166-2-50MC-E	4.5	0.828	1.293	C. floridanus
KNR166-2-50MC-E	4.5	0.580	1.249	C. floridanus
KNR166-2-50MC-E	4.5	0.607	0.993	C. floridanus
KNR166-2-50MC-E	4.5	0.741	1.013	C. floridanus
KNR166-2-50MC-E	4.5	0.701	1.046	C. floridanus
KNR166-2-50MC-E	5.5	1.041	1.455	C. floridanus
KNR166-2-50MC-E	5.5	0.821	1.039	C. floridanus
KNR166-2-50MC-E	5.5	0.638	1.140	C. floridanus
KNR166-2-50MC-E	5.5	0.586	0.948	C. floridanus
KNR166-2-50MC-E	6.5	0.752	1.278	C. floridanus
KNR166-2-50MC-E	6.5	0.675	0.986	C. floridanus
KNR166-2-50MC-E	6.5	0.889	1.223	C. floridanus
KNR166-2-50MC-E	6.5	0.795	0.947	C. floridanus
KNR166-2-50MC-E	7.5	0.741	1.014	C. floridanus
KNR166-2-50MC-E	7.5	0.792	1.052	C. floridanus
KNR166-2-50MC-E	7.5	0.730	1.371	C. floridanus
KNR166-2-50MC-E	7.5	0.818	1.108	C. floridanus
KNR166-2-50MC-E	8.5	0.564	1.372	C. floridanus
KNR166-2-50MC-E	8.5	1.037	1.192	C. floridanus
KNR166-2-50MC-E	8.5	0.887	1.424	C. floridanus
KNR166-2-50MC-E	8.5	0.438	1.167	C. floridanus
KNR166-2-50MC-E	8.5	0.743	1.188	C. floridanus
KNR166-2-50MC-E	9.5	0.610	1.210	C. floridanus
KNR166-2-50MC-E	9.5	0.411	1.108	C. floridanus
KNR166-2-50MC-E	9.5	0.679	1.166	C. floridanus
KNR166-2-50MC-E	9.5	0.534	1.492	C. floridanus
KNR166-2-50MC-E	10	0.903	1.261	C. floridanus
KNR166-2-50MC-E	10.5	0.574	1.312	C. floridanus
KNR166-2-50MC-E	10.5	0.599	1.395	C. floridanus
KNR166-2-50MC-E	10.5	0.556	0.978	C. floridanus
KNR166-2-50MC-E	10.5	0.914	1.407	C. floridanus
KNR166-2-50MC-E	11.5	0.729	0.865	C. floridanus
KNR166-2-50MC-E	11.5	0.920	1.400	C. floridanus
KNR166-2-50MC-E	11.5	0.925	1.224	C. floridanus
KNR166-2-50MC-E	11.5	0.869	1.219	C. floridanus
KNR166-2-50MC-E	12.5	0.522	1.174	C. floridanus
KNR166-2-50MC-E	12.5	0.440	1.070	C. floridanus
KNR166-2-50MC-E	12.5	0.503	1.029	C. floridanus

KNR166-2-50MC-E	12.5	0.330	1.111	C. floridanus
KNR166-2-50MC-E	12.5	0.747	1.180	C. floridanus
KNR166-2-50MC-E	13.5	0.860	1.343	C. floridanus
KNR166-2-50MC-E	13.5	0.751	1.351	C. floridanus
KNR166-2-50MC-E	13.5	0.832	1.141	C. floridanus
KNR166-2-50MC-E	13.5	0.625	1.066	C. floridanus
KNR166-2-50MC-E	13.5	0.636	1.270	C. floridanus
KNR166-2-50MC-E	14.5	0.794	1.194	C. floridanus
KNR166-2-50MC-E	14.5	0.801	1.456	C. floridanus
KNR166-2-50MC-E	14.5	0.781	1.002	C. floridanus
KNR166-2-50MC-E	14.5	0.627	1.292	C. floridanus
KNR166-2-50MC-E	14.5	0.793	1.145	C. floridanus
KNR166-2-50MC-E	15.5	0.846	1.182	C. floridanus
KNR166-2-50MC-E	15.5	0.916	1.141	C. floridanus
KNR166-2-50MC-E	15.5	0.694	1.164	C. floridanus
KNR166-2-50MC-E	15.5	0.711	1.110	C. floridanus
KNR166-2-50MC-E	16.5	0.833	1.317	C. floridanus
KNR166-2-50MC-E	16.5	0.940	1.225	C. floridanus
KNR166-2-50MC-E	16.5	0.694	1.174	C. floridanus
KNR166-2-50MC-E	16.5	0.488	1.274	C. floridanus
KNR166-2-50MC-E	17.5	0.856	1.281	C. floridanus
KNR166-2-50MC-E	17.5	0.659	1.135	C. floridanus
KNR166-2-50MC-E	17.5	0.820	1.330	C. floridanus
KNR166-2-50MC-E	17.5	0.643	1.146	C. floridanus
KNR166-2-50MC-E	18.5	0.492	1.099	C. floridanus
KNR166-2-50MC-E	18.5	0.711	1.178	C. floridanus
KNR166-2-50MC-E	18.5	0.609	1.136	C. floridanus
KNR166-2-50MC-E	18.5	0.821	0.979	C. floridanus
KNR166-2-50MC-E	19.5	0.835	2.497	C. floridanus
KNR166-2-50MC-E	19.5	0.874	1.135	C. floridanus
KNR166-2-50MC-E	19.5	0.773	0.974	C. floridanus
KNR166-2-50MC-E	19.5	0.984	1.092	C. floridanus
KNR166-2-50MC-E	20.5	0.911	1.234	C. floridanus
KNR166-2-50MC-E	20.5	0.675	1.238	C. floridanus
KNR166-2-50MC-E	20.5	0.526	1.264	C. floridanus
KNR166-2-50MC-E	20.5	0.885	1.021	C. floridanus
KNR166-2-50MC-E	21.5	0.591	1.282	C. floridanus
KNR166-2-50MC-E	21.5	0.804	1.086	C. floridanus
KNR166-2-50MC-E	21.5	0.735	1.102	C. floridanus
KNR166-2-50MC-E	21.5	0.769	1.261	C. floridanus
KNR166-2-50MC-E	22.5	0.936	1.299	C. floridanus
KNR166-2-50MC-E	22.5	0.985	1.223	C. floridanus
KNR166-2-50MC-E	22.5	0.950	1.173	C. floridanus
KNR166-2-50MC-E	22.5	1.043	1.123	C. floridanus
KNR166-2-50MC-E	23.5	0.785	1.332	C. floridanus
KNR166-2-50MC-E	23.5	0.706	1.123	C. floridanus
KNR166-2-50MC-E	23.5	0.628	1.027	C. floridanus
KNR166-2-50MC-E	24.5	1.063	1.448	C. floridanus
KNR166-2-50MC-E	24.5	0.782	1.028	C. floridanus
KNR166-2-50MC-E	24.5	0.860	1.210	C. floridanus
KNR166-2-50MC-E	24.5	0.570	1.326	C. floridanus

CORE	DEPTH	C13	O18	SPECIES
KNR166-2-62MC-A	0.25	0.949	1.819	P. ariminensis
KNR166-2-62MC-A	0.25	1.113	1.742	P. ariminensis
KNR166-2-62MC-A	0.25	1.163	1.780	P. ariminensis
KNR166-2-62MC-A	0.25	0.756	1.721	C. floridanus
KNR166-2-62MC-A	0.75	0.998	1.741	P. ariminensis
KNR166-2-62MC-A	0.75	0.184	1.863	C. floridanus
KNR166-2-62MC-A	0.75	1.027	1.903	C. floridanus
KNR166-2-62MC-A	0.75	0.715	1.763	C. floridanus
KNR166-2-62MC-A	1.25	1.155	1.874	P. ariminensis
KNR166-2-62MC-A	1.25	0.838	2.160	C. floridanus
KNR166-2-62MC-A	1.25	1.158	1.629	P. ariminensis
KNR166-2-62MC-A	1.25	0.870	1.748	C. floridanus
KNR166-2-62MC-A	1.75	1.029	1.748	P. ariminensis
KNR166-2-62MC-A	1.75	0.688	1.683	C. floridanus
KNR166-2-62MC-A	1.75	0.927	1.984	C. floridanus
KNR166-2-62MC-A	1.75	1.150	1.719	P. ariminensis
KNR166-2-62MC-A	2.25	1.086	1.697	P. ariminensis
KNR166-2-62MC-A	2.25	0.771	1.891	C. floridanus
KNR166-2-62MC-A	2.25	0.608	1.615	C. floridanus
KNR166-2-62MC-A	2.25	0.867	1.877	C. floridanus
KNR166-2-62MC-A	2.75	1.168	1.854	P. ariminensis
KNR166-2-62MC-A	2.75	0.777	1.616	C. floridanus
KNR166-2-62MC-A	2.75	0.885	1.860	C. floridanus
KNR166-2-62MC-A	2.75	0.918	1.841	C. floridanus
KNR166-2-62MC-A	3.25	1.026	1.719	P. ariminensis
KNR166-2-62MC-A	3.25	0.598	1.707	C. floridanus
KNR166-2-62MC-A	3.25	0.985	2.034	C. floridanus
KNR166-2-62MC-A	3.25	1.047	1.742	P. ariminensis
KNR166-2-62MC-A	3.75	0.728	1.766	C. floridanus
KNR166-2-62MC-A	3.75	0.602	1.557	C. floridanus
KNR166-2-62MC-A	3.75	1.012	1.826	C. floridanus
KNR166-2-62MC-A	3.75	0.696	2.176	C. floridanus
KNR166-2-62MC-A	4.25	1.132	1.636	P. ariminensis
KNR166-2-62MC-A	4.25	0.936	1.891	C. floridanus
KNR166-2-62MC-A	4.25	0.850	1.836	C. floridanus
KNR166-2-62MC-A	4.25	0.937	1.860	C. floridanus
KNR166-2-62MC-A	4.75	1.167	1.701	P. ariminensis
KNR166-2-62MC-A	4.75	1.058	1.910	C. floridanus
KNR166-2-62MC-A	4.75	0.898	1.901	C. floridanus
KNR166-2-62MC-A	4.75	1.097	1.661	P. ariminensis
KNR166-2-62MC-A	5.25	1.070	1.729	P. ariminensis
KNR166-2-62MC-A	5.25	0.975	1.937	C. floridanus
KNR166-2-62MC-A	5.25	0.816	1.903	C. floridanus
KNR166-2-62MC-A	5.25	0.804	1.770	C. floridanus
KNR166-2-62MC-A	5.75	1.070	1.699	P. ariminensis
KNR166-2-62MC-A	5.75	0.840	1.901	C. floridanus
KNR166-2-62MC-A	5.75	1.094	1.811	P. ariminensis
KNR166-2-62MC-A	5.75	0.990	1.809	P. ariminensis
KNR166-2-62MC-A	6.25	1.268	1.822	P. ariminensis
KNR166-2-62MC-A	6.25	0.840	1.756	C. floridanus
KNR166-2-62MC-A	6.25	0.855	1.759	C. floridanus
KNR166-2-62MC-A	6.75	0.983	1.918	C. floridanus
KNR166-2-62MC-A	6.75	0.937	1.693	C. floridanus
KNR166-2-62MC-A	6.75	0.868	2.008	C. floridanus

KNR166-2-62MC-A	6.75	0.938	1.911	C. floridanus
KNR166-2-62MC-A	7.25	1.016	1.822	P. ariminensis
KNR166-2-62MC-A	7.25	0.653	1.839	C. floridanus
KNR166-2-62MC-A	7.25	0.709	1.893	C. floridanus
KNR166-2-62MC-A	7.25	0.994	1.955	C. floridanus
KNR166-2-62MC-A	7.75	1.097	1.762	P. ariminensis
KNR166-2-62MC-A	7.75	0.793	1.857	C. floridanus
KNR166-2-62MC-A	7.75	0.640	1.813	C. floridanus
KNR166-2-62MC-A	7.75	1.005	1.835	C. floridanus
KNR166-2-62MC-A	8.25	1.224	1.801	P. ariminensis
KNR166-2-62MC-A	8.25	0.916	1.807	C. floridanus
KNR166-2-62MC-A	8.25	0.870	1.911	C. floridanus
KNR166-2-62MC-A	8.25	0.990	1.851	C. floridanus
KNR166-2-62MC-A	8.75	1.181	1.804	P. ariminensis
KNR166-2-62MC-A	8.75	0.906	1.670	C. floridanus
KNR166-2-62MC-A	8.75	1.009	1.730	P. ariminensis
KNR166-2-62MC-A	8.75	0.726	1.997	C. floridanus
KNR166-2-62MC-A	9.25	1.169	1.917	P. ariminensis
KNR166-2-62MC-A	9.25	0.916	1.637	C. floridanus
KNR166-2-62MC-A	9.25	0.905	1.893	C. floridanus
KNR166-2-62MC-A	9.25	1.172	1.838	P. ariminensis
KNR166-2-62MC-A	9.75	1.290	1.886	P. ariminensis
KNR166-2-62MC-A	9.75	0.794	2.024	C. floridanus
KNR166-2-62MC-A	9.75	0.878	1.875	C. floridanus
KNR166-2-62MC-A	9.75	0.622	1.796	C. floridanus
KNR166-2-62MC-A	10.25	1.240	1.764	P. ariminensis
KNR166-2-62MC-A	10.25	1.182	1.968	P. ariminensis
KNR166-2-62MC-A	10.25	0.626	1.746	C. floridanus
KNR166-2-62MC-A	10.25	1.033	1.815	P. ariminensis
KNR166-2-62MC-A	10.75	1.103	1.895	P. ariminensis
KNR166-2-62MC-A	10.75	0.833	2.059	C. floridanus
KNR166-2-62MC-A	10.75	0.982	1.869	C. floridanus
KNR166-2-62MC-A	10.75	1.156	1.801	P. ariminensis
KNR166-2-62MC-A	11.25	1.126	1.761	P. ariminensis
KNR166-2-62MC-A	11.25	0.858	1.870	C. floridanus
KNR166-2-62MC-A	11.25	1.084	1.900	P. ariminensis
KNR166-2-62MC-A	11.25	1.159	1.881	P. ariminensis
KNR166-2-62MC-A	11.75	1.146	1.819	P. ariminensis
KNR166-2-62MC-A	11.75	1.181	1.854	P. ariminensis
KNR166-2-62MC-A	11.75	1.092	1.989	P. ariminensis
KNR166-2-62MC-A	11.75	0.968	1.368	C. floridanus
KNR166-2-62MC-A	12.25	1.224	1.894	P. ariminensis
KNR166-2-62MC-A	12.25	0.841	1.814	C. floridanus
KNR166-2-62MC-A	12.25	1.169	1.864	P. ariminensis
KNR166-2-62MC-A	12.25	1.250	1.833	P. ariminensis
KNR166-2-62MC-A	12.75	1.215	1.562	P. ariminensis
KNR166-2-62MC-A	12.75	1.206	1.741	P. ariminensis
KNR166-2-62MC-A	12.75	1.279	1.833	P. ariminensis
KNR166-2-62MC-A	12.75	1.279	1.980	P. ariminensis
KNR166-2-62MC-A	13.25	1.244	1.944	P. ariminensis
KNR166-2-62MC-A	13.25	0.950	2.046	C. floridanus
KNR166-2-62MC-A	13.25	1.058	1.915	C. floridanus
KNR166-2-62MC-A	13.25	1.242	1.883	P. ariminensis
KNR166-2-62MC-A	13.75	1.259	1.782	P. ariminensis
KNR166-2-62MC-A	13.75	0.926	1.824	C. floridanus

KNR166-2-62MC-A	13.75	0.912	2.055	C. floridanus
KNR166-2-62MC-A	13.75	1.091	1.907	P. ariminensis
KNR166-2-62MC-A	14.25	1.205	1.847	P. ariminensis
KNR166-2-62MC-A	14.25	0.851	2.015	C. floridanus
KNR166-2-62MC-A	14.25	0.978	1.890	C. floridanus
KNR166-2-62MC-A	14.25	1.213	1.664	P. ariminensis
KNR166-2-62MC-A	14.75	1.229	1.773	P. ariminensis
KNR166-2-62MC-A	14.75	0.845	1.894	C. floridanus
KNR166-2-62MC-A	14.75	1.329	2.029	P. ariminensis
KNR166-2-62MC-A	14.75	0.829	1.826	C. floridanus
KNR166-2-62MC-A	15.25	1.247	1.832	P. ariminensis
KNR166-2-62MC-A	15.25	0.934	1.827	C. floridanus
KNR166-2-62MC-A	15.25	0.913	1.945	C. floridanus
KNR166-2-62MC-A	15.25	0.701	1.867	C. floridanus
KNR166-2-62MC-A	15.75	1.080	1.845	P. ariminensis
KNR166-2-62MC-A	15.75	0.584	1.914	C. floridanus
KNR166-2-62MC-A	15.75	1.146	1.793	P. ariminensis
KNR166-2-62MC-A	15.75	0.956	1.925	C. floridanus
KNR166-2-62MC-A	16.25	1.152	1.884	P. ariminensis
KNR166-2-62MC-A	16.25	0.765	1.921	C. floridanus
KNR166-2-62MC-A	16.25	0.713	2.077	C. floridanus
KNR166-2-62MC-A	16.25	0.842	1.923	C. floridanus
KNR166-2-62MC-A	16.75	1.220	1.867	P. ariminensis
KNR166-2-62MC-A	16.75	0.830	1.932	C. floridanus
KNR166-2-62MC-A	16.75	0.559	1.927	C. floridanus
KNR166-2-62MC-A	16.75	1.128	2.056	C. floridanus
KNR166-2-62MC-A	17.25	1.194	1.721	P. ariminensis
KNR166-2-62MC-A	17.25	0.952	1.797	C. floridanus
KNR166-2-62MC-A	17.25	0.867	1.763	C. floridanus
KNR166-2-62MC-A	17.25	1.039	1.750	C. floridanus
KNR166-2-62MC-A	17.75	1.072	1.768	P. ariminensis
KNR166-2-62MC-A	17.75	0.874	1.951	C. floridanus
KNR166-2-62MC-A	17.75	0.809	1.903	C. floridanus
KNR166-2-62MC-A	17.75	0.766	1.742	C. floridanus
KNR166-2-62MC-A	18.25	1.056	1.809	P. ariminensis
KNR166-2-62MC-A	18.25	0.927	1.962	C. floridanus
KNR166-2-62MC-A	18.25	0.870	2.071	C. floridanus
KNR166-2-62MC-A	18.25	0.655	1.843	C. floridanus
KNR166-2-62MC-A	18.75	0.985	1.887	C. floridanus
KNR166-2-62MC-A	18.75	0.939	1.925	C. floridanus
KNR166-2-62MC-A	18.75	0.768	2.194	C. floridanus
KNR166-2-62MC-A	18.75	0.926	1.917	C. floridanus
KNR166-2-62MC-A	19.25	1.238	1.757	P. ariminensis
KNR166-2-62MC-A	19.25	0.909	1.952	C. floridanus
KNR166-2-62MC-A	19.25	0.820	1.877	C. floridanus
KNR166-2-62MC-A	19.25	0.860	2.003	C. floridanus
KNR166-2-62MC-A	19.75	1.106	1.912	P. ariminensis
KNR166-2-62MC-A	19.75	0.963	1.924	C. floridanus
KNR166-2-62MC-A	19.75	0.820	1.200	C. floridanus
KNR166-2-62MC-A	19.75	0.625	1.959	C. floridanus
KNR166-2-62MC-A	20.25	1.218	1.837	P. ariminensis
KNR166-2-62MC-A	20.25	0.964	1.779	C. floridanus
KNR166-2-62MC-A	20.25	1.247	1.810	P. ariminensis
KNR166-2-62MC-A	20.25	0.866	2.181	C. floridanus
KNR166-2-62MC-A	20.75	1.063	1.869	P. ariminensis

KNR166-2-62MC-A	20.75	0.888	1.998	C. floridanus
KNR166-2-62MC-A	20.75	0.846	2.068	C. floridanus
KNR166-2-62MC-A	20.75	0.837	1.980	C. floridanus
KNR166-2-62MC-A	21.25	1.093	1.838	P. ariminensis
KNR166-2-62MC-A	21.25	0.881	1.938	C. floridanus
KNR166-2-62MC-A	21.25	0.809	1.912	C. floridanus
KNR166-2-62MC-A	21.25	0.829	1.927	C. floridanus
KNR166-2-62MC-A	21.75	0.847	1.785	C. floridanus
KNR166-2-62MC-A	21.75	0.628	1.899	C. floridanus
KNR166-2-62MC-A	21.75	0.923	1.787	C. floridanus
KNR166-2-62MC-A	21.75	0.644	2.091	C. floridanus
KNR166-2-62MC-A	22.25	1.154	1.821	P. ariminensis
KNR166-2-62MC-A	22.25	0.826	1.847	C. floridanus
KNR166-2-62MC-A	22.25	0.940	1.877	C. floridanus
KNR166-2-62MC-A	22.25	0.849	1.898	C. floridanus
KNR166-2-62MC-A	22.75	1.218	1.793	P. ariminensis
KNR166-2-62MC-A	22.75	0.848	1.930	C. floridanus
KNR166-2-62MC-A	22.75	0.675	2.031	C. floridanus
KNR166-2-62MC-A	22.75	0.566	1.823	C. floridanus
KNR166-2-62MC-A	23.25	1.164	1.883	P. ariminensis
KNR166-2-62MC-A	23.25	0.918	1.997	C. floridanus
KNR166-2-62MC-A	23.25	0.806	1.884	C. floridanus
KNR166-2-62MC-A	23.25	1.028	1.958	C. floridanus
KNR166-2-62MC-A	23.75	1.141	1.834	P. ariminensis
KNR166-2-62MC-A	23.75	0.649	1.834	C. floridanus
KNR166-2-62MC-A	23.75	0.836	2.222	C. floridanus
KNR166-2-62MC-A	23.75	0.839	1.997	C. floridanus
KNR166-2-62MC-A	24.25	1.237	1.869	P. ariminensis
KNR166-2-62MC-A	24.25	1.034	2.035	C. floridanus
KNR166-2-62MC-A	24.25	0.854	2.003	C. floridanus
KNR166-2-62MC-A	24.25	0.755	1.955	C. floridanus
KNR166-2-62MC-A	24.75	1.127	1.830	P. ariminensis
KNR166-2-62MC-A	24.75	0.874	1.860	C. floridanus
KNR166-2-62MC-A	24.75	0.958	2.019	C. floridanus
KNR166-2-62MC-A	24.75	0.870	1.969	C. floridanus
KNR166-2-62MC-A	25.25	1.261	1.715	P. ariminensis
KNR166-2-62MC-A	25.25	0.997	2.093	C. floridanus
KNR166-2-62MC-A	25.25	0.975	1.923	C. floridanus
KNR166-2-62MC-A	25.25	0.522	1.754	C. floridanus
KNR166-2-62MC-A	25.75	1.135	1.798	P. ariminensis
KNR166-2-62MC-A	25.75	0.663	2.085	C. floridanus
KNR166-2-62MC-A	25.75	0.943	2.034	C. floridanus
KNR166-2-62MC-A	25.75	0.514	2.006	C. floridanus
KNR166-2-62MC-A	26.25	1.169	1.895	P. ariminensis
KNR166-2-62MC-A	26.25	1.015	1.911	C. floridanus
KNR166-2-62MC-A	26.25	1.321	2.003	P. ariminensis
KNR166-2-62MC-A	26.25	1.203	1.856	P. ariminensis
KNR166-2-62MC-A	26.75	0.917	2.044	C. floridanus
KNR166-2-62MC-A	26.75	0.918	1.769	C. floridanus
KNR166-2-62MC-A	26.75	1.219	1.772	P. ariminensis
KNR166-2-62MC-A	26.75	1.175	1.774	P. ariminensis
KNR166-2-62MC-A	27.25	1.448	-0.483	P. ariminensis
KNR166-2-62MC-A	27.25	0.854	2.151	C. floridanus
KNR166-2-62MC-A	27.25	0.855	2.237	C. floridanus
KNR166-2-62MC-A	27.25	1.166	1.733	P. ariminensis

KNR166-2-62MC-A	27.75	1.173	1.808	P. ariminensis
KNR166-2-62MC-A	27.75	0.611	2.076	C. floridanus
KNR166-2-62MC-A	27.75	0.744	2.094	C. floridanus
KNR166-2-62MC-A	27.75	0.868	2.171	C. floridanus
KNR166-2-62MC-A	28.25	0.948	1.763	C. floridanus
KNR166-2-62MC-A	28.25	1.013	1.915	C. floridanus
KNR166-2-62MC-A	28.25	0.774	2.154	C. floridanus
KNR166-2-62MC-A	28.25	1.068	2.060	C. floridanus
KNR166-2-62MC-A	28.75	0.650	1.840	C. floridanus
KNR166-2-62MC-A	28.75	0.815	1.898	C. floridanus
KNR166-2-62MC-A	28.75	1.004	1.910	C. floridanus
KNR166-2-62MC-A	29.25	0.976	1.913	C. floridanus
KNR166-2-62MC-A	29.25	0.764	1.885	C. floridanus
KNR166-2-62MC-A	29.25	1.015	1.854	C. floridanus
KNR166-2-62MC-A	29.25	1.216	1.850	P. ariminensis
KNR166-2-62MC-A	29.75	1.178	1.673	P. ariminensis
KNR166-2-62MC-A	29.75	0.884	1.907	C. floridanus
KNR166-2-62MC-A	29.75	0.903	2.112	C. floridanus
KNR166-2-62MC-A	29.75	1.231	1.881	P. ariminensis

CORE	DEPTH	C13	O18	SPECIES
W167-79GGC	0.5	0.919	1.924	C. floridanus
W167-79GGC	2	0.83	1.875	C. floridanus
W167-79GGC	2	1.141	1.913	P. ariminensis
W167-79GGC	3.25	1.036	1.794	P. ariminensis
W167-79GGC	3.25	1.094	1.944	P. ariminensis
W167-79GGC	3.25	1.124	1.664	P. ariminensis
W167-79GGC	3.25	1.162	1.685	P. ariminensis
W167-79GGC	3.75	0.937	1.879	C. floridanus
W167-79GGC	3.75	1.027	1.872	P. ariminensis
W167-79GGC	4.25	0.779	2.164	C. floridanus
W167-79GGC	4.25	0.966	1.846	C. floridanus
W167-79GGC	4.25	0.966	1.953	C. floridanus
W167-79GGC	4.25	1.038	1.642	P. ariminensis
W167-79GGC	4.75	0.7	1.935	C. floridanus
W167-79GGC	4.75	0.794	1.94	C. floridanus
W167-79GGC	4.75	0.942	1.966	C. floridanus
W167-79GGC	4.75	1.2	1.898	P. ariminensis
W167-79GGC	5.25	0.905	1.766	C. floridanus
W167-79GGC	5.25	0.954	1.996	C. floridanus
W167-79GGC	5.25	1.128	1.739	P. ariminensis
W167-79GGC	5.75	0.791	2.099	C. floridanus
W167-79GGC	5.75	0.872	1.584	C. floridanus
W167-79GGC	5.75	1.074	1.719	P. ariminensis
W167-79GGC	6.25	0.98	2.047	C. floridanus
W167-79GGC	6.25	1.062	1.519	P. ariminensis
W167-79GGC	6.25	1.319	2.148	P. ariminensis
W167-79GGC	6.75	0.561	1.944	C. floridanus
W167-79GGC	6.75	1.197	1.986	P. ariminensis
W167-79GGC	6.75	1.198	2.041	P. ariminensis
W167-79GGC	7.25	0.735	2.211	C. floridanus
W167-79GGC	7.25	0.858	2.001	C. floridanus
W167-79GGC	7.25	1.032	2.129	C. floridanus
W167-79GGC	7.75	0.764	1.818	C. floridanus
W167-79GGC	7.75	1.008	2.01	C. floridanus
W167-79GGC	7.75	1.012	2.106	C. floridanus
W167-79GGC	7.75	1.119	1.81	C. floridanus
W167-79GGC	8.25	0.806	1.924	C. floridanus
W167-79GGC	8.25	1.109	1.649	P. ariminensis
W167-79GGC	8.25	1.12	1.767	P. ariminensis
W167-79GGC	8.25	1.187	1.957	P. ariminensis
W167-79GGC	8.75	1.033	1.991	P. ariminensis
W167-79GGC	8.75	1.145	1.751	P. ariminensis
W167-79GGC	8.75	1.185	1.818	P. ariminensis
W167-79GGC	9.25	1.146	1.975	P. ariminensis
W167-79GGC	9.25	1.149	1.947	P. ariminensis
W167-79GGC	9.25	1.164	1.858	P. ariminensis
W167-79GGC	9.75	0.886	1.839	C. floridanus
W167-79GGC	9.75	1.171	1.85	P. ariminensis
W167-79GGC	9.75	1.224	1.933	P. ariminensis
W167-79GGC	10.25	0.744	1.916	C. floridanus
W167-79GGC	10.25	1.029	2.13	C. floridanus
W167-79GGC	10.25	1.134	1.816	P. ariminensis
W167-79GGC	10.75	0.958	1.889	P. ariminensis
W167-79GGC	10.75	1.034	1.828	P. ariminensis

W167-79GGC	11.25	0.917	1.921	C. floridanus
W167-79GGC	11.25	1.167	1.816	P. ariminensis
W167-79GGC	11.25	1.192	1.946	P. ariminensis
W167-79GGC	11.25	1.202	2.05	P. ariminensis
W167-79GGC	11.75	0.873	1.764	P. ariminensis
W167-79GGC	11.75	0.984	1.961	C. floridanus
W167-79GGC	11.75	1.14	2.164	C. floridanus
W167-79GGC	11.75	1.22	2.018	P. ariminensis
W167-79GGC	12.25	1.001	1.948	P. ariminensis
W167-79GGC	12.25	1.08	1.812	P. ariminensis
W167-79GGC	12.25	1.178	1.777	P. ariminensis
W167-79GGC	12.25	1.3	2.072	P. ariminensis
W167-79GGC	12.75	0.771	1.901	C. floridanus
W167-79GGC	12.75	0.798	2.06	C. floridanus
W167-79GGC	12.75	0.927	2.196	C. floridanus
W167-79GGC	13.25	0.804	2.145	C. floridanus
W167-79GGC	13.25	0.811	2.089	C. floridanus
W167-79GGC	13.25	1.224	1.905	P. ariminensis
W167-79GGC	13.75	0.9	1.978	C. floridanus
W167-79GGC	13.75	0.909	1.99	C. floridanus
W167-79GGC	13.75	0.917	2.045	C. floridanus
W167-79GGC	13.75	1.166	1.92	P. ariminensis
W167-79GGC	14.25	0.774	2.136	C. floridanus
W167-79GGC	14.25	0.902	2.067	C. floridanus
W167-79GGC	14.25	1.117	1.959	P. ariminensis
W167-79GGC	14.75	0.802	2.085	C. floridanus
W167-79GGC	14.75	0.821	1.936	C. floridanus
W167-79GGC	14.75	1.053	2.011	P. ariminensis
W167-79GGC	14.75	1.228	1.986	P. ariminensis
W167-79GGC	15.25	0.873	1.879	C. floridanus
W167-79GGC	15.25	0.92	1.947	C. floridanus
W167-79GGC	15.25	0.98	1.546	P. ariminensis
W167-79GGC	15.25	1.063	1.828	P. ariminensis
W167-79GGC	15.75	0.907	2.121	C. floridanus
W167-79GGC	15.75	1.114	1.985	P. ariminensis
W167-79GGC	15.75	1.147	2.046	C. floridanus
W167-79GGC	15.75	1.194	1.883	C. floridanus
W167-79GGC	16.25	0.866	1.723	C. floridanus
W167-79GGC	16.25	1.205	1.788	P. ariminensis
W167-79GGC	16.75	1.032	1.808	P. ariminensis
W167-79GGC	16.75	1.056	1.999	P. ariminensis
W167-79GGC	16.75	1.157	1.794	P. ariminensis
W167-79GGC	17.25	0.667	1.965	C. floridanus
W167-79GGC	17.25	0.877	1.868	C. floridanus
W167-79GGC	17.25	0.917	2.032	C. floridanus
W167-79GGC	17.25	0.95	1.921	C. floridanus
W167-79GGC	17.75	0.854	2.192	C. floridanus
W167-79GGC	17.75	1.051	1.836	P. ariminensis
W167-79GGC	17.75	1.098	2.01	P. ariminensis
W167-79GGC	17.75	1.145	1.738	P. ariminensis
W167-79GGC	18.25	1.022	1.967	C. floridanus
W167-79GGC	18.25	1.03	2.174	C. floridanus
W167-79GGC	18.75	0.779	1.806	C. floridanus
W167-79GGC	18.75	0.875	2.084	C. floridanus
W167-79GGC	18.75	1.152	2.004	P. ariminensis

W167-79GGC	18.75	1.376	2.276	P. ariminensis
W167-79GGC	19.25	0.82	1.9	C. floridanus
W167-79GGC	19.25	0.845	1.938	C. floridanus
W167-79GGC	19.25	1.027	2.109	C. floridanus
W167-79GGC	19.25	1.085	1.792	P. ariminensis
W167-79GGC	19.75	0.917	1.829	C. floridanus
W167-79GGC	19.75	0.938	2.047	C. floridanus
W167-79GGC	19.75	1.109	1.802	P. ariminensis
W167-79GGC	19.75	1.118	1.81	P. ariminensis
W167-79GGC	20.25	0.924	2.111	C. floridanus
W167-79GGC	20.25	1.003	1.891	C. floridanus
W167-79GGC	20.25	1.07	1.613	P. ariminensis
W167-79GGC	20.25	1.17	2.055	P. ariminensis
W167-79GGC	20.75	0.782	2.003	C. floridanus
W167-79GGC	20.75	0.926	1.953	C. floridanus
W167-79GGC	20.75	1.023	1.996	C. floridanus
W167-79GGC	21.25	0.696	1.919	C. floridanus
W167-79GGC	21.25	0.969	2.228	C. floridanus
W167-79GGC	21.25	0.995	2.109	C. floridanus
W167-79GGC	21.25	1.092	1.65	P. ariminensis
W167-79GGC	21.75	1.002	1.885	C. floridanus
W167-79GGC	21.75	1.014	1.884	C. floridanus
W167-79GGC	21.75	1.187	1.909	P. ariminensis
W167-79GGC	21.75	1.194	1.979	P. ariminensis
W167-79GGC	22.25	0.929	1.953	C. floridanus
W167-79GGC	22.25	0.997	1.938	P. ariminensis
W167-79GGC	22.25	1.15	1.942	P. ariminensis
W167-79GGC	22.75	1.083	1.959	P. ariminensis
W167-79GGC	22.75	1.19	1.948	P. ariminensis
W167-79GGC	22.75	1.199	1.912	P. ariminensis
W167-79GGC	22.75	1.28	1.766	P. ariminensis
W167-79GGC	23.25	0.955	2.231	C. floridanus
W167-79GGC	23.25	0.995	1.714	C. floridanus
W167-79GGC	23.25	1.036	2.076	C. floridanus
W167-79GGC	23.75	0.796	1.997	C. floridanus
W167-79GGC	23.75	0.907	2.046	C. floridanus
W167-79GGC	23.75	1.02	2.14	C. floridanus
W167-79GGC	23.75	1.043	2.028	C. floridanus
W167-79GGC	24.25	0.946	2.106	C. floridanus
W167-79GGC	24.25	1.029	1.948	P. ariminensis
W167-79GGC	24.25	1.166	1.917	P. ariminensis
W167-79GGC	24.25	1.173	1.976	P. ariminensis
W167-79GGC	24.75	0.613	1.901	C. floridanus
W167-79GGC	24.75	1.036	1.919	C. floridanus
W167-79GGC	24.75	1.327	1.695	P. ariminensis
W167-79GGC	25.25	0.986	1.921	C. floridanus
W167-79GGC	25.25	1.295	1.977	P. ariminensis
W167-79GGC	25.75	0.648	1.882	C. floridanus
W167-79GGC	25.75	0.867	2.105	C. floridanus
W167-79GGC	25.75	1.046	1.536	P. ariminensis
W167-79GGC	26.25	1.073	2.092	C. floridanus
W167-79GGC	26.25	1.185	1.746	P. ariminensis
W167-79GGC	26.25	1.272	2.013	P. ariminensis
W167-79GGC	26.75	0.823	1.784	C. floridanus
W167-79GGC	26.75	0.969	2.16	C. floridanus

W167-79GGC	26.75	1.022	2.105	C. floridanus
W167-79GGC	27.25	0.919	2.122	C. floridanus
W167-79GGC	27.25	1.217	1.774	P. ariminensis
W167-79GGC	27.75	0.594	1.996	C. floridanus
W167-79GGC	27.75	0.823	1.868	C. floridanus
W167-79GGC	27.75	0.946	1.859	C. floridanus
W167-79GGC	27.75	1.036	1.975	C. floridanus
W167-79GGC	28.25	1.209	1.885	P. ariminensis
W167-79GGC	28.25	1.382	2.048	P. ariminensis
W167-79GGC	28.75	1.153	1.519	P. ariminensis
W167-79GGC	28.75	1.231	1.821	P. ariminensis
W167-79GGC	29.25	0.781	1.589	C. floridanus
W167-79GGC	29.25	0.89	2.078	C. floridanus
W167-79GGC	29.75	1.025	1.971	C. floridanus
W167-79GGC	29.75	1.207	2.217	C. floridanus
W167-79GGC	30.25	0.89	1.85	C. floridanus
W167-79GGC	30.25	1.093	1.856	P. ariminensis
W167-79GGC	30.25	1.156	1.945	P. ariminensis
W167-79GGC	30.75	0.767	1.88	C. floridanus
W167-79GGC	30.75	1.011	1.844	C. floridanus
W167-79GGC	30.75	1.208	1.857	P. ariminensis
W167-79GGC	30.75	1.413	1.937	P. ariminensis
W167-79GGC	31.25	0.88	1.924	C. floridanus
W167-79GGC	31.25	1.098	1.836	P. ariminensis
W167-79GGC	31.75	0.871	1.849	C. floridanus
W167-79GGC	31.75	0.963	1.914	C. floridanus
W167-79GGC	31.75	1.057	1.896	C. floridanus
W167-79GGC	32.25	0.841	1.849	C. floridanus
W167-79GGC	32.25	0.947	1.876	C. floridanus
W167-79GGC	32.25	1.141	1.881	C. floridanus
W167-79GGC	32.75	0.978	2.139	C. floridanus
W167-79GGC	32.75	0.987	1.949	C. floridanus
W167-79GGC	32.75	1.095	1.726	P. ariminensis
W167-79GGC	32.75	1.177	1.742	P. ariminensis
W167-79GGC	33.25	0.927	1.812	C. floridanus
W167-79GGC	33.75	0.96	1.987	C. floridanus
W167-79GGC	33.75	0.965	1.888	C. floridanus
W167-79GGC	34.25	0.479	1.825	C. floridanus
W167-79GGC	34.25	0.906	2.108	C. floridanus
W167-79GGC	34.25	1.043	2.112	P. ariminensis
W167-79GGC	34.75	0.934	1.959	C. floridanus
W167-79GGC	34.75	1.075	2.126	C. floridanus
W167-79GGC	34.75	1.239	1.814	P. ariminensis
W167-79GGC	35.25	0.994	1.977	C. floridanus
W167-79GGC	35.25	1.175	1.837	P. ariminensis
W167-79GGC	35.25	1.258	1.848	P. ariminensis
W167-79GGC	35.75	0.956	1.824	C. floridanus
W167-79GGC	35.75	1.004	1.853	C. floridanus
W167-79GGC	35.75	1.081	2.024	P. ariminensis
W167-79GGC	35.75	1.182	1.953	P. ariminensis
W167-79GGC	36.25	0.887	2.021	C. floridanus
W167-79GGC	36.25	0.906	1.902	C. floridanus
W167-79GGC	36.25	1.025	1.993	C. floridanus
W167-79GGC	36.75	0.978	2.028	C. floridanus
W167-79GGC	36.75	0.985	1.853	C. floridanus

W167-79GGC	36.75	1.205	1.973	P. ariminensis
W167-79GGC	36.75	1.232	1.816	P. ariminensis
W167-79GGC	37.25	0.81	1.845	C. floridanus
W167-79GGC	37.25	0.882	1.798	C. floridanus
W167-79GGC	37.25	1.3	1.956	P. ariminensis
W167-79GGC	37.75	0.97	2.125	C. floridanus
W167-79GGC	37.75	0.972	2.046	C. floridanus
W167-79GGC	37.75	1.151	1.995	P. ariminensis
W167-79GGC	37.75	1.263	1.948	P. ariminensis
W167-79GGC	38.25	0.909	1.814	C. floridanus
W167-79GGC	38.25	1.044	1.984	P. ariminensis
W167-79GGC	38.25	1.212	1.918	P. ariminensis
W167-79GGC	38.75	0.669	1.882	C. floridanus
W167-79GGC	38.75	0.855	2.051	C. floridanus
W167-79GGC	38.75	1.136	1.764	P. ariminensis
W167-79GGC	39.25	0.904	1.862	C. floridanus
W167-79GGC	39.25	0.936	2.179	C. floridanus
W167-79GGC	39.25	0.95	2.214	C. floridanus
W167-79GGC	39.25	1.107	1.67	P. ariminensis
W167-79GGC	39.75	0.32	2.074	C. floridanus
W167-79GGC	39.75	0.873	1.999	C. floridanus
W167-79GGC	39.75	1.254	2.084	P. ariminensis
W167-79GGC	40.25	0.77	2.075	C. floridanus
W167-79GGC	40.25	0.917	2.04	C. floridanus
W167-79GGC	40.25	1.256	1.789	P. ariminensis
W167-79GGC	40.75	0.676	1.963	C. floridanus
W167-79GGC	40.75	0.881	2.072	C. floridanus
W167-79GGC	40.75	0.917	1.825	C. floridanus
W167-79GGC	41.25	0.792	2.193	C. floridanus
W167-79GGC	41.25	0.982	1.883	P. ariminensis
W167-79GGC	41.25	1.19	1.618	P. ariminensis
W167-79GGC	41.75	1.184	1.85	P. ariminensis
W167-79GGC	41.75	1.303	1.709	P. ariminensis
W167-79GGC	42.25	0.263	2.218	C. floridanus
W167-79GGC	42.25	0.336	2.027	C. floridanus
W167-79GGC	42.25	0.969	2.208	C. floridanus
W167-79GGC	42.25	0.995	1.824	C. floridanus
W167-79GGC	42.75	0.834	1.86	C. floridanus
W167-79GGC	42.75	0.971	1.971	C. floridanus
W167-79GGC	42.75	0.991	2.073	C. floridanus
W167-79GGC	42.75	1.019	2.073	P. ariminensis
W167-79GGC	43.25	0.943	1.93	C. floridanus
W167-79GGC	43.25	1.251	1.885	P. ariminensis
W167-79GGC	43.25	1.282	1.735	P. ariminensis
W167-79GGC	43.25	1.285	1.787	P. ariminensis
W167-79GGC	43.75	0.283	2.026	C. floridanus
W167-79GGC	43.75	0.747	1.856	C. floridanus
W167-79GGC	43.75	1.151	1.8	P. ariminensis
W167-79GGC	43.75	1.16	1.705	P. ariminensis
W167-79GGC	44.25	0.691	2.108	C. floridanus
W167-79GGC	44.25	0.878	1.978	C. floridanus
W167-79GGC	44.25	0.964	1.631	C. floridanus
W167-79GGC	44.25	0.968	1.74	P. ariminensis
W167-79GGC	44.75	0.936	1.917	C. floridanus
W167-79GGC	44.75	0.95	1.846	C. floridanus

W167-79GGC	44.75	1.123	2.002	C. floridanus
W167-79GGC	44.75	1.162	2.131	P. ariminensis
W167-79GGC	45.25	0.659	1.903	C. floridanus
W167-79GGC	45.25	1.063	1.941	C. floridanus
W167-79GGC	45.25	1.233	1.939	P. ariminensis
W167-79GGC	45.75	1.007	1.895	C. floridanus
W167-79GGC	45.75	1.166	1.793	P. ariminensis
W167-79GGC	45.75	1.213	1.706	P. ariminensis
W167-79GGC	45.75	1.221	1.796	P. ariminensis
W167-79GGC	46.25	0.821	2.09	C. floridanus
W167-79GGC	46.25	1.149	1.853	P. ariminensis
W167-79GGC	46.25	1.16	1.854	P. ariminensis
W167-79GGC	46.75	1.168	1.799	P. ariminensis
W167-79GGC	46.75	1.203	1.783	P. ariminensis
W167-79GGC	46.75	1.216	2.016	P. ariminensis
W167-79GGC	46.75	1.281	1.951	P. ariminensis
W167-79GGC	47.25	0.661	1.978	C. floridanus
W167-79GGC	47.25	0.957	1.927	C. floridanus
W167-79GGC	47.25	1.202	1.767	P. ariminensis
W167-79GGC	47.25	1.209	1.775	P. ariminensis
W167-79GGC	47.75	1.017	1.951	C. floridanus
W167-79GGC	47.75	1.195	1.932	P. ariminensis
W167-79GGC	47.75	1.381	2.024	P. ariminensis
W167-79GGC	48.25	0.112	2.09	C. floridanus
W167-79GGC	48.25	1.094	1.567	P. ariminensis
W167-79GGC	48.25	1.137	1.777	P. ariminensis
W167-79GGC	48.25	1.186	1.854	P. ariminensis
W167-79GGC	48.75	0.729	1.891	C. floridanus
W167-79GGC	48.75	1.061	1.641	P. ariminensis
W167-79GGC	48.75	1.149	1.687	P. ariminensis
W167-79GGC	48.75	1.155	1.647	P. ariminensis
W167-79GGC	49.25	0.68	1.547	C. floridanus
W167-79GGC	49.25	0.911	1.852	C. floridanus
W167-79GGC	49.25	1.163	1.757	P. ariminensis
W167-79GGC	49.25	1.255	1.903	P. ariminensis
W167-79GGC	49.75	0.91	2.105	C. floridanus
W167-79GGC	49.75	0.98	1.87	C. floridanus
W167-79GGC	49.75	1.008	1.888	C. floridanus
W167-79GGC	49.75	1.14	1.946	P. ariminensis
W167-79GGC	50.25	1.05	2.014	C. floridanus
W167-79GGC	50.25	1.17	1.811	P. ariminensis
W167-79GGC	50.25	1.286	1.415	P. ariminensis
W167-79GGC	50.25	1.304	2.115	P. ariminensis
W167-79GGC	50.75	0.891	2.14	C. floridanus
W167-79GGC	50.75	0.908	2.002	C. floridanus
W167-79GGC	50.75	0.989	1.953	C. floridanus
W167-79GGC	50.75	0.994	1.93	C. floridanus
W167-79GGC	50.75	1.117	1.678	P. ariminensis
W167-79GGC	51.25	1.003	1.907	C. floridanus
W167-79GGC	51.25	1.083	1.608	P. ariminensis
W167-79GGC	51.25	1.109	1.795	P. ariminensis
W167-79GGC	51.25	1.279	2.032	P. ariminensis
W167-79GGC	51.75	0.933	1.972	C. floridanus
W167-79GGC	51.75	0.982	1.858	C. floridanus
W167-79GGC	51.75	1.224	1.559	P. ariminensis

W167-79GGC	52.25	0.893	1.81	C. floridanus
W167-79GGC	52.25	1.107	1.877	P. ariminensis
W167-79GGC	52.25	1.31	2.005	P. ariminensis
W167-79GGC	52.75	0.658	1.82	C. floridanus
W167-79GGC	52.75	0.83	1.949	C. floridanus
W167-79GGC	52.75	0.915	1.987	C. floridanus
W167-79GGC	52.75	0.995	1.872	C. floridanus
W167-79GGC	53.25	1.022	1.931	C. floridanus
W167-79GGC	53.25	1.15	1.754	P. ariminensis
W167-79GGC	53.25	1.24	1.799	P. ariminensis
W167-79GGC	53.25	1.263	1.8	P. ariminensis
W167-79GGC	53.75	0.933	1.971	C. floridanus
W167-79GGC	53.75	1.148	1.886	P. ariminensis
W167-79GGC	53.75	1.157	1.746	P. ariminensis
W167-79GGC	53.75	1.199	1.719	P. ariminensis
W167-79GGC	54.25	0.728	1.825	C. floridanus
W167-79GGC	54.25	0.841	1.751	C. floridanus
W167-79GGC	54.25	0.912	1.932	C. floridanus
W167-79GGC	54.25	1.222	1.814	P. ariminensis
W167-79GGC	54.75	0.216	2.102	C. floridanus
W167-79GGC	54.75	0.879	1.726	C. floridanus
W167-79GGC	54.75	1.005	1.93	C. floridanus
W167-79GGC	54.75	1.098	1.872	P. ariminensis
W167-79GGC	55.25	0.464	1.888	C. floridanus
W167-79GGC	55.25	1.171	1.853	P. ariminensis
W167-79GGC	55.25	1.22	1.509	P. ariminensis
W167-79GGC	55.75	0.908	1.978	C. floridanus
W167-79GGC	55.75	0.913	1.912	C. floridanus
W167-79GGC	55.75	0.949	1.884	C. floridanus
W167-79GGC	55.75	1.243	1.809	P. ariminensis
W167-79GGC	56.25	0.822	1.868	C. floridanus
W167-79GGC	56.25	1.054	1.755	P. ariminensis
W167-79GGC	56.25	1.109	1.805	C. floridanus
W167-79GGC	56.25	1.25	1.736	P. ariminensis
W167-79GGC	56.75	0.736	1.756	C. floridanus
W167-79GGC	56.75	0.984	1.828	C. floridanus
W167-79GGC	56.75	1.047	1.925	C. floridanus
W167-79GGC	56.75	1.226	1.798	P. ariminensis
W167-79GGC	57.25	0.878	1.992	C. floridanus
W167-79GGC	57.25	1.097	1.654	P. ariminensis
W167-79GGC	57.25	1.166	1.788	C. floridanus
W167-79GGC	57.25	1.262	1.777	P. ariminensis
W167-79GGC	57.75	0.83	1.831	C. floridanus
W167-79GGC	57.75	0.938	1.885	C. floridanus
W167-79GGC	57.75	0.957	1.84	C. floridanus
W167-79GGC	57.75	1.132	1.867	P. ariminensis
W167-79GGC	58.25	0.912	1.845	C. floridanus
W167-79GGC	58.25	0.956	1.961	C. floridanus
W167-79GGC	58.25	1.008	1.786	C. floridanus
W167-79GGC	58.25	1.2	1.775	P. ariminensis
W167-79GGC	58.75	0.856	1.815	C. floridanus
W167-79GGC	58.75	0.92	1.808	C. floridanus
W167-79GGC	58.75	0.961	1.771	C. floridanus
W167-79GGC	58.75	1.135	1.757	C. floridanus
W167-79GGC	59.25	0.819	1.642	C. floridanus

W167-79GGC	59.25	0.886	1.855	C. floridanus
W167-79GGC	59.25	1.137	1.808	P. ariminensis
W167-79GGC	59.25	1.227	1.797	P. ariminensis
W167-79GGC	59.75	0.966	1.812	C. floridanus
W167-79GGC	59.75	1.03	1.806	C. floridanus
W167-79GGC	59.75	1.032	1.985	C. floridanus
W167-79GGC	59.75	1.256	1.695	P. ariminensis
W167-79GGC	60.25	0.829	1.868	C. floridanus
W167-79GGC	60.25	0.972	2.085	C. floridanus
W167-79GGC	60.25	1	1.857	C. floridanus
W167-79GGC	60.25	1.054	1.813	C. floridanus
W167-79GGC	60.75	0.857	1.887	C. floridanus
W167-79GGC	60.75	0.909	1.758	C. floridanus
W167-79GGC	60.75	1.057	1.938	C. floridanus
W167-79GGC	60.75	1.199	1.792	P. ariminensis
W167-79GGC	61.25	0.839	1.889	P. ariminensis
W167-79GGC	61.25	0.973	1.797	C. floridanus
W167-79GGC	61.25	0.985	1.912	C. floridanus
W167-79GGC	61.25	0.994	1.916	C. floridanus
W167-79GGC	61.75	0.786	1.764	C. floridanus
W167-79GGC	61.75	0.979	1.972	C. floridanus
W167-79GGC	61.75	1.067	1.839	C. floridanus
W167-79GGC	61.75	1.268	1.718	P. ariminensis
W167-79GGC	62.25	0.863	1.868	C. floridanus
W167-79GGC	62.25	0.957	1.935	C. floridanus
W167-79GGC	62.25	1.036	1.885	C. floridanus
W167-79GGC	62.25	1.09	1.895	C. floridanus
W167-79GGC	62.75	0.875	1.775	C. floridanus
W167-79GGC	62.75	0.877	1.917	C. floridanus
W167-79GGC	62.75	0.895	1.974	C. floridanus
W167-79GGC	62.75	0.952	1.972	C. floridanus
W167-79GGC	63.25	1.005	1.753	C. floridanus
W167-79GGC	63.25	1.028	1.933	C. floridanus
W167-79GGC	63.25	1.033	1.745	C. floridanus
W167-79GGC	63.25	1.233	1.78	P. ariminensis
W167-79GGC	63.75	0.887	1.74	C. floridanus
W167-79GGC	63.75	0.889	1.804	C. floridanus
W167-79GGC	63.75	1.05	1.822	C. floridanus
W167-79GGC	63.75	1.177	1.759	P. ariminensis
W167-79GGC	64.25	0.85	1.998	C. floridanus
W167-79GGC	64.25	0.888	1.749	C. floridanus
W167-79GGC	64.25	0.947	1.882	C. floridanus
W167-79GGC	64.25	1.188	1.87	P. ariminensis
W167-79GGC	64.75	0.792	1.827	C. floridanus
W167-79GGC	64.75	0.899	1.882	C. floridanus
W167-79GGC	64.75	0.91	1.982	C. floridanus
W167-79GGC	64.75	0.965	1.864	C. floridanus
W167-79GGC	65.25	0.899	1.877	C. floridanus
W167-79GGC	65.25	0.936	1.9	C. floridanus
W167-79GGC	65.25	1.04	1.889	C. floridanus
W167-79GGC	65.75	0.148	1.546	C. floridanus
W167-79GGC	65.75	0.874	1.898	C. floridanus
W167-79GGC	65.75	0.952	1.891	C. floridanus
W167-79GGC	65.75	1.034	1.878	C. floridanus
W167-79GGC	66.25	0.858	1.817	C. floridanus

W167-79GGC	66.25	0.956	1.793	C. floridanus
W167-79GGC	66.25	0.973	2.03	C. floridanus
W167-79GGC	66.75	0.697	1.981	C. floridanus
W167-79GGC	66.75	0.869	1.929	C. floridanus
W167-79GGC	66.75	0.996	1.843	C. floridanus
W167-79GGC	66.75	1.086	1.826	P. ariminensis
W167-79GGC	67.25	0.957	2.012	C. floridanus
W167-79GGC	67.25	1.003	1.962	C. floridanus
W167-79GGC	67.25	1.026	1.803	C. floridanus
W167-79GGC	67.25	1.032	1.899	P. ariminensis
W167-79GGC	67.75	0.918	1.942	C. floridanus
W167-79GGC	67.75	0.947	1.788	C. floridanus
W167-79GGC	67.75	1.032	1.936	C. floridanus
W167-79GGC	67.75	1.273	1.879	P. ariminensis
W167-79GGC	68.25	0.948	1.889	C. floridanus
W167-79GGC	68.25	1.001	1.889	C. floridanus
W167-79GGC	68.25	1.172	1.807	P. ariminensis
W167-79GGC	68.25	1.18	1.893	C. floridanus
W167-79GGC	68.75	0.903	1.907	C. floridanus
W167-79GGC	68.75	0.989	1.948	P. ariminensis
W167-79GGC	68.75	0.997	1.826	C. floridanus
W167-79GGC	68.75	1.21	1.845	P. ariminensis
W167-79GGC	69.25	1.022	1.877	C. floridanus
W167-79GGC	69.25	1.049	1.987	C. floridanus
W167-79GGC	69.25	1.147	1.806	P. ariminensis
W167-79GGC	69.25	1.263	1.833	P. ariminensis
W167-79GGC	69.75	1.053	1.873	C. floridanus
W167-79GGC	69.75	1.062	1.825	C. floridanus
W167-79GGC	69.75	1.166	1.786	P. ariminensis
W167-79GGC	69.75	1.177	1.684	P. ariminensis
W167-79GGC	70.25	0.898	1.785	C. floridanus
W167-79GGC	70.25	0.96	1.971	C. floridanus
W167-79GGC	70.25	0.967	1.801	C. floridanus
W167-79GGC	70.25	1.175	1.729	P. ariminensis
W167-79GGC	70.75	0.91	1.944	C. floridanus
W167-79GGC	70.75	0.964	1.915	C. floridanus
W167-79GGC	70.75	1.168	1.793	P. ariminensis
W167-79GGC	70.75	1.236	1.802	P. ariminensis
W167-79GGC	71.25	0.811	1.851	C. floridanus
W167-79GGC	71.25	0.893	1.809	C. floridanus
W167-79GGC	71.25	0.91	1.96	C. floridanus
W167-79GGC	71.25	1.139	1.862	C. floridanus
W167-79GGC	71.75	0.812	1.859	C. floridanus
W167-79GGC	71.75	0.884	1.95	C. floridanus
W167-79GGC	71.75	1.037	1.86	C. floridanus
W167-79GGC	71.75	1.052	1.869	C. floridanus
W167-79GGC	72.25	0.959	2.026	C. floridanus
W167-79GGC	72.25	0.978	1.975	C. floridanus
W167-79GGC	72.25	1.267	1.845	P. ariminensis
W167-79GGC	72.25	1.313	1.712	P. ariminensis
W167-79GGC	72.75	1.086	1.698	P. ariminensis
W167-79GGC	72.75	1.167	1.75	P. ariminensis
W167-79GGC	72.75	1.199	1.762	ariminesis
W167-79GGC	72.75	1.329	1.765	P. ariminensis
W167-79GGC	73.25	0.655	1.656	C. floridanus

W167-79GGC	73.25	0.927	1.939	C. floridanus
W167-79GGC	73.25	0.936	1.759	C. floridanus
W167-79GGC	73.25	1.232	1.726	P. ariminensis
W167-79GGC	73.75	1.079	1.846	P. ariminensis
W167-79GGC	73.75	1.118	2	C. floridanus
W167-79GGC	73.75	1.22	1.726	P. ariminensis
W167-79GGC	73.75	1.267	1.776	P. ariminensis
W167-79GGC	74.25	0.845	1.847	C. floridanus
W167-79GGC	74.25	0.971	1.875	C. floridanus
W167-79GGC	74.25	1.151	1.869	P. ariminensis
W167-79GGC	74.25	1.226	1.703	P. ariminensis
W167-79GGC	74.75	0.845	1.799	C. floridanus
W167-79GGC	74.75	0.937	1.969	C. floridanus
W167-79GGC	74.75	1.074	1.825	C. floridanus
W167-79GGC	74.75	1.147	1.681	P. ariminensis
W167-79GGC	75.25	0.881	1.854	C. floridanus
W167-79GGC	75.25	0.916	2.001	C. floridanus
W167-79GGC	75.25	1.187	1.822	P. ariminensis
W167-79GGC	75.25	1.276	1.709	P. ariminensis
W167-79GGC	75.75	0.71	1.862	C. floridanus
W167-79GGC	75.75	0.838	1.893	C. floridanus
W167-79GGC	75.75	0.9	1.88	C. floridanus
W167-79GGC	75.75	1.003	1.959	C. floridanus
W167-79GGC	76.25	0.776	1.827	C. floridanus
W167-79GGC	76.25	0.851	1.935	C. floridanus
W167-79GGC	76.25	1.082	1.845	C. floridanus
W167-79GGC	76.25	1.103	1.925	C. floridanus
W167-79GGC	76.75	0.682	1.851	C. floridanus
W167-79GGC	76.75	0.908	1.849	C. floridanus
W167-79GGC	76.75	0.912	1.722	C. floridanus
W167-79GGC	76.75	0.993	2.039	C. floridanus
W167-79GGC	77.25	0.853	1.772	C. floridanus
W167-79GGC	77.25	0.87	1.877	C. floridanus
W167-79GGC	77.25	1.076	1.845	C. floridanus
W167-79GGC	77.25	1.252	1.743	P. ariminensis
W167-79GGC	77.75	0.775	1.886	C. floridanus
W167-79GGC	77.75	0.818	1.885	C. floridanus
W167-79GGC	77.75	0.833	1.842	C. floridanus
W167-79GGC	77.75	0.927	1.782	C. floridanus
W167-79GGC	78.25	0.147	2.108	C. floridanus
W167-79GGC	78.25	0.827	1.869	C. floridanus
W167-79GGC	78.25	0.94	1.829	C. floridanus
W167-79GGC	78.25	1.016	1.939	C. floridanus
W167-79GGC	78.75	0.771	1.852	C. floridanus
W167-79GGC	78.75	0.854	1.847	C. floridanus
W167-79GGC	78.75	1.085	1.852	C. floridanus
W167-79GGC	78.75	1.282	1.759	P. ariminensis
W167-79GGC	79.25	0.734	1.857	C. floridanus
W167-79GGC	79.25	0.837	1.81	C. floridanus
W167-79GGC	79.25	0.939	1.823	C. floridanus
W167-79GGC	79.25	1.006	1.9	C. floridanus
W167-79GGC	79.75	0.673	1.828	C. floridanus
W167-79GGC	79.75	0.852	1.906	C. floridanus
W167-79GGC	79.75	0.855	1.878	C. floridanus
W167-79GGC	79.75	1.045	1.9	C. floridanus

W167-79GGC	80.25	0.273	2.141	C. floridanus
W167-79GGC	80.25	0.619	1.875	C. floridanus
W167-79GGC	80.25	0.815	2.045	C. floridanus
W167-79GGC	80.25	0.922	1.57	C. floridanus
W167-79GGC	80.75	0.701	1.899	C. floridanus
W167-79GGC	80.75	0.82	1.807	C. floridanus
W167-79GGC	80.75	0.882	1.908	C. floridanus
W167-79GGC	80.75	1.316	1.707	P. ariminensis
W167-79GGC	81.25	0.924	1.91	C. floridanus
W167-79GGC	81.25	0.962	1.812	C. floridanus
W167-79GGC	81.25	0.966	2.018	C. floridanus
W167-79GGC	81.25	1.246	1.886	P. ariminensis
W167-79GGC	81.75	0.888	1.827	C. floridanus
W167-79GGC	81.75	0.926	2.021	C. floridanus
W167-79GGC	81.75	0.957	1.832	C. floridanus
W167-79GGC	81.75	0.965	1.892	C. floridanus
W167-79GGC	82.25	1.011	1.903	C. floridanus
W167-79GGC	82.25	1.213	1.706	P. ariminensis
W167-79GGC	82.25	1.232	1.796	P. ariminensis
W167-79GGC	82.75	0.811	1.851	C. floridanus
W167-79GGC	82.75	0.86	1.878	C. floridanus
W167-79GGC	82.75	1.22	1.806	P. ariminensis
W167-79GGC	83.25	0.94	1.855	C. floridanus
W167-79GGC	83.25	1	2.013	P. ariminensis
W167-79GGC	83.25	1.025	1.686	P. ariminensis
W167-79GGC	83.25	1.063	1.872	C. floridanus
W167-79GGC	83.25	1.095	1.846	C. floridanus
W167-79GGC	83.75	1.099	1.783	P. ariminensis
W167-79GGC	83.75	1.105	1.786	P. ariminensis
W167-79GGC	83.75	1.196	1.75	P. ariminensis
W167-79GGC	83.75	1.243	1.646	P. ariminensis
W167-79GGC	84.25	0.904	1.919	C. floridanus
W167-79GGC	84.25	0.958	1.875	C. floridanus
W167-79GGC	84.25	1.004	1.894	C. floridanus
W167-79GGC	84.25	1.077	1.826	C. floridanus
W167-79GGC	84.75	0.905	1.851	C. floridanus
W167-79GGC	84.75	0.924	1.798	C. floridanus
W167-79GGC	84.75	0.936	1.872	C. floridanus
W167-79GGC	84.75	0.963	1.904	C. floridanus
W167-79GGC	85.25	0.358	2.053	C. floridanus
W167-79GGC	85.25	0.743	1.821	C. floridanus
W167-79GGC	85.25	0.86	1.842	C. floridanus
W167-79GGC	85.25	1.266	1.775	P. ariminensis
W167-79GGC	85.75	0.879	1.836	C. floridanus
W167-79GGC	85.75	0.879	1.849	C. floridanus
W167-79GGC	85.75	1.069	1.832	C. floridanus
W167-79GGC	85.75	1.206	1.769	P. ariminensis
W167-79GGC	86.25	0.958	1.8	C. floridanus
W167-79GGC	86.25	1.03	1.796	C. floridanus
W167-79GGC	86.25	1.059	1.855	C. floridanus
W167-79GGC	86.75	0.774	1.817	C. floridanus
W167-79GGC	86.75	0.776	1.803	C. floridanus
W167-79GGC	86.75	1.027	1.779	C. floridanus
W167-79GGC	86.75	1.053	1.87	C. floridanus
W167-79GGC	87.25	0.856	1.93	C. floridanus

W167-79GGC	87.25	0.902	1.833	C. floridanus
W167-79GGC	87.25	1.042	1.781	C. floridanus
W167-79GGC	87.25	1.058	1.887	C. floridanus
W167-79GGC	87.75	0.765	1.861	C. floridanus
W167-79GGC	87.75	1.05	1.801	C. floridanus
W167-79GGC	87.75	1.158	1.764	P. ariminensis
W167-79GGC	87.75	1.183	1.813	P. ariminensis
W167-79GGC	88.25	0.944	1.837	C. floridanus
W167-79GGC	88.25	0.971	1.945	C. floridanus
W167-79GGC	88.25	1.075	1.871	C. floridanus
W167-79GGC	88.25	1.141	1.716	P. ariminensis
W167-79GGC	88.75	0.782	1.924	C. floridanus
W167-79GGC	88.75	0.812	2.154	C. floridanus
W167-79GGC	88.75	0.967	1.97	C. floridanus
W167-79GGC	88.75	1.014	1.969	C. floridanus
W167-79GGC	89.25	0.91	2.004	C. floridanus
W167-79GGC	89.25	0.975	1.832	C. floridanus
W167-79GGC	89.25	0.988	1.799	C. floridanus
W167-79GGC	89.25	1.025	1.938	C. floridanus
W167-79GGC	89.75	0.778	2.01	C. floridanus
W167-79GGC	89.75	0.982	1.896	C. floridanus
W167-79GGC	89.75	0.995	1.918	C. floridanus
W167-79GGC	89.75	1.255	1.742	P. ariminensis
W167-79GGC	90.25	0.655	1.798	C. floridanus
W167-79GGC	90.25	0.762	1.847	C. floridanus
W167-79GGC	90.25	1.094	1.791	C. floridanus
W167-79GGC	90.25	1.117	1.862	C. floridanus
W167-79GGC	90.75	0.818	1.642	C. floridanus
W167-79GGC	90.75	0.992	1.846	C. floridanus
W167-79GGC	90.75	1.004	1.91	C. floridanus
W167-79GGC	90.75	1.283	1.808	P. ariminensis
W167-79GGC	91.25	0.832	1.896	C. floridanus
W167-79GGC	91.25	0.935	1.766	C. floridanus
W167-79GGC	91.25	1.021	1.654	C. floridanus
W167-79GGC	91.25	1.028	1.811	C. floridanus
W167-79GGC	91.75	0.894	1.89	C. floridanus
W167-79GGC	91.75	0.957	1.781	C. floridanus
W167-79GGC	91.75	1.004	1.886	C. floridanus
W167-79GGC	91.75	1.058	1.923	C. floridanus
W167-79GGC	92.25	0.74	1.834	C. floridanus
W167-79GGC	92.25	0.823	1.781	C. floridanus
W167-79GGC	92.25	0.922	1.816	C. floridanus
W167-79GGC	92.25	1.144	1.848	C. floridanus
W167-79GGC	92.75	0.199	2.035	C. floridanus
W167-79GGC	92.75	0.756	1.824	C. floridanus
W167-79GGC	92.75	0.973	1.8	C. floridanus
W167-79GGC	92.75	1.014	1.827	C. floridanus
W167-79GGC	92.75	1.065	1.845	C. floridanus
W167-79GGC	93.25	0.74	1.786	C. floridanus
W167-79GGC	93.25	0.982	1.788	C. floridanus
W167-79GGC	93.25	1.024	1.84	C. floridanus
W167-79GGC	93.25	1.094	1.79	C. floridanus
W167-79GGC	93.75	0.904	1.761	C. floridanus
W167-79GGC	93.75	1.042	1.942	C. floridanus
W167-79GGC	93.75	1.079	1.876	C. floridanus

W167-79GGC	93.75	1.099	1.877	C. floridanus
W167-79GGC	94.25	0.882	1.841	C. floridanus
W167-79GGC	94.25	0.981	1.756	C. floridanus
W167-79GGC	94.25	1.049	1.899	C. floridanus
W167-79GGC	94.25	1.308	1.913	P. ariminensis
W167-79GGC	94.75	0.327	2.125	C. floridanus
W167-79GGC	94.75	0.94	1.685	C. floridanus
W167-79GGC	94.75	1.017	1.899	C. floridanus
W167-79GGC	94.75	1.072	1.945	C. floridanus
W167-79GGC	95.25	0.904	1.925	C. floridanus
W167-79GGC	95.25	0.954	1.844	C. floridanus
W167-79GGC	95.25	0.957	1.809	C. floridanus
W167-79GGC	95.25	1.051	1.966	C. floridanus
W167-79GGC	95.75	0.789	1.971	C. floridanus
W167-79GGC	95.75	0.905	1.804	C. floridanus
W167-79GGC	95.75	1.013	1.854	C. floridanus
W167-79GGC	95.75	1.055	1.858	C. floridanus
W167-79GGC	96.25	0.821	1.845	C. floridanus
W167-79GGC	96.25	0.999	1.811	C. floridanus
W167-79GGC	96.25	1.025	1.901	C. floridanus
W167-79GGC	96.25	1.137	1.985	C. floridanus
W167-79GGC	96.75	0.893	1.778	C. floridanus
W167-79GGC	96.75	0.982	1.76	C. floridanus
W167-79GGC	96.75	1.017	1.797	C. floridanus
W167-79GGC	96.75	1.093	1.876	C. floridanus
W167-79GGC	97.25	0.647	2.153	C. floridanus
W167-79GGC	97.25	0.975	1.693	C. floridanus
W167-79GGC	97.25	1.044	1.831	C. floridanus
W167-79GGC	97.25	1.056	1.844	C. floridanus
W167-79GGC	97.25	1.159	1.996	P. ariminensis
W167-79GGC	97.75	0.836	1.827	C. floridanus
W167-79GGC	97.75	0.933	1.978	C. floridanus
W167-79GGC	97.75	1.054	1.907	C. floridanus
W167-79GGC	97.75	1.077	1.933	C. floridanus
W167-79GGC	98.25	0.951	1.845	C. floridanus
W167-79GGC	98.25	1.007	1.874	C. floridanus
W167-79GGC	98.25	1.033	1.814	C. floridanus
W167-79GGC	98.25	1.075	1.824	C. floridanus
W167-79GGC	98.75	0.831	1.778	C. floridanus
W167-79GGC	98.75	0.957	1.858	C. floridanus
W167-79GGC	98.75	1.097	1.942	C. floridanus
W167-79GGC	98.75	1.116	1.873	C. floridanus
W167-79GGC	99.25	0.874	1.91	C. floridanus
W167-79GGC	99.25	0.97	1.775	C. floridanus
W167-79GGC	99.25	0.973	1.915	C. floridanus
W167-79GGC	99.25	0.982	1.965	C. floridanus
W167-79GGC	99.75	0.922	1.963	C. floridanus
W167-79GGC	99.75	0.977	1.88	C. floridanus
W167-79GGC	99.75	1.01	1.944	C. floridanus
W167-79GGC	99.75	1.109	2.002	C. floridanus
W167-79GGC	100.25	0.783	1.789	C. floridanus
W167-79GGC	100.25	0.787	1.985	C. floridanus
W167-79GGC	100.25	1.12	1.918	C. floridanus
W167-79GGC	100.25	1.303	1.702	P. ariminensis
W167-79GGC	100.75	0.832	1.799	C. floridanus

W167-79GGC	100.75	0.891	1.879	C. floridanus
W167-79GGC	100.75	0.981	1.932	C. floridanus
W167-79GGC	100.75	0.992	1.889	C. floridanus
W167-79GGC	101.25	0.867	1.805	C. floridanus
W167-79GGC	101.25	0.935	1.917	C. floridanus
W167-79GGC	101.25	0.993	1.888	C. floridanus
W167-79GGC	101.25	1.057	1.957	C. floridanus
W167-79GGC	101.75	0.875	1.852	C. floridanus
W167-79GGC	101.75	0.897	1.969	C. floridanus
W167-79GGC	101.75	0.987	2.118	C. floridanus
W167-79GGC	101.75	1.014	1.773	C. floridanus
W167-79GGC	102.25	0.124	2.117	C. floridanus
W167-79GGC	102.25	0.954	1.897	C. floridanus
W167-79GGC	102.25	0.983	1.788	C. floridanus
W167-79GGC	102.25	0.993	1.858	C. floridanus
W167-79GGC	102.75	0.491	1.998	C. floridanus
W167-79GGC	102.75	0.768	1.811	C. floridanus
W167-79GGC	102.75	0.985	1.909	C. floridanus
W167-79GGC	102.75	1.249	1.666	P. ariminensis
W167-79GGC	103.25	0.873	1.91	C. floridanus
W167-79GGC	103.25	0.925	1.911	C. floridanus
W167-79GGC	103.25	0.999	1.891	C. floridanus
W167-79GGC	103.25	1.049	2.081	C. floridanus
W167-79GGC	103.75	0.99	1.972	C. floridanus
W167-79GGC	103.75	1.014	1.772	C. floridanus
W167-79GGC	103.75	1.037	1.762	C. floridanus
W167-79GGC	103.75	1.056	1.818	C. floridanus
W167-79GGC	104.25	0.86	1.87	C. floridanus
W167-79GGC	104.25	0.894	1.714	C. floridanus
W167-79GGC	104.25	0.972	1.899	C. floridanus
W167-79GGC	104.25	1.043	1.887	C. floridanus
W167-79GGC	104.75	0.827	1.826	C. floridanus
W167-79GGC	104.75	0.951	1.729	C. floridanus
W167-79GGC	104.75	1.022	1.805	C. floridanus
W167-79GGC	104.75	1.079	1.919	C. floridanus
W167-79GGC	105.25	0.179	2.141	C. floridanus
W167-79GGC	105.25	0.668	1.726	C. floridanus
W167-79GGC	105.25	1.011	1.813	C. floridanus
W167-79GGC	105.25	1.07	1.813	C. floridanus
W167-79GGC	105.75	0.949	1.611	C. floridanus
W167-79GGC	105.75	0.999	1.8	C. floridanus
W167-79GGC	105.75	1.04	1.844	C. floridanus
W167-79GGC	105.75	1.237	1.756	P. ariminensis
W167-79GGC	106.25	0.829	2	C. floridanus
W167-79GGC	106.25	0.901	1.876	C. floridanus
W167-79GGC	106.25	0.957	1.918	C. floridanus
W167-79GGC	106.25	0.991	1.926	C. floridanus
W167-79GGC	106.75	0.774	1.934	C. floridanus
W167-79GGC	106.75	0.965	1.841	C. floridanus
W167-79GGC	106.75	0.967	1.844	C. floridanus
W167-79GGC	106.75	0.971	1.865	C. floridanus
W167-79GGC	107.25	0.599	1.748	C. floridanus
W167-79GGC	107.25	1.011	1.79	C. floridanus
W167-79GGC	107.25	1.071	1.766	C. floridanus
W167-79GGC	107.25	1.074	1.915	C. floridanus

W167-79GGC	107.75	0.764	1.701	C. floridanus
W167-79GGC	107.75	0.981	1.786	C. floridanus
W167-79GGC	107.75	1.038	1.811	C. floridanus
W167-79GGC	107.75	1.27	1.786	P. ariminensis
W167-79GGC	108.25	0.644	2.141	C. floridanus
W167-79GGC	108.25	0.707	1.836	C. floridanus
W167-79GGC	108.25	0.99	1.828	C. floridanus
W167-79GGC	108.25	1.127	1.814	C. floridanus
W167-79GGC	108.75	0.912	1.924	C. floridanus
W167-79GGC	108.75	1.057	1.808	C. floridanus
W167-79GGC	108.75	1.084	1.792	C. floridanus
W167-79GGC	108.75	1.266	1.796	P. ariminensis
W167-79GGC	109.25	0.778	1.791	C. floridanus
W167-79GGC	109.25	0.791	1.858	C. floridanus
W167-79GGC	109.25	1.108	1.941	C. floridanus
W167-79GGC	109.25	1.26	1.819	P. ariminensis
W167-79GGC	109.75	1.014	1.897	C. floridanus
W167-79GGC	109.75	1.101	1.922	C. floridanus
W167-79GGC	109.75	1.19	1.729	P. ariminensis
W167-79GGC	109.75	1.262	1.871	P. ariminensis
W167-79GGC	110.25	1.137	1.458	P. ariminensis
W167-79GGC	110.25	1.155	1.793	P. ariminensis
W167-79GGC	110.25	1.195	1.747	P. ariminensis
W167-79GGC	110.25	1.229	1.75	P. ariminensis
W167-79GGC	110.75	1.075	1.991	C. floridanus
W167-79GGC	110.75	1.185	1.943	C. floridanus
W167-79GGC	110.75	1.259	1.809	P. ariminensis
W167-79GGC	110.75	1.266	1.815	P. ariminensis
W167-79GGC	111.25	1.008	1.874	C. floridanus
W167-79GGC	111.25	1.012	1.962	C. floridanus
W167-79GGC	111.25	1.273	1.84	P. ariminensis
W167-79GGC	111.25	1.328	1.724	P. ariminensis
W167-79GGC	111.75	0.799	1.797	C. floridanus
W167-79GGC	111.75	1.062	1.876	C. floridanus
W167-79GGC	111.75	1.171	1.772	P. ariminensis
W167-79GGC	111.75	1.305	1.749	P. ariminensis
W167-79GGC	112.25	0.961	1.79	C. floridanus
W167-79GGC	112.25	1.03	1.856	C. floridanus
W167-79GGC	112.25	1.213	1.656	P. ariminensis
W167-79GGC	112.25	1.222	1.848	P. ariminensis
W167-79GGC	112.75	0.723	2.089	C. floridanus
W167-79GGC	112.75	0.984	1.899	C. floridanus
W167-79GGC	112.75	1.019	2.009	C. floridanus
W167-79GGC	112.75	1.295	1.717	P. ariminensis
W167-79GGC	113.25	0.303	1.944	C. floridanus
W167-79GGC	113.25	1.03	1.81	C. floridanus
W167-79GGC	113.25	1.105	1.995	P. ariminensis
W167-79GGC	113.25	1.238	1.778	P. ariminensis
W167-79GGC	113.75	0.68	1.588	C. floridanus
W167-79GGC	113.75	0.904	1.856	P. ariminensis
W167-79GGC	113.75	0.969	1.753	C. floridanus
W167-79GGC	113.75	1.064	1.762	P. ariminensis
W167-79GGC	114.25	0.985	1.827	C. floridanus
W167-79GGC	114.25	1.036	1.999	C. floridanus
W167-79GGC	114.25	1.07	1.868	C. floridanus

W167-79GGC	114.25	1.201	1.908	P. ariminensis
W167-79GGC	114.75	0.924	2.009	P. ariminensis
W167-79GGC	114.75	1.057	1.951	C. floridanus
W167-79GGC	114.75	1.2	1.711	P. ariminensis
W167-79GGC	114.75	1.259	1.88	P. ariminensis
W167-79GGC	115.25	0.121	2.127	C. floridanus
W167-79GGC	115.25	0.317	2.152	C. floridanus
W167-79GGC	115.25	0.476	2.001	C. floridanus
W167-79GGC	115.25	1.064	1.755	C. floridanus
W167-79GGC	115.75	0.27	2.042	C. floridanus
W167-79GGC	115.75	0.331	2.243	C. floridanus
W167-79GGC	115.75	0.38	2.011	C. floridanus
W167-79GGC	115.75	0.941	1.887	C. floridanus
W167-79GGC	116.25	0.982	1.806	C. floridanus
W167-79GGC	116.25	1.118	1.895	P. ariminensis
W167-79GGC	116.25	1.24	1.778	C. floridanus
W167-79GGC	116.25	1.318	1.845	P. ariminensis
W167-79GGC	116.75	0.779	1.931	C. floridanus
W167-79GGC	116.75	1.148	1.914	P. ariminensis
W167-79GGC	116.75	1.249	1.789	P. ariminensis
W167-79GGC	116.75	1.304	1.81	P. ariminensis
W167-79GGC	117.25	0.981	2.022	C. floridanus
W167-79GGC	117.25	1.215	1.735	P. ariminensis
W167-79GGC	117.25	1.293	1.74	P. ariminensis
W167-79GGC	117.25	1.308	1.953	P. ariminensis
W167-79GGC	117.75	0.96	1.802	C. floridanus
W167-79GGC	117.75	1.079	1.858	P. ariminensis
W167-79GGC	117.75	1.225	1.725	P. ariminensis
W167-79GGC	117.75	1.288	1.796	P. ariminensis
W167-79GGC	118.25	0.877	1.853	C. floridanus
W167-79GGC	118.25	0.99	1.825	C. floridanus
W167-79GGC	118.25	1.066	1.453	P. ariminensis
W167-79GGC	118.25	1.32	1.729	P. ariminensis
W167-79GGC	118.75	1.081	1.969	C. floridanus
W167-79GGC	118.75	1.11	1.682	C. floridanus
W167-79GGC	118.75	1.256	1.778	P. ariminensis
W167-79GGC	118.75	1.267	1.838	P. ariminensis
W167-79GGC	119.25	0.813	1.986	C. floridanus
W167-79GGC	119.25	0.886	1.791	C. floridanus
W167-79GGC	119.25	1.168	1.625	P. ariminensis
W167-79GGC	119.25	1.324	1.671	P. ariminensis
W167-79GGC	119.75	0.949	1.853	C. floridanus
W167-79GGC	119.75	0.976	1.869	C. floridanus
W167-79GGC	119.75	0.993	1.864	C. floridanus
W167-79GGC	119.75	1.316	1.692	P. ariminensis
W167-79GGC	120.25	1.06	1.92	C. floridanus
W167-79GGC	120.25	1.114	1.846	C. floridanus
W167-79GGC	120.25	1.127	1.905	C. floridanus
W167-79GGC	120.25	1.181	1.786	P. ariminensis
W167-79GGC	120.75	1.143	1.757	P. ariminensis
W167-79GGC	120.75	1.248	1.729	P. ariminensis
W167-79GGC	120.75	1.301	1.855	C. floridanus
W167-79GGC	120.75	1.313	1.732	P. ariminensis
W167-79GGC	121.25	1.089	2.063	C. floridanus
W167-79GGC	121.25	1.099	1.608	P. ariminensis

W167-79GGC	121.25	1.153	1.854	C. floridanus
W167-79GGC	121.25	1.287	1.756	P. ariminensis
W167-79GGC	121.75	0.971	1.721	C. floridanus
W167-79GGC	121.75	0.989	1.89	C. floridanus
W167-79GGC	121.75	1.003	1.813	C. floridanus
W167-79GGC	121.75	1.012	1.851	C. floridanus
W167-79GGC	122.25	0.888	1.961	C. floridanus
W167-79GGC	122.25	0.996	1.802	C. floridanus
W167-79GGC	122.25	1.152	1.609	P. ariminensis
W167-79GGC	122.25	1.167	1.86	P. ariminensis
W167-79GGC	122.75	0.848	1.932	C. floridanus
W167-79GGC	122.75	0.853	1.949	C. floridanus
W167-79GGC	122.75	0.933	1.676	C. floridanus
W167-79GGC	122.75	1.016	1.769	C. floridanus
W167-79GGC	123.25	0.861	1.844	C. floridanus
W167-79GGC	123.25	0.867	1.818	C. floridanus
W167-79GGC	123.25	1.027	1.935	C. floridanus
W167-79GGC	123.25	1.107	1.685	P. ariminensis
W167-79GGC	123.75	0.555	2.058	C. floridanus
W167-79GGC	123.75	0.876	2.047	C. floridanus
W167-79GGC	123.75	1.074	1.882	C. floridanus
W167-79GGC	123.75	1.255	1.7	P. ariminensis
W167-79GGC	124.25	0.604	2.001	C. floridanus
W167-79GGC	124.25	0.994	1.851	C. floridanus
W167-79GGC	124.25	1.106	1.948	C. floridanus
W167-79GGC	124.25	1.241	1.747	P. ariminensis
W167-79GGC	124.75	0.76	1.782	C. floridanus
W167-79GGC	124.75	0.99	1.808	C. floridanus
W167-79GGC	124.75	1.163	1.863	C. floridanus
W167-79GGC	124.75	1.209	1.8	P. ariminensis
W167-79GGC	125.25	0.849	1.718	C. floridanus
W167-79GGC	125.25	1.114	1.866	C. floridanus
W167-79GGC	125.25	1.131	1.864	C. floridanus
W167-79GGC	125.25	1.218	1.767	P. ariminensis
W167-79GGC	125.75	0.763	1.782	C. floridanus
W167-79GGC	125.75	0.794	2.107	C. floridanus
W167-79GGC	125.75	1.025	1.887	C. floridanus
W167-79GGC	125.75	1.126	1.552	P. ariminensis
W167-79GGC	126.25	0.856	2.092	C. floridanus
W167-79GGC	126.25	0.973	1.867	C. floridanus
W167-79GGC	126.25	1.007	1.939	C. floridanus
W167-79GGC	126.25	1.286	1.761	P. ariminensis
W167-79GGC	126.75	0.93	1.938	C. floridanus
W167-79GGC	126.75	1.001	1.86	C. floridanus
W167-79GGC	126.75	1.002	1.771	C. floridanus
W167-79GGC	126.75	1.018	1.866	C. floridanus
W167-79GGC	127.5	0.951	1.884	C. floridanus
W167-79GGC	127.5	1.008	1.865	C. floridanus
W167-79GGC	127.5	1.056	1.855	C. floridanus
W167-79GGC	127.5	1.113	1.851	C. floridanus

GREAT BAHAMA BANK CORE SITES

CORE	DEPTH	C13	O18	SPECIES
KNR166-2-93GGC	38.5	1.854	0.267	C. floridanus
KNR166-2-93GGC	38.5	1.732	0.304	C. floridanus
KNR166-2-93GGC	39.5	1.960	0.120	C. floridanus
KNR166-2-93GGC	42.5	1.707	0.071	C. floridanus
KNR166-2-93GGC	42.5	1.764	0.138	C. floridanus
KNR166-2-93GGC	42.5	1.867	0.018	C. floridanus
KNR166-2-93GGC	43.5	1.683	0.111	C. floridanus
KNR166-2-93GGC	44.5	1.595	0.266	C. floridanus
KNR166-2-93GGC	45.5	1.783	0.178	C. floridanus
KNR166-2-93GGC	46.5	1.533	0.242	C. floridanus
KNR166-2-93GGC	47.5	1.743	0.096	C. floridanus
KNR166-2-93GGC	48.5	1.625	0.144	C. floridanus
KNR166-2-93GGC	49.5	1.742	0.076	C. floridanus
KNR166-2-93GGC	50.5	1.697	0.029	C. floridanus
KNR166-2-93GGC	51.5	1.636	0.014	C. floridanus
KNR166-2-93GGC	52.5	1.736	0.209	C. floridanus
KNR166-2-93GGC	53.5	1.656	0.211	C. floridanus
KNR166-2-93GGC	54.5	1.824	0.107	C. floridanus
KNR166-2-93GGC	55.5	1.540	0.141	C. floridanus
KNR166-2-93GGC	56.5	1.733	0.136	C. floridanus
KNR166-2-93GGC	58.5	1.601	0.187	C. floridanus
KNR166-2-93GGC	60.5	1.748	0.088	C. floridanus
KNR166-2-93GGC	62.5	1.829	0.187	C. floridanus
KNR166-2-93GGC	64.5	1.604	0.109	C. floridanus
KNR166-2-93GGC	66.5	1.720	0.068	C. floridanus
KNR166-2-93GGC	68.5	1.632	0.301	C. floridanus
KNR166-2-93GGC	70.5	1.581	0.067	C. floridanus
KNR166-2-93GGC	70.5	1.723	0.215	C. floridanus
KNR166-2-93GGC	74.5	1.579	0.199	C. floridanus
KNR166-2-93GGC	76.5	1.686	0.186	C. floridanus
KNR166-2-93GGC	78.5	1.733	0.107	C. floridanus
KNR166-2-93GGC	82.5	1.689	0.230	C. floridanus
KNR166-2-93GGC	82.5	1.493	0.137	C. floridanus
KNR166-2-93GGC	82.5	1.729	0.045	C. floridanus
KNR166-2-93GGC	86.5	1.761	0.093	C. floridanus
KNR166-2-93GGC	93.5	1.728	0.236	C. floridanus
KNR166-2-93GGC	94.5	1.699	0.241	C. floridanus
KNR166-2-93GGC	96.5	1.640	0.115	C. floridanus
KNR166-2-93GGC	98.5	1.843	0.249	C. floridanus
KNR166-2-93GGC	100.5	1.607	0.265	C. floridanus
KNR166-2-93GGC	102.5	1.730	0.117	C. floridanus
KNR166-2-93GGC	106.5	1.696	0.412	C. floridanus
KNR166-2-93GGC	106.5	1.687	0.153	C. floridanus
KNR166-2-93GGC	108.5	1.678	0.123	C. floridanus
KNR166-2-93GGC	108.5	1.677	0.395	C. floridanus
KNR166-2-93GGC	114.5	1.552	0.204	C. floridanus
KNR166-2-93GGC	116.5	1.536	0.201	C. floridanus
KNR166-2-93GGC	118.5	1.678	0.209	C. floridanus
KNR166-2-93GGC	118.5	1.772	0.238	C. floridanus
KNR166-2-93GGC	124.5	1.867	0.328	C. floridanus

KNR166-2-93GGC	124.5	1.679	0.129	C. floridanus
KNR166-2-93GGC	126.5	1.754	0.137	C. floridanus
KNR166-2-93GGC	130.5	1.912	0.180	C. floridanus
KNR166-2-93GGC	130.5	1.758	0.208	C. floridanus
KNR166-2-93GGC	132.5	1.707	0.177	C. floridanus
KNR166-2-93GGC	134.5	1.624	0.203	C. floridanus
KNR166-2-93GGC	136.5	2.009	0.112	C. floridanus
KNR166-2-93GGC	151.5	1.595	0.145	C. floridanus
KNR166-2-93GGC	151.5	1.678	0.066	C. floridanus
KNR166-2-93GGC	155.5	1.862	-0.076	C. floridanus
KNR166-2-93GGC	155.5	1.839	0.182	C. floridanus
KNR166-2-93GGC	155.5	1.620	0.177	C. floridanus
KNR166-2-93GGC	157.5	1.776	0.161	C. floridanus
KNR166-2-93GGC	157.5	1.574	-0.083	C. floridanus
KNR166-2-93GGC	159.5	1.964	0.185	C. floridanus
KNR166-2-93GGC	159.5	1.895	0.044	C. floridanus
KNR166-2-93GGC	159.5	1.867	0.089	C. floridanus
KNR166-2-93GGC	161.5	1.807	0.045	C. floridanus
KNR166-2-93GGC	161.5	1.453	0.096	C. floridanus
KNR166-2-93GGC	163.5	1.557	0.133	C. floridanus
KNR166-2-93GGC	163.5	1.780	0.180	C. floridanus
KNR166-2-93GGC	165.5	1.688	0.096	C. floridanus
KNR166-2-93GGC	165.5	1.895	0.100	C. floridanus
KNR166-2-93GGC	167.5	1.512	0.098	C. floridanus
KNR166-2-93GGC	167.5	1.771	0.159	C. floridanus
KNR166-2-93GGC	167.5	1.905	0.323	C. floridanus
KNR166-2-93GGC	169.5	1.623	0.106	C. floridanus
KNR166-2-93GGC	169.5	1.830	0.205	C. floridanus
KNR166-2-93GGC	169.5	1.726	0.133	C. floridanus
KNR166-2-93GGC	171.5	1.691	0.129	C. floridanus
KNR166-2-93GGC	171.5	1.642	0.033	C. floridanus
KNR166-2-93GGC	173.5	1.929	0.194	C. floridanus
KNR166-2-93GGC	173.5	1.998	0.214	C. floridanus
KNR166-2-93GGC	175.5	1.878	0.140	C. floridanus
KNR166-2-93GGC	175.5	1.819	0.138	C. floridanus
KNR166-2-93GGC	179.5	1.795	0.155	C. floridanus
KNR166-2-93GGC	179.5	1.744	0.234	C. floridanus
KNR166-2-93GGC	181.5	1.924	0.112	C. floridanus
KNR166-2-93GGC	181.5	1.704	0.141	C. floridanus
KNR166-2-93GGC	181.5	1.847	0.224	C. floridanus
KNR166-2-93GGC	183.5	1.705	0.081	C. floridanus
KNR166-2-93GGC	183.5	1.764	0.113	C. floridanus
KNR166-2-93GGC	183.5	1.835	0.257	C. floridanus
KNR166-2-93GGC	185.5	1.594	-0.158	C. floridanus
KNR166-2-93GGC	185.5	1.712	0.175	C. floridanus
KNR166-2-93GGC	185.5	1.734	-0.035	C. floridanus
KNR166-2-93GGC	187.5	1.696	0.059	C. floridanus
KNR166-2-93GGC	189.5	1.715	0.048	C. floridanus
KNR166-2-93GGC	189.5	1.629	-0.031	C. floridanus
KNR166-2-93GGC	189.5	2.048	-0.046	C. floridanus
KNR166-2-93GGC	191.5	1.765	0.052	C. floridanus
KNR166-2-93GGC	191.5	1.763	0.132	C. floridanus
KNR166-2-93GGC	191.5	1.794	0.127	C. floridanus
KNR166-2-93GGC	193.5	1.757	0.264	C. floridanus
KNR166-2-93GGC	193.5	1.769	0.243	C. floridanus

KNR166-2-93GGC	195.5	1.722	0.082	C. floridanus
KNR166-2-93GGC	195.5	1.711	0.057	C. floridanus
KNR166-2-93GGC	195.5	1.932	0.156	C. floridanus
KNR166-2-93GGC	197.5	2.039	0.057	C. floridanus
KNR166-2-93GGC	197.5	2.019	0.118	C. floridanus
KNR166-2-93GGC	199.5	1.781	0.084	C. floridanus
KNR166-2-93GGC	199.5	1.648	0.062	C. floridanus
KNR166-2-93GGC	201.5	1.974	0.118	C. floridanus
KNR166-2-93GGC	201.5	1.713	0.059	C. floridanus
KNR166-2-93GGC	203.5	1.785	0.153	C. floridanus
KNR166-2-93GGC	203.5	1.668	0.045	C. floridanus
KNR166-2-93GGC	203.5	1.794	0.144	C. floridanus
KNR166-2-93GGC	205.5	1.900	0.005	C. floridanus
KNR166-2-93GGC	205.5	1.778	0.030	C. floridanus
KNR166-2-93GGC	221.5	1.559	0.217	C. floridanus
KNR166-2-93GGC	221.5	1.696	0.236	C. floridanus
KNR166-2-93GGC	221.5	1.609	0.141	C. floridanus
KNR166-2-93GGC	223.5	1.660	0.074	C. floridanus
KNR166-2-93GGC	223.5	1.608	0.091	C. floridanus
KNR166-2-93GGC	223.5	1.672	0.040	C. floridanus
KNR166-2-93GGC	225.5	1.558	0.106	C. floridanus
KNR166-2-93GGC	225.5	1.755	0.195	C. floridanus
KNR166-2-93GGC	225.5	1.766	0.059	C. floridanus
KNR166-2-93GGC	227.5	1.846	0.008	C. floridanus
KNR166-2-93GGC	227.5	1.569	0.151	C. floridanus
KNR166-2-93GGC	227.5	1.821	0.051	C. floridanus
KNR166-2-93GGC	229.5	1.505	0.133	C. floridanus
KNR166-2-93GGC	229.5	1.737	0.214	C. floridanus
KNR166-2-93GGC	231.5	1.773	0.109	C. floridanus
KNR166-2-93GGC	231.5	1.830	0.239	C. floridanus
KNR166-2-93GGC	231.5	1.546	0.195	C. floridanus
KNR166-2-93GGC	233.5	1.532	0.230	C. floridanus
KNR166-2-93GGC	233.5	1.673	0.063	C. floridanus
KNR166-2-93GGC	233.5	1.692	0.194	C. floridanus
KNR166-2-93GGC	237.5	1.749	0.146	C. floridanus
KNR166-2-93GGC	237.5	1.673	0.201	C. floridanus
KNR166-2-93GGC	239.5	1.757	0.223	C. floridanus
KNR166-2-93GGC	243.5	1.579	0.235	C. floridanus
KNR166-2-93GGC	245.5	1.770	0.150	C. floridanus
KNR166-2-93GGC	247.5	1.825	0.201	C. floridanus
KNR166-2-93GGC	249.5	1.748	0.172	C. floridanus
KNR166-2-93GGC	249.5	1.737	0.210	C. floridanus
KNR166-2-93GGC	251.5	1.678	0.243	C. floridanus
KNR166-2-93GGC	255.5	1.845	0.286	C. floridanus
KNR166-2-93GGC	257.5	1.684	0.206	C. floridanus
KNR166-2-93GGC	257.5	1.593	0.178	C. floridanus
KNR166-2-93GGC	259.5	1.611	0.139	C. floridanus
KNR166-2-93GGC	259.5	1.780	0.281	C. floridanus
KNR166-2-93GGC	263.5	1.645	0.078	C. floridanus
KNR166-2-93GGC	263.5	1.742	0.114	C. floridanus
KNR166-2-93GGC	263.5	1.675	0.141	C. floridanus
KNR166-2-93GGC	265.5	1.640	0.131	C. floridanus
KNR166-2-93GGC	265.5	1.556	0.047	C. floridanus
KNR166-2-93GGC	267.5	1.333	-0.020	C. floridanus
KNR166-2-93GGC	267.5	1.749	0.115	C. floridanus

KNR166-2-93GGC	267.5	1.671	0.132	C. floridanus
KNR166-2-93GGC	269.5	1.675	0.150	C. floridanus
KNR166-2-93GGC	269.5	1.620	0.097	C. floridanus
KNR166-2-93GGC	269.5	1.698	0.221	C. floridanus
KNR166-2-93GGC	271.5	1.677	0.228	C. floridanus
KNR166-2-93GGC	271.5	1.677	0.154	C. floridanus
KNR166-2-93GGC	271.5	1.725	0.098	C. floridanus
KNR166-2-93GGC	271.5	1.844	0.088	C. floridanus

CORE	DEPTH	C13	O18	SPECIES
KNR166-2-94MC-C	0.5	1.751	0.182	C. floridanus
KNR166-2-94MC-C	0.5	1.133	0.194	C. floridanus
KNR166-2-94MC-C	0.5	1.174	0.069	C. floridanus
KNR166-2-94MC-C	0.5	1.152	0.090	C. floridanus
KNR166-2-94MC-C	1.5	1.095	-0.051	C. floridanus
KNR166-2-94MC-C	1.5	1.217	0.137	C. floridanus
KNR166-2-94MC-C	1.5	1.608	-0.030	C. floridanus
KNR166-2-94MC-C	1.5	1.120	0.055	C. floridanus
KNR166-2-94MC-C	2.5	1.405	-0.248	C. floridanus
KNR166-2-94MC-C	2.5	1.299	0.124	C. floridanus
KNR166-2-94MC-C	2.5	1.571	0.072	C. floridanus
KNR166-2-94MC-C	2.5	1.001	0.028	C. floridanus
KNR166-2-94MC-C	3.5	1.051	-0.036	C. floridanus
KNR166-2-94MC-C	3.5	1.597	0.146	C. floridanus
KNR166-2-94MC-C	3.5	1.430	0.031	C. floridanus
KNR166-2-94MC-C	3.5	1.023	0.046	C. floridanus
KNR166-2-94MC-C	4.5	1.408	0.144	C. floridanus
KNR166-2-94MC-C	4.5	1.628	0.066	C. floridanus
KNR166-2-94MC-C	4.5	1.778	0.090	C. floridanus
KNR166-2-94MC-C	4.5	1.327	0.039	C. floridanus
KNR166-2-94MC-C	5.5	1.383	0.120	C. floridanus
KNR166-2-94MC-C	5.5	1.332	0.167	C. floridanus
KNR166-2-94MC-C	5.5	1.277	-0.020	C. floridanus
KNR166-2-94MC-C	5.5	1.585	0.149	C. floridanus
KNR166-2-94MC-C	6.5	1.305	0.015	C. floridanus
KNR166-2-94MC-C	6.5	1.659	0.189	C. floridanus
KNR166-2-94MC-C	6.5	1.153	0.097	C. floridanus
KNR166-2-94MC-C	6.5	1.118	-0.246	C. floridanus
KNR166-2-94MC-C	7.5	1.636	0.128	C. floridanus
KNR166-2-94MC-C	7.5	1.244	0.146	C. floridanus
KNR166-2-94MC-C	7.5	1.355	0.095	C. floridanus
KNR166-2-94MC-C	7.5	1.860	0.173	C. floridanus
KNR166-2-94MC-C	8.5	1.500	0.147	C. floridanus
KNR166-2-94MC-C	8.5	1.757	0.199	C. floridanus
KNR166-2-94MC-C	8.5	1.440	0.067	C. floridanus
KNR166-2-94MC-C	8.5	1.619	0.067	C. floridanus
KNR166-2-94MC-C	9.5	1.330	0.210	C. floridanus
KNR166-2-94MC-C	9.5	1.569	0.220	C. floridanus
KNR166-2-94MC-C	9.5	1.609	0.086	C. floridanus
KNR166-2-94MC-C	9.5	1.328	0.218	C. floridanus
KNR166-2-94MC-C	10.5	1.867	0.157	C. floridanus
KNR166-2-94MC-C	10.5	1.261	0.138	C. floridanus
KNR166-2-94MC-C	10.5	1.181	0.038	C. floridanus
KNR166-2-94MC-C	11.5	1.723	0.155	C. floridanus
KNR166-2-94MC-C	11.5	1.719	0.354	C. floridanus
KNR166-2-94MC-C	11.5	1.603	0.038	C. floridanus
KNR166-2-94MC-C	11.5	1.634	0.165	C. floridanus
KNR166-2-94MC-C	11.5	1.483	0.199	C. floridanus
KNR166-2-94MC-C	12.5	1.494	0.211	C. floridanus
KNR166-2-94MC-C	12.5	1.936	-0.186	C. floridanus
KNR166-2-94MC-C	12.5	1.671	0.111	C. floridanus
KNR166-2-94MC-C	12.5	1.503	0.219	C. floridanus
KNR166-2-94MC-C	13.5	1.625	0.182	C. floridanus
KNR166-2-94MC-C	13.5	1.316	0.203	C. floridanus

KNR166-2-94MC-C	13.5	1.371	0.189	C. floridanus
KNR166-2-94MC-C	13.5	1.683	0.227	C. floridanus
KNR166-2-94MC-C	14.5	1.790	0.165	C. floridanus
KNR166-2-94MC-C	14.5	1.484	0.086	C. floridanus
KNR166-2-94MC-C	14.5	1.725	0.014	C. floridanus
KNR166-2-94MC-C	14.5	1.261	0.194	C. floridanus
KNR166-2-94MC-C	15.5	1.989	-0.044	C. floridanus
KNR166-2-94MC-C	15.5	1.506	0.122	C. floridanus
KNR166-2-94MC-C	16.5	1.610	0.082	C. floridanus
KNR166-2-94MC-C	16.5	1.867	0.300	C. floridanus
KNR166-2-94MC-C	16.5	1.790	0.002	C. floridanus
KNR166-2-94MC-C	16.5	1.257	0.195	C. floridanus
KNR166-2-94MC-C	17.5	1.822	0.102	C. floridanus
KNR166-2-94MC-C	17.5	1.702	0.231	C. floridanus
KNR166-2-94MC-C	17.5	1.736	0.087	C. floridanus
KNR166-2-94MC-C	17.5	1.844	0.316	C. floridanus
KNR166-2-94MC-C	19.5	1.682	0.246	C. floridanus
KNR166-2-94MC-C	19.5	1.344	0.042	C. floridanus
KNR166-2-94MC-C	19.5	1.870	0.048	C. floridanus
KNR166-2-94MC-C	19.5	1.631	0.178	C. floridanus
KNR166-2-94MC-C	20.5	1.857	0.182	C. floridanus
KNR166-2-94MC-C	20.5	1.751	0.212	C. floridanus
KNR166-2-94MC-C	20.5	1.605	0.218	C. floridanus
KNR166-2-94MC-C	21.5	1.338	0.088	C. floridanus
KNR166-2-94MC-C	21.5	1.194	0.032	C. floridanus
KNR166-2-94MC-C	21.5	1.697	0.211	C. floridanus
KNR166-2-94MC-C	21.5	1.687	0.236	C. floridanus
KNR166-2-94MC-C	22.5	1.571	0.022	C. floridanus
KNR166-2-94MC-C	22.5	1.657	0.262	C. floridanus
KNR166-2-94MC-C	22.5	1.279	0.107	C. floridanus
KNR166-2-94MC-C	22.5	1.327	0.125	C. floridanus
KNR166-2-94MC-C	23.5	1.526	0.113	C. floridanus
KNR166-2-94MC-C	23.5	1.976	0.149	C. floridanus
KNR166-2-94MC-C	23.5	1.621	0.123	C. floridanus
KNR166-2-94MC-C	23.5	1.564	0.029	C. floridanus
KNR166-2-94MC-C	24.5	1.936	0.194	C. floridanus
KNR166-2-94MC-C	24.5	1.819	0.116	C. floridanus
KNR166-2-94MC-C	24.5	1.766	0.221	C. floridanus
KNR166-2-94MC-C	24.5	1.979	-0.046	C. floridanus
KNR166-2-94MC-C	25.5	2.090	0.130	C. floridanus
KNR166-2-94MC-C	25.5	1.660	0.157	C. floridanus
KNR166-2-94MC-C	26.5	1.674	-0.056	C. floridanus
KNR166-2-94MC-C	26.5	1.626	0.112	C. floridanus
KNR166-2-94MC-C	26.5	1.722	0.108	C. floridanus
KNR166-2-94MC-C	27.5	1.779	0.144	C. floridanus
KNR166-2-94MC-C	27.5	2.152	-0.022	C. floridanus
KNR166-2-94MC-C	27.5	1.888	0.227	C. floridanus
KNR166-2-94MC-C	28.5	1.771	0.174	C. floridanus
KNR166-2-94MC-C	28.5	1.888	0.074	C. floridanus
KNR166-2-94MC-C	28.5	1.875	0.060	C. floridanus
KNR166-2-94MC-C	28.5	1.841	0.106	C. floridanus
KNR166-2-94MC-C	28.5	2.202	0.188	C. floridanus
KNR166-2-94MC-C	29.5	1.719	0.263	C. floridanus
KNR166-2-94MC-C	29.5	1.947	0.086	C. floridanus
KNR166-2-94MC-C	29.5	1.771	0.205	C. floridanus

KNR166-2-94MC-C	30.5	1.850	0.152	C. floridanus
KNR166-2-94MC-C	30.5	1.624	0.196	C. floridanus
KNR166-2-94MC-C	30.5	1.906	0.327	C. floridanus
KNR166-2-94MC-C	31.5	1.570	0.160	C. floridanus
KNR166-2-94MC-C	31.5	1.890	0.161	C. floridanus
KNR166-2-94MC-C	31.5	1.479	0.275	C. floridanus
KNR166-2-94MC-C	31.5	1.666	0.152	C. floridanus
KNR166-2-94MC-C	32.5	1.670	0.095	C. floridanus
KNR166-2-94MC-C	32.5	1.732	0.167	C. floridanus
KNR166-2-94MC-C	32.5	1.869	0.227	C. floridanus
KNR166-2-94MC-C	32.5	1.918	0.218	C. floridanus
KNR166-2-94MC-C	33.5	1.901	0.107	C. floridanus
KNR166-2-94MC-C	33.5	1.835	0.189	C. floridanus
KNR166-2-94MC-C	33.5	1.730	0.143	C. floridanus
KNR166-2-94MC-C	33.5	1.883	0.118	C. floridanus
KNR166-2-94MC-C	34.5	1.707	0.199	C. floridanus
KNR166-2-94MC-C	34.5	1.825	0.015	C. floridanus
KNR166-2-94MC-C	34.5	2.074	0.139	C. floridanus
KNR166-2-94MC-C	34.5	2.025	0.135	C. floridanus
KNR166-2-94MC-C	35.5	1.803	0.188	C. floridanus
KNR166-2-94MC-C	35.5	1.761	0.107	C. floridanus
KNR166-2-94MC-C	35.5	1.829	0.120	C. floridanus
KNR166-2-94MC-C	35.5	1.863	0.124	C. floridanus
KNR166-2-94MC-C	36.5	1.762	0.088	C. floridanus
KNR166-2-94MC-C	36.5	1.325	-0.007	C. floridanus
KNR166-2-94MC-C	36.5	1.572	0.114	C. floridanus
KNR166-2-94MC-C	36.5	1.865	0.220	C. floridanus

CORE	DEPTH	C13	O18	SPECIES
KNR166-2-117GGC	30.5	1.408	0.986	C. floridanus
KNR166-2-117GGC	30.5	1.447	0.996	C. floridanus
KNR166-2-117GGC	30.5	1.436	1.130	C. floridanus
KNR166-2-117GGC	30.5	1.508	1.144	C. floridanus
KNR166-2-117GGC	31.5	1.392	0.917	C. floridanus
KNR166-2-117GGC	31.5	1.380	0.922	C. floridanus
KNR166-2-117GGC	31.5	1.232	0.997	C. floridanus
KNR166-2-117GGC	31.5	1.244	0.998	C. floridanus
KNR166-2-117GGC	32.5	1.408	0.924	C. floridanus
KNR166-2-117GGC	32.5	1.254	0.969	C. floridanus
KNR166-2-117GGC	32.5	1.603	1.029	C. floridanus
KNR166-2-117GGC	32.5	1.179	1.116	C. floridanus
KNR166-2-117GGC	33.5	1.329	0.804	C. floridanus
KNR166-2-117GGC	33.5	1.339	0.928	C. floridanus
KNR166-2-117GGC	33.5	1.181	1.032	C. floridanus
KNR166-2-117GGC	33.5	1.327	1.064	C. floridanus
KNR166-2-117GGC	34.5	1.432	0.828	C. floridanus
KNR166-2-117GGC	34.5	1.294	0.928	C. floridanus
KNR166-2-117GGC	34.5	1.533	1.113	C. floridanus
KNR166-2-117GGC	34.5	1.327	1.176	C. floridanus
KNR166-2-117GGC	35.5	1.341	0.838	C. floridanus
KNR166-2-117GGC	35.5	1.338	0.956	C. floridanus
KNR166-2-117GGC	35.5	1.385	1.010	C. floridanus
KNR166-2-117GGC	35.5	1.419	1.041	C. floridanus
KNR166-2-117GGC	36.5	1.404	0.849	C. floridanus
KNR166-2-117GGC	36.5	1.313	0.926	C. floridanus
KNR166-2-117GGC	36.5	1.525	1.029	C. floridanus
KNR166-2-117GGC	36.5	1.216	1.148	C. floridanus
KNR166-2-117GGC	37.5	1.418	0.867	C. floridanus
KNR166-2-117GGC	37.5	1.369	0.926	C. floridanus
KNR166-2-117GGC	37.5	1.348	0.993	C. floridanus
KNR166-2-117GGC	37.5	1.411	1.178	C. floridanus
KNR166-2-117GGC	38.5	1.368	0.949	C. floridanus
KNR166-2-117GGC	38.5	1.355	0.950	C. floridanus
KNR166-2-117GGC	38.5	1.264	1.002	C. floridanus
KNR166-2-117GGC	38.5	1.413	1.229	C. floridanus
KNR166-2-117GGC	39.5	1.200	0.819	C. floridanus
KNR166-2-117GGC	39.5	1.198	0.919	C. floridanus
KNR166-2-117GGC	39.5	1.452	0.928	C. floridanus
KNR166-2-117GGC	39.5	1.366	1.018	C. floridanus
KNR166-2-117GGC	40.5	1.472	0.799	C. floridanus
KNR166-2-117GGC	40.5	1.306	0.830	C. floridanus
KNR166-2-117GGC	40.5	1.364	0.922	C. floridanus
KNR166-2-117GGC	40.5	1.214	1.319	C. floridanus
KNR166-2-117GGC	41.5	1.459	0.919	C. floridanus
KNR166-2-117GGC	41.5	1.368	0.937	C. floridanus
KNR166-2-117GGC	41.5	1.224	0.994	C. floridanus
KNR166-2-117GGC	41.5	1.376	1.092	C. floridanus
KNR166-2-117GGC	42.5	1.456	0.880	C. floridanus
KNR166-2-117GGC	42.5	1.288	1.010	C. floridanus
KNR166-2-117GGC	42.5	1.457	1.058	C. floridanus
KNR166-2-117GGC	43.5	1.382	0.850	C. floridanus
KNR166-2-117GGC	43.5	1.307	0.897	C. floridanus
KNR166-2-117GGC	43.5	1.314	0.970	C. floridanus

KNR166-2-117GGC	43.5	1.282	1.027	C. floridanus
KNR166-2-117GGC	44.5	1.359	0.896	C. floridanus
KNR166-2-117GGC	44.5	1.460	0.987	C. floridanus
KNR166-2-117GGC	44.5	1.483	1.000	C. floridanus
KNR166-2-117GGC	44.5	1.442	1.064	C. floridanus
KNR166-2-117GGC	45.5	1.346	0.907	C. floridanus
KNR166-2-117GGC	45.5	1.208	0.912	C. floridanus
KNR166-2-117GGC	45.5	1.490	0.946	C. floridanus
KNR166-2-117GGC	45.5	1.378	0.984	C. floridanus
KNR166-2-117GGC	46.5	1.355	0.909	C. floridanus
KNR166-2-117GGC	46.5	1.298	0.944	C. floridanus
KNR166-2-117GGC	46.5	1.447	0.965	C. floridanus
KNR166-2-117GGC	46.5	1.339	1.050	C. floridanus
KNR166-2-117GGC	47.5	1.454	0.853	C. floridanus
KNR166-2-117GGC	47.5	1.349	0.995	C. floridanus
KNR166-2-117GGC	47.5	1.294	0.996	C. floridanus
KNR166-2-117GGC	47.5	1.273	1.095	C. floridanus
KNR166-2-117GGC	48.5	1.343	0.868	C. floridanus
KNR166-2-117GGC	48.5	1.300	0.873	C. floridanus
KNR166-2-117GGC	48.5	1.545	0.894	C. floridanus
KNR166-2-117GGC	48.5	1.345	0.904	C. floridanus
KNR166-2-117GGC	49.5	1.283	0.925	C. floridanus
KNR166-2-117GGC	49.5	1.425	0.944	C. floridanus
KNR166-2-117GGC	49.5	1.353	1.015	C. floridanus
KNR166-2-117GGC	49.5	1.261	1.035	C. floridanus
KNR166-2-117GGC	50.5	1.350	0.902	C. floridanus
KNR166-2-117GGC	50.5	1.394	1.020	C. floridanus
KNR166-2-117GGC	50.5	1.432	1.086	C. floridanus
KNR166-2-117GGC	50.5	1.469	1.105	C. floridanus
KNR166-2-117GGC	51.5	1.258	0.802	C. floridanus
KNR166-2-117GGC	51.5	1.343	0.963	C. floridanus
KNR166-2-117GGC	51.5	1.343	1.012	C. floridanus
KNR166-2-117GGC	52.5	1.230	0.856	C. floridanus
KNR166-2-117GGC	52.5	1.195	0.930	C. floridanus
KNR166-2-117GGC	52.5	1.311	1.010	C. floridanus
KNR166-2-117GGC	52.5	1.473	1.049	C. floridanus
KNR166-2-117GGC	53.5	1.331	0.902	C. floridanus
KNR166-2-117GGC	53.5	1.336	0.907	C. floridanus
KNR166-2-117GGC	53.5	1.220	1.005	C. floridanus
KNR166-2-117GGC	53.5	1.431	1.085	C. floridanus
KNR166-2-117GGC	53.5	1.321	1.170	C. floridanus
KNR166-2-117GGC	54.5	1.138	0.869	C. floridanus
KNR166-2-117GGC	54.5	1.328	0.968	C. floridanus
KNR166-2-117GGC	54.5	1.274	1.020	C. floridanus
KNR166-2-117GGC	55.5	1.424	0.942	C. floridanus
KNR166-2-117GGC	55.5	1.353	0.975	C. floridanus
KNR166-2-117GGC	55.5	1.410	0.985	C. floridanus
KNR166-2-117GGC	55.5	1.474	1.043	C. floridanus
KNR166-2-117GGC	56.5	1.479	0.963	C. floridanus
KNR166-2-117GGC	56.5	1.388	0.966	C. floridanus
KNR166-2-117GGC	56.5	1.326	0.976	C. floridanus
KNR166-2-117GGC	56.5	1.243	1.021	C. floridanus
KNR166-2-117GGC	57.5	1.422	0.928	C. floridanus
KNR166-2-117GGC	57.5	1.398	0.930	C. floridanus
KNR166-2-117GGC	57.5	1.457	0.933	C. floridanus

KNR166-2-117GGC	57.5	1.507	0.969	C. floridanus
KNR166-2-117GGC	58.5	1.261	0.864	C. floridanus
KNR166-2-117GGC	58.5	1.308	0.951	C. floridanus
KNR166-2-117GGC	58.5	1.485	1.029	C. floridanus
KNR166-2-117GGC	58.5	1.288	1.130	C. floridanus
KNR166-2-117GGC	59.5	1.316	0.958	C. floridanus
KNR166-2-117GGC	59.5	1.288	0.973	C. floridanus
KNR166-2-117GGC	59.5	1.311	0.973	C. floridanus
KNR166-2-117GGC	59.5	1.229	1.002	C. floridanus
KNR166-2-117GGC	60.5	1.286	0.875	C. floridanus
KNR166-2-117GGC	60.5	1.270	0.957	C. floridanus
KNR166-2-117GGC	60.5	1.351	0.973	C. floridanus
KNR166-2-117GGC	60.5	1.452	1.042	C. floridanus
KNR166-2-117GGC	61.5	1.406	0.959	C. floridanus
KNR166-2-117GGC	61.5	1.453	0.974	C. floridanus
KNR166-2-117GGC	61.5	1.486	1.087	C. floridanus
KNR166-2-117GGC	61.5	1.408	1.097	C. floridanus
KNR166-2-117GGC	61.5	1.451	1.185	C. floridanus
KNR166-2-117GGC	62.5	1.269	0.848	C. floridanus
KNR166-2-117GGC	62.5	1.406	0.948	C. floridanus
KNR166-2-117GGC	62.5	1.406	1.031	C. floridanus
KNR166-2-117GGC	62.5	1.526	1.119	C. floridanus
KNR166-2-117GGC	63.5	1.483	0.956	C. floridanus
KNR166-2-117GGC	63.5	1.375	0.970	C. floridanus
KNR166-2-117GGC	63.5	1.315	1.085	C. floridanus
KNR166-2-117GGC	63.5	1.464	1.146	C. floridanus
KNR166-2-117GGC	64.5	1.354	0.950	C. floridanus
KNR166-2-117GGC	64.5	1.334	0.977	C. floridanus
KNR166-2-117GGC	64.5	1.345	1.038	C. floridanus
KNR166-2-117GGC	64.5	1.534	1.154	C. floridanus
KNR166-2-117GGC	65.5	1.236	0.943	C. floridanus
KNR166-2-117GGC	65.5	1.432	1.039	C. floridanus
KNR166-2-117GGC	65.5	1.307	1.090	C. floridanus
KNR166-2-117GGC	65.5	1.398	1.104	C. floridanus
KNR166-2-117GGC	73.5	1.303	0.792	P. ariminensis
KNR166-2-117GGC	73.5	1.102	0.856	C. floridanus
KNR166-2-117GGC	73.5	0.988	0.898	C. floridanus
KNR166-2-117GGC	73.5	1.466	0.960	C. floridanus
KNR166-2-117GGC	73.5	1.526	1.109	C. floridanus
KNR166-2-117GGC	74.5	1.482	0.925	C. floridanus
KNR166-2-117GGC	75.5	1.476	0.870	C. floridanus
KNR166-2-117GGC	76.5	1.242	1.116	C. floridanus
KNR166-2-117GGC	77.5	1.373	0.820	C. floridanus
KNR166-2-117GGC	77.5	1.257	1.423	C. floridanus
KNR166-2-117GGC	78.5	1.261	0.654	C. floridanus
KNR166-2-117GGC	78.5	1.252	1.217	C. floridanus
KNR166-2-117GGC	79.5	1.438	0.829	C. floridanus
KNR166-2-117GGC	80.5	1.425	0.761	C. floridanus
KNR166-2-117GGC	80.5	1.198	1.503	C. floridanus
KNR166-2-117GGC	81.5	1.428	0.835	C. floridanus
KNR166-2-117GGC	82.5	1.476	0.928	C. floridanus
KNR166-2-117GGC	82.5	1.437	0.968	C. floridanus
KNR166-2-117GGC	83.5	1.337	0.766	C. floridanus
KNR166-2-117GGC	83.5	1.401	0.825	C. floridanus
KNR166-2-117GGC	84.5	1.394	0.884	C. floridanus

KNR166-2-117GGC	84.5	1.335	0.924	C. floridanus
KNR166-2-117GGC	85.5	1.381	0.887	C. floridanus
KNR166-2-117GGC	85.5	1.442	0.955	C. floridanus
KNR166-2-117GGC	86.5	1.397	0.880	C. floridanus
KNR166-2-117GGC	86.5	1.390	0.890	C. floridanus
KNR166-2-117GGC	87.5	1.268	0.819	C. floridanus
KNR166-2-117GGC	87.5	1.380	0.867	C. floridanus
KNR166-2-117GGC	88.5	1.190	0.773	C. floridanus
KNR166-2-117GGC	88.5	1.455	0.970	C. floridanus
KNR166-2-117GGC	89.5	1.217	0.782	C. floridanus
KNR166-2-117GGC	89.5	1.461	0.795	C. floridanus
KNR166-2-117GGC	89.5	1.171	0.984	C. floridanus
KNR166-2-117GGC	91.5	1.566	0.959	C. floridanus
KNR166-2-117GGC	91.5	1.508	1.014	C. floridanus
KNR166-2-117GGC	91.5	1.416	1.075	C. floridanus
KNR166-2-117GGC	93.5	1.466	0.705	C. floridanus
KNR166-2-117GGC	93.5	1.497	0.814	C. floridanus
KNR166-2-117GGC	93.5	1.553	0.856	C. floridanus
KNR166-2-117GGC	93.5	1.479	0.877	C. floridanus
KNR166-2-117GGC	93.5	1.232	0.988	C. floridanus
KNR166-2-117GGC	95.5	1.526	0.884	C. floridanus
KNR166-2-117GGC	95.5	1.503	0.917	C. floridanus
KNR166-2-117GGC	95.5	1.504	0.976	C. floridanus
KNR166-2-117GGC	95.5	1.466	0.992	C. floridanus
KNR166-2-117GGC	97.5	1.468	0.838	C. floridanus
KNR166-2-117GGC	99.5	1.290	0.510	C. floridanus
KNR166-2-117GGC	101.5	1.522	0.870	C. floridanus
KNR166-2-117GGC	101.5	1.387	1.067	C. floridanus
KNR166-2-117GGC	103.5	1.452	0.868	C. floridanus
KNR166-2-117GGC	103.5	1.473	0.953	C. floridanus
KNR166-2-117GGC	103.5	1.571	1.009	C. floridanus
KNR166-2-117GGC	105.5	1.565	0.829	C. floridanus
KNR166-2-117GGC	105.5	1.494	0.961	C. floridanus
KNR166-2-117GGC	105.5	1.273	0.991	C. floridanus
KNR166-2-117GGC	107.5	1.383	0.793	C. floridanus
KNR166-2-117GGC	107.5	1.391	0.827	C. floridanus
KNR166-2-117GGC	107.5	1.323	0.920	C. floridanus
KNR166-2-117GGC	107.5	1.488	0.964	C. floridanus
KNR166-2-117GGC	109.5	1.408	0.856	C. floridanus
KNR166-2-117GGC	109.5	1.474	1.041	C. floridanus
KNR166-2-117GGC	111.5	1.436	0.912	C. floridanus
KNR166-2-117GGC	111.5	1.587	0.930	C. floridanus
KNR166-2-117GGC	111.5	1.531	0.957	C. floridanus
KNR166-2-117GGC	111.5	1.516	0.983	C. floridanus
KNR166-2-117GGC	111.5	1.440	0.994	C. floridanus
KNR166-2-117GGC	113.5	1.450	0.911	C. floridanus
KNR166-2-117GGC	113.5	1.482	0.920	C. floridanus
KNR166-2-117GGC	115.5	1.415	0.791	C. floridanus
KNR166-2-117GGC	115.5	1.550	0.815	C. floridanus
KNR166-2-117GGC	115.5	1.433	0.893	C. floridanus
KNR166-2-117GGC	115.5	1.326	1.066	C. floridanus
KNR166-2-117GGC	117.5	1.253	0.816	C. floridanus
KNR166-2-117GGC	117.5	1.445	0.867	C. floridanus
KNR166-2-117GGC	117.5	1.444	0.912	C. floridanus
KNR166-2-117GGC	117.5	1.501	1.061	C. floridanus

KNR166-2-117GGC	119.5	1.498	0.940	C. floridanus
KNR166-2-117GGC	119.5	1.421	0.960	C. floridanus
KNR166-2-117GGC	126.5	1.475	0.854	C. floridanus
KNR166-2-117GGC	126.5	1.465	0.936	C. floridanus
KNR166-2-117GGC	126.5	1.362	0.941	C. floridanus
KNR166-2-117GGC	126.5	1.579	1.000	C. floridanus
KNR166-2-117GGC	128.5	1.570	0.841	C. floridanus
KNR166-2-117GGC	128.5	1.518	0.864	C. floridanus
KNR166-2-117GGC	128.5	1.513	0.929	C. floridanus
KNR166-2-117GGC	128.5	1.492	1.034	C. floridanus
KNR166-2-117GGC	130.5	1.600	0.935	C. floridanus
KNR166-2-117GGC	130.5	1.462	0.966	C. floridanus
KNR166-2-117GGC	130.5	1.437	0.980	C. floridanus
KNR166-2-117GGC	132.5	1.239	0.792	C. floridanus
KNR166-2-117GGC	132.5	1.451	0.928	C. floridanus
KNR166-2-117GGC	132.5	1.531	1.000	C. floridanus
KNR166-2-117GGC	132.5	1.508	1.008	C. floridanus
KNR166-2-117GGC	134.5	1.504	0.999	C. floridanus
KNR166-2-117GGC	134.5	1.316	1.045	C. floridanus
KNR166-2-117GGC	136.5	1.369	0.684	C. floridanus
KNR166-2-117GGC	136.5	1.442	0.847	C. floridanus
KNR166-2-117GGC	136.5	1.565	0.906	C. floridanus
KNR166-2-117GGC	138.5	1.365	0.915	C. floridanus
KNR166-2-117GGC	138.5	1.574	0.916	C. floridanus
KNR166-2-117GGC	138.5	1.471	0.945	C. floridanus
KNR166-2-117GGC	138.5	1.366	0.967	C. floridanus
KNR166-2-117GGC	140.5	1.426	0.759	C. floridanus
KNR166-2-117GGC	140.5	1.518	0.796	C. floridanus
KNR166-2-117GGC	140.5	1.505	0.972	C. floridanus
KNR166-2-117GGC	140.5	1.379	0.975	C. floridanus
KNR166-2-117GGC	142.5	1.364	0.903	C. floridanus
KNR166-2-117GGC	142.5	1.490	0.934	C. floridanus
KNR166-2-117GGC	142.5	1.572	0.988	C. floridanus
KNR166-2-117GGC	142.5	1.469	1.005	C. floridanus
KNR166-2-117GGC	144.5	1.363	0.844	C. floridanus
KNR166-2-117GGC	144.5	1.401	0.918	C. floridanus
KNR166-2-117GGC	144.5	1.474	0.919	C. floridanus
KNR166-2-117GGC	144.5	1.354	1.039	C. floridanus
KNR166-2-117GGC	146.5	1.459	0.758	C. floridanus
KNR166-2-117GGC	146.5	1.428	0.991	C. floridanus
KNR166-2-117GGC	146.5	1.504	1.027	C. floridanus
KNR166-2-117GGC	148.5	1.247	1.023	C. floridanus
KNR166-2-117GGC	150.5	1.464	0.833	C. floridanus
KNR166-2-117GGC	150.5	1.421	0.888	C. floridanus
KNR166-2-117GGC	150.5	1.420	0.986	C. floridanus
KNR166-2-117GGC	152.5	1.391	0.886	C. floridanus
KNR166-2-117GGC	152.5	1.459	0.900	C. floridanus
KNR166-2-117GGC	152.5	1.477	0.984	C. floridanus
KNR166-2-117GGC	154.5	1.534	0.855	C. floridanus
KNR166-2-117GGC	154.5	1.302	0.951	C. floridanus
KNR166-2-117GGC	154.5	1.583	0.958	C. floridanus
KNR166-2-117GGC	154.5	1.480	0.993	C. floridanus
KNR166-2-117GGC	156.5	1.394	0.925	C. floridanus
KNR166-2-117GGC	156.5	1.360	0.930	C. floridanus
KNR166-2-117GGC	156.5	1.514	0.996	C. floridanus

KNR166-2-117GGC	156.5	1.388	1.013	C. floridanus
KNR166-2-117GGC	158.5	1.629	0.894	C. floridanus
KNR166-2-117GGC	158.5	1.443	0.970	C. floridanus
KNR166-2-117GGC	158.5	1.401	1.078	C. floridanus
KNR166-2-117GGC	158.5	1.523	1.163	C. floridanus
KNR166-2-117GGC	160.5	1.394	0.701	C. floridanus
KNR166-2-117GGC	160.5	1.476	0.987	C. floridanus
KNR166-2-117GGC	160.5	1.535	1.032	C. floridanus
KNR166-2-117GGC	160.5	1.471	1.093	C. floridanus
KNR166-2-117GGC	162.5	1.726	0.417	C. floridanus
KNR166-2-117GGC	162.5	1.474	0.976	C. floridanus
KNR166-2-117GGC	164.5	1.390	0.822	C. floridanus
KNR166-2-117GGC	164.5	1.634	0.877	C. floridanus
KNR166-2-117GGC	164.5	1.605	0.998	C. floridanus
KNR166-2-117GGC	166.5	1.527	0.809	C. floridanus
KNR166-2-117GGC	166.5	1.651	0.821	C. floridanus
KNR166-2-117GGC	166.5	1.351	0.896	C. floridanus
KNR166-2-117GGC	166.5	1.447	1.078	C. floridanus
KNR166-2-117GGC	168.5	1.462	0.835	C. floridanus
KNR166-2-117GGC	168.5	1.369	0.857	C. floridanus
KNR166-2-117GGC	168.5	1.544	0.937	C. floridanus
KNR166-2-117GGC	170.5	1.066	0.861	C. floridanus
KNR166-2-117GGC	170.5	1.500	0.893	C. floridanus
KNR166-2-117GGC	172.5	1.507	0.758	C. floridanus
KNR166-2-117GGC	172.5	1.548	0.796	C. floridanus
KNR166-2-117GGC	172.5	1.513	0.854	C. floridanus
KNR166-2-117GGC	172.5	1.558	0.972	C. floridanus
KNR166-2-117GGC	174.5	1.439	0.809	C. floridanus
KNR166-2-117GGC	174.5	1.464	0.815	C. floridanus
KNR166-2-117GGC	174.5	1.483	0.856	C. floridanus
KNR166-2-117GGC	176.5	1.393	0.758	C. floridanus
KNR166-2-117GGC	176.5	1.678	0.848	C. floridanus
KNR166-2-117GGC	176.5	1.518	0.941	C. floridanus
KNR166-2-117GGC	176.5	1.471	0.971	C. floridanus
KNR166-2-117GGC	178.5	1.346	0.781	C. floridanus
KNR166-2-117GGC	178.5	1.497	0.945	C. floridanus
KNR166-2-117GGC	180.5	1.565	0.840	C. floridanus
KNR166-2-117GGC	180.5	1.520	0.915	C. floridanus
KNR166-2-117GGC	182.5	1.390	0.782	C. floridanus
KNR166-2-117GGC	182.5	1.427	0.799	C. floridanus
KNR166-2-117GGC	182.5	1.401	0.905	C. floridanus
KNR166-2-117GGC	182.5	1.336	0.949	C. floridanus
KNR166-2-117GGC	182.5	1.440	0.971	C. floridanus
KNR166-2-117GGC	184.5	0.672	0.592	C. floridanus
KNR166-2-117GGC	184.5	1.405	0.881	C. floridanus
KNR166-2-117GGC	184.5	1.383	0.910	C. floridanus
KNR166-2-117GGC	184.5	1.364	1.019	C. floridanus
KNR166-2-117GGC	186.5	1.398	0.627	C. floridanus
KNR166-2-117GGC	186.5	1.523	0.874	C. floridanus
KNR166-2-117GGC	186.5	1.535	0.881	C. floridanus
KNR166-2-117GGC	186.5	1.441	0.906	C. floridanus
KNR166-2-117GGC	188.5	1.450	0.852	C. floridanus
KNR166-2-117GGC	188.5	1.505	0.952	C. floridanus
KNR166-2-117GGC	188.5	1.409	0.978	C. floridanus
KNR166-2-117GGC	188.5	1.320	1.068	C. floridanus

CORE	DEPTH	C13	O18	SPECIES
KNR166-2-118MC-A	0.5	1.374	0.827	C. floridanus
KNR166-2-118MC-A	0.5	1.397	0.794	C. floridanus
KNR166-2-118MC-A	0.5	1.463	0.917	C. floridanus
KNR166-2-118MC-A	0.5	1.208	0.854	C. floridanus
KNR166-2-118MC-A	0.5	1.447	0.829	P. ariminensis
KNR166-2-118MC-A	1.5	1.170	0.867	C. floridanus
KNR166-2-118MC-A	1.5	1.223	0.788	C. floridanus
KNR166-2-118MC-A	1.5	1.346	0.784	C. floridanus
KNR166-2-118MC-A	1.5	1.020	0.912	C. floridanus
KNR166-2-118MC-A	2.5	0.847	0.843	C. floridanus
KNR166-2-118MC-A	2.5	1.065	0.765	C. floridanus
KNR166-2-118MC-A	2.5	1.016	0.662	C. floridanus
KNR166-2-118MC-A	2.5	1.314	0.920	C. floridanus
KNR166-2-118MC-A	3.5	1.564	0.812	C. floridanus
KNR166-2-118MC-A	3.5	1.110	0.901	C. floridanus
KNR166-2-118MC-A	3.5	1.417	0.789	C. floridanus
KNR166-2-118MC-A	4.5	1.421	0.518	C. floridanus
KNR166-2-118MC-A	4.5	1.350	0.925	C. floridanus
KNR166-2-118MC-A	5.5	1.195	0.841	C. floridanus
KNR166-2-118MC-A	5.5	1.143	0.819	C. floridanus
KNR166-2-118MC-A	5.5	1.315	0.867	C. floridanus
KNR166-2-118MC-A	5.5	1.395	0.753	C. floridanus
KNR166-2-118MC-A	6.5	0.940	0.862	C. floridanus
KNR166-2-118MC-A	6.5	1.415	0.976	C. floridanus
KNR166-2-118MC-A	6.5	1.193	0.886	C. floridanus
KNR166-2-118MC-A	6.5	1.192	0.916	C. floridanus
KNR166-2-118MC-A	7.5	1.330	0.879	C. floridanus
KNR166-2-118MC-A	7.5	1.420	0.929	C. floridanus
KNR166-2-118MC-A	7.5	1.287	0.821	C. floridanus
KNR166-2-118MC-A	7.5	1.446	0.905	C. floridanus
KNR166-2-118MC-A	7.5	1.199	0.947	C. floridanus
KNR166-2-118MC-A	8.5	1.567	1.083	C. floridanus
KNR166-2-118MC-A	8.5	1.322	1.014	C. floridanus
KNR166-2-118MC-A	8.5	1.118	0.930	C. floridanus
KNR166-2-118MC-A	9.5	1.318	0.859	C. floridanus
KNR166-2-118MC-A	9.5	1.466	0.936	C. floridanus
KNR166-2-118MC-A	9.5	1.365	0.838	C. floridanus
KNR166-2-118MC-A	9.5	1.362	0.986	C. floridanus
KNR166-2-118MC-A	10.5	1.286	0.993	C. floridanus
KNR166-2-118MC-A	10.5	1.509	0.902	C. floridanus
KNR166-2-118MC-A	10.5	1.446	0.829	C. floridanus
KNR166-2-118MC-A	10.5	1.101	0.744	C. floridanus
KNR166-2-118MC-A	11.5	1.389	0.996	C. floridanus
KNR166-2-118MC-A	11.5	0.861	0.647	C. floridanus
KNR166-2-118MC-A	11.5	1.383	0.991	C. floridanus
KNR166-2-118MC-A	11.5	1.477	0.828	C. floridanus
KNR166-2-118MC-A	12.5	1.333	0.944	C. floridanus
KNR166-2-118MC-A	12.5	1.417	0.967	C. floridanus
KNR166-2-118MC-A	12.5	1.454	0.954	C. floridanus
KNR166-2-118MC-A	12.5	1.482	0.831	C. floridanus
KNR166-2-118MC-A	13.5	1.326	0.851	C. floridanus
KNR166-2-118MC-A	13.5	1.396	1.020	C. floridanus
KNR166-2-118MC-A	13.5	1.479	1.062	C. floridanus
KNR166-2-118MC-A	13.5	1.499	0.991	C. floridanus

KNR166-2-118MC-A	14.5	1.346	0.857	C. floridanus
KNR166-2-118MC-A	14.5	1.355	1.019	C. floridanus
KNR166-2-118MC-A	14.5	1.474	0.922	C. floridanus
KNR166-2-118MC-A	14.5	1.389	0.980	C. floridanus
KNR166-2-118MC-A	15.5	1.383	0.957	C. floridanus
KNR166-2-118MC-A	15.5	1.312	1.004	C. floridanus
KNR166-2-118MC-A	15.5	1.682	0.904	P. ariminensis
KNR166-2-118MC-A	15.5	1.266	0.860	C. floridanus
KNR166-2-118MC-A	16.5	1.397	0.903	C. floridanus
KNR166-2-118MC-A	16.5	1.467	0.994	C. floridanus
KNR166-2-118MC-A	16.5	1.343	0.988	C. floridanus
KNR166-2-118MC-A	16.5	1.353	0.909	C. floridanus
KNR166-2-118MC-A	17.5	1.476	0.903	C. floridanus
KNR166-2-118MC-A	17.5	1.398	0.745	C. floridanus
KNR166-2-118MC-A	17.5	1.384	1.026	C. floridanus
KNR166-2-118MC-A	18.5	1.296	0.738	C. floridanus
KNR166-2-118MC-A	18.5	1.424	0.952	C. floridanus
KNR166-2-118MC-A	18.5	1.197	0.897	C. floridanus
KNR166-2-118MC-A	18.5	1.484	0.997	C. floridanus
KNR166-2-118MC-A	19.5	1.346	0.974	C. floridanus
KNR166-2-118MC-A	19.5	1.282	0.962	C. floridanus
KNR166-2-118MC-A	19.5	1.347	0.911	C. floridanus
KNR166-2-118MC-A	19.5	1.410	0.899	C. floridanus
KNR166-2-118MC-A	20.5	1.339	0.827	C. floridanus
KNR166-2-118MC-A	20.5	1.336	0.954	C. floridanus
KNR166-2-118MC-A	20.5	1.442	0.851	C. floridanus
KNR166-2-118MC-A	20.5	1.451	0.879	C. floridanus
KNR166-2-118MC-A	21.5	1.456	0.912	C. floridanus
KNR166-2-118MC-A	21.5	1.456	0.996	C. floridanus
KNR166-2-118MC-A	22.5	1.291	0.579	C. floridanus
KNR166-2-118MC-A	22.5	1.154	0.793	C. floridanus
KNR166-2-118MC-A	22.5	1.344	1.238	C. floridanus
KNR166-2-118MC-A	22.5	1.425	0.833	C. floridanus
KNR166-2-118MC-A	22.5	1.492	0.850	C. floridanus
KNR166-2-118MC-A	23.5	1.331	0.872	C. floridanus
KNR166-2-118MC-A	23.5	1.333	0.848	C. floridanus
KNR166-2-118MC-A	23.5	1.372	1.002	C. floridanus
KNR166-2-118MC-A	23.5	1.280	0.886	C. floridanus
KNR166-2-118MC-A	23.5	1.730	0.989	P. ariminensis
KNR166-2-118MC-A	24.5	1.301	0.971	C. floridanus
KNR166-2-118MC-A	24.5	1.402	0.866	C. floridanus
KNR166-2-118MC-A	24.5	1.349	0.989	C. floridanus
KNR166-2-118MC-A	24.5	1.443	0.976	C. floridanus
KNR166-2-118MC-A	25.5	1.334	0.865	C. floridanus
KNR166-2-118MC-A	25.5	1.362	1.061	C. floridanus
KNR166-2-118MC-A	25.5	1.377	1.023	C. floridanus
KNR166-2-118MC-A	25.5	1.106	0.819	C. floridanus
KNR166-2-118MC-A	26.5	1.406	0.976	C. floridanus
KNR166-2-118MC-A	26.5	1.334	0.982	C. floridanus
KNR166-2-118MC-A	26.5	1.237	0.912	C. floridanus
KNR166-2-118MC-A	27.5	1.319	1.003	C. floridanus
KNR166-2-118MC-A	27.5	1.263	0.915	C. floridanus
KNR166-2-118MC-A	28.5	1.257	0.857	C. floridanus
KNR166-2-118MC-A	28.5	1.341	1.021	C. floridanus
KNR166-2-118MC-A	28.5	1.402	0.832	C. floridanus

KNR166-2-118MC-A	28.5	1.374	0.964	C. floridanus
KNR166-2-118MC-A	29.5	1.267	0.923	C. floridanus
KNR166-2-118MC-A	29.5	1.314	0.929	C. floridanus
KNR166-2-118MC-A	29.5	1.306	0.498	C. floridanus
KNR166-2-118MC-A	29.5	1.284	0.943	C. floridanus
KNR166-2-118MC-A	30.5	1.442	0.630	C. floridanus
KNR166-2-118MC-A	30.5	1.429	0.853	C. floridanus
KNR166-2-118MC-A	30.5	1.361	0.896	C. floridanus
KNR166-2-118MC-A	30.5	1.416	0.937	C. floridanus
KNR166-2-118MC-A	31.5	1.333	0.918	C. floridanus
KNR166-2-118MC-A	31.5	1.399	0.823	C. floridanus
KNR166-2-118MC-A	31.5	1.349	0.846	C. floridanus
KNR166-2-118MC-A	31.5	1.362	1.086	C. floridanus
KNR166-2-118MC-A	32.5	1.320	0.828	C. floridanus
KNR166-2-118MC-A	32.5	1.170	0.917	C. floridanus
KNR166-2-118MC-A	32.5	1.222	0.915	C. floridanus
KNR166-2-118MC-A	32.5	1.469	0.963	C. floridanus
KNR166-2-118MC-A	33.5	1.327	0.884	C. floridanus
KNR166-2-118MC-A	33.5	1.224	0.912	C. floridanus
KNR166-2-118MC-A	33.5	1.362	0.802	C. floridanus
KNR166-2-118MC-A	33.5	1.277	0.925	C. floridanus
KNR166-2-118MC-A	34.5	1.274	0.958	C. floridanus
KNR166-2-118MC-A	34.5	1.413	0.987	C. floridanus
KNR166-2-118MC-A	34.5	1.284	0.899	C. floridanus
KNR166-2-118MC-A	34.5	1.355	0.954	C. floridanus
KNR166-2-118MC-A	35.5	1.448	0.886	C. floridanus
KNR166-2-118MC-A	35.5	1.427	0.834	C. floridanus
KNR166-2-118MC-A	35.5	1.352	0.984	C. floridanus
KNR166-2-118MC-A	35.5	1.338	0.971	C. floridanus
KNR166-2-118MC-A	36.5	1.219	0.867	C. floridanus
KNR166-2-118MC-A	36.5	1.217	0.877	C. floridanus
KNR166-2-118MC-A	36.5	1.198	0.939	C. floridanus
KNR166-2-118MC-A	36.5	1.265	0.947	C. floridanus

CORE	DEPTH	C13	O18	SPECIES
KNR166-2-118MC-A	0.5	0.473	-1.687	G. ruber-w
KNR166-2-118MC-A	0.5	0.639	-1.885	G. ruber-w
KNR166-2-118MC-A	0.5	0.590	-2.059	G. ruber-w
KNR166-2-118MC-A	0.5	0.277	-1.719	G. ruber-w
KNR166-2-118MC-A	1.5	1.116	-1.738	G. ruber-w
KNR166-2-118MC-A	1.5	0.873	-1.993	G. ruber-w
KNR166-2-118MC-A	1.5	0.739	-1.962	G. ruber-w
KNR166-2-118MC-A	1.5	0.509	-1.805	G. ruber-w
KNR166-2-118MC-A	2.5	1.048	-1.847	G. ruber-w
KNR166-2-118MC-A	2.5	0.707	-1.967	G. ruber-w
KNR166-2-118MC-A	2.5	0.905	-1.864	G. ruber-w
KNR166-2-118MC-A	2.5	0.486	-1.816	G. ruber-w
KNR166-2-118MC-A	3.5	0.518	-1.855	G. ruber-w
KNR166-2-118MC-A	3.5	0.894	-1.860	G. ruber-w
KNR166-2-118MC-A	3.5	0.551	-1.903	G. ruber-w
KNR166-2-118MC-A	3.5	0.334	-2.010	G. ruber-w
KNR166-2-118MC-A	4.5	0.827	-2.102	G. ruber-w
KNR166-2-118MC-A	4.5	0.627	-1.777	G. ruber-w
KNR166-2-118MC-A	4.5	0.304	-2.008	G. ruber-w
KNR166-2-118MC-A	4.5	0.607	-1.957	G. ruber-w
KNR166-2-118MC-A	5.5	0.661	-1.853	G. ruber-w
KNR166-2-118MC-A	5.5	0.874	-1.825	G. ruber-w
KNR166-2-118MC-A	5.5	0.531	-1.960	G. ruber-w
KNR166-2-118MC-A	6.5	0.605	-2.076	G. ruber-w
KNR166-2-118MC-A	6.5	0.407	-2.112	G. ruber-w
KNR166-2-118MC-A	6.5	0.720	-1.843	G. ruber-w
KNR166-2-118MC-A	6.5	0.539	-2.046	G. ruber-w
KNR166-2-118MC-A	7.5	0.665	-2.104	G. ruber-w
KNR166-2-118MC-A	7.5	1.119	-2.102	G. ruber-w
KNR166-2-118MC-A	7.5	0.575	-1.762	G. ruber-w
KNR166-2-118MC-A	7.5	0.287	-1.807	G. ruber-w
KNR166-2-118MC-A	8.5	0.261	-2.104	G. ruber-w
KNR166-2-118MC-A	8.5	0.544	-2.142	G. ruber-w
KNR166-2-118MC-A	8.5	0.390	-1.866	G. ruber-w
KNR166-2-118MC-A	8.5	0.533	-1.775	G. ruber-w
KNR166-2-118MC-A	9.5	0.484	-1.810	G. ruber-w
KNR166-2-118MC-A	9.5	0.213	-2.058	G. ruber-w
KNR166-2-118MC-A	9.5	0.393	-1.726	G. ruber-w
KNR166-2-118MC-A	9.5	0.210	-1.975	G. ruber-w
KNR166-2-118MC-A	10.5	0.477	-1.992	G. ruber-w
KNR166-2-118MC-A	10.5	-0.114	-2.011	G. ruber-w
KNR166-2-118MC-A	10.5	0.707	-2.209	G. ruber-w
KNR166-2-118MC-A	10.5	-0.165	-2.022	G. ruber-w
KNR166-2-118MC-A	11.5	-0.116	-2.302	G. ruber-w
KNR166-2-118MC-A	11.5	0.238	-2.172	G. ruber-w
KNR166-2-118MC-A	11.5	0.872	-1.938	G. ruber-w
KNR166-2-118MC-A	11.5	0.277	-1.913	G. ruber-w
KNR166-2-118MC-A	12.5	0.718	-2.116	G. ruber-w
KNR166-2-118MC-A	12.5	0.326	-2.022	G. ruber-w
KNR166-2-118MC-A	12.5	0.278	-2.103	G. ruber-w
KNR166-2-118MC-A	12.5	0.842	-1.904	G. ruber-w
KNR166-2-118MC-A	13.5	0.744	-2.225	G. ruber-w
KNR166-2-118MC-A	13.5	-0.373	-2.051	G. ruber-w
KNR166-2-118MC-A	13.5	0.223	-1.966	G. ruber-w

KNR166-2-118MC-A	13.5	0.163	-2.030	G. ruber-w
KNR166-2-118MC-A	14.5	0.299	-1.861	G. ruber-w
KNR166-2-118MC-A	14.5	0.713	-2.097	G. ruber-w
KNR166-2-118MC-A	14.5	0.441	-1.942	G. ruber-w
KNR166-2-118MC-A	14.5	-0.402	-2.367	G. ruber-w
KNR166-2-118MC-A	15.5	0.193	-2.269	G. ruber-w
KNR166-2-118MC-A	15.5	0.204	-2.021	G. ruber-w
KNR166-2-118MC-A	15.5	0.179	-2.089	G. ruber-w
KNR166-2-118MC-A	15.5	0.399	-2.162	G. ruber-w
KNR166-2-118MC-A	16.5	-0.094	-2.036	G. ruber-w
KNR166-2-118MC-A	16.5	0.573	-1.953	G. ruber-w
KNR166-2-118MC-A	16.5	0.586	-2.094	G. ruber-w
KNR166-2-118MC-A	16.5	0.298	-1.974	G. ruber-w
KNR166-2-118MC-A	17.5	0.628	-1.734	G. ruber-w
KNR166-2-118MC-A	17.5	0.422	-1.903	G. ruber-w
KNR166-2-118MC-A	17.5	0.008	-2.239	G. ruber-w
KNR166-2-118MC-A	17.5	0.295	-1.890	G. ruber-w
KNR166-2-118MC-A	18.5	0.115	-2.047	G. ruber-w
KNR166-2-118MC-A	18.5	0.271	-2.351	G. ruber-w
KNR166-2-118MC-A	18.5	0.168	-1.870	G. ruber-w
KNR166-2-118MC-A	18.5	-0.338	-2.133	G. ruber-w
KNR166-2-118MC-A	19.5	-0.060	-2.052	G. ruber-w
KNR166-2-118MC-A	19.5	0.353	-1.976	G. ruber-w
KNR166-2-118MC-A	19.5	0.234	-1.882	G. ruber-w
KNR166-2-118MC-A	19.5	0.384	-2.131	G. ruber-w
KNR166-2-118MC-A	20.5	0.487	-2.057	G. ruber-w
KNR166-2-118MC-A	20.5	0.386	-2.127	G. ruber-w
KNR166-2-118MC-A	20.5	0.332	-2.034	G. ruber-w
KNR166-2-118MC-A	20.5	-0.459	-2.165	G. ruber-w
KNR166-2-118MC-A	21.5	0.087	-1.770	G. ruber-w
KNR166-2-118MC-A	21.5	0.813	-1.830	G. ruber-w
KNR166-2-118MC-A	21.5	-0.171	-2.312	G. ruber-w
KNR166-2-118MC-A	21.5	1.027	-1.837	G. ruber-w
KNR166-2-118MC-A	22.5	0.658	-2.014	G. ruber-w
KNR166-2-118MC-A	22.5	0.417	-1.975	G. ruber-w
KNR166-2-118MC-A	22.5	0.229	-2.148	G. ruber-w
KNR166-2-118MC-A	22.5	0.456	-2.121	G. ruber-w
KNR166-2-118MC-A	23.5	0.274	-2.181	G. ruber-w
KNR166-2-118MC-A	23.5	-0.014	-2.101	G. ruber-w
KNR166-2-118MC-A	23.5	0.320	-1.984	G. ruber-w
KNR166-2-118MC-A	23.5	-0.130	-2.069	G. ruber-w
KNR166-2-118MC-A	24.5	-0.163	-2.117	G. ruber-w
KNR166-2-118MC-A	24.5	0.617	-1.754	G. ruber-w
KNR166-2-118MC-A	24.5	0.832	-1.785	G. ruber-w
KNR166-2-118MC-A	24.5	0.164	-2.036	G. ruber-w
KNR166-2-118MC-A	25.5	0.036	-2.158	G. ruber-w
KNR166-2-118MC-A	25.5	0.283	-1.721	G. ruber-w
KNR166-2-118MC-A	25.5	0.022	-1.955	G. ruber-w
KNR166-2-118MC-A	25.5	0.320	-1.898	G. ruber-w
KNR166-2-118MC-A	26.5	0.184	-2.111	G. ruber-w
KNR166-2-118MC-A	26.5	0.393	-1.821	G. ruber-w
KNR166-2-118MC-A	26.5	-0.107	-2.297	G. ruber-w
KNR166-2-118MC-A	26.5	0.361	-2.100	G. ruber-w
KNR166-2-118MC-A	27.5	0.138	-2.140	G. ruber-w
KNR166-2-118MC-A	27.5	0.194	-2.069	G. ruber-w

KNR166-2-118MC-A	27.5	0.521	-1.861	G. ruber-w
KNR166-2-118MC-A	27.5	0.213	-2.130	G. ruber-w
KNR166-2-118MC-A	28.5	-0.118	-2.172	G. ruber-w
KNR166-2-118MC-A	28.5	0.347	-2.074	G. ruber-w
KNR166-2-118MC-A	28.5	-0.015	-1.884	G. ruber-w
KNR166-2-118MC-A	28.5	0.561	-1.838	G. ruber-w
KNR166-2-118MC-A	29.5	-0.039	-2.225	G. ruber-w
KNR166-2-118MC-A	29.5	0.198	-1.910	G. ruber-w
KNR166-2-118MC-A	29.5	0.064	-2.003	G. ruber-w
KNR166-2-118MC-A	29.5	-0.165	-2.129	G. ruber-w
KNR166-2-118MC-A	30.5	0.448	-2.064	G. ruber-w
KNR166-2-118MC-A	30.5	-0.181	-2.343	G. ruber-w
KNR166-2-118MC-A	30.5	0.299	-1.966	G. ruber-w
KNR166-2-118MC-A	30.5	0.403	-2.104	G. ruber-w
KNR166-2-118MC-A	31.5	0.385	-1.913	G. ruber-w
KNR166-2-118MC-A	31.5	0.043	-2.180	G. ruber-w
KNR166-2-118MC-A	31.5	0.262	-2.147	G. ruber-w
KNR166-2-118MC-A	31.5	-0.079	-2.234	G. ruber-w
KNR166-2-118MC-A	32.5	0.351	-2.284	G. ruber-w
KNR166-2-118MC-A	32.5	0.223	-1.927	G. ruber-w
KNR166-2-118MC-A	32.5	0.156	-2.084	G. ruber-w
KNR166-2-118MC-A	32.5	-0.122	-2.123	G. ruber-w
KNR166-2-118MC-A	33.5	0.086	-2.003	G. ruber-w
KNR166-2-118MC-A	33.5	0.150	-2.285	G. ruber-w
KNR166-2-118MC-A	33.5	-0.053	-1.895	G. ruber-w
KNR166-2-118MC-A	33.5	0.096	-2.104	G. ruber-w
KNR166-2-118MC-A	34.5	0.409	-2.022	G. ruber-w
KNR166-2-118MC-A	34.5	0.374	-2.204	G. ruber-w
KNR166-2-118MC-A	34.5	0.256	-2.045	G. ruber-w
KNR166-2-118MC-A	34.5	0.038	-2.183	G. ruber-w
KNR166-2-118MC-A	35.5	0.420	-2.234	G. ruber-w
KNR166-2-118MC-A	35.5	0.205	-1.914	G. ruber-w
KNR166-2-118MC-A	35.5	-0.103	-2.010	G. ruber-w
KNR166-2-118MC-A	35.5	0.102	-2.255	G. ruber-w
KNR166-2-118MC-A	35.5	0.997	-2.039	G. ruber-w
KNR166-2-118MC-A	36.5	0.366	-2.124	G. ruber-w
KNR166-2-118MC-A	36.5	-0.067	-1.829	G. ruber-w
KNR166-2-118MC-A	36.5	0.395	-2.061	G. ruber-w
KNR166-2-118MC-A	36.5	-0.377	-1.929	G. ruber-w
KNR166-2-118MC-A	36.5	0.473	-1.914	G. ruber-w

CORE	DEPTH	C13	O18	SPECIES
KNR166-2-124GGC	6.5	1.381	1.607	P. ariminensis
KNR166-2-124GGC	6.5	1.316	1.621	P. ariminensis
KNR166-2-124GGC	6.5	1.254	1.555	C. floridanus
KNR166-2-124GGC	6.5	1.351	1.719	P. ariminensis
KNR166-2-124GGC	7.5	1.184	1.521	C. floridanus
KNR166-2-124GGC	7.5	1.060	1.535	C. floridanus
KNR166-2-124GGC	7.5	1.208	1.484	C. floridanus
KNR166-2-124GGC	7.5	1.363	1.575	P. ariminensis
KNR166-2-124GGC	8.5	1.010	1.493	C. floridanus
KNR166-2-124GGC	8.5	1.167	1.702	C. floridanus
KNR166-2-124GGC	8.5	1.325	1.661	C. floridanus
KNR166-2-124GGC	8.5	1.076	1.661	C. floridanus
KNR166-2-124GGC	9.5	1.227	1.601	C. floridanus
KNR166-2-124GGC	9.5	1.155	1.583	C. floridanus
KNR166-2-124GGC	9.5	1.122	1.507	C. floridanus
KNR166-2-124GGC	9.5	1.318	1.717	P. ariminensis
KNR166-2-124GGC	10.5	1.152	1.512	C. floridanus
KNR166-2-124GGC	10.5	1.122	1.603	C. floridanus
KNR166-2-124GGC	10.5	1.393	1.536	P. ariminensis
KNR166-2-124GGC	10.5	1.388	1.604	P. ariminensis
KNR166-2-124GGC	11.5	1.210	1.664	C. floridanus
KNR166-2-124GGC	11.5	1.340	1.533	P. ariminensis
KNR166-2-124GGC	11.5	1.328	1.517	P. ariminensis
KNR166-2-124GGC	11.5	1.399	1.525	P. ariminensis
KNR166-2-124GGC	12.5	1.252	1.562	C. floridanus
KNR166-2-124GGC	12.5	1.344	1.635	P. ariminensis
KNR166-2-124GGC	12.5	1.425	1.498	P. ariminensis
KNR166-2-124GGC	12.5	1.458	1.782	P. ariminensis
KNR166-2-124GGC	13.5	1.098	1.443	C. floridanus
KNR166-2-124GGC	13.5	1.165	1.249	C. floridanus
KNR166-2-124GGC	13.5	1.217	1.699	C. floridanus
KNR166-2-124GGC	13.5	1.236	1.567	P. ariminensis
KNR166-2-124GGC	14.5	1.176	1.579	C. floridanus
KNR166-2-124GGC	14.5	1.207	1.797	C. floridanus
KNR166-2-124GGC	14.5	1.398	1.648	P. ariminensis
KNR166-2-124GGC	14.5	1.397	1.651	P. ariminensis
KNR166-2-124GGC	15.5	1.264	1.701	C. floridanus
KNR166-2-124GGC	15.5	1.137	1.693	C. floridanus
KNR166-2-124GGC	15.5	1.358	1.387	P. ariminensis
KNR166-2-124GGC	15.5	1.348	1.679	P. ariminensis
KNR166-2-124GGC	16.5	1.204	1.683	C. floridanus
KNR166-2-124GGC	16.5	1.170	1.539	C. floridanus
KNR166-2-124GGC	16.5	1.134	1.665	C. floridanus
KNR166-2-124GGC	16.5	1.334	1.622	P. ariminensis
KNR166-2-124GGC	17.5	1.083	1.664	C. floridanus
KNR166-2-124GGC	17.5	1.117	1.521	C. floridanus
KNR166-2-124GGC	17.5	1.364	1.607	P. ariminensis
KNR166-2-124GGC	17.5	1.411	1.605	P. ariminensis
KNR166-2-124GGC	18.5	1.154	1.600	C. floridanus
KNR166-2-124GGC	18.5	1.221	1.536	C. floridanus
KNR166-2-124GGC	18.5	1.131	1.524	C. floridanus
KNR166-2-124GGC	18.5	1.389	1.498	P. ariminensis
KNR166-2-124GGC	19.5	1.124	1.535	C. floridanus
KNR166-2-124GGC	19.5	1.255	1.579	C. floridanus

KNR166-2-124GGC	19.5	1.086	1.707	C. floridanus
KNR166-2-124GGC	19.5	1.398	1.574	P. ariminensis
KNR166-2-124GGC	20.5	1.205	1.576	C. floridanus
KNR166-2-124GGC	20.5	1.194	1.702	C. floridanus
KNR166-2-124GGC	20.5	1.200	1.630	C. floridanus
KNR166-2-124GGC	20.5	1.388	1.539	P. ariminensis
KNR166-2-124GGC	21.5	1.185	1.570	C. floridanus
KNR166-2-124GGC	21.5	1.091	1.353	C. floridanus
KNR166-2-124GGC	21.5	1.361	1.514	P. ariminensis
KNR166-2-124GGC	21.5	1.355	1.610	P. ariminensis
KNR166-2-124GGC	22.5	1.193	1.432	C. floridanus
KNR166-2-124GGC	22.5	1.244	1.639	C. floridanus
KNR166-2-124GGC	22.5	1.265	1.777	C. floridanus
KNR166-2-124GGC	22.5	1.380	1.403	P. ariminensis
KNR166-2-124GGC	23.5	1.167	1.584	C. floridanus
KNR166-2-124GGC	23.5	1.406	1.439	P. ariminensis
KNR166-2-124GGC	23.5	1.306	1.601	P. ariminensis
KNR166-2-124GGC	23.5	1.428	1.612	P. ariminensis
KNR166-2-124GGC	24.5	1.198	1.589	C. floridanus
KNR166-2-124GGC	24.5	1.265	1.690	C. floridanus
KNR166-2-124GGC	24.5	1.080	1.524	C. floridanus
KNR166-2-124GGC	24.5	1.316	1.556	P. ariminensis
KNR166-2-124GGC	25.5	1.170	1.621	C. floridanus
KNR166-2-124GGC	25.5	1.324	1.593	C. floridanus
KNR166-2-124GGC	25.5	1.329	1.399	P. ariminensis
KNR166-2-124GGC	25.5	1.383	1.512	P. ariminensis
KNR166-2-124GGC	26.5	1.154	1.629	C. floridanus
KNR166-2-124GGC	26.5	1.320	1.632	P. ariminensis
KNR166-2-124GGC	26.5	1.438	1.386	P. ariminensis
KNR166-2-124GGC	26.5	1.249	1.661	P. ariminensis
KNR166-2-124GGC	27.5	1.107	1.460	C. floridanus
KNR166-2-124GGC	27.5	1.442	1.499	P. ariminensis
KNR166-2-124GGC	27.5	1.406	1.557	P. ariminensis
KNR166-2-124GGC	28.5	1.395	1.208	C. floridanus
KNR166-2-124GGC	28.5	1.255	1.619	C. floridanus
KNR166-2-124GGC	28.5	1.346	1.567	C. floridanus
KNR166-2-124GGC	28.5	1.283	1.660	C. floridanus
KNR166-2-124GGC	28.5	1.230	1.481	C. floridanus
KNR166-2-124GGC	29.5	1.300	1.410	C. floridanus
KNR166-2-124GGC	29.5	1.183	1.511	C. floridanus
KNR166-2-124GGC	29.5	1.248	1.560	C. floridanus
KNR166-2-124GGC	29.5	1.255	1.550	C. floridanus
KNR166-2-124GGC	29.5	1.394	1.567	P. ariminensis
KNR166-2-124GGC	30.5	1.258	1.539	C. floridanus
KNR166-2-124GGC	30.5	1.266	1.642	C. floridanus
KNR166-2-124GGC	30.5	1.320	1.639	C. floridanus
KNR166-2-124GGC	30.5	1.414	1.690	P. ariminensis
KNR166-2-124GGC	31.5	1.103	1.568	C. floridanus
KNR166-2-124GGC	31.5	1.270	1.515	C. floridanus
KNR166-2-124GGC	31.5	1.363	1.639	P. ariminensis
KNR166-2-124GGC	32.5	1.269	1.557	C. floridanus
KNR166-2-124GGC	32.5	1.138	1.396	C. floridanus
KNR166-2-124GGC	32.5	1.189	1.580	C. floridanus
KNR166-2-124GGC	32.5	1.186	1.525	C. floridanus
KNR166-2-124GGC	32.5	1.295	1.521	P. ariminensis

KNR166-2-124GGC	33.5	1.256	1.137	C. floridanus
KNR166-2-124GGC	33.5	1.308	1.691	C. floridanus
KNR166-2-124GGC	33.5	1.404	1.512	P. ariminensis
KNR166-2-124GGC	33.5	1.436	1.363	P. ariminensis
KNR166-2-124GGC	33.5	1.377	1.641	P. ariminensis
KNR166-2-124GGC	34.5	1.343	1.704	C. floridanus
KNR166-2-124GGC	34.5	1.254	1.573	C. floridanus
KNR166-2-124GGC	34.5	1.131	1.380	C. floridanus
KNR166-2-124GGC	34.5	1.327	1.740	C. floridanus
KNR166-2-124GGC	34.5	1.172	1.521	C. floridanus
KNR166-2-124GGC	35.5	1.037	1.338	C. floridanus
KNR166-2-124GGC	35.5	1.237	1.667	C. floridanus
KNR166-2-124GGC	35.5	1.449	1.539	P. ariminensis
KNR166-2-124GGC	35.5	1.380	1.440	P. ariminensis
KNR166-2-124GGC	36.5	1.068	1.489	C. floridanus
KNR166-2-124GGC	36.5	1.207	1.526	C. floridanus
KNR166-2-124GGC	36.5	1.244	1.724	C. floridanus
KNR166-2-124GGC	36.5	1.328	1.524	C. floridanus
KNR166-2-124GGC	36.5	1.316	1.575	C. floridanus
KNR166-2-124GGC	37.5	1.132	1.617	C. floridanus
KNR166-2-124GGC	37.5	1.216	1.750	C. floridanus
KNR166-2-124GGC	37.5	1.336	1.597	P. ariminensis
KNR166-2-124GGC	37.5	1.516	1.684	P. ariminensis
KNR166-2-124GGC	37.5	1.380	1.574	P. ariminensis
KNR166-2-124GGC	38.5	1.180	1.757	C. floridanus
KNR166-2-124GGC	38.5	1.244	1.587	C. floridanus
KNR166-2-124GGC	38.5	1.154	1.457	C. floridanus
KNR166-2-124GGC	38.5	1.406	1.532	P. ariminensis
KNR166-2-124GGC	38.5	1.164	1.524	C. floridanus
KNR166-2-124GGC	39.5	1.311	1.561	C. floridanus
KNR166-2-124GGC	39.5	1.191	1.631	C. floridanus
KNR166-2-124GGC	39.5	1.317	1.606	P. ariminensis
KNR166-2-124GGC	39.5	1.483	1.497	P. ariminensis
KNR166-2-124GGC	39.5	1.377	1.505	P. ariminensis
KNR166-2-124GGC	40.5	1.236	1.504	C. floridanus
KNR166-2-124GGC	40.5	1.266	1.699	C. floridanus
KNR166-2-124GGC	40.5	1.441	1.578	P. ariminensis
KNR166-2-124GGC	40.5	1.464	1.604	P. ariminensis
KNR166-2-124GGC	40.5	1.349	1.431	P. ariminensis
KNR166-2-124GGC	41.5	1.207	1.563	C. floridanus
KNR166-2-124GGC	41.5	1.447	1.539	P. ariminensis
KNR166-2-124GGC	41.5	1.448	1.749	P. ariminensis
KNR166-2-124GGC	41.5	1.490	2.117	P. ariminensis
KNR166-2-124GGC	41.5	1.365	1.509	P. ariminensis
KNR166-2-124GGC	42.5	1.217	1.197	C. floridanus
KNR166-2-124GGC	42.5	1.225	1.602	C. floridanus
KNR166-2-124GGC	42.5	1.187	1.244	P. ariminensis
KNR166-2-124GGC	42.5	0.968	1.867	P. ariminensis
KNR166-2-124GGC	42.5	1.362	1.552	P. ariminensis
KNR166-2-124GGC	43.5	1.221	1.650	C. floridanus
KNR166-2-124GGC	43.5	1.575	1.056	P. ariminensis
KNR166-2-124GGC	43.5	1.177	1.509	C. floridanus
KNR166-2-124GGC	43.5	1.123	1.747	P. ariminensis
KNR166-2-124GGC	43.5	1.431	1.559	P. ariminensis
KNR166-2-124GGC	44.5	1.442	1.480	P. ariminensis

KNR166-2-124GGC	44.5	1.496	1.521	P. ariminensis
KNR166-2-124GGC	44.5	1.433	1.587	P. ariminensis
KNR166-2-124GGC	44.5	1.175	1.511	P. ariminensis
KNR166-2-124GGC	44.5	1.477	1.533	P. ariminensis
KNR166-2-124GGC	45.5	1.326	1.622	C. floridanus
KNR166-2-124GGC	45.5	1.323	1.542	C. floridanus
KNR166-2-124GGC	45.5	1.415	1.701	P. ariminensis
KNR166-2-124GGC	45.5	1.472	1.502	P. ariminensis
KNR166-2-124GGC	45.5	1.280	1.540	C. floridanus
KNR166-2-124GGC	46.5	1.367	1.558	P. ariminensis
KNR166-2-124GGC	46.5	1.467	1.645	P. ariminensis
KNR166-2-124GGC	46.5	1.399	1.453	C. floridanus
KNR166-2-124GGC	46.5	1.435	1.546	P. ariminensis
KNR166-2-124GGC	47.5	1.437	1.604	P. ariminensis
KNR166-2-124GGC	47.5	1.482	1.682	P. ariminensis
KNR166-2-124GGC	47.5	1.473	1.649	P. ariminensis
KNR166-2-124GGC	47.5	1.452	1.718	P. ariminensis
KNR166-2-124GGC	47.5	1.371	1.613	P. ariminensis
KNR166-2-124GGC	48.5	1.261	1.711	C. floridanus
KNR166-2-124GGC	48.5	1.272	1.734	C. floridanus
KNR166-2-124GGC	48.5	1.365	1.637	P. ariminensis
KNR166-2-124GGC	48.5	1.388	1.518	P. ariminensis
KNR166-2-124GGC	48.5	1.513	1.608	P. ariminensis
KNR166-2-124GGC	48.5	1.479	1.757	P. ariminensis
KNR166-2-124GGC	49.5	1.382	1.549	P. ariminensis
KNR166-2-124GGC	49.5	1.457	1.437	P. ariminensis
KNR166-2-124GGC	49.5	1.472	1.591	P. ariminensis
KNR166-2-124GGC	49.5	1.476	1.602	P. ariminensis
KNR166-2-124GGC	49.5	1.435	1.680	P. ariminensis
KNR166-2-124GGC	50.5	1.398	1.685	P. ariminensis
KNR166-2-124GGC	50.5	1.535	1.655	P. ariminensis
KNR166-2-124GGC	50.5	1.434	1.613	P. ariminensis

CORE	DEPTH	C13	O18	SPECIES
KNR166-2-124GGC	6.5	-0.043	-2.208	G. ruber-w
KNR166-2-124GGC	6.5	0.811	-1.898	G. ruber-w
KNR166-2-124GGC	6.5	0.100	-2.190	G. ruber-w
KNR166-2-124GGC	6.5	0.557	-1.986	G. ruber-w
KNR166-2-124GGC	7.5	0.389	-2.065	G. ruber-w
KNR166-2-124GGC	7.5	0.439	-1.979	G. ruber-w
KNR166-2-124GGC	7.5	0.290	-1.862	G. ruber-w
KNR166-2-124GGC	7.5	0.479	-2.021	G. ruber-w
KNR166-2-124GGC	8.5	0.098	-1.949	G. ruber-w
KNR166-2-124GGC	8.5	0.520	-1.948	G. ruber-w
KNR166-2-124GGC	8.5	0.281	-1.899	G. ruber-w
KNR166-2-124GGC	8.5	0.222	-2.017	G. ruber-w
KNR166-2-124GGC	9.5	0.168	-1.993	G. ruber-w
KNR166-2-124GGC	9.5	0.545	-1.957	G. ruber-w
KNR166-2-124GGC	9.5	0.445	-1.888	G. ruber-w
KNR166-2-124GGC	9.5	0.428	-2.060	G. ruber-w
KNR166-2-124GGC	10.5	0.671	-1.836	G. ruber-w
KNR166-2-124GGC	10.5	0.630	-1.833	G. ruber-w
KNR166-2-124GGC	10.5	0.230	-1.897	G. ruber-w
KNR166-2-124GGC	10.5	0.446	-1.932	G. ruber-w
KNR166-2-124GGC	11.5	0.438	-2.155	G. ruber-w
KNR166-2-124GGC	11.5	0.414	-1.991	G. ruber-w
KNR166-2-124GGC	11.5	0.457	-2.067	G. ruber-w
KNR166-2-124GGC	11.5	0.347	-1.982	G. ruber-w
KNR166-2-124GGC	12.5	0.186	-1.993	G. ruber-w
KNR166-2-124GGC	12.5	0.333	-2.061	G. ruber-w
KNR166-2-124GGC	12.5	-0.017	-2.031	G. ruber-w
KNR166-2-124GGC	12.5	0.172	-2.102	G. ruber-w
KNR166-2-124GGC	13.5	0.188	-1.930	G. ruber-w
KNR166-2-124GGC	13.5	0.401	-1.824	G. ruber-w
KNR166-2-124GGC	13.5	0.212	-2.053	G. ruber-w
KNR166-2-124GGC	13.5	0.364	-1.924	G. ruber-w
KNR166-2-124GGC	14.5	0.287	-1.912	G. ruber-w
KNR166-2-124GGC	14.5	0.300	-2.017	G. ruber-w
KNR166-2-124GGC	14.5	0.425	-1.872	G. ruber-w
KNR166-2-124GGC	14.5	0.451	-1.980	G. ruber-w
KNR166-2-124GGC	15.5	0.137	-2.000	G. ruber-w
KNR166-2-124GGC	15.5	0.232	-1.867	G. ruber-w
KNR166-2-124GGC	15.5	0.372	-1.942	G. ruber-w
KNR166-2-124GGC	15.5	-0.096	-2.039	G. ruber-w
KNR166-2-124GGC	16.5	-0.439	-2.059	G. ruber-w
KNR166-2-124GGC	16.5	0.164	-2.070	G. ruber-w
KNR166-2-124GGC	16.5	0.224	-1.933	G. ruber-w
KNR166-2-124GGC	16.5	0.388	-1.934	G. ruber-w
KNR166-2-124GGC	17.5	0.231	-2.021	G. ruber-w
KNR166-2-124GGC	17.5	0.431	-1.994	G. ruber-w
KNR166-2-124GGC	17.5	0.393	-2.110	G. ruber-w
KNR166-2-124GGC	17.5	0.263	-1.975	G. ruber-w
KNR166-2-124GGC	18.5	0.433	-1.886	G. ruber-w
KNR166-2-124GGC	18.5	0.289	-2.171	G. ruber-w
KNR166-2-124GGC	18.5	0.224	-1.968	G. ruber-w
KNR166-2-124GGC	18.5	0.337	-1.909	G. ruber-w
KNR166-2-124GGC	19.5	0.112	-2.133	G. ruber-w
KNR166-2-124GGC	19.5	0.489	-1.875	G. ruber-w

KNR166-2-124GGC	19.5	0.404	-2.024	G. ruber-w
KNR166-2-124GGC	19.5	0.224	-2.205	G. ruber-w
KNR166-2-124GGC	20.5	0.160	-2.174	G. ruber-w
KNR166-2-124GGC	20.5	0.612	-1.939	G. ruber-w
KNR166-2-124GGC	20.5	0.528	-2.036	G. ruber-w
KNR166-2-124GGC	20.5	0.467	-2.054	G. ruber-w
KNR166-2-124GGC	21.5	0.415	-2.206	G. ruber-w
KNR166-2-124GGC	21.5	0.406	-1.942	G. ruber-w
KNR166-2-124GGC	21.5	0.460	-2.061	G. ruber-w
KNR166-2-124GGC	21.5	0.422	-2.105	G. ruber-w
KNR166-2-124GGC	22.5	0.329	-2.037	G. ruber-w
KNR166-2-124GGC	22.5	0.240	-2.112	G. ruber-w
KNR166-2-124GGC	22.5	0.258	-1.963	G. ruber-w
KNR166-2-124GGC	23.5	0.346	-2.056	G. ruber-w
KNR166-2-124GGC	23.5	0.353	-2.142	G. ruber-w
KNR166-2-124GGC	23.5	0.278	-1.932	G. ruber-w
KNR166-2-124GGC	23.5	0.611	-2.020	G. ruber-w
KNR166-2-124GGC	24.5	0.420	-1.822	G. ruber-w
KNR166-2-124GGC	24.5	0.386	-2.073	G. ruber-w
KNR166-2-124GGC	24.5	0.370	-1.983	G. ruber-w
KNR166-2-124GGC	24.5	0.565	-1.989	G. ruber-w
KNR166-2-124GGC	25.5	0.040	-2.071	G. ruber-w
KNR166-2-124GGC	25.5	-0.339	-2.106	G. ruber-w
KNR166-2-124GGC	25.5	0.328	-2.173	G. ruber-w
KNR166-2-124GGC	25.5	0.311	-1.874	G. ruber-w
KNR166-2-124GGC	26.5	0.182	-2.130	G. ruber-w
KNR166-2-124GGC	26.5	0.198	-1.965	G. ruber-w
KNR166-2-124GGC	26.5	0.362	-1.974	G. ruber-w
KNR166-2-124GGC	26.5	0.385	-1.940	G. ruber-w
KNR166-2-124GGC	27.5	0.085	-1.939	G. ruber-w
KNR166-2-124GGC	27.5	0.309	-2.191	G. ruber-w
KNR166-2-124GGC	27.5	0.115	-2.027	G. ruber-w
KNR166-2-124GGC	27.5	0.578	-2.041	G. ruber-w
KNR166-2-124GGC	28.5	0.388	-2.028	G. ruber-w
KNR166-2-124GGC	28.5	0.488	-2.067	G. ruber-w
KNR166-2-124GGC	28.5	0.389	-2.095	G. ruber-w
KNR166-2-124GGC	28.5	0.666	-1.914	G. ruber-w
KNR166-2-124GGC	29.5	0.391	-2.069	G. ruber-w
KNR166-2-124GGC	29.5	0.357	-1.924	G. ruber-w
KNR166-2-124GGC	29.5	0.529	-1.975	G. ruber-w
KNR166-2-124GGC	29.5	0.461	-2.108	G. ruber-w
KNR166-2-124GGC	30.5	0.263	-2.189	G. ruber-w
KNR166-2-124GGC	30.5	0.360	-1.975	G. ruber-w
KNR166-2-124GGC	30.5	0.233	-2.051	G. ruber-w
KNR166-2-124GGC	30.5	0.241	-2.190	G. ruber-w
KNR166-2-124GGC	31.5	0.237	-1.837	G. ruber-w
KNR166-2-124GGC	31.5	0.131	-1.978	G. ruber-w
KNR166-2-124GGC	31.5	0.133	-2.031	G. ruber-w
KNR166-2-124GGC	31.5	0.197	-1.984	G. ruber-w
KNR166-2-124GGC	32.5	0.383	-1.800	G. ruber-w
KNR166-2-124GGC	32.5	0.507	-1.879	G. ruber-w
KNR166-2-124GGC	32.5	0.553	-1.879	G. ruber-w
KNR166-2-124GGC	32.5	0.348	-1.831	G. ruber-w
KNR166-2-124GGC	33.5	0.282	-2.044	G. ruber-w
KNR166-2-124GGC	33.5	0.545	-1.890	G. ruber-w

KNR166-2-124GGC	33.5	0.382	-2.007	G. ruber-w
KNR166-2-124GGC	33.5	0.450	-1.966	G. ruber-w
KNR166-2-124GGC	34.5	0.232	-2.020	G. ruber-w
KNR166-2-124GGC	34.5	0.081	-1.944	G. ruber-w
KNR166-2-124GGC	34.5	0.462	-2.142	G. ruber-w
KNR166-2-124GGC	34.5	0.022	-2.207	G. ruber-w
KNR166-2-124GGC	35.5	0.067	-1.993	G. ruber-w
KNR166-2-124GGC	35.5	0.507	-1.917	G. ruber-w
KNR166-2-124GGC	35.5	0.382	-2.033	G. ruber-w
KNR166-2-124GGC	35.5	0.541	-1.987	G. ruber-w
KNR166-2-124GGC	36.5	0.337	-2.264	G. ruber-w
KNR166-2-124GGC	36.5	0.400	-2.119	G. ruber-w
KNR166-2-124GGC	36.5	-0.091	-2.356	G. ruber-w
KNR166-2-124GGC	36.5	0.203	-2.161	G. ruber-w
KNR166-2-124GGC	37.5	0.363	-2.007	G. ruber-w
KNR166-2-124GGC	37.5	0.250	-2.159	G. ruber-w
KNR166-2-124GGC	37.5	0.133	-2.091	G. ruber-w
KNR166-2-124GGC	37.5	0.369	-2.059	G. ruber-w
KNR166-2-124GGC	38.5	0.557	-2.037	G. ruber-w
KNR166-2-124GGC	38.5	0.453	-1.999	G. ruber-w
KNR166-2-124GGC	38.5	0.745	-2.054	G. ruber-w
KNR166-2-124GGC	38.5	0.321	-2.070	G. ruber-w
KNR166-2-124GGC	39.5	0.281	-2.077	G. ruber-w
KNR166-2-124GGC	39.5	0.060	-2.160	G. ruber-w
KNR166-2-124GGC	39.5	0.509	-1.959	G. ruber-w
KNR166-2-124GGC	39.5	0.247	-2.162	G. ruber-w
KNR166-2-124GGC	40.5	0.525	-2.020	G. ruber-w
KNR166-2-124GGC	40.5	0.590	-2.186	G. ruber-w
KNR166-2-124GGC	40.5	0.463	-2.153	G. ruber-w
KNR166-2-124GGC	40.5	0.574	-2.051	G. ruber-w
KNR166-2-124GGC	41.5	0.451	-1.919	G. ruber-w
KNR166-2-124GGC	41.5	0.388	-2.146	G. ruber-w
KNR166-2-124GGC	41.5	0.258	-2.182	G. ruber-w
KNR166-2-124GGC	41.5	0.526	-1.893	G. ruber-w
KNR166-2-124GGC	42.5	0.586	-1.943	G. ruber-w
KNR166-2-124GGC	42.5	0.165	-2.177	G. ruber-w
KNR166-2-124GGC	42.5	0.434	-1.993	G. ruber-w
KNR166-2-124GGC	42.5	0.348	-2.162	G. ruber-w
KNR166-2-124GGC	43.5	0.483	-1.845	G. ruber-w
KNR166-2-124GGC	43.5	0.174	-2.121	G. ruber-w
KNR166-2-124GGC	43.5	0.060	-2.279	G. ruber-w
KNR166-2-124GGC	43.5	0.287	-2.114	G. ruber-w
KNR166-2-124GGC	44.5	0.098	-1.909	G. ruber-w
KNR166-2-124GGC	44.5	0.624	-2.055	G. ruber-w
KNR166-2-124GGC	44.5	0.474	-2.129	G. ruber-w
KNR166-2-124GGC	44.5	0.458	-1.810	G. ruber-w
KNR166-2-124GGC	45.5	0.363	-2.105	G. ruber-w
KNR166-2-124GGC	45.5	0.272	-2.097	G. ruber-w
KNR166-2-124GGC	45.5	0.479	-2.140	G. ruber-w
KNR166-2-124GGC	45.5	0.484	-2.127	G. ruber-w
KNR166-2-124GGC	46.5	0.200	-2.096	G. ruber-w
KNR166-2-124GGC	46.5	0.365	-2.154	G. ruber-w
KNR166-2-124GGC	46.5	0.440	-2.046	G. ruber-w
KNR166-2-124GGC	46.5	0.335	-2.133	G. ruber-w
KNR166-2-124GGC	47.5	0.231	-2.071	G. ruber-w

KNR166-2-124GGC	47.5	0.488	-2.114	G. ruber-w
KNR166-2-124GGC	47.5	0.049	-2.089	G. ruber-w
KNR166-2-124GGC	47.5	0.305	-2.069	G. ruber-w
KNR166-2-124GGC	48.5	0.074	-2.170	G. ruber-w
KNR166-2-124GGC	48.5	0.178	-2.093	G. ruber-w
KNR166-2-124GGC	48.5	0.262	-2.077	G. ruber-w
KNR166-2-124GGC	48.5	0.219	-2.201	G. ruber-w
KNR166-2-124GGC	49.5	0.092	-1.997	G. ruber-w
KNR166-2-124GGC	49.5	0.113	-1.984	G. ruber-w
KNR166-2-124GGC	49.5	0.043	-2.013	G. ruber-w
KNR166-2-124GGC	49.5	0.187	-2.068	G. ruber-w
KNR166-2-124GGC	50.5	-0.100	-2.222	G. ruber-w
KNR166-2-124GGC	50.5	0.249	-1.891	G. ruber-w
KNR166-2-124GGC	50.5	-0.044	-1.891	G. ruber-w
KNR166-2-124GGC	50.5	0.195	-2.155	G. ruber-w

CORE	DEPTH	C13	O18	SPECIES
KNR166-2-125MC-D	0.5	1.013	1.410	C. floridanus
KNR166-2-125MC-D	0.5	1.081	1.642	C. floridanus
KNR166-2-125MC-D	0.5	1.178	1.466	P. ariminensis
KNR166-2-125MC-D	0.5	1.130	1.502	C. floridanus
KNR166-2-125MC-D	0.5	1.378	1.527	P. ariminensis
KNR166-2-125MC-D	1.5	0.795	1.376	C. floridanus
KNR166-2-125MC-D	1.5	1.033	1.422	C. floridanus
KNR166-2-125MC-D	1.5	1.145	1.373	C. floridanus
KNR166-2-125MC-D	1.5	1.037	1.436	C. floridanus
KNR166-2-125MC-D	1.5	1.218	1.602	C. floridanus
KNR166-2-125MC-D	2.5	0.847	1.528	C. floridanus
KNR166-2-125MC-D	2.5	1.301	1.721	P. ariminensis
KNR166-2-125MC-D	2.5	1.419	1.587	P. ariminensis
KNR166-2-125MC-D	2.5	1.360	1.494	P. ariminensis
KNR166-2-125MC-D	2.5	1.196	1.537	P. ariminensis
KNR166-2-125MC-D	3.5	1.184	1.565	C. floridanus
KNR166-2-125MC-D	3.5	1.269	1.625	C. floridanus
KNR166-2-125MC-D	3.5	1.315	1.567	P. ariminensis
KNR166-2-125MC-D	3.5	1.442	1.581	P. ariminensis
KNR166-2-125MC-D	4.5	1.210	1.580	C. floridanus
KNR166-2-125MC-D	4.5	1.209	1.622	C. floridanus
KNR166-2-125MC-D	4.5	1.451	1.553	P. ariminensis
KNR166-2-125MC-D	4.5	1.207	1.534	C. floridanus
KNR166-2-125MC-D	4.5	1.248	1.558	P. ariminensis
KNR166-2-125MC-D	5.5	1.110	1.627	C. floridanus
KNR166-2-125MC-D	5.5	1.082	1.579	C. floridanus
KNR166-2-125MC-D	5.5	1.328	1.569	P. ariminensis
KNR166-2-125MC-D	5.5	1.483	1.391	P. ariminensis
KNR166-2-125MC-D	5.5	1.360	1.682	P. ariminensis
KNR166-2-125MC-D	6.5	1.102	1.545	C. floridanus
KNR166-2-125MC-D	6.5	1.322	1.627	C. floridanus
KNR166-2-125MC-D	6.5	1.087	1.571	C. floridanus
KNR166-2-125MC-D	6.5	1.263	1.541	C. floridanus
KNR166-2-125MC-D	6.5	1.293	1.657	P. ariminensis
KNR166-2-125MC-D	7.5	1.216	1.675	C. floridanus
KNR166-2-125MC-D	7.5	1.335	1.553	C. floridanus
KNR166-2-125MC-D	7.5	1.441	1.521	P. ariminensis
KNR166-2-125MC-D	7.5	1.140	1.520	C. floridanus
KNR166-2-125MC-D	7.5	1.370	1.563	P. ariminensis
KNR166-2-125MC-D	8.5	1.249	1.584	P. ariminensis
KNR166-2-125MC-D	8.5	1.313	1.810	C. floridanus
KNR166-2-125MC-D	8.5	1.384	1.558	P. ariminensis
KNR166-2-125MC-D	8.5	1.356	1.528	P. ariminensis
KNR166-2-125MC-D	8.5	1.317	1.600	P. ariminensis
KNR166-2-125MC-D	9.5	1.105	1.585	C. floridanus
KNR166-2-125MC-D	9.5	1.041	1.694	C. floridanus
KNR166-2-125MC-D	9.5	0.938	1.595	C. floridanus
KNR166-2-125MC-D	9.5	1.375	1.569	P. ariminensis
KNR166-2-125MC-D	9.5	1.340	1.560	P. ariminensis
KNR166-2-125MC-D	10.5	1.183	1.572	C. floridanus
KNR166-2-125MC-D	10.5	1.180	1.558	C. floridanus
KNR166-2-125MC-D	10.5	1.094	1.575	C. floridanus
KNR166-2-125MC-D	10.5	1.103	1.524	C. floridanus
KNR166-2-125MC-D	10.5	1.370	1.712	P. ariminensis

KNR166-2-125MC-D	11.5	1.206	1.169	C. floridanus
KNR166-2-125MC-D	11.5	1.124	1.680	C. floridanus
KNR166-2-125MC-D	11.5	1.050	1.433	C. floridanus
KNR166-2-125MC-D	11.5	1.046	1.547	C. floridanus
KNR166-2-125MC-D	11.5	1.181	1.727	C. floridanus
KNR166-2-125MC-D	12.5	1.045	1.523	C. floridanus
KNR166-2-125MC-D	12.5	1.185	1.468	C. floridanus
KNR166-2-125MC-D	12.5	1.205	1.554	C. floridanus
KNR166-2-125MC-D	12.5	1.200	1.702	C. floridanus
KNR166-2-125MC-D	12.5	1.086	1.676	C. floridanus
KNR166-2-125MC-D	13.5	1.177	1.455	C. floridanus
KNR166-2-125MC-D	13.5	1.201	1.471	C. floridanus
KNR166-2-125MC-D	13.5	1.095	1.467	C. floridanus
KNR166-2-125MC-D	13.5	1.211	1.618	C. floridanus
KNR166-2-125MC-D	13.5	1.283	1.606	C. floridanus
KNR166-2-125MC-D	14.5	1.217	1.577	C. floridanus
KNR166-2-125MC-D	14.5	1.256	1.445	C. floridanus
KNR166-2-125MC-D	14.5	1.196	1.522	C. floridanus
KNR166-2-125MC-D	14.5	1.185	1.705	C. floridanus
KNR166-2-125MC-D	14.5	1.394	1.531	P. ariminensis
KNR166-2-125MC-D	15.5	1.148	1.443	C. floridanus
KNR166-2-125MC-D	15.5	1.066	1.433	C. floridanus
KNR166-2-125MC-D	15.5	1.193	1.549	C. floridanus
KNR166-2-125MC-D	15.5	1.420	1.607	P. ariminensis
KNR166-2-125MC-D	15.5	1.433	1.520	P. ariminensis
KNR166-2-125MC-D	16.5	1.206	1.628	C. floridanus
KNR166-2-125MC-D	16.5	1.160	1.581	C. floridanus
KNR166-2-125MC-D	16.5	1.139	1.589	C. floridanus
KNR166-2-125MC-D	16.5	1.199	1.419	C. floridanus
KNR166-2-125MC-D	16.5	1.294	1.663	C. floridanus
KNR166-2-125MC-D	17.5	1.234	1.551	C. floridanus
KNR166-2-125MC-D	17.5	1.195	1.475	C. floridanus
KNR166-2-125MC-D	17.5	1.060	1.639	C. floridanus
KNR166-2-125MC-D	17.5	1.276	1.634	C. floridanus
KNR166-2-125MC-D	17.5	1.407	1.515	P. ariminensis
KNR166-2-125MC-D	18.5	1.085	1.449	C. floridanus
KNR166-2-125MC-D	18.5	1.173	1.350	C. floridanus
KNR166-2-125MC-D	18.5	1.036	1.587	C. floridanus
KNR166-2-125MC-D	18.5	1.321	1.595	P. ariminensis
KNR166-2-125MC-D	18.5	1.405	1.532	P. ariminensis
KNR166-2-125MC-D	19.5	0.680	1.598	C. floridanus
KNR166-2-125MC-D	19.5	1.389	1.525	P. ariminensis
KNR166-2-125MC-D	19.5	1.212	1.583	C. floridanus
KNR166-2-125MC-D	19.5	1.354	1.543	P. ariminensis
KNR166-2-125MC-D	19.5	1.378	1.469	P. ariminensis
KNR166-2-125MC-D	20.5	1.149	1.433	C. floridanus
KNR166-2-125MC-D	20.5	1.172	1.525	C. floridanus
KNR166-2-125MC-D	20.5	1.214	1.669	C. floridanus
KNR166-2-125MC-D	20.5	1.179	1.341	C. floridanus
KNR166-2-125MC-D	20.5	1.277	1.439	P. ariminensis
KNR166-2-125MC-D	21.5	1.157	1.608	C. floridanus
KNR166-2-125MC-D	21.5	1.096	1.550	C. floridanus
KNR166-2-125MC-D	21.5	1.095	1.623	C. floridanus
KNR166-2-125MC-D	21.5	1.361	1.604	P. ariminensis
KNR166-2-125MC-D	21.5	1.424	1.523	P. ariminensis

KNR166-2-125MC-D	22.5	1.273	1.578	C. floridanus
KNR166-2-125MC-D	22.5	1.262	1.602	C. floridanus
KNR166-2-125MC-D	22.5	1.069	1.620	C. floridanus
KNR166-2-125MC-D	22.5	1.332	1.565	P. ariminensis
KNR166-2-125MC-D	23.5	1.248	1.582	C. floridanus
KNR166-2-125MC-D	23.5	1.375	1.620	P. ariminensis
KNR166-2-125MC-D	23.5	1.201	1.574	C. floridanus
KNR166-2-125MC-D	23.5	1.368	1.535	P. ariminensis
KNR166-2-125MC-D	23.5	1.159	1.494	C. floridanus
KNR166-2-125MC-D	24.5	1.126	1.658	C. floridanus
KNR166-2-125MC-D	24.5	1.210	1.543	C. floridanus
KNR166-2-125MC-D	24.5	1.179	1.556	C. floridanus
KNR166-2-125MC-D	24.5	1.122	1.540	C. floridanus
KNR166-2-125MC-D	24.5	1.338	1.616	P. ariminensis
KNR166-2-125MC-D	25.5	1.142	1.577	C. floridanus
KNR166-2-125MC-D	25.5	1.323	1.661	P. ariminensis
KNR166-2-125MC-D	25.5	1.249	1.700	P. ariminensis
KNR166-2-125MC-D	25.5	1.212	1.759	P. ariminensis
KNR166-2-125MC-D	25.5	1.155	1.579	C. floridanus
KNR166-2-125MC-D	26.5	1.245	1.580	C. floridanus
KNR166-2-125MC-D	26.5	1.373	1.627	P. ariminensis
KNR166-2-125MC-D	26.5	1.197	1.581	C. floridanus
KNR166-2-125MC-D	26.5	1.222	1.513	C. floridanus
KNR166-2-125MC-D	26.5	1.390	1.374	P. ariminensis
KNR166-2-125MC-D	27.5	1.184	1.556	C. floridanus
KNR166-2-125MC-D	27.5	1.114	1.522	C. floridanus
KNR166-2-125MC-D	27.5	1.117	1.550	C. floridanus
KNR166-2-125MC-D	27.5	1.185	1.556	C. floridanus
KNR166-2-125MC-D	27.5	1.361	1.535	P. ariminensis

CORE	DEPTH	C13	O18	SPECIES
KNR166-2-125MC-D	0.5	0.692	-2.200	G. ruber-w
KNR166-2-125MC-D	0.5	0.698	-1.827	G. ruber-w
KNR166-2-125MC-D	0.5	0.422	-1.921	G. ruber-w
KNR166-2-125MC-D	0.5	0.364	-2.190	G. ruber-w
KNR166-2-125MC-D	1.5	0.660	-1.717	G. ruber-w
KNR166-2-125MC-D	1.5	0.835	-1.889	G. ruber-w
KNR166-2-125MC-D	1.5	0.788	-1.880	G. ruber-w
KNR166-2-125MC-D	1.5	0.167	-1.980	G. ruber-w
KNR166-2-125MC-D	2.5	0.620	-1.922	G. ruber-w
KNR166-2-125MC-D	2.5	0.547	-1.874	G. ruber-w
KNR166-2-125MC-D	2.5	0.525	-1.778	G. ruber-w
KNR166-2-125MC-D	2.5	0.531	-2.106	G. ruber-w
KNR166-2-125MC-D	3.5	0.704	-2.021	G. ruber-w
KNR166-2-125MC-D	3.5	0.329	-2.045	G. ruber-w
KNR166-2-125MC-D	3.5	0.501	-1.898	G. ruber-w
KNR166-2-125MC-D	3.5	0.302	-2.215	G. ruber-w
KNR166-2-125MC-D	4.5	-0.331	-2.092	G. ruber-w
KNR166-2-125MC-D	4.5	0.185	-1.326	G. ruber-w
KNR166-2-125MC-D	4.5	0.561	-2.012	G. ruber-w
KNR166-2-125MC-D	4.5	0.252	-2.231	G. ruber-w
KNR166-2-125MC-D	4.5	0.068	-2.286	G. ruber-w
KNR166-2-125MC-D	4.5	-0.188	-2.078	G. ruber-w
KNR166-2-125MC-D	5.5	0.193	-2.000	G. ruber-w
KNR166-2-125MC-D	5.5	-0.110	-2.096	G. ruber-w
KNR166-2-125MC-D	5.5	-0.225	-1.954	G. ruber-w
KNR166-2-125MC-D	5.5	0.212	-2.205	G. ruber-w
KNR166-2-125MC-D	5.5	-0.363	-2.171	G. ruber-w
KNR166-2-125MC-D	6.5	0.257	-2.238	G. ruber-w
KNR166-2-125MC-D	6.5	0.321	-2.126	G. ruber-w
KNR166-2-125MC-D	6.5	0.200	-2.037	G. ruber-w
KNR166-2-125MC-D	6.5	0.504	-2.008	G. ruber-w
KNR166-2-125MC-D	6.5	0.135	-2.087	G. ruber-w
KNR166-2-125MC-D	7.5	0.041	-1.873	G. ruber-w
KNR166-2-125MC-D	7.5	0.109	-1.856	G. ruber-w
KNR166-2-125MC-D	7.5	0.479	-2.115	G. ruber-w
KNR166-2-125MC-D	7.5	0.428	-2.033	G. ruber-w
KNR166-2-125MC-D	7.5	0.339	-2.026	G. ruber-w
KNR166-2-125MC-D	8.5	0.633	-1.801	G. ruber-w
KNR166-2-125MC-D	8.5	0.394	-1.979	G. ruber-w
KNR166-2-125MC-D	8.5	0.316	-1.969	G. ruber-w
KNR166-2-125MC-D	8.5	0.368	-1.932	G. ruber-w
KNR166-2-125MC-D	8.5	0.312	-1.820	G. ruber-w
KNR166-2-125MC-D	9.5	0.194	-2.019	G. ruber-w
KNR166-2-125MC-D	9.5	0.404	-2.048	G. ruber-w
KNR166-2-125MC-D	9.5	0.216	-2.116	G. ruber-w
KNR166-2-125MC-D	9.5	0.502	-2.179	G. ruber-w
KNR166-2-125MC-D	9.5	0.023	-1.841	G. ruber-w
KNR166-2-125MC-D	10.5	0.509	-1.973	G. ruber-w
KNR166-2-125MC-D	10.5	-0.094	-2.199	G. ruber-w
KNR166-2-125MC-D	10.5	-0.297	-2.301	G. ruber-w
KNR166-2-125MC-D	10.5	0.373	-1.882	G. ruber-w
KNR166-2-125MC-D	10.5	-0.053	-2.091	G. ruber-w
KNR166-2-125MC-D	11.5	0.422	-1.785	G. ruber-w
KNR166-2-125MC-D	11.5	0.286	-1.960	G. ruber-w

KNR166-2-125MC-D	11.5	0.008	-2.027	G. ruber-w
KNR166-2-125MC-D	11.5	0.484	-2.043	G. ruber-w
KNR166-2-125MC-D	12.5	0.247	-2.034	G. ruber-w
KNR166-2-125MC-D	12.5	-0.198	-2.199	G. ruber-w
KNR166-2-125MC-D	12.5	0.051	-2.081	G. ruber-w
KNR166-2-125MC-D	12.5	-0.164	-1.968	G. ruber-w
KNR166-2-125MC-D	13.5	0.460	-1.886	G. ruber-w
KNR166-2-125MC-D	13.5	0.006	-2.064	G. ruber-w
KNR166-2-125MC-D	13.5	-0.106	-2.209	G. ruber-w
KNR166-2-125MC-D	13.5	0.192	-2.122	G. ruber-w
KNR166-2-125MC-D	14.5	0.177	-2.045	G. ruber-w
KNR166-2-125MC-D	14.5	0.675	-2.102	G. ruber-w
KNR166-2-125MC-D	14.5	0.474	-2.012	G. ruber-w
KNR166-2-125MC-D	14.5	0.329	-2.074	G. ruber-w
KNR166-2-125MC-D	15.5	0.038	-2.146	G. ruber-w
KNR166-2-125MC-D	15.5	0.863	-2.104	G. ruber-w
KNR166-2-125MC-D	15.5	0.472	-1.968	G. ruber-w
KNR166-2-125MC-D	15.5	-0.110	-2.195	G. ruber-w
KNR166-2-125MC-D	16.5	0.291	-2.093	G. ruber-w
KNR166-2-125MC-D	16.5	0.163	-2.070	G. ruber-w
KNR166-2-125MC-D	16.5	0.247	-2.166	G. ruber-w
KNR166-2-125MC-D	16.5	-0.181	-1.942	G. ruber-w
KNR166-2-125MC-D	17.5	0.234	-2.031	G. ruber-w
KNR166-2-125MC-D	17.5	0.137	-2.371	G. ruber-w
KNR166-2-125MC-D	17.5	0.251	-2.055	G. ruber-w
KNR166-2-125MC-D	17.5	-0.172	-2.310	G. ruber-w
KNR166-2-125MC-D	18.5	0.686	-2.215	G. ruber-w
KNR166-2-125MC-D	18.5	-0.215	-2.277	G. ruber-w
KNR166-2-125MC-D	18.5	0.098	-1.933	G. ruber-w
KNR166-2-125MC-D	18.5	-0.232	-2.142	G. ruber-w
KNR166-2-125MC-D	19.5	0.256	-2.157	G. ruber-w
KNR166-2-125MC-D	19.5	0.562	-2.068	G. ruber-w
KNR166-2-125MC-D	19.5	0.550	-1.655	G. ruber-w
KNR166-2-125MC-D	19.5	0.427	-1.988	G. ruber-w
KNR166-2-125MC-D	19.5	0.394	-1.984	G. ruber-w
KNR166-2-125MC-D	20.5	0.195	-1.911	G. ruber-w
KNR166-2-125MC-D	20.5	-0.387	-2.109	G. ruber-w
KNR166-2-125MC-D	20.5	0.563	-2.105	G. ruber-w
KNR166-2-125MC-D	20.5	0.630	-1.943	G. ruber-w
KNR166-2-125MC-D	21.5	-0.075	-2.200	G. ruber-w
KNR166-2-125MC-D	21.5	0.151	-2.103	G. ruber-w
KNR166-2-125MC-D	21.5	0.375	-1.928	G. ruber-w
KNR166-2-125MC-D	22.5	-0.577	-2.035	G. ruber-w
KNR166-2-125MC-D	22.5	0.261	-2.121	G. ruber-w
KNR166-2-125MC-D	22.5	-0.057	-1.891	G. ruber-w
KNR166-2-125MC-D	23.5	0.133	-2.046	G. ruber-w
KNR166-2-125MC-D	23.5	0.288	-2.233	G. ruber-w
KNR166-2-125MC-D	23.5	0.566	-1.684	G. ruber-w
KNR166-2-125MC-D	24.5	0.019	-2.287	G. ruber-w
KNR166-2-125MC-D	24.5	0.204	-2.002	G. ruber-w
KNR166-2-125MC-D	24.5	0.069	-2.115	G. ruber-w
KNR166-2-125MC-D	25.5	0.272	-2.246	G. ruber-w
KNR166-2-125MC-D	25.5	0.476	-1.652	G. ruber-w
KNR166-2-125MC-D	25.5	0.485	-1.869	G. ruber-w
KNR166-2-125MC-D	26.5	0.551	-1.888	G. ruber-w

KNR166-2-125MC-D	26.5	0.403	-1.888	G. ruber-w
KNR166-2-125MC-D	26.5	0.181	-1.842	G. ruber-w
KNR166-2-125MC-D	27.5	0.557	-1.926	G. ruber-w
KNR166-2-125MC-D	27.5	0.536	-2.096	G. ruber-w
KNR166-2-125MC-D	27.5	0.552	-1.755	G. ruber-w

CORE	DEPTH	C13	O18	SPECIES
KNR166-2-134MC-A	2.5	1.054	0.582	C. floridanus
KNR166-2-134MC-A	2.5	1.127	0.394	C. floridanus
KNR166-2-134MC-A	2.5	1.081	0.474	C. floridanus
KNR166-2-134MC-A	2.5	1.034	0.487	C. floridanus
KNR166-2-134MC-A	3.5	1.242	0.504	C. floridanus
KNR166-2-134MC-A	3.5	0.999	0.551	C. floridanus
KNR166-2-134MC-A	3.5	1.296	0.385	C. floridanus
KNR166-2-134MC-A	4.5	0.971	0.454	C. floridanus
KNR166-2-134MC-A	5.5	1.494	0.363	C. floridanus
KNR166-2-134MC-A	6.5	1.422	0.452	C. floridanus
KNR166-2-134MC-A	7.5	1.405	0.379	C. floridanus
KNR166-2-134MC-A	7.5	1.857	0.323	C. floridanus
KNR166-2-134MC-A	7.5	1.286	0.484	C. floridanus
KNR166-2-134MC-A	7.5	1.349	0.542	C. floridanus
KNR166-2-134MC-A	8.5	1.473	0.366	C. floridanus
KNR166-2-134MC-A	8.5	1.634	0.527	C. floridanus
KNR166-2-134MC-A	8.5	1.400	0.583	C. floridanus
KNR166-2-134MC-A	9.5	1.520	0.613	C. floridanus
KNR166-2-134MC-A	9.5	1.445	0.665	C. floridanus
KNR166-2-134MC-A	10.5	1.485	0.498	C. floridanus
KNR166-2-134MC-A	10.5	1.766	0.377	C. floridanus
KNR166-2-134MC-A	11.5	1.500	0.509	C. floridanus
KNR166-2-134MC-A	11.5	1.532	0.413	C. floridanus
KNR166-2-134MC-A	11.5	1.573	0.511	C. floridanus
KNR166-2-134MC-A	12.5	1.480	0.640	C. floridanus
KNR166-2-134MC-A	12.5	1.460	0.691	C. floridanus
KNR166-2-134MC-A	12.5	1.637	0.621	C. floridanus
KNR166-2-134MC-A	12.5	1.623	0.566	C. floridanus
KNR166-2-134MC-A	13.5	1.663	0.499	C. floridanus
KNR166-2-134MC-A	13.5	1.614	0.568	C. floridanus
KNR166-2-134MC-A	14.5	1.784	0.574	C. floridanus
KNR166-2-134MC-A	14.5	1.581	0.631	C. floridanus
KNR166-2-134MC-A	15.5	1.285	0.572	C. floridanus
KNR166-2-134MC-A	15.5	1.422	0.401	C. floridanus
KNR166-2-134MC-A	16.5	1.722	0.062	C. floridanus
KNR166-2-134MC-A	16.5	1.449	0.693	C. floridanus
KNR166-2-134MC-A	16.5	1.572	0.589	C. floridanus